THE BELL SYSTEM
Technical Journal

Volume 51 January 1972 Number 1

SOIL BURIAL TESTS OF MATERIALS AND STRUCTURES

(Continued on inside back cover)

THE BELL SYSTEM TECHNICAL JOURNAL

ADVISORY BOARD

D. E. PROCKNOW, *President, Western Electric Company*

J. B. FISK, *President, Bell Telephone Laboratories*

W. L. LINDHOLM, *Executive Vice President, American Telephone and Telegraph Company*

EDITORIAL COMMITTEE

W. E. DANIELSON, *Chairman*

F. T. ANDREWS, JR.
S. J. BUCHSBAUM
R. P. CLAGETT
I. DORROS
D. GILLETTE
A. E. JOEL, JR.
H. H. LOAR
B. E. STRASSER
D. G. THOMAS
C. R. WILLIAMSON

EDITORIAL STAFF

W. W. MINES, *Editor*
R. E. GILLIS, *Associate Editor*
H. M. PURVIANCE, *Production and Illustrations*
F. J. SCHWETJE, *Circulation*
R. A. CONNOLLY, *Coordinating Editor of Soil Burial Articles*

THE BELL SYSTEM TECHNICAL JOURNAL is published ten times a year by the American Telephone and Telegraph Company, H. I. Romnes, Chairman and President, J. J. Scanlon, Vice President and Treasurer, R. W. Ehrlich, Secretary. Checks for subscriptions should be made payable to American Telephone and Telegraph Company and should be addressed to the Treasury Department, Room 2312C, 195 Broadway, New York, N. Y. 10007. Subscriptions $10.00 per year; single copies $1.25 each. Foreign postage $1.00 per year; 15 cents per copy. Printed in U.S.A.

THE BELL SYSTEM
TECHNICAL JOURNAL

DEVOTED TO THE SCIENTIFIC AND ENGINEERING
ASPECTS OF ELECTRICAL COMMUNICATION

Volume 51 January 1972 Number 1

Copyright © 1972, American Telephone and Telegraph Company. Printed in U.S.A.

Soil Burial Tests:

Soil Burial of Materials and Structures

By R. A. CONNOLLY

(Manuscript received July 28, 1971)

The Bell System emphasis on burying the transmission media plant directly in the soil resulted in the initiation of a study in 1956 designed to determine the behavior of commercial and experimental materials in the soil. For this study, two test sites representative of soils of large sections of the country were employed: one in Bainbridge, Georgia, and the other in Roswell, New Mexico, typical acid and alkaline soils, respectively. The soil characteristics, test plot design, sample preparation, installation and removal schedules, and overall areas of responsibilities are discussed in this paper. A detailed discussion of the effect of up to eight years of soil burial exposure on molded plastics, casting resins, rubbers and metal-to-rubber bonds, electrical and structural laminates, adhesives, tapes, and coated conductors are covered in companion papers. The history of the problems with buried structures and the engineering implications are stressed.

I. INTRODUCTION

In the late 1950s, the Bell System started to bury exchange area plant directly in the soil and now some 80 percent of annual additions to service individual homes are buried. By 1975, almost all newly

installed distribution plant will be in this environment. Figure 1, from H. Southworth,[1] shows the trends in the underground, aerial, and buried telephone cable plant over the last sixteen years. The advantages of buried plant over conventional aerial plant are that it is potentially lower in first cost, less subject to service interruptions by natural causes, not affected by trees, faster to install, and more aesthetic.[2] In contrast to this, it is less flexible and additions are costly while workmen in other operations may cause damage to buried lines. In addition, armored cable and wire must be used in rock and gopher-infested areas.

In the mid-1950s, the accelerating trend to bury the telephone distribution circuits to homes was thwarted somewhat by problems in the areas of wire and cable design, materials, and construction techniques. The long-range economy of buried plant depends in large measure on the ability of materials to withstand factors in soil environments

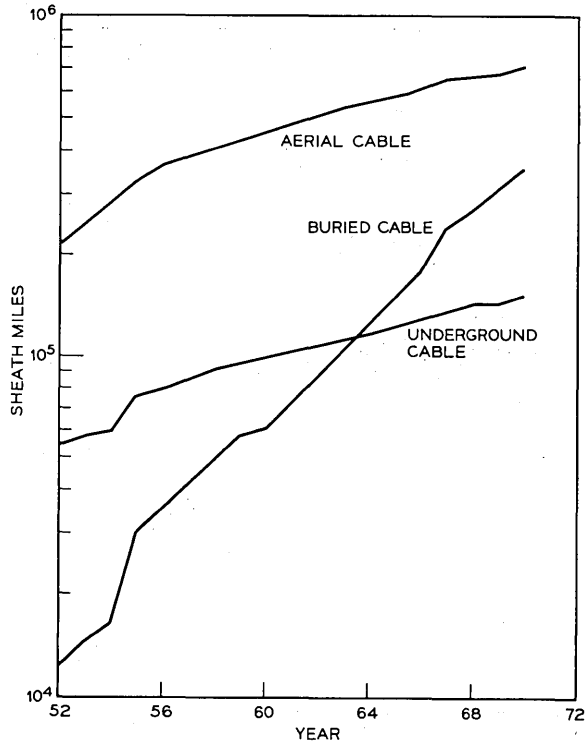

Fig. 1—Cable sheath miles in Bell System (excluding Long Lines).

which may affect their performance. Therefore, it was considered important that the wires, cables, structures, and the materials which might be used in their fabrication be evaluated in subterranean environments to determine their resistance to physical, chemical, and biological degradation under conditions expected to accelerate such attack. Consequently, in 1956 a committee was set up to design an appropriate program and to implement the necessary action to meet this need for accumulating environmental data on material performance. Their program included the study of materials in use at that time and those which might find application in the form of cable, wire, terminals, splices, and ducts. The soil environment presents many factors that may affect the buried telephone plant, and some explanation of these is necessary for an understanding of the problems to be faced.

II. CHARACTERISTICS OF SOIL ENVIRONMENTS

The soil, which provides a more severe environment than underground duct exposure, is complex and difficult to describe. There are some 200 different soil types within the continental United States, including fertile agricultural soils, prairies, forest land, sand dunes, bogs, and swamps, all of which differ chemically, physically, and biologically. Our buried telephone plant must be capable of functioning in all these situations.

2.1 *Chemical*

The bulk of most soils is made up of inorganic matter which ranges from 60 percent to 99 percent of the total weight, averaging 95 percent. About 47 percent is oxygen, as shown in Table I. The abundance of oxygen and its oxides clearly suggests that the environment can cause chemical modifications of materials. The trace elements, such as Cl and S, are especially active.

The organic matter in the soil is as complex as any existing in nature. Constituents include plant and animal tissues, living and dead microbial cells, microbial synthesized compounds, and endless arrays of derivatives of these materials produced as the result of microbial activity. Soils contain most, if not all, of the naturally occurring organic compounds, such as sugars, starches, carbohydrates, hemicellulose, pectins, celluloses, lignins, fats, and proteins. However, the concentration of organic matter in most soils is less than 5 percent[3] as an overall average.

The natural composition of the soil, although varied, is generally made up of only the above materials. In addition, however, there

TABLE I—AVERAGE CHEMICAL COMPOSITION OF THE EARTH'S CRUST*

Element	% Element	% Oxide
O	46.5	
Si	27.6	59.7
Al	8.1	15.22
Fe	5.1	6.81
Ca	3.6	5.10
Mg	2.1	3.45
Na	2.8	3.71
K	2.6	3.11
Ti	0.6	1.03
P	0.12	0.30
Mn	0.09	0.11
S	0.06	1.30
Cl	0.05	
C	0.04	

* Based on 95 percent igneous rocks, 4 percent shales, 0.75 percent sandstone and 0.25 percent limestone (F. E. Bear[3]).

can be many other chemicals that, through man's activities, find their way into the soil. These include: gasoline, diesel fuel, lubricating oil, grease, trichloroethylene, and organic chemical wastes in general. Many of these materials can adversely affect the performance of the plastic components of the cable, as for example, swelling of polymers exposed to petroleum derivatives. Also, cinders may contribute acid conditions and provide a highly corrosive environment for many metallic materials.

2.2 *Biological*

The soil abounds with plant and animal life, and no soil is completely free from living organisms. The organisms that can be found in at least some locations that are of concern include bacteria, fungi, insects, and rodents. Because of the complexity of the interactions of the above organisms, laboratory tests to duplicate the natural environment are not yet possible.

2.2.1 *Microorganisms*

The most numerous and the smallest organisms are the one-celled bacteria which range from 0.5 μm to 10 μm in length. A cubic inch may contain as many as a trillion individual cells. They range in shape from spheres to straight, curved, or helical rods. They occur in the air, in the soil, in natural bodies of water, and even in the deepest

parts of the oceans. Among the bacteria, many types are able to decompose organic material into carbon dioxide, water, and ammonia. These are heterotrophic organisms in contrast to species which are capable of using carbon from inorganic sources. C. E. ZoBell and J. D. Beckwith[4] found that rubber is attacked by a large number of bacterial species, as indicated by oxygen consumption, carbon dioxide production, loss in weight, and swelling of the rubber. This study also showed that rubber is decomposed faster by mixed cultures than by pure cultures.

P. L. Steinberg[5] found that with biochemical oxygen demand tests (BOD) using enrichment cultures of bacteria at 5 and 20°C, externally plasticized poly (vinyl chloride) and elastomeric materials, except neoprene containing zinc oxide and magnesium oxide, showed significant oxygen consumption. Polyethylene and internally plasticized poly (vinyl chloride) copolymers and pure poly (vinyl chloride) resins were not attacked at either temperature. W. G. Walter, et al.,[6] found that a large list of plastics, including polyethylene, poly (vinyl chloride), nylon, Teflon, and Saran would not inhibit growth of *Micrococcus pyogenes* and *Streptoccus sp.* in the presence of milk. Experiments[7] with polyethylene of different molecular weights have shown that the bacterial activity was most significant at the lowest molecular weight, 4800, which is well below that used in wire and cable structures.

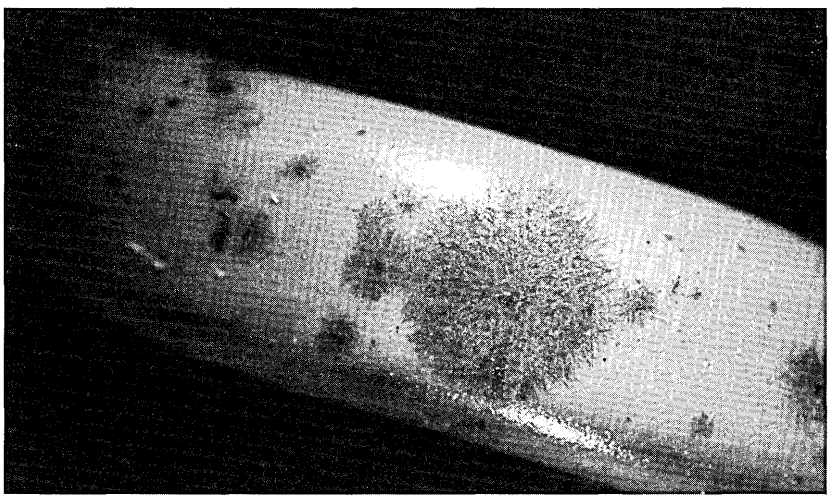

Fig. 2—Fungal growth, *Aureobasidium pullulans*, and *Cladosporium cladosporiodes*, on vinyl chloride coating.

In recent years, more interest has been shown in fungi with respect to materials degradation than any other group of organisms. It is estimated that there are between 10^4 and 10^6 viable fungal organisms per gram of soil, and, although smaller in number, they probably equal the bacteria in sheer weight of microbial protoplasm. Fungi lack chlorophyll and, therefore, are unable to utilize energy directly from the sun. The fungi of greatest interest in degradation are the molds or mildews which can manufacture organic constituents. As heterotrophic organisms, the fungi are exceptionally well equipped to undertake the rapid decomposition of virtually all the major plant constituents, including cellulose.

It is a generally accepted fact that fungi are not capable of attacking the base resins of synthetic polymers such as polyethylene, poly (vinyl chloride), etc. When attack does occur, it is because of additives such as plasticizers, lubricants, oils, and waxes which are added to alter the properties of the base resin.[8] An example of this is the fungal attack on vinyl chloride plastic wire coating, as illustrated in Fig. 2, which is due to susceptible plasticizers and stabilizers. Figure 3 clearly shows the effect of fungi on elongation and tensile strength of a plasticized poly (vinyl chloride).[9] Likewise, J. T. Blake, et al.,[10] demonstrated

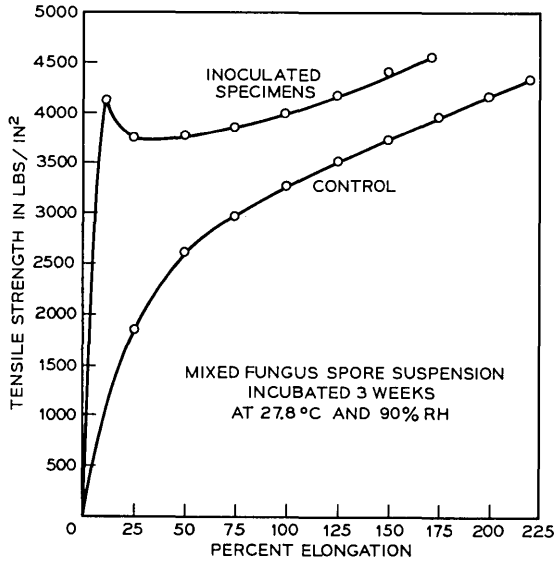

Fig. 3—Effect of fungi on tensile strength and elongation of vinyl chloride plastic containing a nutrient plasticizer.

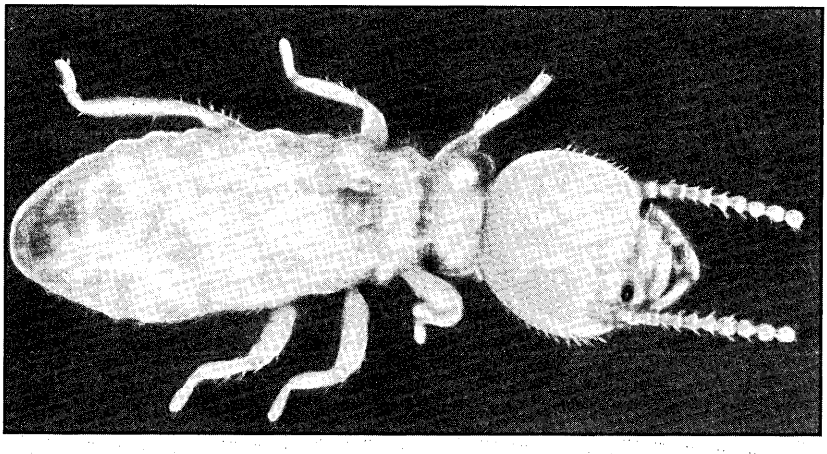

Fig. 4—Native termite worker.

that natural rubber and GRS insulation (which are mixtures of many materials) are inherently vulnerable to fungi to the point where they will fail electrically in moist environments.

2.2.2 *Macroorganisms*

The macroorganisms in the soil capable of damaging engineering materials include a large number of species. For example, entomologists estimate there are as many as 500,000 different species of insects. Because of food habits and behavior patterns exhibited cover a wide range, it is not surprising that many articles made from organic materials are totally destroyed by insect attack. Various species of termites (Fig. 4), ants, and beetles which damage telephone structures in the same way comprise the predominant groups of insects that damage materials in the soil. Recently, the Formosan termite has been introduced into this country in the Houston, Texas, area and has subsequently spread to Louisiana and South Carolina.[11–13] This species has caused considerable damage to buried telephone and power cables in Japan, Hawaii, and Australia, and indications are that it will be a more destructive pest than our native species.

Insect damage to the transmission media plant is not nearly as spectacular as that of the rodents, but is just as sure since there are almost an infinite number of individuals. One of the best examples of damage by termites and/or ants is presented in Fig. 5 which shows an underground wire that has been chewed. The armor of this particular wire eventually corroded, and the structure ultimately failed electrically.

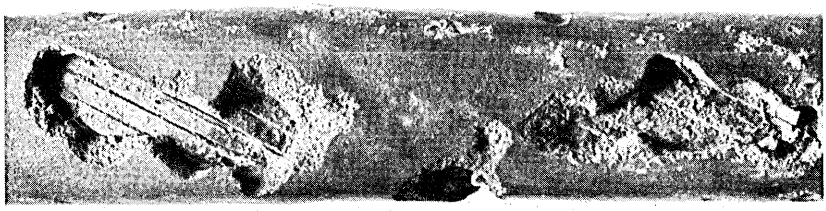

Fig. 5—Underground wire damaged by insects after two years of service in Decatur, Alabama.

G. Flatau[14] stated in 1966 that as much as 5 percent of the sheath faults to plastic jacketed cables in Australia are caused by insects. More recently,[15] the Australians have demonstrated that they can extrude a nylon jacket on cables up to 1.5 inches in diameter to provide adequate insect protection for direct burial cables. F. J. Gay and A. H. Wetherly[16] found that changing the nature and amount of plasticizer can materially improve the termite resistance of plasticized poly (vinyl chloride), and a similar improvement can be effected in polyethylene by changing from a low- to high-density resin.

Rodents represent the largest class of animals that consistently attack buried underground structures, including cable. They possess characteristic chisel-like incisor teeth, especially adapted for gnawing, which they use in their search for food or shelter. By far, the most serious rodent enemy of buried wire and cable is the pocket gopher (*Geomes bursarius*), shown in Fig. 6, which ranges from 4.5 to 9 inches in length. These animals have external cheek pouches which are fur-

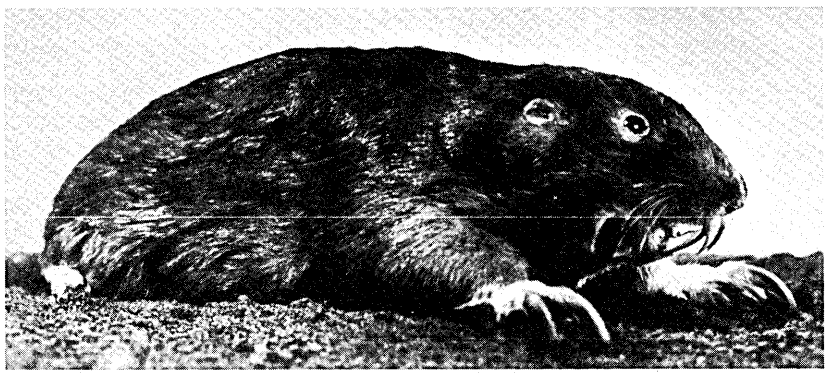

Fig. 6—The pocket gopher (*Geomes bursarius*).

lined so they do not have to ingest the material they chew. It is reported by R. Blain[17] that the two upper incisors of adult pocket gophers grow 9 inches per year, while the two lower incisors average 14 inches per year for a total of 46 inches tooth growth per year per animal. The food of pocket gophers consists entirely of plant material which they consume at the rate of as much as four pounds per day. It is not clear why they sometimes gnaw on things other than plant material such as cable. Some say it is because cables are rootlike in appearance, while others think that they serve as barriers to the animals. A typical example of gopher damage is shown in Fig. 7 where the tooth marks are clearly evident on the polyethylene jacket and lead sheath of a Lepeth cable. Gross damage such as this may cause immediate service interruption in paired cable, or eventually allow water to enter the cable with resulting transmission problems and ultimately service interruptions.

There have been many examples of gopher damage to Bell System plant. R. A. Connolly and R. E. Landstrom[18] have reported that the damage in a given location does not necessarily decrease with time and may even increase significantly. This idea is in contrast to the earlier view that the incidence of damage becomes less as the soil becomes more compact. This study showed that the pocket gopher does not damage cables much larger than 2 inches in diameter.

The Alberta Government Telephone Company reported[19] that 29 percent of the sheath faults in 1966–67 were caused by pocket gophers, *Thomomys talpoides*. They reported that there has not been a single instance of attack on an aluminum shield which is contrary

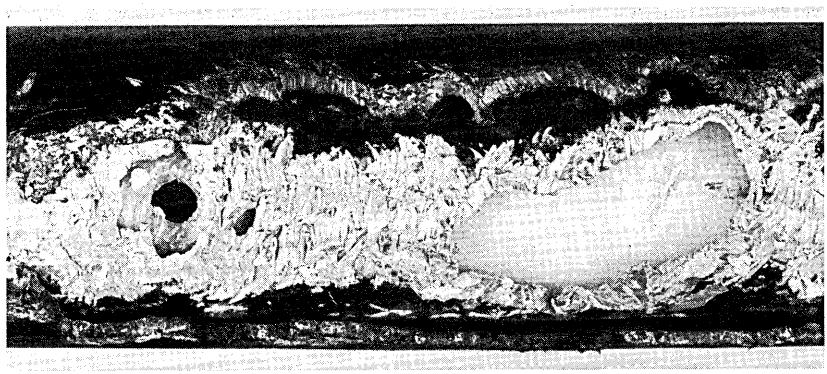

Fig. 7—Lepeth cable damaged by gophers after six years of exposure in Omaha, Nebraska, showing tooth marks and significant loss of material.

to laboratory test data and the expected field performance. They also stated that a far more serious rodent problem than gopher attack on cables is posed by mice in pedestal terminals where they chew on the conductor insulation. In 1953, W. E. Howard[20] found that materials that have resisted gopher attack include 0.005-inch steel armor, aluminum basket weave, and 1/4 inch and 1/8 inch hardware cloth mesh wrapped around the outer jackets of experimental samples. In addition, there was rapid penetration of all nonmetallic cable armor using the following materials: cotton braid, asphaltic saturant asbestos, polyethylene, polychloroprene, vinyl, glass braid, and glass yarn.

Over the years the Bell System has not experienced large losses due to insects and rodents because of good cable and wire design. However, the trend of the combined incidences of rodent and insect damage to the Bell System from 1957 to 1968 are shown in Fig. 8 where it is clear that the rate is increasing more rapidly than for corrosion and lightning. The prediction is that if the Formosan termite becomes more widely spread the rate of increase will be even more pronounced.

2.3 *Physical*

The physical soil environment varies from location to location throughout the continental United States and varies within small

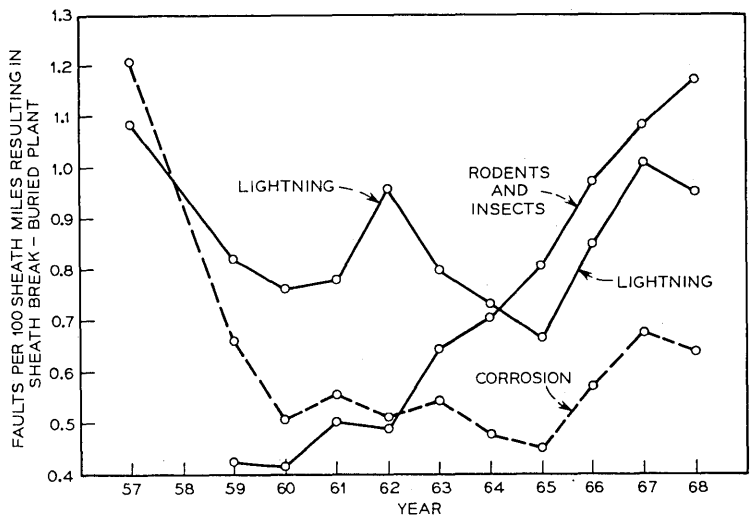

Fig. 8—Rate of sheath break faults with time from insects and rodents, lightning, and corrosion (excluding Long Lines).

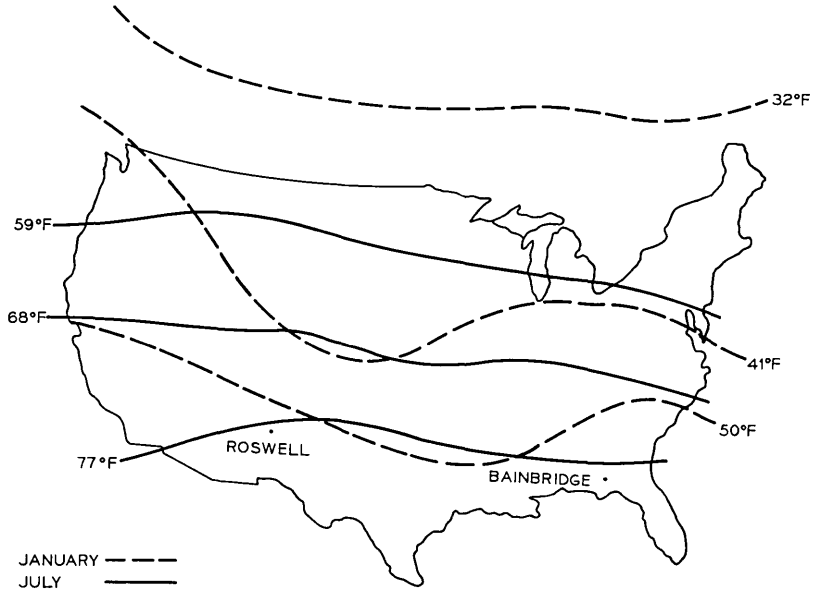

Fig. 9—Ground temperature at 120 cm (from J. H. Chang[21]).

areas and includes factors such as temperature, moisture, soil texture, and lightning.

2.3.1 *Temperature*

Soil temperature, of course, varies with depth, season, and time of day. With respect to materials performance, temperature is not usually critical except where metal and plastics are used in the same structure, and differential thermal expansion becomes a factor. Figure 9 roughly shows the temperature for July and January for the continental United States[21] at a depth of 120 cm. It is clear that at this depth the annual fluctuations are in the neighborhood of 17 to 18°F and that freezing and thawing is not generally a problem except where the cable and wire leaves the ground. The National Electric Light Association[22] measured minimum and maximum earth temperatures at depths from 2 to 8 feet in eleven U. S. cities. The data at the 4-foot level show an annual fluctuation of 15°F in Bloomfield, New Jersey, and 27°F at Clarksburg, West Virginia, which bracket the above figures.

2.3.2 *Moisture*

The annual rainfall of the continental United States varies from

nearly zero in the Western deserts to 60 inches of rain in the Southeast and Pacific Northwest. Generally the Eastern states receive 40–50 inches per year. Though a wide range of precipitation is evident, Bell System equipment must be designed to function in the worst situation, which is effectively soil saturated with water.

2.3.3 *Soil Texture*

The presence of rocks and/or hardpan, where with effort cables and wires can be buried, presents very real problems of damage to the cable in the backfilling operations. When the problem becomes severe enough, especially with critical cables, mechanical protection is added in the form of steel tapes. However, such protection is not always used when it should be and rock damage may result. Small rocks and concretions, if tamped, or if a vehicle is used to compact the soil, may cause sheath damage, which can expose the metallic elements of the cable. Of course, where large rocks are used in backfilling, damage invariably results even if tamping is not done.

2.3.4 *Lightning*

When lightning strikes a plastic jacketed cable, it punctures the jacket by fusion, resulting in a hole 2 mils or larger in diameter. The current then travels along the shield and jumps to earth and punctures the jacket again, possibly at 5- to 10-foot intervals for as long as a mile in either direction from the initial strike.[23] The frequency of damage by lightning varies markedly throughout the country. E. D. Sunde[24] has shown that the number of days with lightning storms per year ranges from a high of 90 in Florida to a low of 5 on the West Coast. There is no location in the United States where lightning is not a potential problem. The nature of the soil affects the behavior of strokes once they hit the ground and how they act once they find their way on a buried telephone structure since the soil resistivity can vary from hundreds of ohm centimeters to hundreds of thousands of ohm centimeters. Figure 8 shows that the detected service interrupting (as reported by the Operating Bell Telephone Companies) faults due to lightning have varied from 0.7 to 1.1 per hundred sheath miles over the last ten years.

III. PREFERRED CHARACTERISTICS FOR BURIED PLANT MATERIALS

Any transmission media system must be able to withstand the adverse forces of nature, as discussed above, for the forty-year design

life of the system. This means that the unprotected materials exposed to the environment must be chemically stable, provide a water barrier, and be resistant to biological attack.

One type of buried cable consists (from the core outward) of a layer of polyethylene, an aluminum shield, and a steel armor coated on the outside with asphalt flooding, followed by a polyethylene jacket.

On any cable, the outermost element will generally be organic rather than metallic because of the problems with corrosion of any of the metals used in cable construction. Consequently, one of the major functions of these materials is corrosion protection. They also offer some mechanical strength to the core and provide a smooth, relatively slippery surface necessary in installing cables with plows or trenchers. Specific properties required of the outer plastic element include resistance to environmental stress-cracking, low water permeability, tensile strength, abrasion resistance, cut-through resistance, flexibility, toughness, and good low-temperature brittleness characteristics.

The present tin-plated steel and aluminum used in sheath construction are not basically highly corrosion resistant materials. The steel offers high tensile strength and permits soldering to obtain an hermetic seal, while the aluminum offers high conductivity. The plastic jacket and the asphaltic flooding used on the steel are designed to isolate and protect these metals from the soil enviromnent.

IV. DESIGN OF SOIL BURIAL PROGRAM

Although the above considerations have a bearing on material performance, this test program was designed primarily to evaluate the effect of microbial, chemical, and physical factors. The sample selection, sample shapes, and exposure methods were not aimed at determining the effect of lightning, rocks, temperature, etc., on material performance.

It is impossible in any soil test to duplicate each of the countless combinations of biological and chemical associations which exist in the natural environment throughout the country. Consequently, it was immediately clear that one test site would not serve the purpose, and the Soil Burial Committee decided that two test plots should be established, one typical of acid and one typical of alkaline soils that were, in turn, representative of large sections of the country.

4.1 *Test Site Selection*

The first step in selecting the sites was to examine the isothermal and regional soil maps of the United States to define areas of interest.[25]

Then, detailed soil maps of the states and counties in the selected regions were examined to find the most appropriate soil types. With this information, local telephone company personnel assisted in locating specific sites. Laboratories representatives then extracted soil samples at various locations and depths in more than twenty-five candidate tracts. They analyzed these samples chemically and physically, and ultimately selected an 11-acre site in Georgia and a 15-acre site in New Mexico designated, respectively, the Bainbridge and Roswell Environmental Test Plots.

The soil analysis was a vital consideration in the selection of the test plots. Table II gives the chemical characteristics of the two sites finally chosen. The pH of the Bainbridge soil shows it to be a strongly acid environment in contrast to the Roswell plot which is only mildly alkaline. The resistivity of the two soils was not measured originally, but was found to be 2000 and 40,000 ohm centimeters, respectively, in 1969. N. D. Tomashov[26] classifies soils in the 1000 to 2000 ohm cm range as medium to high, and soils above 10,000 ohm cm as low in electrolytic aggressiveness. Although the plots were not selected on the basis of their corrosiveness, it is useful information for certain classes of materials such as the metal-to-rubber bonds.

The Bainbridge soil, Tifton Fine Sandy Loam, contains a large quantity of iron concretions which may comprise as much as 20 to 25 percent of the soil. The topsoil is a dark gray loam containing some organic matter in contrast to the subsoil which is a deep yellow, mealy, heavy, sandy clay which contains some imperfectly formed soft brown

TABLE II—SOIL BURIAL TEST PLOT CHARACTERISTICS

Characteristics	Topsoil		Subsoil	
	Bainbridge	Roswell	Bainbridge	Roswell
pH	5.3	8.1	5.1	7.9
Resistivity, ohm-cm	2000*	48,000*	2000*	48,000*
Organic matter	2.0%	1.2%	0.94%	0.35%
Magnesium	23 ppm	369 ppm	17 ppm	266 ppm
Phosphorus	5 ppm	4 ppm	4 ppm	7 ppm
Potasium	24 ppm	111 ppm	7 ppm	58 ppm
Calcium	244 ppm	4236 ppm	120 ppm	4455 ppm
Total nitrogen	0.03%	0.09%	0.015%	0.05%
Chloride	<10 ppm	50 ppm	<10 ppm	50 ppm
Sulfate	<10 ppm	100 ppm	<20 ppm	100 ppm

* Combined topsoil and subsoil.

concretions. The Reagan Clay Loam at Roswell is dark brown, calcareous with little organic matter. The subsoil is gray due to an accumulation of carbonate of lime and is firm or slightly cemented.

4.2 *Test Plot Layout*

The two test plots have essentially the same layout and are divided into quadrants by roadways, as shown in Fig. 10, to provide easy access to the sample locations. Two of the quadrants are used for exposure of the material samples, the third quadrant is for the insulated wires, and the fourth quadrant is for cables and cable hardware (these samples will not be covered in these papers). The quadrants were laid out such that the individual rows of samples are 10 feet apart to allow trucks to be driven close to the samples during installation and removal periods. This spacing also allows room for the necessary periodic maintenance operations.

For protection of the samples, a 25-foot fire lane bounds the test plot proper just outside a 7-foot-high Cyclone fence. It is of interest that to date there has been no vandalism or fire damage to the test plots, either inside or outside the fence. A 20-foot-square cinder block test house, located near the center of the plot, was designed to store the equipment and samples before installation, and to house services such as telephone, water, and power.

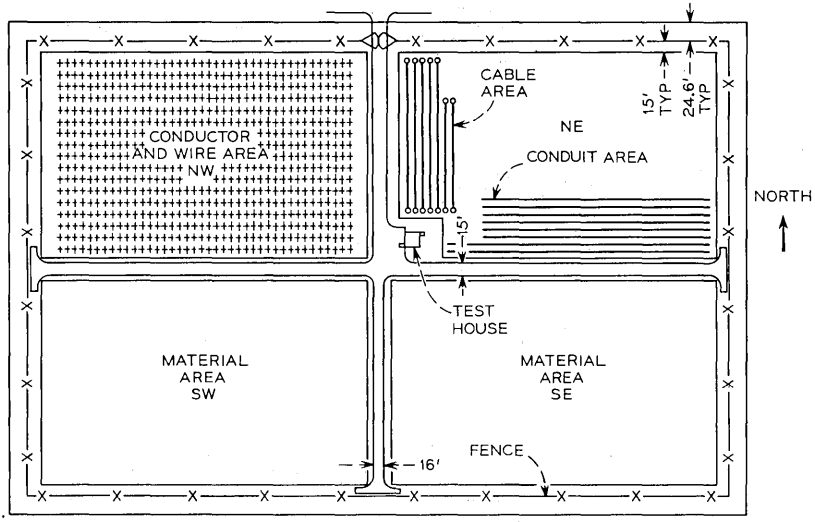

Fig. 10—Roswell environmental test plot.

4.3 *Samples*

All the materials groups participating in this program prepared samples according to their standard methods of testing. However, for the most part, the rubber and thermoplastic samples are in the form of 1/8 inch thick dumbbell-shaped specimens, injection molded or stamped from sheet stock. The thermosetting materials such as casting resins, structural laminates, and electrical laminates were exposed as 1/8 inch thick rectangular sheets. A wide range of polyolefins, poly (vinyl chloride), and rubber insulated or jacketed wires have been under test. All the plastic coated wires were extruded on both copper and aluminum conductors while the rubber was applied to copper-steel lead and brass plated conductors as well as on aluminum. The wires were generally 22 AWG wires with 30 mils of insulation.

Table III gives the general breakdown of the types and numbers of material and wire samples tested in this program. To date some 25,000 individual samples have been tested representing 287 different materials and combinations.

The number of replicates installed ranged from material to material, but basically, enough specimens were put in originally so that at each inspection a minimum of two (but an average of about five) samples could be removed for testing after each exposure period.

4.4 *Exposure Methods*

For exposure purposes, the material samples are attached to 3-foot-long polyethylene tubes with polyethylene rivets. The tubes are sub-

TABLE III—MATERIALS UNDER SOIL BURIAL TESTING

Materials Under Test	Number of Types	Number of Samples
Molded plastics	75	5,720
Casting resins	3	216
Electrical grade reinforced plastics	23	7,922
Structural reinforced plastics	20	2,600
Bonded structural laminates and stainless steel samples	4	431
	25	2,040
Rubber	17	1,080
Rubber-to-metal bonds	15	300
Rubber covered conductors	25	880
Plastic covered conductors	78	3,120
Tapes	6	936
	287	24,814

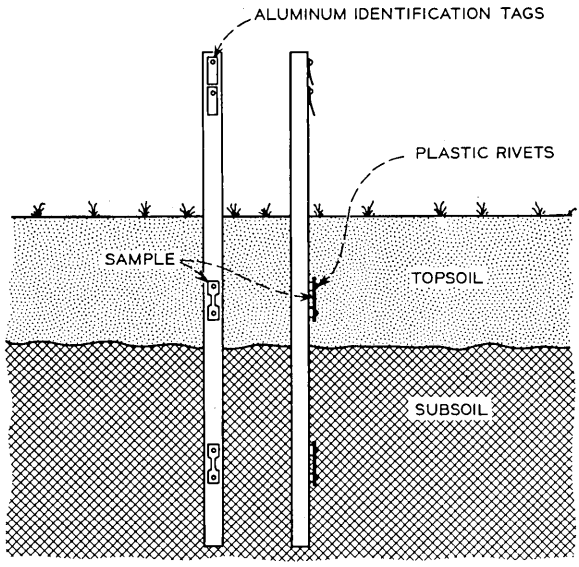

Fig. 11—Front and side view of rubber and molded plastics tensile samples mounted on polyethylene pipe.

sequently buried vertically in the ground in such a manner that the center of the top sample is in the topsoil, 6 inches below the surface, and the bottom sample is in the subsoil, 18 inches below the surface. The material used for the supporting structures was low-density polyethylene plus 2.5 percent fine channel black and 0.1 percent thiocresol antioxidant. Figures 11 and 12 illustrate how these samples were mounted. When in place, 12 inches of the tube protrude above

Fig. 12—Material section of Bainbridge environmental test plot.

the ground; aluminum identification tags are attached to this portion of the tube, as shown in Fig. 11.

The insulated wire samples were exposed in the form of helixes, 12 inches in diameter, and were connected to a terminal in such a way that half of the replicates of a given material were initially under constant 48-volt potential and half were not. About 4 feet of each end of the coil was in the topsoil, and the remainder of the sample was in the subsoil down to a depth of 2 feet. The design of the exposure of these samples is shown in Fig. 13.

The exposure schedule initially selected was the geometric progression 1, 2, 4, 8, 16, and 32 years. The eight-year inspections have been made, and no further samples are scheduled to be removed until 1974 at Bainbridge and 1976 at Roswell with the exception of samples installed after the initial installations and, therefore, on a different removal schedule.

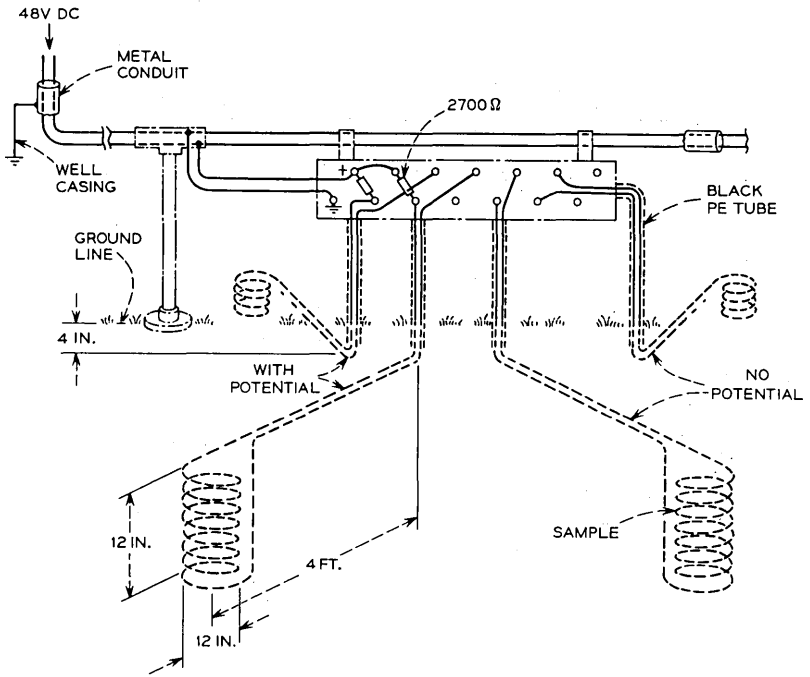

Fig. 13—Method of exposure for insulated wire samples.

TABLE IV—LIST OF TESTS CONDUCTED ON EXPOSED SAMPLES

Material	Visual	Adhesion	Tensile Strength	Tensile Modulus	Tensile Yield	Tensile Shear	Ultimate Elongation	Modulus of Rupture	Modulus of Elasticity	Flexural Strength	Flexural Modulus	Rockwell Hardness	Barcol Hardness	Insulation Resistance	Dielectric Strength	Capacitance
Molded plastics	X		X	X	X		X			X	X	X		X		
Casting resins	X		X				X	X	X	X		X	X	X		
Electrical laminates	X								X	X				X		
Glass fiber reinforced plastics	X								X	X						
Adhesives	X					X										
Rubber	X		X			X										
Rubber-to-metal bonds	X															
Rubber coated conductors	X													X	X	X
Plastic coated conductors	X													X	X	X
Tapes	X	X	X				X									

4.5 *Sample Evaluation*

The samples are carefully removed from the ground by shovel or by hand, and a casual visual examination is made on each one at that time. Next, the samples are packed and sent back to Murray Hill where a more detailed visual examination is made after cleaning the samples of adhering soil and debris. Physical and biological degradation is specifically noted, i.e., loss of material, cracks, decay, insect damage, discoloration, etc. The samples are then returned to the group responsible for them who then make the appropriate mechanical and electrical tests to detect any changes that may have occurred due to exposure. The tests conducted on the various classes of materials are given in Table IV.

V. RESULTS

Only two papers have been published on this project to date. One by Connolly[25] described the overall program and some of the preliminary observations on the first set of samples removed from Bainbridge in 1959. The second one by J. B. DeCoste[27] reported in detail on the performance of vinyl chloride plastics used as electrical insulations or cable jackets after four years of exposure. He found that performance was affected more by composition, particularly the choice and concentration of plasticizers, than by burial location or depth, electrical potential, or metallic conductors used. Nonmigratory and/or inherently resistant plasticizers such as tricresyl phosphate, polyesters, nitrile rubber, and dipentaerythrital esters give the best performance, while phthalate plasticizers were more susceptible to attack.

The test results after up to eight years of exposure will be discussed in the following papers by those responsible for each class of materials.

REFERENCES

1. Southworth, H., private communication, December 15, 1968.
2. Blain, R., "Buried Wire and Cable Construction," Telephony, August 23, 1958, pp. 19, 19–24, 60–61.
3. Bear, F. E., *Chemistry of the Soil*, Second Ed., New York: Reinhold, Publishing Corp., 1964, p. 74.
4. ZoBell, C. E., and Beckwith, J. D., "The Deterioration of Rubber Products by Microorganisms," American Water Works Association Journal, *36*, No. 4 (April 1944).
5. Steinberg, P. L., "Resistance of Organic Materials to Attack by Marine Bacteria at Low Temperatures," B.S.T.J., *40*, No. 5 (September 1961), pp. 1369–1395.
6. Walter, W. G., Beadle, B., Rodriquez, R., and Chaffey, D., "The Effect of Plastics on Bacteria," Society of Plastics Engineering Journal, August 1958, pp. 36–37, 54.
7. Jen-hao, L., and Greifswald, A. S., "The Behavior of Bacterial Mixtures with

Respect to Polyethylenes of Various Average Molecular Weights," Kunststoffe, *51*, June 1961, pp. 317–319.
8. Brown, A. E., "The Problem of Fungal Growth," Modern Plastics, April 1946, pp. 189–195.
9. DeCoste, J. B., "Advances in Vinyl Plastics Test Methods," SPE Journal, October 1960, pp. 1129–1133.
10. Blake, J. T., Kitchin, D. W., and Pratt, O. S., "The Microbial Deterioration of Rubber Insulation," AIEE Transactions, 1953, 10 pages.
11. U.S. Department of Agriculture, *Formosan-Subterranean Termite*, U.S.D.A. Coop. Econ. Ins. Report 16(24): 562–564, 1966.
12. Weldon, D., *A Review of Ecology and Control Studies of Formosan Termites*, American Wood Preservers Association, January 1, 1970, pp. 1–3.
13. Shiga, T., and Inagaki, Y., "Termite Damage to Cable and Its Prevention," Sumitome Electric Technical Review, March 1969.
14. Flatau, G., "Protection of Telephone Cables from Attack by Insects," presented at the Fifteenth Annual Wire and Cable Symposium, December 7–9, 1966, 18 pages.
15. Blain, R., "Australians Protect Cable with Thin Nylon Jacket," Telephone, February 22, 1969, p. 38.
16. Gay, F. J., and Wetherly, A. H., *Laboratory Studies of Termite Resistance, IV*, "The Termite Resistance of Plastics," Division of Entomology Technical Paper No. 5, Commonwealth Scientific and Industrial Research Organization, Melbourne, Australia, 1962, 31 pages.
17. Blain, R., "Gopher Protection of Buried Cable Plant," Telephony, April 24, 1965, pp. 12, 46, 48, 98.
18. Connolly, R. A., and Landstrom R. E., "Gopher Damage to Buried Cable Materials," Materials Research and Standards, *9*, No. 12, 1969.
19. Kirk, J. D., Brooks, R. C., and Saul, D. G., "Progress and Pitfalls of Rural Buried Plant," Telephone Engineering and Management, April 15, 1970. pp. 64–67.
20. Howard, W. E., "Test of Pocket Gophers Gnawing Electric Cables," Journal of Wildlife Management, *17*, 1953, pp. 296–300.
21. Chang, J. H., *Ground Temperature*, Vol. 1, Harvard University, Quartermaster Research and Development Command under Contract No. DA 19-129-QM-348, 1958.
22. National Electric Light Association, *Earth Temperatures and Their Use in Rating Cables*, Publication No. 021, December 1929.
23. Douglass, D. A., private communication.
24. Sunde, E. D., *Earth Conduction Effects in Transmission Systems*, New York: Dover Publications, 1967, p. 295.
25. Connolly, R. A., "Soil Testing Materials and Apparatus," Bell Laboratories Record, April 1962, pp. 124–129.
26. Tomashov, N. D., *Theory of Corrosion and Protection of Metals*, 1966, p. 428.
27. DeCoste, J. B., "Soil Burial Resistance of Vinyl Chloride Plastics," I & EC Product Research and Development, *7*, December 1968, pp. 238–247.

Copyright © 1972 American Telephone and Telegraph Company
THE BELL SYSTEM TECHNICAL JOURNAL
Vol. 51, No. 1, January, 1972
Printed in U.S.A.

Soil Burial Tests:

Effect of Soil Burial Exposure on the Properties of Molded Plastics

By R. J. MINER

(Manuscript received May 10, 1971)

An evaluation of the effect of soil burial on a wide variety of thermoplastic and thermoset plastic molding compounds has been completed for specimens interred eight years at the soil burial test plots in Georgia and New Mexico. In general, the effect of soil environment has been mild on most of the molded plastics. The most significant changes occur to those materials most sensitive to moisture. These changes take place independently of either burial site or depth of soil burial (6 and 18 inches).

I. INTRODUCTION

The molded plastics selected for soil burial tests represented a limited cross section of those commercially available at the time the program was started. Many of the materials evaluated are now being used in diverse telephone apparatus, including telephone sets, terminals, relays, covers, switches, connectors, underwater repeaters, and many other applications. It can be anticipated, as buried plant becomes more common, that many of these materials will be considered for underground applications.

Any plastic used in a buried telephone plant system would represent a long-time investment and a minimum life expectancy of twenty years is not an unusual requirement. Therefore, before any applications are developed for employing plastics underground, it is necessary to assess the general effect of soil burial on the different plastics that are commercially available. Most molded plastics are synthetic organic compounds and subject to normal aging processes such as oxidation or hydrolysis. Continuous exposure to any of the overall complex soil environments, whether they are physical, chemical, or biological, may increase the rate at which these plastics age. Earlier studies have led

to a greater understanding of why some materials fail in certain environments while others do not.

II. CHEMISTRY OF MOLDED PLASTIC COMPOUNDS

The chemistry of the molded plastics covered in this paper has been described adequately in most standard polymer textbooks. Three such books are listed in the references.[1-3]

2.1 *Base Polymers*

2.1.1 *Thermoplastic Compounds*

We have chosen twenty-six thermoplastics representing ten basic materials for soil burial exposure. Table I lists those materials selected

TABLE I—THERMOPLASTIC MOLDING COMPOUNDS FOR SOIL BURIAL

Butyrate, Black Butyrate, Clear Propionate, Black	*Cellulose Compounds*
Polystyrene, GP, Clear Styrene Acrylonitrile Copolymer, Natural Acrylonitrile-Butadiene-Styrene, Natural Acrylonitrile-Butadiene-Styrene, Black	*Styrene Compounds*
Nylon, Type 610, Natural Nylon, Type 6, Natural	*Polyamides*
Poly (methyl methacrylate), Clear	*Acrylic*
Polyethylene H. D., Black Polypropylene, Ivory Ethylene-ethyl-acrylate, Natural Ethylene-vinyl-acetate, Natural	*Polyolefin Compounds*
PVC, Semirigid, Gray PVC, Rigid, Dark Gray PVC, Rigid, Sheet, Gray	*Poly(vinyl chloride) Compounds*
Acetal, Homopolymer, Natural Acetal, Homopolymer, Black Acetal, Copolymer, Natural	*Acetals*
Polychlorotrifluorethylene, Natural Polytetrafluorethylene, Natural	*Fluorocarbon Polymers*
Polycarbonate, Natural Polysulfone, Natural	*Bisphenol A Polymers*
Polyurethane, Natural	*Polyurethane Molding Compound*
Polyphenylene Oxide, Beige	*Poly-(2, 6-dimehyl-1, 4-phenylene oxide)*

TABLE II—THERMOSET MOLDING COMPOUNDS FOR SOIL BURIAL

Phenolplastic Two Stage Wood-Flour, Black Phenolplastic One Stage Wood-Flour, Black Phenolplastic Two Stage Asbestos, Black Phenolplastic Two Stage Mineral, Black	*Phenolic Compounds*
DAP, Orlon, Green DAP, Mineral, Gray	*Diallyl Phthalate Compounds*
Melamine, Glass, Natural	*Melamine*
Styrene-Polyester, Glass Bulk Molding Compound	*Styrene-Polyester*
Alkyd, Glass, Sheet	*Alkyd*
Styrene-Butadiene, Crosslinked Silica Filled, Gray	*Crosslinked Styrene-Butadiene*

and identifies the thermoplastics that make up each group. Of course, as new and promising materials are developed, they are added to the program. The materials selected to date vary greatly in their mechanical and electrical properties and in their ability to resist moisture.

2.1.2 *Thermoset Compounds*

We have included ten compounds representative of six basic thermosetting materials for soil burial testing. These compounds are listed in Table II. Although thermoset compounds, like the thermoplastic compounds, have similar electrical and mechanical properties, one important difference is that thermoset compounds must contain reinforcing fillers in order to achieve their optimum characteristics.

2.2 *Additives, Reinforcing, Fillers, Plasticizers, etc.*

In addition to fillers, however, most plastic molding compounds contain other ingredients. Many contain an antioxidant to protect the material against oxidation either in processing or in service and thereby improve the resistance to aging. Lubricants are sometimes used to improve processing conditions or to facilitate molding. In some cases, plasticizers are added to impart flexibility or to soften the polymer for processing. There are also special additives used for specific purposes such as colorants, flame retarders, and ultraviolet absorbers. These substances may be present in quite high proportions which may substantially alter the physical properties of the basic

plastic material. In addition to these additives, thermoset molding compounds use various types of filler to enhance their properties and characteristics. Roughly half of the compound is made up of filler. This allows a wide latitude of electrical and mechanical properties, depending on the type of filler used.

2.3 *Commercial Compounds*

In most cases, the commercial molded plastics selected for soil burial tests contain some or all of the additives mentioned above. These are proprietary compounds and the additives are not often disclosed. The types of fillers used in the thermoset compounds are generally known, but the amounts and types of chemical additives are not. However, the purpose of the soil burial program on molded plastics was not to evaluate the performance of a specific filler or additive, but to determine the relative resistance of a group of commercial plastic materials to a soil environment.

III. TEST METHODS

The effect of soil burial on the various molded plastics was primarily followed by quantitatively observing the changes in their mechanical and electrical properties. Qualitative visual examinations were also noted for any changes in the general appearance that could indicate a deterioration of the plastic.

3.1 *Types of Mechanical and Electrical Tests*

The effect of soil burial on molded plastics was followed by changes in the mechanical and the dc insulation resistance properties. Samples were removed from the soil test plot after 1, 2, 4, and 8 years of exposure. All exhumed specimens were conditioned for six months at 23°C and 50 percent relative humidity. Each group of molded plastics was examined for changes in tensile, hardness, and electrical properties after each soil exposure period. In addition to these tests, flexural properties were also recorded for the thermoset compounds. The tensile properties include tensile strength, yield, modulus, and ultimate elongation and were determined in accordance with the general procedures of ASTM D638. Flexural strength and modulus were determined for the more rigid thermoset compounds using ASTM D790. Hardness tests were performed according to ASTM D785. Several indentation scales were needed to cover the entire range of molded plastic materials. The dc electrical insulation resistance measurements

were made on all materials using the flat end of the 8-1/2 inch test bar with the prescribed terminal distance. This is not the shape of specimen called for in ASTM D257, but it has yielded comparative data in the soil burial program.

3.2 *Basis for Selection*

The mechanical properties of the molded plastics selected for soil burial vary over a wide range from soft and flexible to hard and brittle, with many intermediate combinations. It was, therefore, difficult in some cases to select standard tests for the measurement of a particular property which would be suitable for all materials. However, because we have had some understanding of the nature of most of these plastics, and their behavior under conditions of stress, we chose a group of tests to accomplish the following:

(*i*) Assess the initial differences among the plastics and establish a control value.
(*ii*) Measure the effect of soil burial on all materials.
(*iii*) Provide guidelines useful to design engineers.

All of these tests are useful for following the parameters of a large group of materials whose properties vary widely.

3.3 *Preconditioning*

One very important consideration is the moisture content of the specimen at the time of testing. Ideally, it would be desirable to perform the tests directly in the field at the time the samples are unearthed. This would indicate their actual mechanical characteristics under soil conditions. However, this procedure is impractical. Another possibility is to test the exposed samples immediately upon their return to the laboratories. However, their moisture content would depend on the length of time in transit from the burial site. Very often a number of weeks elapse before the specimens are finally made available for testing. Consequently, it was decided to condition the exposed samples for six months at 23°C and 50 percent relative humidity to bring the specimens back to a moisture content reasonably comparable to that of the initial samples. Essentially, the data then measured would be the permanent changes that have occurred in the molded plastics as a result of soil burial. There are a sufficient number of control specimens of each material in storage to determine whether any changes in mechanical properties are actually the results of soil burial or of natural aging. Most of the materials are relatively stable at room conditions

TABLE III—TENSILE BREAK STRENGTH OF THERMOPLASTICS (PERCENT CHANGE AFTER SOIL BURIAL)

Material	Location	Topsoil				Subsoil			
		1 Yr	2 Yrs	4 Yrs	8 Yrs	1 Yr	2 Yrs	4 Yrs	8 Yrs
Cellulose Acetate Butyrate, Black	Georgia	+23	+22	+41	+50	+14	+11	+30	+50
	New Mexico		+26	+49			+21	+47	
Cellulose Propionate, Black	Georgia	+30	+9	+32	+38	+22	+10	+35	+40
	New Mexico		+13	+36			+14	+37	
Cellulose Acetate Butyrate, Clear	Georgia	+16	+11	+36	+46	+2	+5	+27	+41
	New Mexico		+21	+42			+19	+37	
Polystyrene, General Purpose, Clear	Georia	NC	−7	NC	NC	NC	−9	NC	+3
	New Mexico		−1	−2			−1	−1	
Styrene-Acrylonitrile Copolymer, Natural	Georgia	NC	−3	NC	NC	−3	−4	NC	NC
	New Mexico		+1	−1			−1	−3	
Acrylonitrile-Butadiene-Styrene, Natural	Georgia	−6	−12	−1	−1	−12	−15	−3	NC
	New Mexico		−1	−9			−6	−5	
Acrylonitrile-Butadiene-Styrene, Black	Georgia	−2	−2	+2	+1	−2	−3	+2	+5
	New Mexico		NC	NC			NC	−1	
Acetal, Homopolymer, Natural	Georgia	NC	−1	−3	NC	NC	+3	+3	NC
	New Mexico		NC	−3			NC	−3	
Acetal, Copolymer, Natural	Georgia	−2	−1	NC		−2	+2	−1	
	New Mexico	−1	−2			−5	+2		
Acetal, Homopolymer, Black	Georgia	+1	NC	−4	+2	+2	−1	−3	+1
	New Mexico		−1	−3			NC	−2	

NC = No change

TABLE IV—TENSILE BREAK STRENGTH OF THERMOSET PLASTICS (PERCENT CHANGE AFTER SOIL BURIAL)

Material	Location	Topsoil				Subsoil			
		1 Yr	2 Yrs	4 Yrs	8 yrs	1 Yr	2 Yrs	4 Yrs	8 Yrs
Phenolic 2/s Wood-Flour, Black	Georgia	−20	+29	+36	+21	−10	+20	+32	+20
	New Mexico		+34	+33			+22	+43	
Phenolic 1/s Wood-Flour, Black	Georgia	−31	−15	+9	+2	−14	−10	−3	+9
	New Mexico		+7	−3			−1	−8	
Phenolic 2/s Asbestos, Black	Georgia	−15	+8	+28	−2	−31	−5	+26	+15
	New Mexico		+14	+13			+11	+12	
Phenolic 2/s Mineral, Black	Georgia	−8	+7	+1	+2	NC	+9	+3	+11
	New Mexico		+13	+4			+22	+4	
DAP, Orlon, Green	Georgia	−26	−9	−5	−11	−27	−17	+9	−6
	New Mexico		+8	+8			−2	+1	
DAP, Mineral, Gray	Georgia	−2	−1	+7	+1	−9	+9	+11	+1
	New Mexico		+8	+1			−2	+1	
Styrene-Butadiene, Crosslinked, Silica	Georgia	+35	+23	+27		+37	+30	+26	
	New Mexico	+33	+28	+33		+36	+30	+37	

NC = No change

and therefore no deterioration in mechanical properties is anticipated for the reference specimens over a period of many years.

IV. RESULTS

4.1 *Effect of Soil Test Plot Site and Depth of Burial*

Tables III and IV clearly show that neither the variations in the soil conditions nor the depth at which the specimens are buried is critical. Individual materials exhibit similar behavior at each location and at each burial level. Since this has been the case for all of the examination periods, it was evident that the only way to handle the massive amount of data was to make a composite of all the information for a given exposure period and take the average for the individual types of plastic compounds. Consequently, we have taken the results of each test from each location and burial level and have combined them for each basic group of common materials listed in Tables I and II. The results of all of the tests correlate quite well and the average change is entered as either a percent increase or a percent decrease for the mechanical properties and as orders of magnitude of change for the insulation resistance measurements. Thus we have reduced the total number of tables necessary for data display without adversely affecting the value of the information obtained.

4.2 *Thermoplastic Changes*

Significant changes in the tensile strength at break for thermoplastic compounds are limited to those that are sensitive to moisture. These include the cellulosic molding resins and the type 6 polyamide (nylon) compound. Figure 1 shows the results of cellulose compounds buried 1, 2, 4, and 8 years and includes both the cellulose acetate butyrate and cellulose propionate compounds. Both materials have changed substantially from their original values, indicating their instability in a soil system.

Type 6 nylon deteriorates steadily in tensile properties. This material has changed from a hard, tough thermoplastic to such a rigid, brittle material that rupture occurs before any appreciable elongation (Fig. 2) can take place. Type 610 nylon showed much superior resistance properties than type 6 nylon. Type 610 nylon absorbs 75 percent less moisture than nylon 6.

After eight years of soil burial the semirigid poly (vinyl chloride) compound has generally increased in hardness and tensile strength and diminished in extensibility. In every testing period there were

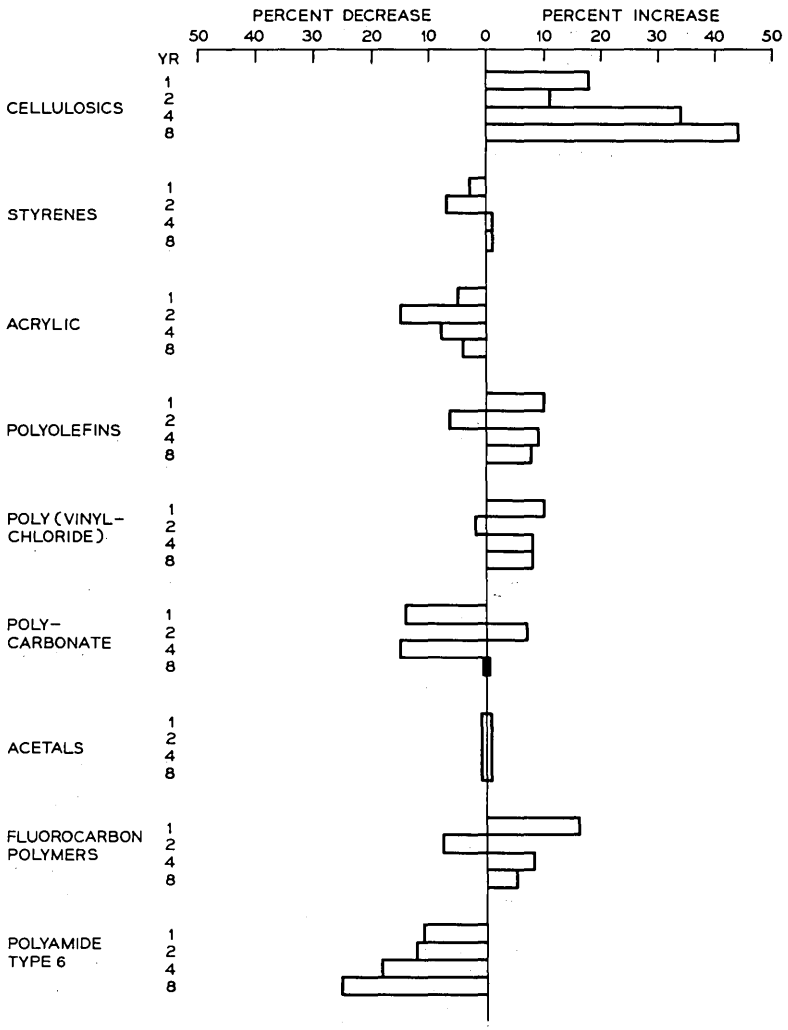

Fig. 1.—Changes in tensile break strength for thermoplastics.

some signs of microbiological action on the surface of the plasticized PVC test specimens. This consisted of mainly black greasy surface deposits which were not totally removed by the cleaning method employed.

4.3 *Unchanged Thermoplastics*

The effects of soil burial on the tensile and hardness properties of the other thermoplastics shown in Figs. 1, 2, and 3 are quite mild.

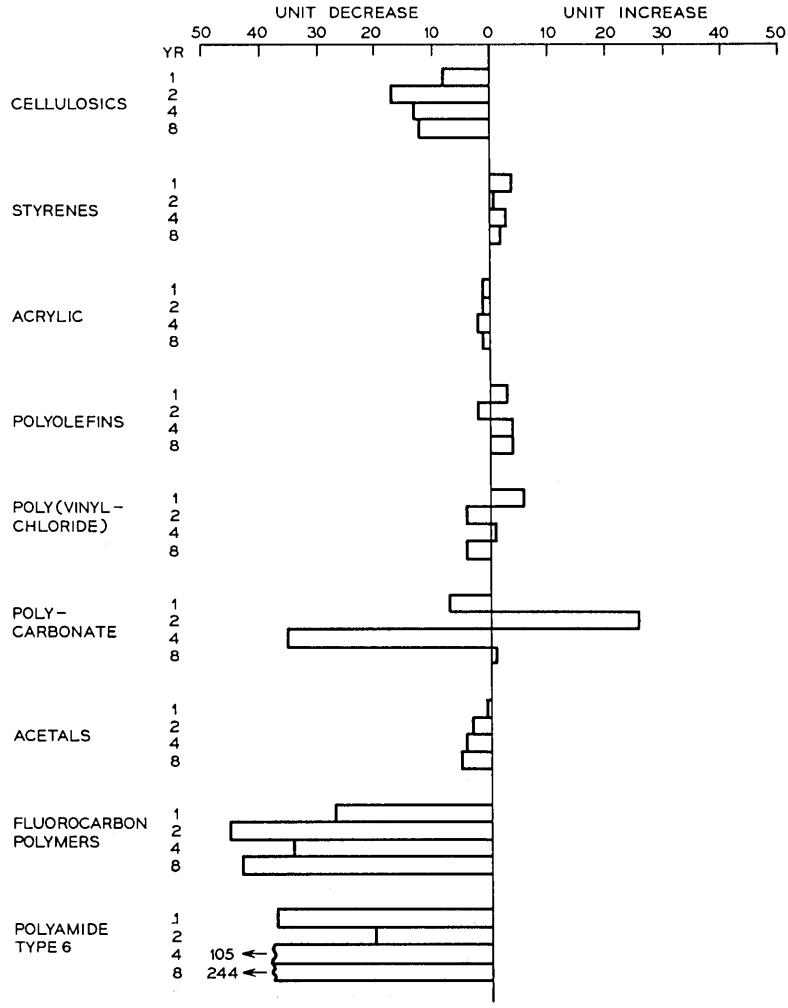

Fig. 2—Changes in ultimate elongation of thermoplastics.

In most cases there are small changes in property values from year to year, but these are generally considered to be within experimental error. For this reason, judgment is required in evaluating differences in test data to make certain a valid difference exists. Some errors are associated with the test method itself, while others may arise through defects in test specimens. Anomalous behavior is especially evident

for the ultimate elongation results of polycarbonate and fluorocarbon polymers shown in Fig. 2. While changes in elongation for polycarbonate vary from negative to positive, the fluorocarbon polymers show a continuous loss. Since these results do not correlate with those of other mechanical tests, we can only conclude that a real change has not occurred.

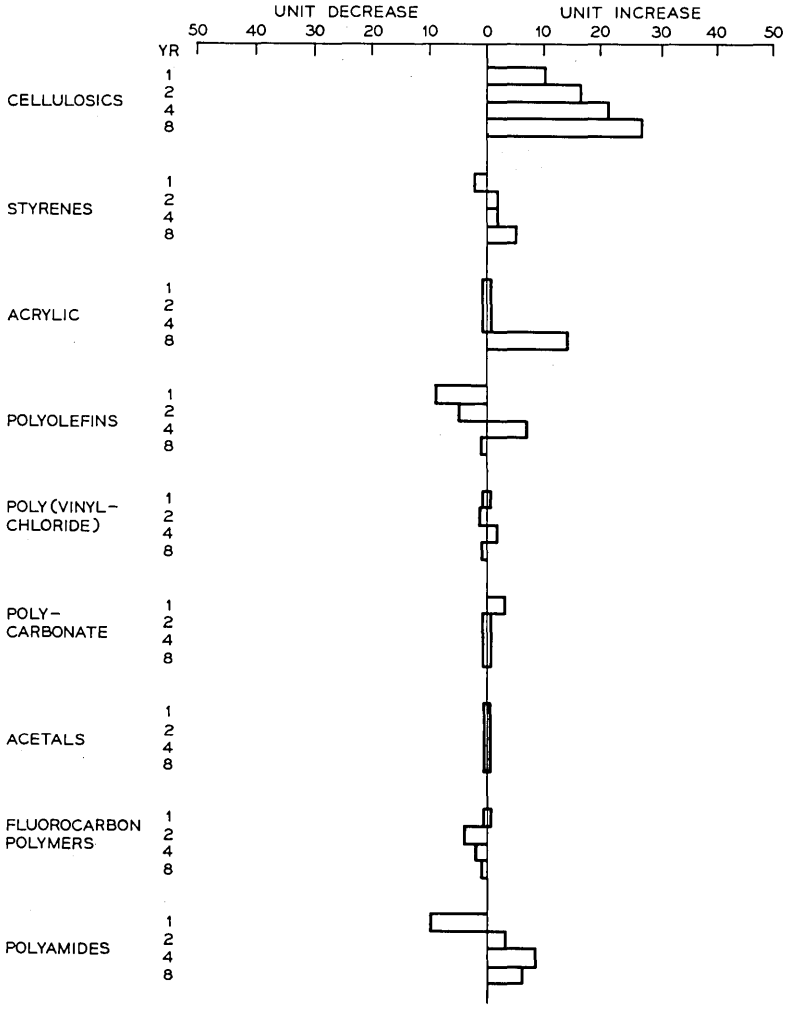

Fig. 3—Changes in hardness for thermoplastics.

The remaining thermoplastic compounds that do not show any significant change at this time are the styrene group, the polyolefins, the two rigid poly (vinyl chloride) compounds, and the acetal homopolymer. The individual materials that compose each group are given in Table I.

4.4 *Late Starting Thermoplastics*

Several variations of commercial molding plastics, as well as compounds based on new polymers, have been developed since the burial program was first initiated. In 1965 we selected six new compounds: a natural color acetal copolymer, a beige polyphenylene oxide compound, a natural color thermoplastic polyurethane molding compound, a natural polysulfone resin, and two natural color polyethylene copolymers–ethylene-ethyl acrylate and ethylene-vinyl-acetate.

These materials have been in the program for four years and have been tested for the effects of soil burial for 1, 2, and 4 years. None of the mechanical or electrical properties of these materials has changed significantly. For example, Table III clearly shows that the tensile strength at break for the natural acetal copolymer has not changed during 1, 2, and 4 years of soil burial.

4.5 *Thermoset Changes*

The effects of soil burial on the mechanical properties of thermoset molding compounds are shown in Figs. 4 thru 7. Tensile strength and modulus data shown in Fig. 4 indicate there have been some significant changes in these properties during the first four exposure periods. This is also true for the flexural properties shown in Figs. 5 and 6, but not for the hardness values given in Fig. 7.

The individual compounds that constitute the thermoset groups are given in Table II. Of all the thermoset compounds, soil burial had the least effect on the mechanical properties of the diallyl phthalate compounds. One of these materials has a mineral filler while the other depends on a synthetic fiber filler for impact strength. The phenolic compounds show a slight to moderate effect. A significant difference was noted in the phenolic compounds containing wood-flour and those using asbestos or mineral filler. For instance, wood-flour-filled phenolics show a greater loss in tensile strength at break than those having mineral or asbestos as a filler. However, in flexural properties, just the opposite appears to be the case where the mineral and asbestos compounds have shown the greatest change. The slight decrease in hardness shown in Fig. 7 is further evidence that a soil environment

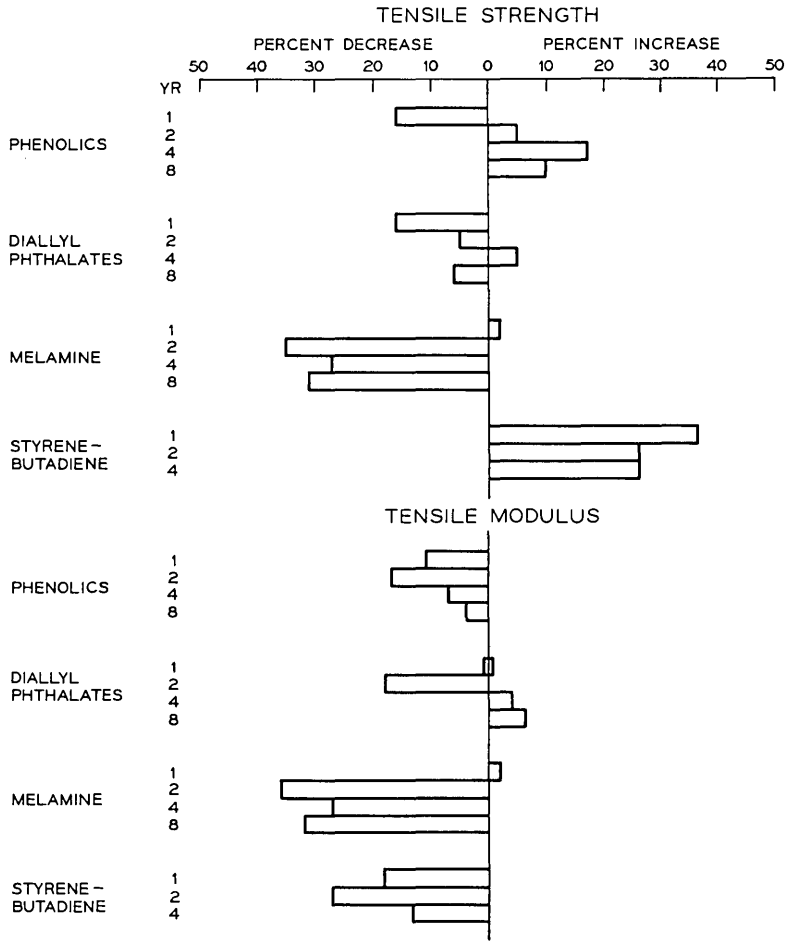

Fig. 4—Changes in tensile properties of thermoset plastics.

has a definite weakening affect on the mechanical properties of phenolic compounds.

The effects of soil burial on all three glass-reinforced thermoset compounds, melamine, styrene-polyester, and alkyd, are generally the same, causing an almost complete deterioration of the mechanical properties. Figures 4, 5, 6, and 7 show there is a significant loss in tensile, flexural, and hardness values for all of these glass-filled compounds.

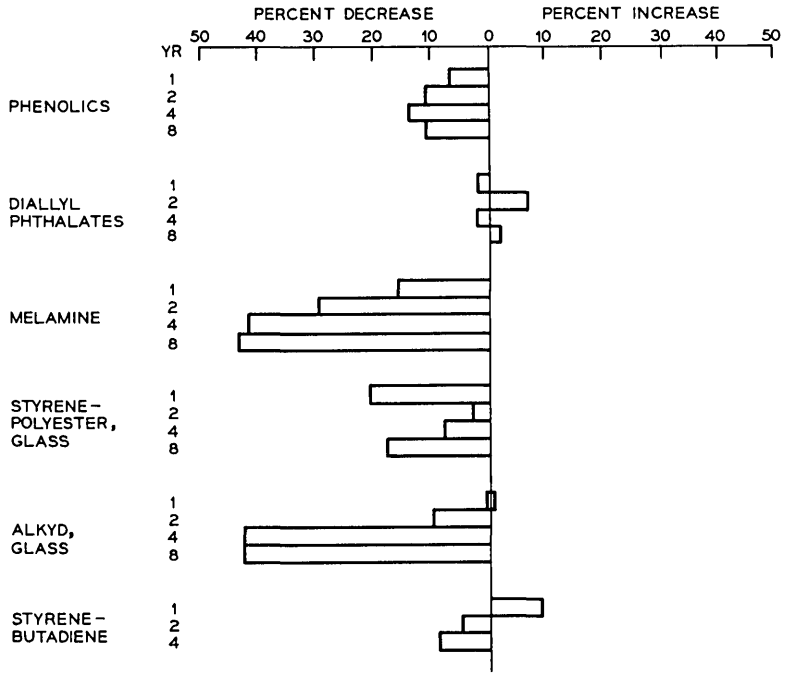

Fig. 5—Changes in flexural strength of thermoset plastics.

4.6 *Insulation Resistance*

The dc insulation resistance of molded plastics after eight years of soil burial in Georgia and New Mexico is given in Table V. These results are not the actual values, but are the orders of magnitude change over the four exposure periods.

The same materials that show the greatest change in mechanical properties, i.e., polyamides, phenolics, melamine, styrene-polyester, alkyd, styrene-butadiene, and cellulosic compounds, also exhibit the largest loss in insulation resistance. Most of these changes are not unexpected. These materials started with relatively low levels of resistance and any surface deterioration would increase their sensitivity to moisture, thereby decreasing the insulation resistance. The styrene and diallyl phthalate molding compounds are reduced 1/2 to 1 order of magnitude. However, their initial values are so high that these changes are not that significant. The remaining plastic materials, all of which started with high insulation resistance, show little or no change after eight years of soil burial.

DISCUSSION OF RESULTS

Many of these changes were physical instead of chemical or biological. The change in mechanical and electrical properties as a result of soil burial was caused mainly by moisture. Many of the plastics tested, such as polyethylene, polystyrene, polypolyamides, poly (vinyl chlorides), and the thermosets, are generally resistant to chemicals that may be found in the soil. This is most likely why soil chemicals played only a minor role in these changes since the results from both Georgia, an acid soil, and New Mexico, an alkaline soil, were similar. The chemical effects will be discussed first.

5.1 *Chemical Changes*

Chemical changes for molded plastics were limited to those materials subject to hydrolysis. The loss of extension in the mechanical properties of nylon 6 is attributed to the moisture content of the soil and the subsequent degradation caused by hydrolysis. The general structure

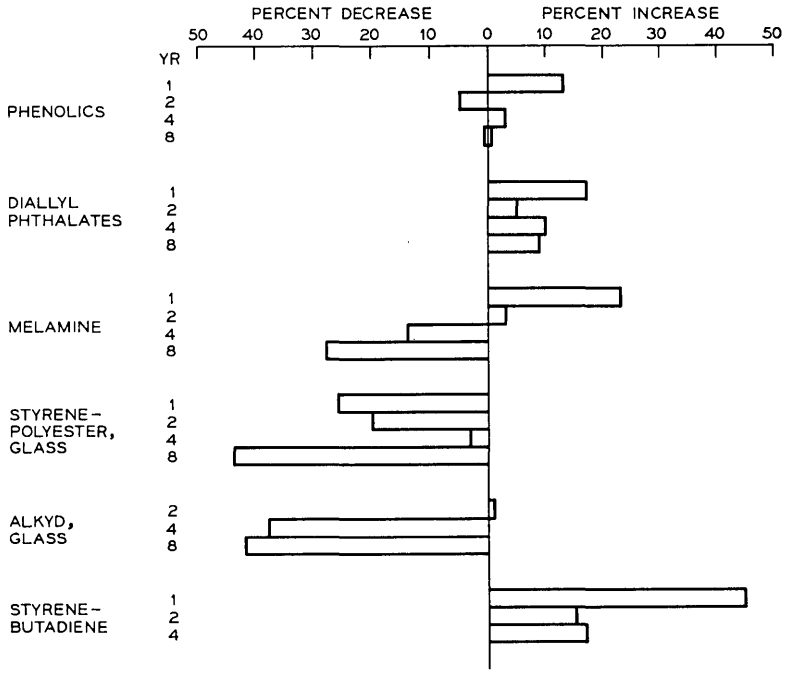

Fig. 6—Changes in flexural modulus of thermoset plastics.

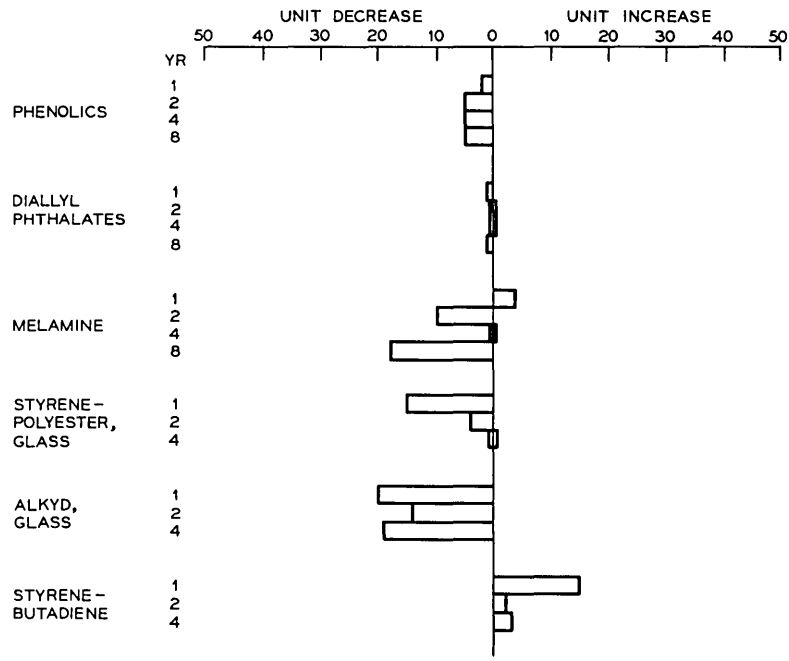

Fig. 7—Changes in hardness for thermoset plastics.

of nylons results from the condensation reaction of an organic acid with an amine.[2] The longer the hydrocarbon part of the chain, for instance, the less the attraction between the chains and therefore the lower the softening point, tensile strength, and stiffness because the hydrogen bonding is, in effect, diluted along the chain. However, the longer hydrocarbon groups are advantageous since they lead to a reduction in water absorption. Type 610 nylon absorbs 75 percent less moisture than nylon 6 and suffers no appreciable loss in mechanical properties due to soil burial.

5.2 *Physical Changes*

Physical changes to molded plastics buried in soil are attributed to loss of plasticizer, moisture absorption, and, in two cases, biological attack.

5.2.1 *Leaching*

Leaching occurs when water removes soluble constituents as they migrate to the surface of the plastic. In most cases this is probably a plasticizer or chemical additive used for some specific purpose. It

is believed that loss of plasticizer in cellulosic compounds is more responsible for the change in tensile properties than the degradation through hydrolysis. The more plasticized cellulose acetate butyrate compounds show more change in these properties than cellulose propionate. No evidence for cellulosic polymer degradation was found by infrared analysis.

The semirigid poly (vinyl chloride) compound contains 43 phr (parts per hundred of resin) of DNODP (di-n-octyl-n-decyl phthalate) plasticizer. In addition to the loss of mechanical properties, semirigid PVC had black greasy surface deposits which were not totally removed by the cleaning method employed. Both of these results suggest that plasticizer is exuding. However, since this compound also contains 10 phr of di-basic lead phosphite (a lead stabilizer) and fatty acid lubricants, these components may be migrating to the surface. The black discoloration could be lead sulfate. As pointed out before, changes in the plasticizer content can have a marked effect on mechanical properties, but there is no evidence that the PVC resin itself has been degraded. Another mechanism for plasticized composition deterioration would be the absorption of the plasticizer by the surrounding dry soil. Since there were no major differences at either the Georgia or New Mexico locations, this mechanism may be more important than leaching.

5.2.2 *Moisture Absorption*

In general, cellulose compounds, polyamides, and those compounds with hydrophilic OH, COOH, or NH groups are sensitive to moisture,

TABLE V—DC INSULATION RESISTANCE

Materials/Exposure Periods	Orders of Magnitude of Change			
	1 Yr	2 Yrs	4 Yrs	8 Yrs
Cellulosics	0	0	2 1/2	1/2
Styrenes	1/2	1 1/2	1/2	1/2
Acrylic	0	0	1	0
Polyolefins	0	0	0	0
Poly (vinyl chloride)	0	0	0	0
Polycarbonate	0	0	0	0
Acetals	0	0	0	0
Fluorocarbon Polymers	0	0	0	0
Polyamides	2	2	2	2
Phenolics	1 1/2	1	1/2	1
Diallyl Phthalates	1	2	1/2	1
Melamine, Glass	3	3	2	3
Styrene-Polyester, Glass	3	3	3	
Alkyd, Glass	2	2	3	
Styrene-Butadiene	3	4	4	

while compounds low in oxygen and nitrogen but rich in carbon, hydrogen, or halogen are moisture resistant.[4] The styrene and acetal group can absorb up to 1 percent moisture at saturation while the polyolefins and fluorocarbon polymers absorb less than 0.1 percent. All of these latter materials are structurally stable compounds in a soil environment.

Wood-flour-filled phenolics would be expected to have greater changes than either mineral- or asbestos-filled formulations since the former can absorb a maximum of 7 to 8 percent of water while the latter equilibrate after absorbing only 1 to 2 percent. Diallyl phthalates show no large change due to the 1 to 2 percent moisture they can absorb.

Although moisture plays an important part in the glass-filled materials' susceptibility to soil burial, the mechanism of water attack is somewhat different from that of the wood-flour-filled phenolics. The melamine, styrene-polyester, and alkyd glass-filled compounds absorb about 1 to 3 percent moisture. However, the effect of soil burial on these compounds has been caused by the erosion of the resin-rich surface of the test specimens leaving the glass fibers close to the outer surface exposed. Whereas the wood-flour fillers actually absorb moisture, water is introduced into the glass-filled material by a "wicking" action at the resin/glass interface. Apparently these materials do not possess an adequate chemical bonding or coupling agent to achieve good adhesion between the glass reinforcement and the resin. The result has been a gradual decrease in the resin/glass bond and a subsequent failure in the material's mechanical properties. It should be pointed out, however, that in recent years significant advances have been made in glass finishes, providing much better adhesion between glass and resin than that available in the compounds studied.

5.2.3 *Biological Attack*

Only two compounds were susceptible to attack by gnawing insects. Both of these were copolymers of polyethylene, ethylene-ethyl acrylate and ethylene-vinyl acetate, and were natural in color. Most of the damage occurred at the edges of the specimen; however, there were some isolated spots throughout the surface of some of the specimens that were eaten away.

5.2.4 *Appearance Changes*

While the functional and structural integrity of a molded plastic buried in a soil environment is of more concern than the aesthetic

value, a change in appearance can sometimes indicate the cause of failure. All of the following changes were noted after the first exposure period, indicating that there is very little induction time and that these changes start to occur almost immediately after soil burial.

The cellulose acetate butyrate and the semirigid poly (vinyl chloride) showed evidence of plasticizer migration on the surface. The cellulosic compounds were covered with a white soapy substance, while the vinyl material had black greasy deposits along its surface. The exuded plasticizer of both of these compounds has apparently reacted with the surrounding soil chemicals or carried some of the other compound ingredients to the surface.

Those compounds that have been stained by the imprints of plant root systems include the cellulosics, type 6 nylon, semirigid poly (vinyl chloride), and the thermoplastic polyurethane molding compound. The glass-filled melamine, styrene-polyester, and alkyd thermoset compounds showed areas of blotchy orange-yellow stains. In addition, erosion of the resin of these materials has left the surfaces extremely rough as a result of the exposed glass fibers.

As far as the other materials are concerned, once the soil is removed from the test specimens using tap water, there is no indication that they have been exposed to soil. Many of the materials still retain their original high gloss.

VI. ENGINEERING IMPLICATIONS

In conclusion, the changes in mechanical and electrical properties of the materials reported on in this paper represent the permanent cumulative damage that has occurred over the past eight years of soil burial. The most significant changes were to those materials most sensitive to the effect of moisture. These include the cellulosic compounds, type 6 nylon, wood-flour-filled phenolics, silica-filled styrene-butadiene resin, and the glass-filled melamine, alkyd, and styrene-polyester compounds. These molded plastics would not be recommended for applications underground.

Most changes were independent of either burial location (Georgia or New Mexico) or depth of soil burial (6 and 18 inches). In general, the effect of soil burial has been mild on most of the other molded plastics which would be suitable for underground plant.

REFERENCES

1. Billmeyer, Fred W., *Textbook of Polymer Science*, New York: John Wiley and Sons, 1966.

2. Miles, D. C., and Briston, J. H., *Polymer Technology,* New York: Chemical Publishing Company, 1965.
3. *Modern Plastics Encyclopedia,* New York: McGraw-Hill, 1970.
4. Carswell, T. S., and Nason, H. K., *Symposium on Plastics,* Spec. Tech. Publ. No. 59, Amer. Soc. Testing and Materials, Philadelphia, 1944, pp. 22–45.

Copyright © 1972 American Telephone and Telegraph Company
THE BELL SYSTEM TECHNICAL JOURNAL
Vol. 51, No. 1, January, 1972
Printed in U.S.A.

Soil Burial Tests:

Effect of Soil Burial Exposure on the Properties of Casting Resins

By F. X. VENTRICE

(Manuscript received June 30, 1971)

Styrene-polyester and epoxy casting formulations have been used in the Bell System for over ten years and have a minimum service life requirement of twenty years. The styrene-polyester formulation is a filled phthalic maleic/diethylene glycol ester catalyzed with methyl ethyl ketone peroxide and is by far the most stable and least affected by eight years of soil contact or aging. Two epoxy formulations, unfilled and silica-filled, have the same base diglycidyl ether of bisphenol A resin which is cured with a proprietary epoxy adduct of diethylene triamine. After eight years, unfilled specimens from both burial sites were not significantly degraded but the flexural strength of buried silica-filled specimens was reduced by approximately 40 percent within the first year and then remained relatively constant for the following seven years.

I. INTRODUCTION

Casting resins are thermosetting materials (thermosets) which are hardened by crosslinking at ambient or elevated temperatures. Casting compounds consist of a resin and a hardener or curing agent in one or more parts. The cured plastic can have a wide range of properties by selectively compounding inert additives, such as particulate or fibrous fillers, flexibilizers, colorants, and fire retardants. In production, the two-part formulations are metered, mixed, and finally dispensed into molds or potting containers to encapsulate electronic devices. The encapsulated units may be heated to develop the optimum in physical and electrical properties. Casting resins most commonly used are styrene-polyesters, epoxies, polyurethanes, and silicones.[1] Representative casting formulations used widely in the Bell System, styrene-polyester and epoxy, have been used over ten years and have a minimum service life requirement of twenty years.

II. CHEMISTRY OF CASTING RESINS

2.1 *Styrene-Polyester*

Polyesters are prepared by reacting a polyhydroxy alcohol with a mixture of saturated and unsaturated dibasic acids. The styrene monomer dissolves the polyester resin and reacts with the ester's unsaturated groups to form a crosslinked thermoset. Inhibitors are added to the styrene-polyester to prevent premature gelling. Peroxides are added to overcome the inhibitor action and, finally, to initiate the curing mechanism to form the thermoset. Detailed chemistry of styrene-polyesters appears in numerous references.[2,3]

The proprietary styrene-polyester formulation included in the soil burial program is a phthalic maleic/diethylene glycol ester type which contains 21 percent styrene, 38 percent silica, and 3 percent milled glass fiber. It is catalyzed with methyl ethyl ketone peroxide. Specimens were gelled 45 minutes at 52°C and post-cured one hour at 120°C. Formulation details are listed in Table I.

2.2 *Epoxy*

The conventional epoxy included in this program is a diglycidyl ether of bisphenol A containing 13 percent butyl glycidyl ether as a reactive diluent. It is cured with a proprietary epoxy adduct of diethylene triamine. Chemical reactions of epoxides are detailed in the literature.[4]

The two epoxy formulations are composed of the same base resin and hardener; one formulation contains a fine particle size silica and is tinted with titanium dioxide. Each formulation was gelled at room temperature and post-cured two hours at 85°C. Complete formulations are in Table I.

TABLE I—FORMULATIONS

Material Description	Parts by Weight
Styrene-Polyester	
Fiber glass in silica-filled styrene-polyester	100.0
Methyl ethyl ketone peroxide	1.0
Epoxy	
Diglycidyl ether of bisphenol A containing 13% butyl glycidyl ether resin	100.0
Epoxy adduct of diethylene triamine hardener	20.0
Silica, fine particle size	125.0

III. DISCUSSION OF SOIL BURIAL DATA

3.1 *Styrene-Polyester*

All eight-year specimens, buried and control, prepared from this proprietary formulation retained their original Barcol Hardness of 55, flexural strength, and modulus. Of the three castings buried, the styrene-polyester is by far the most stable and least affected by soil contact or aging (Table II).

3.2 *Epoxies*

The hardnesses, flexural strengths, and moduli of unfilled and silica-filled control specimens remained essentially unchanged over eight

TABLE II—EFFECT OF SOIL BURIAL ON FLEXURAL PROPERTIES OF CASTINGS

Years	Flexural Strength (psi)			Flexural Modulus (psi × 10^{-6})		
	Control	Georgia	New Mexico	Control	Georgia	New Mexico
			Styrene-Polyester			
0	10,400	10,400	10,400	0.860	0.860	0.860
1	12,600	8,400	—	0.980	0.865	—
2	—	12,100	10,400	—	0.830	0.950
4	12,100	11,800	10,300	—	—	0.910
6	—	—	10,100	—	—	0.800
8	9,230	9,550	14,400	0.800	0.830	0.860
			Epoxy			
0	18,700	18,700	18,700	0.540	0.540	0.540
1	19,500	18,300	—	0.570	0.470	—
2	—	18,800	19,600	—	0.510	0.550
4	20,600	18,500	18,000	—	0.560	0.530
6	—	—	17,200	—	—	0.500
8	19,400	17,000	18,000	0.560	0.490	0.500
			Silica-Filled Epoxy			
0	14,100	14,100	14,100	1.100	1.100	1.100
1	12,100	8,500	—	1.200	1.000	—
2	—	9,130	8,790	—	1.000	1.300
4	13,500	8,640	8,700	—	1.300	1.100
6	—	—	—	—	—	1.030
8	11,600	8,190	8,440	1.240	0.960	1.030

years. After eight years, unfilled specimens from both burial sites were not significantly degraded. The Barcol Hardnesses of the unfilled and silica-filled specimens were unaffected by soil contact and remained constant at 35 and 55 respectively.

The flexural strength of buried silica-filled specimens was reduced by approximately 40 percent within the first year of burial and then remained relatively constant for the next seven years as indicated in Table II. Possibly their contact with soil moisture quickly weakens the most vulnerable mechanical bonds between the cured epoxy and silica. The most stable bonds remain unaffected as the flexural strength of the buried specimens fell to a minimum within one year (Table II) and then remained constant.

IV. ENGINEERING IMPLICATIONS

Styrene-polyester and epoxy resins of the type described herein are the basis for many electronic encapsulants. The excellent stability of these casting compositions is dependent on the basic chemical structure of the polymers themselves.

REFERENCES

1. Harper, C. A., *Plastics For Electronics*, Chicago: Kiver Publications, Inc., 1964.
2. Lawrence, J. R., *Polyester Resins*, New York: Reinhold Publishing Corp., 1960.
3. Teach, W. C., and Kiessling, G. C., *Polystyrene*, New York: Reinhold Publishing Corp., 1960.
4. Lee, H., and Neville, K., *Handbook of Epoxy Resins*, Appendix 5-1, New York: McGraw-Hill, Inc., 1967.

Copyright © 1972 American Telephone and Telegraph Company
THE BELL SYSTEM TECHNICAL JOURNAL
Vol. 51, No. 1, January, 1972
Printed in U.S.A.

Soil Burial Tests:

Effect of Soil Burial Exposure on the Properties of Electrical Grade Reinforced Plastic Laminates

By T. K. KWEI

(Manuscript received September 24, 1971)

Twenty-three types of unclad laminates based on phenolic, melamine, silicone, epoxy, and polyester resins were examined after exposure in alkaline soil at Roswell, New Mexico, and in acid soil at Bainbridge, Georgia. The laminates have initial insulation resistance values ranging from 1.4 × 10^6 to less than 30 megohms. Each suffers a large decrease in insulation resistance upon exposure. The percentage decrease can be in excess of 90 percent after four years underground exposure in New Mexico or Georgia. Moderate decreases in flexural strengths also were observed.

I. INTRODUCTION

Twenty-three types of unclad laminates based on phenolic, melamine, silicone, epoxy, and polyester resins were examined after exposure in alkaline soil at Roswell, New Mexico, and in acid soil at Bainbridge, Georgia.[1-3] The laminate thickness was 1/16 inch nominal in all cases. Tests were made of insulation resistance, flexural strength, and flexural modulus.

The properties evaluated included:

(*i*) Insulation resistance after conditioning four days at 90 percent relative humidity and 95°F, using a tapered pin method in accordance with ASTM D257. Five replicates for each below-ground exposure condition were tested, each of which provided three readings to give fifteen readings for averaging. Two replicates were measured for each of the shelf-aging specimens, to give six readings for averaging.

(*ii*) Flexural strength and modulus of elasticity in flexure in accordance with ASTM D790. Five replicates for each exposure condition were tested.

(*iii*) The exposed samples were examined visually for deterioration, color change, staining, and overall physical appearance.

II. RESULTS AND DISCUSSION

2.1 *Insulation Resistance*

The laminates included in this study have initial insulation resistance values ranging from 1.4×10^6 megohms to less than 30 megohms. Each suffers a large decrease in insulation resistance upon exposure and the trend of change is similar for all laminates. For this reason, only eight laminates with initial insulation resistance of greater than 1000 megohms are listed in Table I. The laminates possessing high initial IR values still maintain their *numerical* superiority after exposure, although the percentage decrease can be in excess of 90 percent after four years underground exposure in New Mexico or Georgia. The alkaline soil environment is somewhat more detrimental than the acid soil environment. The depth of burial does not appear to be a significant influence on the IR values.

2.2 *Flexural Strength and Flexural Modulus*

Moderate decreases in flexural strengths, about 20 to 30 percent, and in flexural moduli, about 10 to 28 percent, were observed.

2.3 *Biological Attack*

Paper-base phenolic laminates having low resin contents (not listed in Table I) exhibited noticeable biological attack of the core material

TABLE I—AVERAGE PERCENT DECREASE IN INSULATION RESISTANCE

Material	Type	Initial IR, Megohms	4 Years Exposure in Roswell, N.M.		4 Years Exposure in Bainbridge, Ga.	
			6 in	12 in	6 in	12 in
Phenolic-Paper	XXP	11,300	−99	−99	−58	−22
	XXX	8,350	−92	−91	−87	−84
	XXXPC	390,000	−98	−98	−98	−97
	XXXP	212,000	−96	−95	−95	−95
Melamine-Glass	G-5	4,380	−96	−96	−98	−97
Silicone-Glass	G-7	1,510,000	−83	−80	−99	−98
Epoxy-Glass	G-10	616,000	−86	−86	−80	−79
Phenolic-Nylon	N-1	1,720,000	−99	−99	−99	−98

on burial. Many laminates, aged above ground at both locations for the purpose of comparison, showed fungus growth.

REFERENCES

1. Pape, N. R., and Schlabach, T. D., unpublished work.
2. Schlabach, T. D., and Pape, N. R., unpublished work.
3. Pape, N. R., unpublished work.

Copyright © 1972 American Telephone and Telegraph Company
THE BELL SYSTEM TECHNICAL JOURNAL
Vol. 51, No. 1, January, 1972
Printed in U.S.A.

Soil Burial Tests:

Effect of Soil Burial Exposure on the Properties of Structural Grade Reinforced Plastic Laminates

By T. H. KLEIN

(Manuscript received October 1, 1971)

This paper is a summary of the effects of long-term soil burial on the properties of reinforced plastic laminates. The interactions of reinforcement, resin, and fabrication technique, as they relate to the laminates' ability to resist the effects of soil burial, are discussed. The method of soil burial attack is explained. Recommendations for the best laminate construction and methods of protection from the soil environment are made. These include:

(i) Where there is a need for a laminate structure with the maximum initial mechanical properties and the largest percent retention of these values, a fully cured laminate with fiberglass cloth reinforcement and an epoxy resin matrix is recommended.

(ii) Laminates made with an epoxy resin matrix or a polyester resin matrix show the same rate of degradation due to soil burial.

(iii) The use of resin-rich face plies in a sandwich construction with fiberglass chopped strand mat (FCSM) as the core plies showed better resistance to the effects of soil burial than does an all-FCSM laminate.

I. INTRODUCTION

The effects of long-term soil burial on reinforced plastic laminates is of major significance because of their present and projected increased use in intimate soil contact. Reinforced plastic manholes and pipe structures are two examples of projected uses that depend upon the application of these soil burial data.

II. CHEMISTRY OF REINFORCED PLASTIC LAMINATES

Laminates discussed herein are made of two or more layers of reinforcement with a resin matrix. The physical, mechanical, chemical, and electrical properties of the resultant laminate are dependent upon the selection of the proper reinforcement, resin system, and fabrication method.

2.1 *Resins*

This paper concerns itself with laminates made of polyester and epoxy resin matrices.

2.1.1 *Polyester Resins*

Polyester resins are polycondensation products of a polycarboxylic acid and a polyhydroxy alcohol. These polyesters can be characterized as possessing a number of ester groups ($-\overset{\overset{O}{\|}}{C}-O-$) and ethylenic groups ($-\overset{|}{C}=\overset{|}{C}-$) in the polymer chain. The long linear chains are crosslinked by vinyl monomers. The polyester resins in the buried laminates almost exclusively contain styrene as the vinyl monomer.

The following is a brief description of the three polyester resins evaluated.

(*i*) A general purpose orthophthalate polyester resin that typically contains styrene monomer.

(*ii*) A fire-retardant polyester resin based upon chlorendic anhydride with styrene monomer added.

(*iii*) An acrylic-modified polyester resin and methyl methacrylate monomer, to which was added styrene monomer.

2.1.1.1 *Polyester Initiators.* Polyester addition polymerization is initiated by free radicals, which are obtained by the breakdown of peroxides. There are several different catalysts with a wide range of activation temperatures. The selection of the catalyst is dependent upon the desired curing conditions. Methyl ethyl ketone peroxide (DDM) and benzoyl peroxide (BPO) were the catalysts selected in this program.

2.1.1.2 *The Polyester-Styrene Curing Mechanism.*[1]

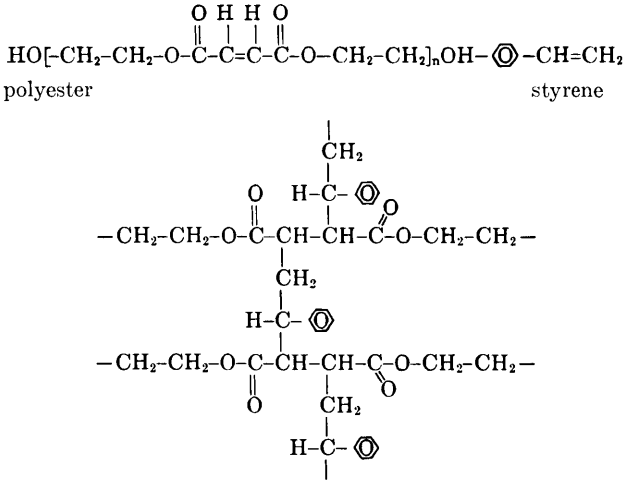

2.1.2 *Epoxy Resins*

Epoxy resins are available in a wide range of molecular weights. The epoxy resins referred to in this part of the soil burial program are the reaction products of epichlorohydrin and bisphenol A. A typical epoxy resin has the following structural formula.

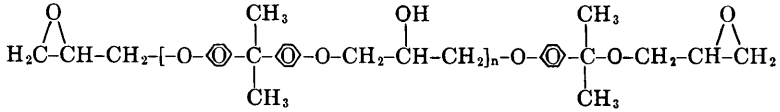

These epoxy resins were cured by amine catalysts. The reaction is shown by the following schematic representation.

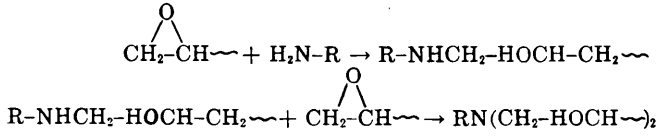

Two commercially available epoxy resins were evaluated: (*i*) a diglycidyl ether of bisphenol A, a liquid resin with a viscosity of 10,000 to 16,000 centipoises; (*ii*) the same base resin as above but diluted with 11 percent butyl glycidyl ether, a reactive diluent, to an average viscosity of 6000 centipoises.

2.1.2.1 *Epoxy Curing Agents.* Epon Curing Agent "Z", a commercial eutectic blend of methylene dianiline (MDA) and metaphenylene diamine (MPDA), and Epon Curing Agent "D", a commercial product of 2-ethyl hexoic acid salt of tris (dimethylaminomethyl) phenol,[2] and diethylene triamine (DTA) are the curing agents used in the curing of the epoxy resin laminates.

2.1.2.2 *Epoxy Additives.* The resin matrix in one of the laminates contained 50 parts of a saturated polyester resin added to 50 parts of the higher viscosity epoxy resin. Saturated polyesters impart flexibility and impact resistance to cured epoxy resins.

2.2 *Reinforcements*

Three classes of fibrous reinforcements were evaluated: glass fibers, a polyester fiber, and an acrylonitrile-vinyl chloride copolymer fiber. The glass fiber reinforcements were fabricated into three different forms: continuous filament woven cloth (FC), continuous filament rovings woven into a cloth (FWR), and glass rovings chopped into 2-inch strands and formed into a mat (FCSM). The fiberglass mat in some cases was the sole reinforcement in the laminate. It was also used as the core plies of reinforcement in laminates of sandwich type construction, Fig. 1. The fiberglass as woven roving is used only as the face plies of the sandwich construction.

The polyester fibers and the acrylonitrile-vinyl chloride copolymer fibers were used in a mat form as the face plies of the sandwich construction only.

III. TEST METHODS

3.1 *Laminate Fabrication*

The laminates were molded in a press under heat and pressure. The polyester resin laminates were cured at 245°F for 7 minutes. The

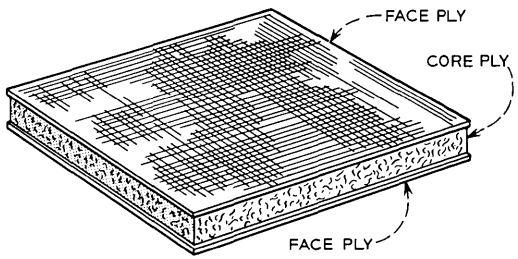

Fig. 1—Sandwich construction type laminate.

epoxy resin laminate molding conditions varied with the catalyst system. The individual laminate number and fabrication data are in Table I.

3.2 *Sample Preparation and Burial*[3]

The laminates were cut into specimens 1 inch by 4 inches and attached by means of polyethylene rivets to the polyethylene tubes. Thirty replicates of each laminate were exposed at each depth at each site.

3.3 *Test Procedure*

Following exposure, a 1/4 inch strip was cut from each side of one- and two-year soil burial specimens to reduce the "edge effect." This reduced the test specimens to 1/2 inch width. The sides of the four-, six-, and eight-year specimens were polished with an emery wheel to 1-inch width.

The flexural strength and the flexural modulus of elasticity tests were performed in accordance with ASTM D790.

A condensation and comparison of the values obtained are in Tables II, III, and IV.

IV. DISCUSSION OF DATA

4.1 *Test Selection*

In a study of this nature one is concerned with: (*i*) the effects of the soil environment on the reinforcement, (*ii*) the resin matrix, (*iii*) the interface between the resin matrix and the reinforcement, and (*iv*) the manner in which these forces come to bear on a structural laminate.

Flexural tests subject the specimen to tensile stresses in the outer extreme fiber and to compression in the inner extreme fiber. The tensile property is largely determined by the reinforcement whereas the compressive strength is dependent on the resin.

The measured resultant combination of these forces is an indication of the effects of soil burial conditioning on the fiber-reinforced plastic (FRP).

4.2 *Control—Shelf Aging at Murray Hill, N. J.*

Representative samples of the specimens buried at the two test sites were shelf aged in a Standard Laboratory Atmosphere per ASTM D618. The samples were tested as received, and after 2, 4, 6, and 8 years of shelf aging.

The greatest initial strength was exhibited by the fiberglass cloth laminates, followed by laminates of sandwich construction consisting of woven fiberglass rovings as the face plies and fiberglass chopped strand mat as the core plies. Laminates made entirely of FCSM and laminates made of FCSM as the core plies and polyester fiber mat or acrylonitrile-vinyl chloride copolymer fiber mat as face plies showed the lowest initial mechanical strengths. In this last group of laminates, the all-fiberglass chopped strand mat with epoxy resin matrix showed approximately 30 percent greater initial strength than the same construction using a polyester resin matrix.

The all-FCSM polyester resin matrix laminate and laminate with the polyester fiber mat or acrylonitrile-vinyl chloride copolymer fiber mat face plies all had initial flexural strengths in the range of 36,000 psi.

The four- and eight-year data showed a wide range of values that may be attributed to deviations in the samples rather than the effect of ambient conditions on the laminate. Samples may differ as to the degree of cure and location of the particular sample in the laminate.

4.3 *Soil Burial Effects*

4.3.1 *Visual Examination*

In practically all cases, gross examination of the specimens subjected to soil burial showed no severe attack upon the physical integrity of the laminate. A few laminates showed abnormalities traced to improper laminate preparation. For example, Laminate No. 157 showed a tendency to delaminate between the first and second plies of fiberglass cloth. The comparatively high initial flexural strength indicates that the laminate is adequately cured and that the delamination is probably due to insufficient resin or poor resin wet-out in the base laminate. Laminate No. 155 developed many hairline cracks due to shrinkage in resin-rich areas on the surface of the laminate. Laminate 169, the only laminate to show a significant staining, was made of an epoxy resin and a saturated polyester resin additive.

4.3.2 *Mechanical Properties*

The rate and percent degradation of the laminate mechanical properties due to soil burial is independent of soil depth and test location.

4.3.3 *Resin Systems Evaluation*

All laminates made using FCSM were compared in order to assess the effect of soil burial on the various resin systems. Data are tabulated

in Table II. Although the two epoxy resin based laminates showed the highest initial flexural strength, these data show that the epoxy resin and the polyester resin laminates both exhibited the same degree of mechanical degradation. After eight years of soil burial these laminates maintained 65–70 percent of their initial flexural strength.

4.3.4 *Reinforcement Systems Evaluation*

Table III lists data obtained on laminates of the same polyester resin matrix and different reinforcements. This table shows the effect of soil burial as it relates to the reinforcement.

The evidence leaves no doubt that the laminates made of all fiberglass cloth reinforcement have superior resistance to the effect of long-term soil burial to any other reinforcement or combinations of reinforcements evaluated. The fiberglass cloth laminates show the highest initial flexural strength (54,000 psi) and a retention of 80 to 85 percent of their initial mechanical properties. The FCSM laminates maintained 55 to 60 percent of their original mechanical properties. The utilization of a fiberglass woven roving fabric as the two face plies and the fiberglass mat as the core plies enhanced the laminates' ability to resist degradation. This was particularly true with an epoxy resin as the matrix in which it retained at least 75 to 80 percent of its original properties. The data also indicate that the use of polyester fiber mat or acrylonitrile-vinyl chloride copolymer fiber mat face plies did show an improvement in soil burial resistance over laminates made of all-fiberglass chopped strand mat. These data demonstrate that the nature of the reinforcement has a greater influence on the laminates' ability to resist the effects of soil burial than does the resin.

4.3.5 *Cure*

Table IV demonstrates that the degree of cure is directly related to the laminates' ability to resist the effect of long-term soil burial.

V. CONCLUSIONS

A fully cured laminate with fiberglass cloth reinforcement and an epoxy resin matrix is recommended where there is need for a laminate structure with high initial mechanical strength and little change with time.

The fiberglass cloth is woven from long lengths of continuous filament yarn presenting relatively few filament ends to the hostile environment. Fiberglass chopped strand mat is made of many 2-inch lengths of

fiberglass yarn. Each filament end presents loci for chemical attack by the environment, largely by capillary action, and thereby weakening of the bond between the glass fiber and the resin.[4] Laminates with an all fiberglass mat construction suffered the greatest damage due to the effect of soil burial regardless of the choice of resin.

Laminates with an epoxy resin matrix possess higher initial mechanical properties than do laminates made of a polyester resin matrix. However, both of these systems show the same rate of degradation due to soil burial. The study shows that to derive the best properties from the laminates the resin matrix must be fully cured.

The use of a polyester fiber mat, an acrylonitrile-vinyl chloride copolymer fiber mat, or fiberglass woven roving face plies in a sandwich construction with FCSM as the core plies showed better resistance to the effects of soil burial than does an all-FCSM laminate. The polyester fiber mat and the acrylonitrile-vinyl chloride copolymer fiber mat resin-rich surfaces act as a protective barrier for the ends of the glass fibers of the FCSM.

No precautions were taken to protect the exposed ends of fibers on the edges of the buried laminate. Although the exposed edges were machined from the soil burial samples to reduce the edge effect, the damaging effect of the soil burial had already been done. If only one surface of the laminate with protected edges were subjected to soil conditioning the effects on the laminate would be significantly less.

In considering the information in this evaluation program we must acknowledge the program's limitations. The laminates selected for the soil burial program were representative of the best glass, glass finish, resin, and fabrication technology available at the outset of the program in 1958. Since then there have been many new and significant developments in the above technologies. The following recent developments are cited to indicate the extent and areas that have shown advancement:

(*i*) "S" glass fibers—a new high-strength glass.

(*ii*) A thermochemical desizing agent that reduces or eliminates the need to use high-heat treating to remove the starch sizing from the glass fiber. Heat treatments of this nature degrade the mechanical properties of the glass fibers.

(*iii*) Sheet molding compounds (SMC) and parts made from SMC present a new technology in its entirety, along with its unique resin systems.

The soil burial program of these materials will be continued, reflecting the latest developments in the FRP field.

VI. ACKNOWLEDGMENTS

The author of this paper wishes to acknowledge the contributions of D. J. Maccia, and N. R. Pape, retired.

REFERENCES

1. Oleesky, S. S., and Mohr, J. G., *Handbook of Reinforced Plastics*, New York: Reinhold Publishing Corp., 1964.
2. Dow Chemical Company, *Epoxy Resin Manual*, Midland, Michigan: The Dow Chemical Company, 1970.
3. Pape, N. R., unpublished work.
4. Asbee, K. H. G., and Wyatt, R. C., "Water Damage in Glass Fibre/Resin Composites," Proc. Royal Soc., A312 (1969), pp. 553–564.

TABLE I—LAMINATE COMPOSITION AND FABRICATION DATA*

Laminate No.	151	152	153	154
Reinforcement				
Face ply	—	—	1 ply PM	1 ply AM
Core plies	4 plies FCSM	4 plies FCSM	4 plies FCSM	4 plies FCSM
Face ply	—	—	1 ply PM	1 ply AM
Resin Matrix				
Resin	Ortho P'ester	Ortho P'ester	Ortho P'ester	Ortho P'ester
Catalyst	0.05% BPO	1.0% DDM	1.0% DDM	1.0% DDM
Cure				
Time-Temp	7 min, 245°F	7 min, 245°F	7 min, 245°F	7 min, 245°F
Laminate No.	**155**	**156**	**157**	**158**
Reinforcement				
Face ply	1 ply FWR	—	—	—
Core plies	1 ply FCSM	11 plies 181FC	11 plies 181FC	11 plies 181FC
Face ply	1 ply FWR	—	—	—
Resin Matrix				
Resin	Ortho P'ester	Ortho P'ester	Ortho P'ester	Chlor P'ester
Catalyst	1.0% DDM	1.0% DDM	0.5% ATC	0.5% BPO, 0.5% DDM
Cure				
Time-Temp	7 min, 245°F	7 min, 245°F	7 min, 245°F	7 min, 245°F
Laminate No.	**159**	**160**	**161**	**162**
Reinforcement				
Face ply	—	—	—	1 ply PM
Core plies	4 plies FCSM	4 plies FCSM	4 plies FCSM	4 plies FCSM
Face ply	—	—	—	1 ply PM
Resin Matrix				
Resin	Chlor P'ester	Acryl P'ester	8 Epoxy	8 Epoxy
Catalyst	1.0% DDM	1.0% DDM	20 phr Z	20 phr Z
Cure				
Time-Temp	7 min, 245°F	7 min, 245°F	90 min, 180°F	90 min, 180°F
Post-cure				
Time-Temp	—	—	120 min, 300°F	120 min, 300°F
Laminate No.	**163**	**164**	**165**	**166**
Reinforcement				
Face ply	1 ply AM	1 ply FWR	—	—
Core plies	4 plies FCSM	1 ply FCSM	4 plies FCSM	4 plies FCSM
Face ply	1 ply AM	1 ply FWR	—	—
Resin Matrix				
Resin	8 Epoxy	8 Epoxy	5 Epoxy	8 Epoxy
Catalyst	20 phr Z	20 phr Z	20 phr Z	13 phr D
Cure				
Time-Temp	90 min, 180°F	90 min, 180°F	90 min, 180°F	30 min, 245°F
Post-Cure				
Time-Temp	120 min, 300°F	12 min, 300°F	120 min, 300°F	—
Laminate No.	**167**	**168**	**169**	**170**
Reinforcement				
Face ply	1 ply FWR	—	—	1 ply FWR
Core plies	1 ply FCSM	4 plies FCSM	4 plies FCSM	1 ply FCSM
Face ply	1 ply FWR	—	—	1 ply FWR
Resin Matrix				
Resin	Ortho P'ester	60 Part 5 Epoxy	50 Part 8 Epoxy	8 Epoxy
Catalyst	1.0% DDM	40 Part V125	15 Part Sat P'ester	20 phr Z
Cure				
Time-Temp	7 min, 245°F	30 min, 250°F	4 hrs, 158°F	90 min, 180°F
Post-Cure				
Time-Temp	—	—	—	120 min, 300°F

* See appended list of abbreviations.

TABLE II—COMPARISON OF RESIN MATRICES* (FCSM REINFORCEMENT)

Laminate No.	151	152	159	160	161	166	169	165	168
Resin	Ortho P'ester	Ortho P'ester	Chlor P'ester	Acryl P'ester	8 Epoxy	8 Epoxy	8 Epoxy Sat. P'ester	5 Epoxy	5 Epoxy
Catalyst or curing agent	BPO	DDM	DDM	DDM	Z	D	DTA	Z	V125
Initial flex str avg, psi	33,800	34,100	33,500	35,800	43,800	49,600	13,600	50,100	37,700
% Change:									
MH-shelf aging, 8 yrs	+7.1	+8.5	+1.5	−5.6	−11.6	−8.5	−38.8	−19.2	−17.5
Ga-topsoil, 8 yrs	−39.6	−42.2	−42.4	−40.3	−41.3	−33.9	+16.9	−33.5	−35.3
Ga-subsoil, 8 yrs	−41.7	−34.6	−42.7	−92.2	−36.5	−25.9	+14.0	−34.3	−35.0
NM-topsoil, 6 yrs	−34.3	−32.3	−31.3	−38.3	−32.9	−30.4	+13.2	−33.5	−29.4
NM-subsoil, 6 yrs	−31.4	−33.7	−31.9	−34.1	−30.6	−32.1	+15.4	−29.1	−30.0

* See appended list of abbreviations.

TABLE III—COMPARISON OF REINFORCEMENTS* (ORTHOPHTHALATE POLYESTER/1.0% DDM RESIN MATRIX, CURED AT 245°F FOR 7 MINUTES)

Laminate No.	152	153	154	155	156
Reinforcement					
Face plies	—	1 ply PM	1 ply AM	1 ply FWR	—
Core plies	4 plies FCSM	4 plies FCSM	4 plies FCSM	1 ply FCSM	11 plies 181FC
Face plies	—	1 ply PM	1 ply AM	1 ply FWR	—
Initial flex str avg, psi	34,100	33,800	33,200	46,100	57,300
% Change:					
MH-shelf aging, 8 yrs	+8.5	−8.0	+2.7	−14.5	−3.3
Ga-topsoil, 8 yrs	−42.2	−37.3	−29.5	−32.1	−4.4
Ga-subsoil, 8 yrs	−34.6	−38.2	−31.3	−25.4	−8.7
NM-topsoil, 6 yrs	−32.3	−31.4	−23.2	−34.1	−5.6
NM-subsoil, 6 yrs	−33.7	−25.4	−17.2	−29.1	−9.2

* See appended list of abbreviations.

TABLE IV—EFFECT OF DEGREE OF CURE OF EPOXY MATRIX*

Laminate No.	164	170
	Same Formulation (See Table I)	
Cure Time-Temp	90 min, 180°F	90 min, 180°F
Post-Cure Time-Temp	12 min, 300°F	120 min, 300°F
Initial flex str avg, psi	47,900	50,000
% Change:		
MH-shelf aging, 8 yrs	−27.8	+5.2
Ga-topsoil, 8 yrs	−29.6	−11.8
Ga-subsoil, 8 yrs	−25.1	+8.6
NM-topsoil, 6 yrs	−28.6	+5.8
NM-subsoil, 6 yrs	−24.6	+2.0

* See appended list of abbreviations.

ABBREVIATIONS

Reinforcements

AM—Acrylonitrile-vinyl chloride copolymer fiber mat
FC—Fiberglass cloth, continuous filament, style 181
FCSM—Fiberglass chopped strand mat, 2 oz per sq/ft
FWR—Fiberglass woven roving
PM—Polyester fiber mat

Resins

Acryl P'ester—Acrylic modified polyester resin
Chlor P'ester—Chlorendic anhydride based polyester resin
Ortho P'ester—Orthophthalate based polyester resin
Sat P'ester—Saturated polyester flexibilizer
5 Epoxy—Diglycidyl ether of bisphenol A, diluted to 6000 centipoises with butyl glycidyl ether
8 Epoxy—Diglycidyl ether of bisphenol A, liquid resin with a viscosity of approximately 13,000 centipoises

Catalysts and Hardeners

ATC—A paste of 50 parts benzoyl peroxide and 50 parts diallyl phthalate
BPO—Benzoyl peroxide
D—2-ethyl hexoic acid salt of tris (dimethylaminomethyl) phenol
DDM—60% solution of methyl ethyl ketone peroxide in dimethyl phthalate
DTA—Diethylene triamine
V125—Liquid polyamide hardener
Z—Blend of methylene dianiline (MDA) and methaphenylene diamine (MPDA)

Copyright © 1972 American Telephone and Telegraph Company
THE BELL SYSTEM TECHNICAL JOURNAL
Vol. 51, No. 1, January, 1972
Printed in U.S.A.

Soil Burial Tests:

Effect of Soil Burial Exposure on the Properties of Plastics for Wire and Cable

By J. B. DE COSTE

(Manuscript received April 27, 1971)

This paper describes the studies that have been made on polyethylene and vinyl chloride plastic wire and cable coatings after up to eight years soil burial at sites in Georgia and New Mexico. The initial samples of both types of plastics were exposed in the form of extruded wire while the more recent studies on vinyl plastics have been made on molded sheet. The polyethylenes were observed to have excellent resistance to deterioration, but certain of them may be susceptible to adverse changes in physical properties that appear to be associated with polymer crystallization. The vinyl plastics vary in their resistance to deterioration, depending primarily upon the choice of plasticization. Compositions of both types of plastics can be prepared that may be expected to provide satisfactory long-term service as wire or cable coatings in a soil environment.

I. INTRODUCTION

A soil burial study was undertaken on polyethylene and vinyl chloride plastics in order to develop a background of knowledge concerning these materials that would be useful in the design of buried wire and cable. These plastics were selected for study because of their wide acceptance as coatings on communications wire and cable and because their chemical structure suggested that they might be expected to possess good resistance to soil burial.

In the initial phase of this program, wires with extruded plastic coatings on copper and aluminum conductors were buried at the Georgia and New Mexico test sites. Half of the samples were exposed with a 48-volt positive dc potential on the conductors and half without

it. An interim report on the vinyl plastics in these tests was made at the end of four years of soil burial.[1] The observations at that time indicated that the nature of the conductor, potential, and variations in the depth of burial (within the limits studied) were not critical variables. On the basis of these observations, it was decided, henceforth, to examine only coatings on copper conductor without potential from a mean depth.

In the second phase of this program, molded sheet samples of vinyl plastics were buried mounted on polyethylene tubes. These were introduced because they permitted the preparation of samples from small roller mill mixed lots which facilitated the study of compositional variables. The objectives of this work have been to study the performance of a number of new plasticizers and to confirm certain earlier observations made on wire samples.

The information compiled thus far has been of assistance in understanding the mechanisms involved in the changes that may occur in plastics on soil burial and is serving as a valuable guide in selecting the most permanent types of coatings for use on buried structures.

II. CHEMISTRY OF PLASTICS FOR WIRE AND CABLE

The polyethylene plastics buried as extruded wire coatings were chosen from available commercial compositions (see Table I). The resins from which these plastics were manufactured were of both low- and high-density types (0.92 to 0.96) with subdivisions of low and high molecular weight grades (melt indices 2.0 to 0.3). The low-density resins used in this study are similar to grades commonly used today, but the high-density resins were first generation low-pressure grades that are now only of academic interest since they suffered from thermal embrittlement[2] and have been superseded by reportedly improved grades.

Ordinarily, polyethylenes inherently possess suitable mechanical and electrical properties and are modified with only minor percentages of additives to aid stabilization in processing and service or to modify superficial properties. Among the additives investigated were antioxidants, carbon black, and butyl rubber. Also buried were coatings crosslinked by electron beam irradiation as well as a coating foamed with azodicarbonamide.

The vinyl plastics buried as wire coatings ranged from semirigid to highly flexible grades and consisted of both commercial and experimental formulations. The compositions were based on high molecular

TABLE I—COMPOSITION OF POLYETHYLENE PLASTIC WIRE COATINGS USED IN SOIL BURIAL TESTS

Compound No. −57	Polyethylene Wire Coating			
	Base Polymer		Modification	
	Density	Melt Index‡	Antioxidant	Other Additives and/or Treatment
450	0.92	2.0	—	—
464, 468	0.92	2.0	0.1% Thiocresol*	—
456	0.92	1.1	0.1% Thiocresol*	—
451, 481§	0.92	0.3	0.1% Thiocresol*	—
455, 472§	0.92	0.3	0.1% Thiocresol*	2.7% Medium Channel Carbon Black
453	0.92	0.3	0.1% Thiocresol*	5% Butyl Rubber (IIR)
470	0.92	0.3	0.1% Thiocresol*	25% Butyl Rubber (IIR); plus 3% Medium Channel Carbon Black
460	0.92	0.3	0.1% Thiocresol*	Irradiated with Crosslinking Agent
466	0.92	0.3	0.1% Thiocresol*	Irradiated with Crosslinking Agent; plus 2.7% Medium Channel Carbon Black
452	0.92	2.0	0.07% Aryl Diamine**	Foamed with Azodicarbonamide
454, 457§	0.95	—	—	—
458	0.96	0.5	0.01% Tertbutyl Phenol†	—
483	0.95	—	—	Irradiated with Crosslinking Agent
475	Polypropylene, Natural			

* 4,4′ Thiobis (6-tertbutyl m-cresol)
** N, N′ Diphenyl-p-phenylene diamine
† 2,6 Di-tertbutyl-4-methyl phenol
‡ ASTM Method D1238, Condition E (190°C, 216g load)
§ Compounds obtained from different manufacturing sources

weight homopolymer suspension resins conforming approximately to a GP6-grade per ASTM D1755,[3] with the exception of coating No. 403, which was based on a 5-percent acetate copolymer. To obtain the desired processing and ultimate properties in a vinyl plastic, it is necessary to incorporate with the resin plasticizers, fillers, colorants, stabilizers, and lubricants totaling, sometimes, as much as 50 percent by weight of the plastic. The various ingredients are thermoplastically mixed with the resin to obtain a homogeneous plastic. To accomplish the mixing, a roller mill, banbury, screw plasticator, or one or more of these in combination, are ordinarily used.

The plasticizer content of the vinyl wire coatings is given in Figs. 5 and 6. Wherever octyl ester plasticizers are referred to, the ester intended is that of 2-ethylhexanol. Details regarding other ingredients in these coatings are a matter of record.[1]

The vinyl compounds used in the second phase of the investigation employing molded sheet samples were all experimentally prepared. They were formulated with a number of new plasticizers, as well as some previously used in the wire coatings, and they included a series of compounds to examine the effect of various inorganic fillers at rather high loading (see Tables IV and V). Among the new plasticizers examined were two trimellitates, a chlorinated hydrocarbon, a chlorinated polyethylene, and a chlorophenyl diphenyl phosphate. The chlorinated hydrocarbon was a liquid having 52 percent chlorine on an essentially normal C_{15} fraction. The chlorinated polyethylene was a solid amorphous polymer of 40 percent chlorination based on a linear medium-high molecular weight polyethylene. The purpose of re-examining pentaerythritol plasticizers was to obtain confirmation regarding conclusions reached from the earlier wire studies relative to the merits of monomeric and dimer esters. The polyesters were obtained from several commercial sources and have, according to trade information, a molecular weight range from 1000 to 5000. The polyesters in compositions No. 118-67 and No. 121-67 (see Table IV) differ from the others in that they contain phthalic groups.

III. SAMPLE PREPARATION AND BURIAL

Wire samples of the various plastics were extruded with coatings having a 0.030-inch-thick wall on 22 AWG conductors of copper and aluminum. Lengths of 37.5 feet were buried in the form of an open helix 12 inches in diameter to a maximum depth of 28 inches. For the two- and four-year inspections, two samples of each type of conductor

were dug up, one with potential and one without. At the eight-year inspection, only two samples on copper without potential were removed. All samples were returned to the Murray Hill laboratory for evaluation.

Sheet samples were molded to a thickness of 0.030 inch from the various experimental vinyls. From these 1.5 × 3.0-inch rectangular pieces were cut and then mounted on the polyethylene tubes in the conventional manner for exposure below the surface. At inspections, two tubes representing each plastic are removed for evaluation.

IV. EVALUATION METHODS

The wire samples from soil burial were evaluated first for electrical properties using a test length of 30 feet. This was subsequently cut into topsoil and subsoil sections (from average depths of 10 and 24 inches) for tensile tests on the coating after the conductor was removed. Where tensile tests were made on coatings from a mean depth, sections that had been buried at an average depth of 16 inches were used. Lengths of wire adjacent to those taken for tensile tests were visually examined for insect attack, discoloration, and corrosion of the conductors. Sheet vinyl samples, taken from polyethylene supporting tubes after soil burial, were die punched to obtain tensile specimens for evaluation.

Electrical measurements were made using conventional ac (1 kHz) and dc bridge techniques on wire samples immersed in tap water at 23°C. Tensile tests on wire coatings and sheet specimens were performed in accordance with ASTM methods D470 and D412, respectively.[3] In order to economize on material, micro-tensile specimens (see Figs. 7 and 8) were used in performing D412 instead of the larger one specified. The tensile stress at 100-percent elongation, or S-100 modulus, is a particularly useful parameter for following changes in vinyl plastics as it is sensitive to small differences in plasticizer concentration and is not subject to minor imperfections in the manner of a fracture parameter.

The analysis of vinyl sheets for plasticizer retention was made by means of an ethyl ether extraction per ASTM D2124. Where polyester plasticizers were known to be present, an additional four-hour extraction was preformed with a mixture of carbon tetrachloride and methanol, 2:1 by volume.

Infrared analysis was used to determine changes that may have occurred in the chemical structure of the polyethylenes as a result of soil burial. Specimens for scanning were remolded between polished

chrome-plated steel plates to 0.010-inch-thick films. Discs about 2 inches in diameter were obtained and scanned in a Perkin-Elmer spectrophotometer, Model 521.

V. POLYETHYLENES—RESULTS AND DISCUSSION

5.1 *Results*

The various polyethylene wire coatings remained generally intact after soil burial and were almost devoid of any noticeable color change. Minor isolated attacks by insects were observed on about half of the samples. These took the form of short chewed areas that did not penetrate to the conductor (see Fig. 1). The polyethylenes showed little or no tendency to react with the metallic conductors. Tarnish was

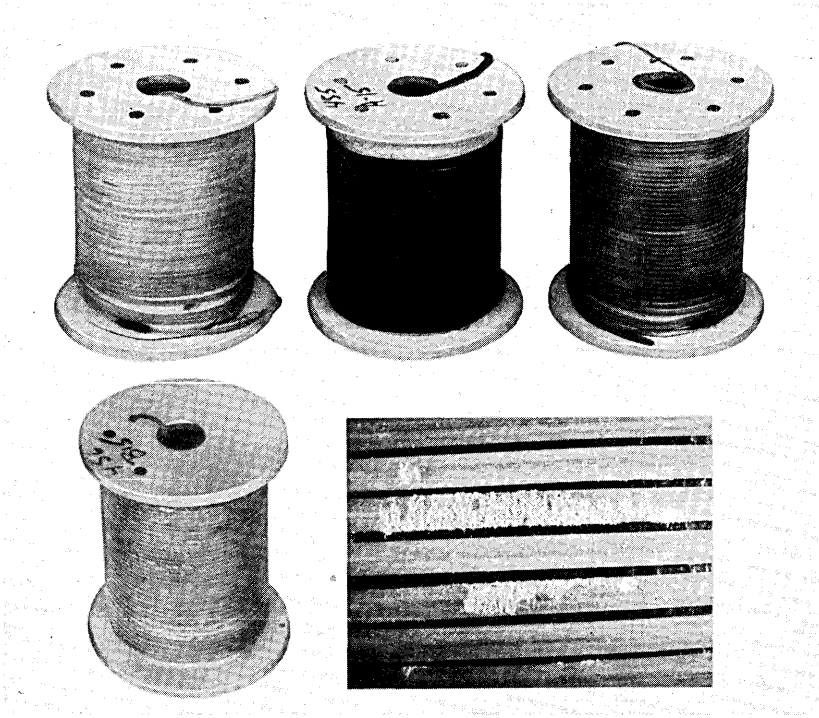

Fig. 1—Polyethylene coated wire samples after six years soil burial. Upper spools (left to right, Nos. 456, 455, and 450) are from Georgia. Lower spool (No. 456) is from New Mexico and shows insect attack, a section of which is magnified in the insert.

common on the copper conductors but only three cases of spotty green corrosion were detected (Nos. 452, 483, and 450).

The polyethylenes varied in their retention of tensile properties, depending upon the density of the resins from which they were prepared. Those based on low-density resins showed a relatively small change in tensile properties after up to eight years soil burial (see Tables II and III and Fig. 2). With few exceptions, there is a slight increase in tensile strength and yield with some loss in elongation in these coatings. Variations in the molecular weight, as characterized by melt index, do not appear to have an appreciable effect on the retention of tensile properties nor did the addition of carbon black. The only compound tested without antioxidant (No 450) showed a somewhat greater loss in elongation than was common among those in which it was used. The polyethylene plastics based on high-density resins, in contrast, suffered major losses in elongation, in some cases to the point of embrittlement, and decreased somewhat in strength. Polyethylene wire coatings shelf-aged for eight years at room temperature show essentially the same results as those obtained on the polyethylenes after soil burial.

Among the low-density coatings there were also instances where a significant loss in elongation was noted. These occurred where 25 percent butyl rubber had been added (No. 470) and in two of the coatings crosslinked by irradiation. The natural irradiated coating (No. 460) on aluminum lost most of its elongation after four years burial in Georgia (Fig. 2) while the black irradiated coating (No. 466) on copper did likewise after eight years shelf aging. It is interesting to note that G. H. Bebbington, in his paper in this series on rubber-like materials, also reports observing a loss in mechanical properties for a peroxide crosslinked polyethylene without channel black.

The principal change in electrical properties after soil burial occurred in ac breakdown strength where a sizable loss was observed for both high- and low-density types (see Fig. 3). No essential change was noted in the capability of the majority of the coatings to maintain a high dc insulation resistance equal to or greater than 6×10^4 MΩ/10^3 ft. Capacitance measurements on the conductors showed, in general, a slight decrease after soil burial. Notable exceptions in this regard were the foam sample, No. 452, and the high-density sample, No. 483, which increased in capacitance.

A number of low-density coatings were examined for chemical change by comparing the spectra of soil burial and shelf-aged samples.[4] The spectra from most of the buried samples examined (Nos. 451, 453, 456,

TABLE II—ORIGINAL TENSILE AND ELECTRICAL PROPERTIES OF ETHYLENE PLASTIC WIRE COATINGS (AVERAGE OF SAMPLES ON BOTH COPPER AND ALUMINUM)

	Tensile Properties			Electrical Properties (on wire)		
Plastic No. −57	Tensile St. psi	Yield psi	Ultimate Elongation %	Capacitance, 1 kHz pF/ft	AC Breakdown kV	Insulation Proof Test 6×10^4 MΩ/10^3 ft
450	1910	1280	520	32.1	22.0	OK
464	1930	1350	480	31.2	26.0	OK
468	1910	1440	495	33.9	25.0	OK
456	2430	1610	549	30.9	27.5	OK
472	2170	1790	535	36.9	31.5	OK
451	2410	1510	480	32.6	27.0	OK
455	2580	1270	520	37.0	23.5	OK
481	1890	1280	435	33.1	21.5	OK
453	2100	1200	495	32.4	22.0	OK
470	1470	990	485	38.8	29.5	OK
460	1990	1340	370	33.4	22.0	OK
466	1960	1450	340	33.0	22.0	OK
452	620	520	360	21.7	10.5	NG
454	2130	2140	575	33.2	30.5	OK
457	2600	2380	578	32.9	34.5	OK
458	3220	3370	775	32.9	34.5	OK
483	2630	2800	780	30.5	27.0	OK
475	3570	3580	563	32.2	27.5	OK

TABLE III—CHANGE IN TENSILE PROPERTIES OF POLYETHYLENE WIRE COATINGS AFTER 8 YEARS SOIL BURIAL IN NEW MEXICO AND AFTER SHELF AGING*

		Tensile Strength			Yield			Elongation		
		Percent Change			Percent Change			Percent Change		
		8 Yrs Shelf Aging		8 Yrs N.M.†	8 Yrs Shelf Aging		8 Yrs N.M.†	8 Yrs Shelf Aging		8 Yrs N.M.†
Plastic No.	−57	Cu	Al	Cu	Cu	Al	Cu	Cu	Al	Cu
Low density, low mol wt	450	−7.9	+29.2	−7.7	+1.9	+12.2	−3.3	−30.0	+11.2	−17.3
	464	+12.1	+21.8	+28.0	0.0	+16.7	−4.9	+5.3	+2.0	+35.5
	468	+17.5	−5.7	+22.7	+5.9	+5.9	−1.0	−6.1	−9.0	+27.1
	456	−3.6	+50.9	−4.5	+3.7	+7.5	−1.1	−16.1	+28.7	+7.7
Low density, high mol wt	451	−9.7	+25.8	+3.1	+1.0	+4.0	−3.3	−18.6	+4.4	−7.8
	481	+53.1	+50.0	+41.0	−2.7	+4.7	−6.4	+18.5	+26.8	+26.1
	455	+4.8	+15.2	−5.0	+12.6	+14.5	−0.2	−8.3	−1.0	−0.6
	472	+27.2	+38.2	+23.3	+4.0	+5.1	−0.1	−0.9	+2.8	+10.2
	453	−1.7	+44.1	−13.7	+12.9	+12.4	+5.0	−11.0	+25.0	−9.8
	470	−1.7	−5.1	−7.6	+0.5	+8.9	−1.1	−3.7	−17.3	−9.4
	460	—	+16.0	+20.1	—	+11.1	+4.6	—	+27.0	+5.4
	466	+26.0	—	+16.6	+68.0	—	+6.1	−97.1	—	+9.7
Foam	452	−2.2	+4.4	+0.6	+4.5	+13.4	+6.1	−15.3	+29.2	−19.7
MEDIAN, % CHANGE		+1.5	+23.8	+3.1	+3.9	+10.0	−1.0	−9.7	+7.8	+5.4
High density	454	−1.7	+0.8	−9.7	−6.9	−16.6	−1.9	−1.9	−20.6	−0.6
	457	+33.9	−14.7	−10.6	+66.7	+7.7	−90.5	<−98.1	<−98.4	−96.0
	458	−24.1	−12.1	−27.6	−19.0	−19.9	+1.4	<−98.7	<−98.7	−97.7
	483	—	−11.6	+2.6	—	—	+14.5	—	—	−97.6
Polypropylene	475	−9.7	+10.3	−8.6	−10.5	−5.4	+5.6	+59.8	−15.9	+70.0

* Shelf aging was conducted in the dark at average indoor room conditions
† Mean depth (avg 16 inches) data

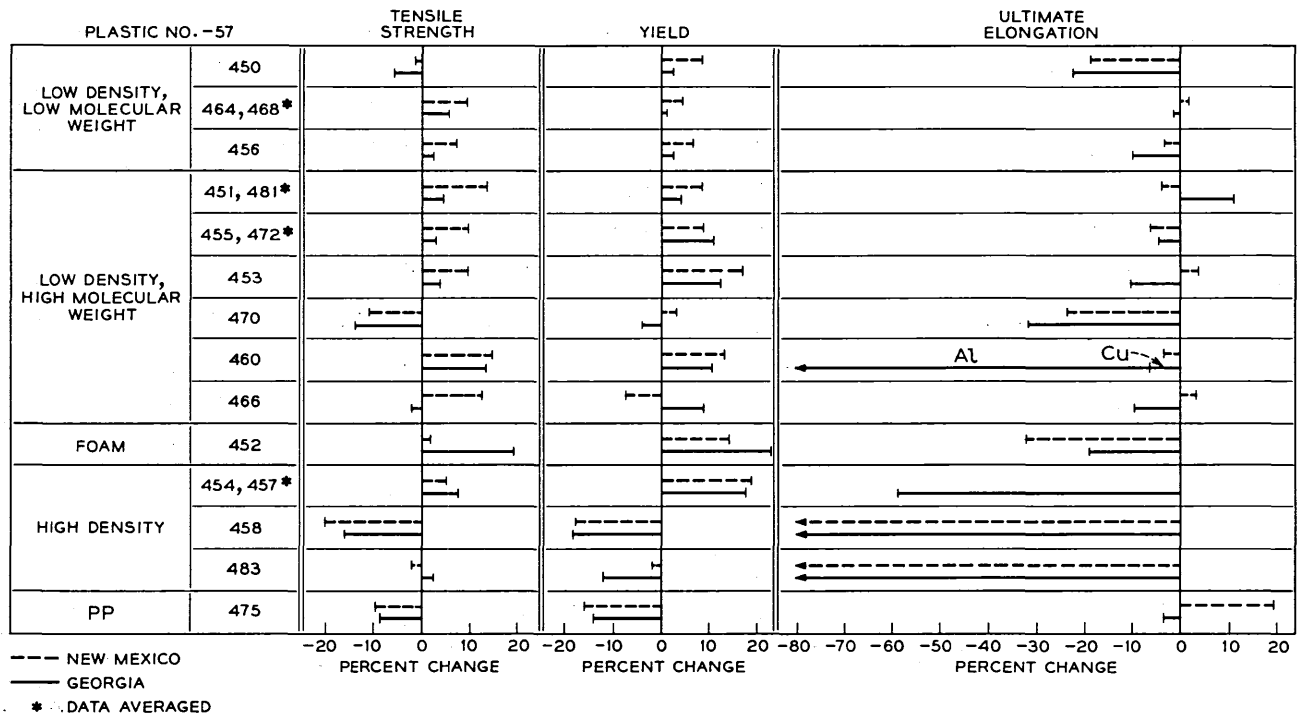

Fig. 2—Change in tensile properties of polyethylene plastic wire coatings after four years soil burial; average values for samples with and without potential on both Cu and Al conductors.

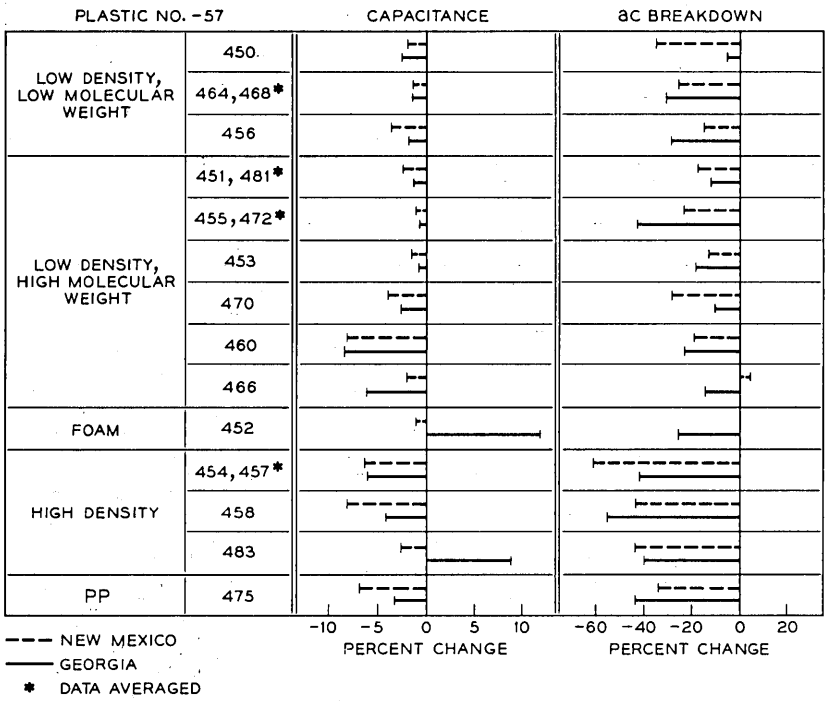

Fig. 3—Change in electrical properties of polyethylene plastic wire coatings after four years soil burial; average values for samples with and without potential on both Cu and Al conductors.

and 464) were found to be identical with the shelf-aged controls except for the appearance of a weak carbonyl band in the 1705 cm^{-1} region. The plastic showing the most noticeable carbonyl absorption (No. 450) contained a natural resin without antioxidant (see Fig. 4). The one high-density coating examined (No. 454) had no detectable carbonyl after either kind of aging.

5.2 *Discussion*

The good soil burial resistance observed for the low-density polyethylenes is consistent with results reported in the literature on these materials. Tensile tests on polyethylene cable coatings buried in inoculated and sterile soil were found[5] to be immune to deterioration. Excellent retention of tensile and other physical properties has been observed for 10-mil polyethylene sheet after seven years accelerated laboratory soil burial tests and after four years field burial service

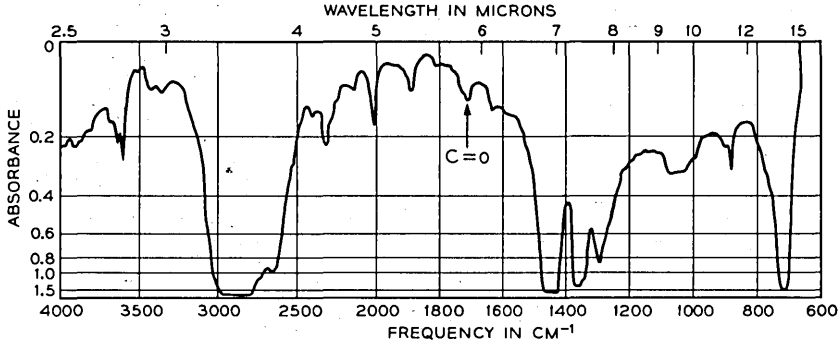

Fig. 4—Infrared spectrum of natural low-density polyethylene (No. 450) showing carbonyl absorption after four years soil burial in Georgia.

in New Mexico.[6] Although no differences of any consequence were noted in our studies among the low-density resins with respect to molecular weight, evidence of biological attack by bacteria has been reported in studies involving exceptionally low molecular weight grades of polyethylene ordinarily not used on wire and cable.[7]

There is some question as to whether the severe loss in elongation observed in the high-density coatings is attributable to the soil environment. Since essentially the same changes occurred in samples retained at room conditions, which are too mild to expect oxidative effects, we are probably dealing with a time-temperature phenomena recognized to occur in these polymers and referred to as thermal embrittlement.[2,8] This embrittlement has also been observed in cable jacketing of these high-density polymers following extended ocean exposure.[9]

The infrared spectra obtained on polyethylenes indicated that they were, with few exceptions, essentially free of chemical decomposition as a result of soil burial or shelf aging. The slight increases detected in the carbonyl content of the low-density coatings may be attributable to either oxidation or possibly to the absorption by the resins of foreign substances. An argument favoring the oxidation is found in the No. 450 coating, which contained no antioxidant and had the most intense carbonyl band. However, since the resin used was a high-pressure branched type polymer with a broad molecular weight distribution, it could also be argued that it might be expected to be fairly absorptive, hence the source of the carbonyl cannot be pinpointed.

The good retention of dielectric and insulation resistance properties are what would have been predicted from the chemical stability exhibited by the polyethylenes. The decrease in ac breakdown strength is

probably related to highly localized damage to the coatings sustained during burial or excavation, or from insect attack.

VI. VINYLS—RESULTS AND DISCUSSION

6.1 *Results*

6.1.1 *Wire Coatings*

The vinyl chloride plastics differ from the polyethylenes in that they show some discoloration after soil burial and undergo compositional changes that alter their properties. The appearance of the coatings after eight years burial has not particularly changed since the earlier four-year inspection. Mottling was common with yellow or purple spots appearing frequently, although brown, gray, and pink were also noted. Isolated attacks on the coatings by insects occurred while the condition of the conductors was about the same as that observed for the polyethylenes.

A general aging pattern appears to have developed for most of the vinyl wire coatings (see Figs. 5 and 6). Following an early rapid increase in S-100 modulus, they level off or, at most, continue to increase at

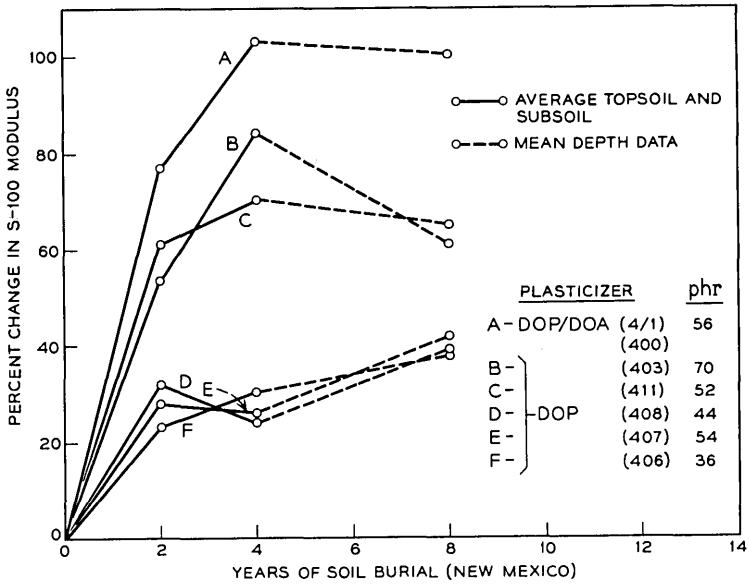

Fig. 5—Effect of soil burial with time on the modulus of vinyl wire coatings containing dioctyl phthalate at various concentrations.

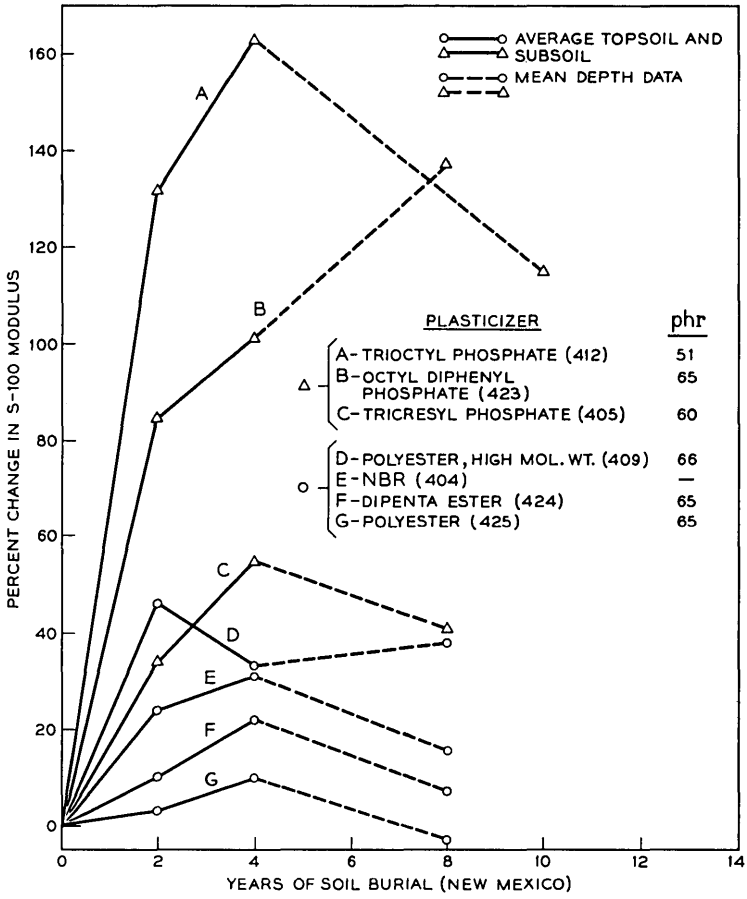

Fig. 6—Effect of soil burial with time on the modulus of vinyl wire coatings varying in plasticization.

a slow rate. A number of coatings formulated with dioctyl phthalates are in this category as well as those prepared with polyesters, nitrile rubber, and tricresyl phosphate. Exceptions are found in the curves for coatings containing octyl diphenyl phosphate (No. 423) which continued to rise sharply and that containing trioctyl phosphate which declined.

6.1.2 *Sheet Tests*

The sheet vinyls after thirty-two months soil burial were found to have undergone some superficial changes which included discoloration,

shrinkage, warping, and insect attack. The discoloration, in general, (see Fig. 7) was similar to that previously mentioned for the wire coatings. One unusual color development was noted in the case of the compound prepared with chlorophenyl diphenyl phosphate (No. 120-67) which turned an overall pink.

Shrinkage and warpage was noted in samples where there had been an excessive loss in plasticizer as determined by analysis (see Table VI) or deduced from a large change in modulus. An example of shrinkage may be seen in the dioctyl adipate compound (No. 84-67) shown in Fig. 7; a noticeable difference in size between this and the other samples is readily apparent. Warping appears to be associated with samples which show a large increase in modulus or stiffness and suggests that the plasticizer loss may not be uniform over the surface of the samples. There was also an indication of nonuniformity of attack on vinyl wire coatings which was occasionally apparent as a variation in stiffness along a coating from which the conductor had been removed.

The insect attack on sheet vinyls was typical in that it was confined to the edges of the samples (see Fig. 8). Scalloped sections were removed from the edge of what were originally rectangular samples. This occurred on a relatively few samples and presented no problem in obtaining sound areas from which to punch tensile specimens. It is evident from these observations that prepunched specimens should be avoided as they are liable to edge damage, which would render them unsuitable for measurement.

Significant differences have been noted among the various vinyls with respect to their permanence, as reflected by tensile tests. Data

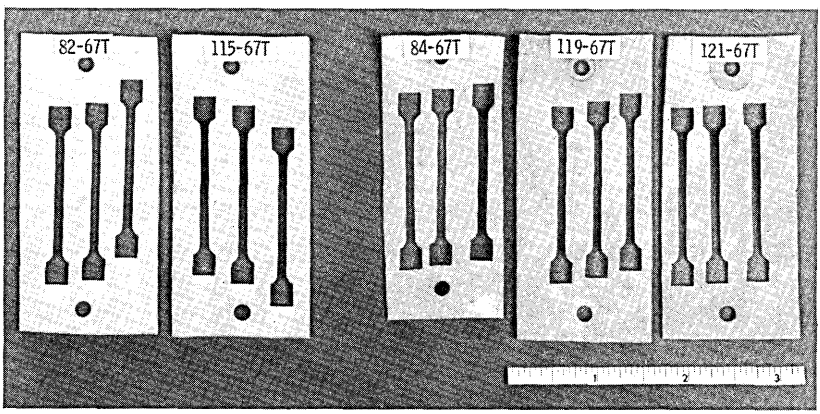

Fig. 7—Range in discoloration observed in vinyl sheet samples after 32 months soil burial in Georgia (cutouts are from micro specimens).

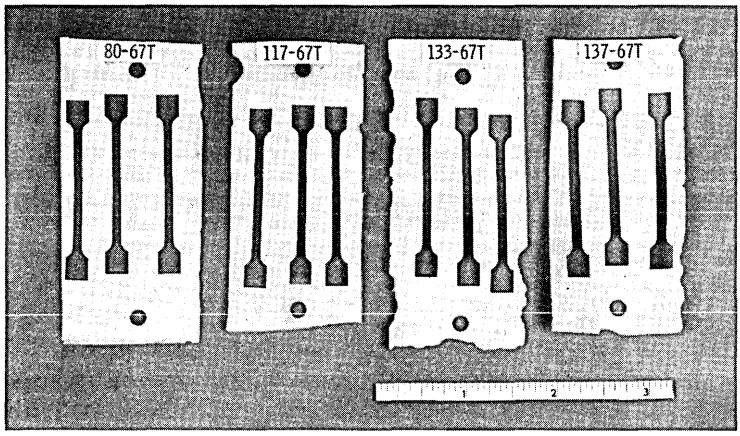

Fig. 8—Examples of edge damage by insects to vinyl sheet samples after 32 months soil burial in Georgia.

on the sheet samples are presented in Tables IV and V and Figs. 9, 10, and 11. The large increase in the moduli of those vinyls containing azelate and adipate esters (Nos. 83- and 84-67) was expected (see Fig. 9) since these plasticizers, which are known to be biodegradable, were included to provide assurance of the microbiological activity of the soil at the test sites. A large increase in modulus was also noted for the monomeric penta ester vinyl (No. 79-67) while compositions prepared with two dimer penta esters (Nos. 80- and 81-67) showed much smaller changes clearly confirming the superiority of the dimer as previously reported from data on wire coatings. Among the monomeric plasticizers, exceptional permanence was shown by both trioctyl and the mixed n-octyl n-decyl trimellitates (Nos. 115- and 116-67) as judged from their small changes in modulus. Although there is no difference in the tensile data of these trimellitates, plasticizer loss by extraction analysis favors the trioctyl trimellitate, which showed a very small loss (see Table VI).

The polyester plasticizers vary in their response to soil burial with the medium and high molecular weight types showing the best performance (Fig. 10). A notable difference was observed between the two low molecular weight polyesters with the one containing phthalic groups (No. 121-67) showing the best permanence. Since polyester plasticizers are proprietary materials of undisclosed composition, any generalizations with regard to performance are risky and only those with proven integrity may be depended upon.

TABLE IV—EFFECT OF SOIL BURIAL ON THE TENSILE PROPERTIES OF PVC PLASTICS

No.	PVC Plastic* Plasticizer, 65 phr	Tensile Strength				Elongation				S-100 Modulus			
		Orig psi	% Change After 32 Months			Orig %	% Change After 32 Months			Orig psi	% Change After 32 Months		
			Shelf	Topsoil	Subsoil		Shelf	Topsoil	Subsoil		Shelf	Topsoil	Subsoil
115-67	TOTM	2533	+5.5	+7.9	+8.3	353	−10.7	+4.2	−5.7	1480	+3.8	+8.3	+10.3
116-67	NODTM	2405	−8.3	+5.3	+2.8	300	0.0	+8.0	+4.3	1468	−9.2	+9.4	+3.2
80-67	DIPENTA Ester (A)	2533	+4.7	+8.3	+14.1	300	+13.3	+3.0	+2.3	1696	−0.1	+13.3	+18.8
81-67	DIPENTA Ester (B)	2507	+5.7	+13.6	+9.0	323	+5.3	+1.2	+0.3	1444	−0.2	+20.1	+20.2
82-67	DOP	2442	−0.8	+10.4	+10.8	350	+1.4	+5.4	+4.8	1140	−2.3	+11.7	+17.5
120-67	Chloro Aryl Phosphate†	3207	+5.3	+5.6	+5.9	307	+5.9	−5.5	−0.6	1760	+2.4	+20.7	+25.4
79-67	PENTA Ester	2492	+7.5	+26.6	+26.4	357	+0.8	−3.9	−7.5	1242	+2.6	+46.1	+55.3
83-67	DOZ	2119	+4.8	+26.0	+39.1	377	+2.1	+1.8	−6.4	968	−1.6	+38.1	+83.9
84-67	DOA	2109	+6.4	+38.5	+22.7	390	+2.6	−19.5	−12.7	876	+3.5	+110.7	+77.6
119-67	Polyester, high Mol. wt	2645	+1.9	+3.1	+5.1	320	+4.7	+0.6	+2.8	1749	−1.4	+12.6	+10.8
122-67	Polyester, high Mol wt	2489	+4.0	+6.7	+17.4	327	−8.3	−7.0	−6.1	1565	+7.1	+18.1	+8.5
118-67	Polyester, med mol wt	2815	−3.1	+3.7	+3.3	340	−4.4	−0.6	−8.0	1864	+1.9	+14.3	+14.6
121-67	Polyester, low mol Wt	3048	−1.6	+7.7	+9.5	350	0.0	−8.0	−9.4	1817	−1.2	+20.8	+21.2
117-67	Polyester, low mol Wt	2534	+2.4	+14.8	+21.5	333	+6.6	+2.1	+0.3	1396	+0.8	+36.3	+46.7

* Base formulation (pts by wt): PVC resin—100 pts; plasticizer (as indicated)—65 pts; dibasic lead phthalate—8.0 pts; low mol wt polyethylene—1.0 pt

† Chlorophenyl Diphenyl Phosphate

TABLE V—EFFECT OF SOIL BURIAL ON THE TENSILE PROPERTIES OF PVC PLASTICS

No.	PVC Plastic*		Tensile Strength				Elongation				S-100 Modulus			
	Plasticizer, 65 phr (Blends 45/20 phr)	Filler 50 phr	Orig psi	% Change After 32 Months			Orig %	% Change After 32 Months			Orig psi	% Change After 32 Months		
				Shelf	Topsoil	Subsoil		Shelf	Topsoil	Subsoil		Shelf	Topsoil	Subsoil
126-67	DOP/Nitrile Rubber	None	2195	−2.1	+1.0	+9.6	303	−4.3	+1.6	+11.5	1335	−2.2	−4.4	−0.1
128-67	DOP/Cl Hydrocarbon	None	3014	−6.5	+0.7	+0.6	383	−2.1	−7.3	−5.5	1504	−3.4	+6.0	+3.7
127-67	DOP/Cl Polyethylene	None	2580	+0.7	+9.3	+7.4	297	+4.4	+5.4	+6.4	1631	+1.8	+7.5	+7.0
124-67	DOP/Polyester M.M. Wt	None	2611	−5.4	+3.9	+9.6	367	−3.3	−7.6	+0.3	1215	−1.9	+16.5	+18.0
125-67	DOP/Polyester H.M. Wt	None	2422	+1.6	+13.7	+13.3	360	+9.7	−1.4	−3.6	1099	+1.0	+20.8	+23.7
130-67	TCP/Cl Hydrocarbon	None	3213	−5.7	−1.1	+0.4	347	−9.2	−13.5	−7.8	1836	−4.6	+7.8	+2.4
129-67	DIPENTA Ester/Cl Hydrocarbon	None	2751	+1.3	+5.7	+7.6	353	−2.3	−5.1	−3.1	1758	+2.2	+4.0	+11.3
131-67	DOP	$CaCO_3$, ppt	2120	−3.4	+9.4	+2.0	300	−8.3	−5.0	−1.7	1232	+5.7	+11.0	+5.0
132-67	DIPENTA Ester	$CaCO_3$, ppt	1994	−2.3	+4.0	+5.7	247	−10.9	+0.8	+4.0	1551	−0.8	+1.0	+1.4
133-67	DOP	$CaCO_3$, limestone	2270	−0.4	−0.4	−4.6	260	+26.9	+15.4	+17.3	1489	−15.3	−15.6	−17.1
134-67	DOP	$CaCO_3$, limestone†	2064	−2.5	−2.2	+4.3	277	+19.7	+18.1	+12.6	1194	−14.2	−16.1	−12.5
135-67	DOP	Clay, calcined	2000	−6.4	+0.6	+1.3	290	−1.7	−2.1	−4.5	1416	−5.6	−5.2	−1.6
136-67	DIPENTA Ester	Clay, calcined	1744	+6.7	+9.8	+11.3	170	+11.8	+19.4	+8.2	1628	+3.9	+4.7	+7.2
137-67	DOP	Hydrated Alumina‡	1710	+2.2	+9.5	+7.1	260	+11.5	+20.8	+12.7	1275	−1.7	−0.2	−2.9

* Base formulation (pts by wt)—PVC resin—100 pts; plasticizer (as indicated)—65 pts; dibasic lead phthalate—8 pts; filler (as indicated)—50.0 pts; low mol wt polyethylene—1.0 pt
† Treated with organic coating
‡ 65 phr

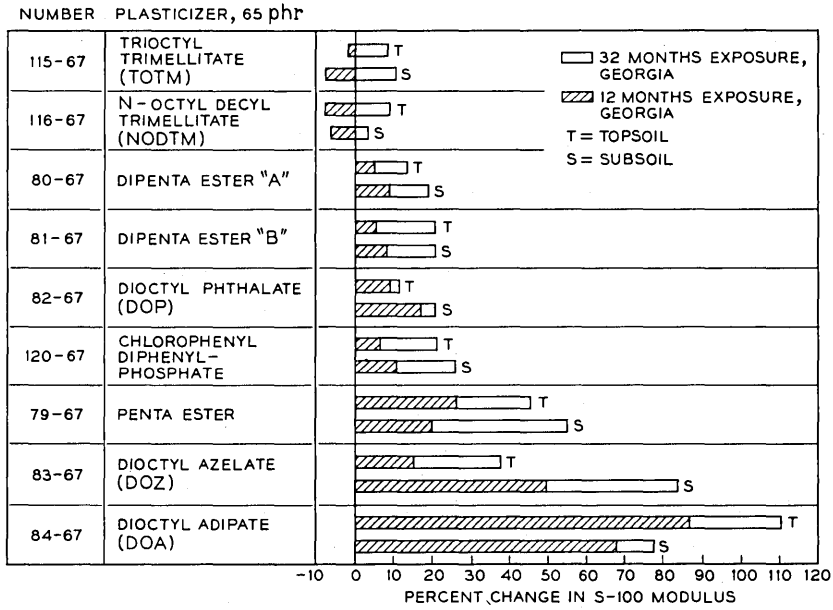

Fig. 9—Effect of soil burial on the modulus of sheet vinyls containing monomeric and dimeric plasticizers.

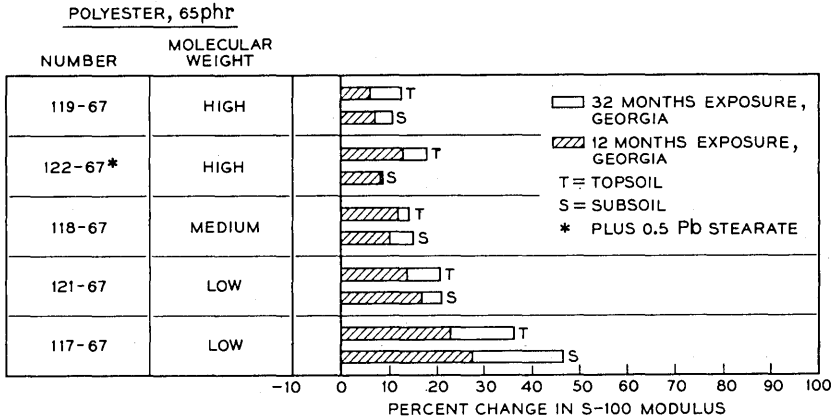

Fig. 10—Effect of soil burial on the modulus of sheet vinyls containing polyester plasticizers.

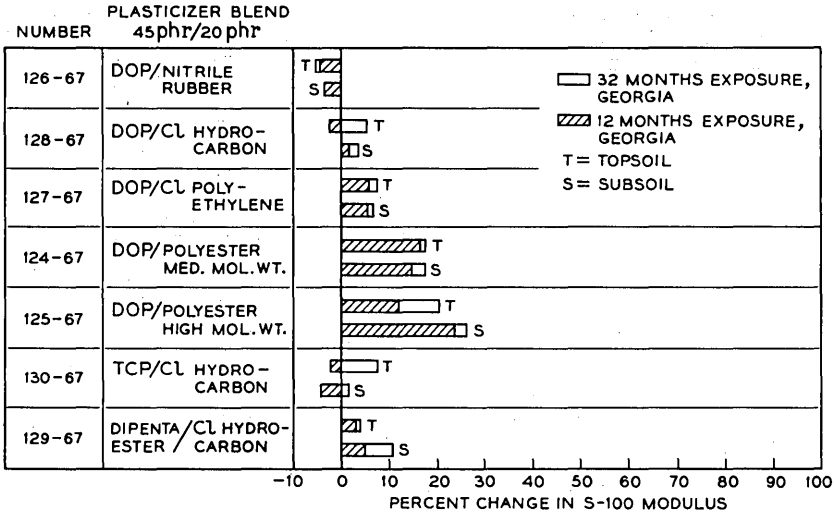

Fig. 11—Effect of soil burial on the modulus of sheet vinyls containing plasticizer blends.

TABLE VI—PLASTICIZER ANALYSIS ON SHEET SAMPLES AFTER SOIL BURIAL

No.	Plasticizer	Percent Plasticizer			
		Original	32 Months Soil Burial, Ga.		Loss After Exposure (Avg)
			Topsoil	Subsoil	
115-67	TOTM	37.2	36.9	36.5	−0.48
116-67	NODTM	38.1	36.0	36.2	−2.07
80-67	DIPENTA ESTER "A"	37.2	36.7	36.2	−0.80
82-67	DOP	37.2	36.3	34.7	−1.69
83-67	DOZ	37.1	28.9	26.6	−9.35
84-67	DOA	37.0	27.0	26.3	−10.33
119-67	Polyester, high mol wt	38.9	34.6	34.0	−4.60
118-67	Polyester, med. mol wt	39.5	35.9	35.7	−3.75
121-67	Polyester, low mol wt	38.7	36.0	35.8	−2.82
117-67	Polyester, low mol wt	38.0	32.8	30.4	−6.44
128-67	DOP/Cl Hydrocarbon	37.3	36.2	35.8	−1.05
130-67	TCP/Cl Hyrdocarbon	37.4	37.1	37.3	−0.20
129-67	DIPENTA ESTER/ Cl Hydrocarbon	37.3	36.8	36.3	−0.78

A number of compositions exhibiting good permanence were prepared with plasticizer blends in which a strong primary was partially replaced with a secondary or less efficient plasticizer (Fig. 11). Where the replacements were nitrile rubber, chlorinated hydrocarbon, or chlorinated polyethylene, an improvement was observed over 100 percent of the primary (see Figs. 9 and 11). No advantage was observed in the use of polyesters in such blends.

The addition of high loadings of inorganic fillers does not seem to have had a critical effect on resistance to soil burial (see Table V). In general, the loaded compositions showed equal or superior permanence in tensile tests when compared with unfilled controls. The limited changes recorded correspond to those observed over the same period during shelf aging and are believed to reflect testing variables.

6.2 *Discussion*

The observed tendency of vinyl plastics to increase in stiffness or modulus with soil burial is in general agreement with the literature in which a loss in extensibility and an increase in tensile strength are reported. Results of this nature were obtained in studies made by the Bureau of Reclamation on 8–10-mil vinyl sheeting in seven-year accelerated laboratory soil burial tests and on samples taken from field service in Wyoming (seven years) and in New Mexico (four years).[6] A vinyl tape pipe coating plasticized with dioctyl phthalate was found by B. I. Borisov, et al., to have lower extensibility and higher tensile strength after five years burial on the Dashave-Minsk gas pipe line.[10] Infrared spectra of films pressed from the coating showed an intensification of hydroxyl and carbonyl bands. It was inferred by the authors that this resulted from oxidation of both the resin and the plasticizer induced by micro-organisms. This deduction is debatable since an attack on the resin would be expected to reduce strength rather than increase it, as observed, and, further, our experience has shown that dioctyl phthalate extracted from soil burial samples is unchanged. An alternate explanation for the intensification of these bands might be found in the possibility that fractions from a bitumen primer on the pipe line might have been absorbed by the vinyl tape to yield the observed spectra.

Where an increase in stiffness occurs in a vinyl it may be attributed to a loss in plasticizer and the magnitude of the increase is roughly proportional to the plasticizer loss (see Table VI). Plasticizer is believed to be lost through diffusion to the surface of the coating, followed by migration to the soil environment. Utilization of plasticizers by micro-

organisms in their life cycle is recognized as a primary cause of plasticizer loss in vinyls.[11,12] It has been postulated that this utilization by both bacteria and fungi occurs as an interfacial absorption and that the micro-organisms do not, as a rule, penetrate the plastic mass.[1] This is believed to be the case since there is no evidence of the decomposition of the retained plasticizer or the presence of by-products that might result from such decomposition.

Other migration forces, such as those presented by soil minerals and water, should not be overlooked as causes of plasticizer loss. Powdered silicas and calcium carbonate in intimate contact with vinyl plastics have been shown to have the capability of removing plasticizer.[13,14] The extraction of plasticizer from vinyl plastics by water has been demonstrated to take place by E. F. Schultz, who investigated the variables involved.[15] In the case of both inorganic powders and water, when saturation conditions occur, the further removal of plasticizer is prevented. This might be a partial explanation for the leveling effects observed in Figs. 5 and 6.

VII. ENGINEERING IMPLICATIONS

From the results of these studies it is evident that both polyethylene and vinyl chloride plastics may be selected that resist soil degradation and maintain, to a high degree, their engineering properties after long-term soil burial. They cannot be expected, however, to provide, in all cases, completely continuous coatings over a conductor because of chance damage by macro-organisms. Thus, they represent a poor risk as a primary electrical insulation unless additional protection, for example, in the form of a metal foil, is forthcoming. As sheath or jacketing on buried wire and cable they may be expected to perform satisfactorily where an occasional discontinuity may be tolerated. In these applications they would offer mechanical protection and serve as a secondary insulation. Since the environmental resistance of properly selected polyethylene and vinyl chloride plastic are adequate, their selection for a given application will depend mainly on unrelated properties, such as toughness, low-temperature flexibility, or flammability.

VIII. CONCLUSIONS

8.1 *Polyethylene*

Polyethylenes show excellent resistance to decomposition after long-term soil burial. The principal changes observed in the tensile

properties of the coatings are believed to result from alterations in their crystallinity with time and to be unrelated to the soil environment. Coatings prepared with low-density resins, in general, show only minor changes in tensile properties, whereas those prepared with high-density resins may suffer a severe loss in elongation.

The electrical insulation and capacitance of the coatings remained essentially constant, which is believed to reflect the absence of chemical change in these coatings. The decrease observed in the breakdown strength is attributed to chance mechanical damage which, in part, is the result of insect attack.

8.2 *Vinyl Chloride Plastics*

Vinyl chloride plastics vary with regard to their resistance to soil burial, depending primarily on their plasticizer content. The more permanent vinyls show a moderate initial increase in stiffness with time and then appear to level off while they still retain a high percentage of their original properties.

Among the recently examined plasticizers found to show promise in vinyls for soil burial are the trioctyl and n-octyl n-decyl trimellitate, and blends of nitrile rubber, a chlorinated hydrocarbon, and a chlorinated polyethylene with a primary plasticizer such as dioctyl phthalate. Confirmation was obtained for the superiority of the dimer esters of pentaerythritol over the monomeric esters and that vinyls prepared with polyesters may resist change on soil burial.

Loading vinyls with various types of inorganic fillers does not appear to have any significant effect on their resistance to soil burial.

IX. ACKNOWLEDGMENTS

The author expresses appreciation to H. M. Zupko and D. Sgroi for sample preparation, R. P. Wentz for physical testing, E. H. Brilhart and W. E. Williamson for electrical measurements, and H. Gaupp for analytical data. The voluminous records for this study were ably kept by L. Dorrance.

REFERENCES

1. DeCoste, J. B., "Soil Burial Resistance of Vinyl Chloride Plastics," I & EC Product Research and Development, *7*, 1968, pp. 238–247.
2. Howard, J. B., *Crystalline Olefin Polymers, Part II, Stress-Cracking*, R. A. Raff and K. W. Doak, Eds., New York: Interscience, 1964, p. 47.
3. Amer. Soc. For Testing and Materials, Philadelphia, Pa., "ASTM Standards—Parts 26, 27 & 28," 1970.
4. Luongo, J. P., "Infrared Study of Oxygenated Groups Formed in Polyethylene During Oxidation," J. Polymer Sci., *42*, 1960, pp. 139–150.

5. Kulman, F. E., "Microbiological Deterioration of Buried Pipe and Cable Coatings," Corrosion, *14*, 1958, pp. 213t–222t.
6. U. S. Dept. of the Interior, Bureau of Reclamation Research Report No. 19, *Investigations of Plastic Films for Canal Linings*, Washington: U. S. Govt. Print. Off., 1969.
7. Jen-Hao, L. and Schwartz, A., "The Action of Bacteria Mixtures on Polyethylene of Various Molecular Weights," Kunstoffee, *51*, 1961, pp. 317–319.
8. Howard, J. B., "Engineering Thermoplastics for Ocean Telephone Cables," Plastics Technology, *5*, 1959, pp. 57–61, 68.
9. Connolly, R. A., DeCoste, J. B., and Gaupp, H. L., "Marine Exposure of Polymeric Materials and Cables After Fifteen Years," ASTM J. Materials, *5*, No. 2 (1970), pp. 339–362.
10. Borisov, B. I., Valuiskaya, D. P., Rozova, E. D., and Noskov, S. K., "Changes in the Properties of Vinyl Chloride Films Under Subterranean Conditions," Zhurnal Prikladnol Khiml, *41*, 1968, pp. 877–882.
11. Dolezel, B., "The Resistance of Plastics to Micro-Organisms," British Plastics, *40*, 1967, p. 105.
12. Tirpak, G., "Microbial Degradation of Plasticized PVC," SPE J., *26*, 1970, pp. 26–30.
13. Geenty, J. R., "A Study of Plasticizer Migration in Vinyl Compounds," India Rubber World, *126*, 1952, pp. 646–649.
14. Reed, M. C., Klemm, H. F., and Schultz, E. F., "Plasticizers in Vinyl Chloride Resins—Removal by Oil, Soapy Water, and Dry Powders," Ind. & Eng. Chem., *46*, 1954, pp. 1344–1349.
15. Schultz, E. F., "Improved Water Extraction Test for Poly(vinyl chloride) Elastomers," ASTM Bull., *183*, 1952, pp. 75–78.

Copyright © 1972 American Telephone and Telegraph Company
THE BELL SYSTEM TECHNICAL JOURNAL
Vol. 51, No. 1, January, 1972
Printed in U.S.A.

Soil Burial Tests:

Effect of Soil Burial Exposure on the Properties of Rubber, Crosslinked Polyethylene, and Vulcanized Wire Coatings

By G. H. BEBBINGTON

(Manuscript received August 24, 1971)

Vulcanized rubber and polyethylene coated wires, molded specimens, and rubber-to-metal bonded test samples were buried in both alkaline and acid soils to determine the effects of these environments. Results show that:

(i) Most wire samples suffered a loss in insulation resistance, but retained their physical strength.

(ii) Insect and rodent chewing have caused varying test results in the dumbbell-shaped molded samples.

(iii) Rubber-to-metal bonds have failed due to corrosion in most samples using aluminum and cold-rolled steel, while stainless steel samples have retained strong bonds. The adhesion of insulations to aluminum conductors has also failed.

(iv) Black, chemically crosslinked polyethylene has been essentially unaffected by soil exposure.

Soil burial test exposures of improved and more recent materials are continuing.

I. INTRODUCTION

Rubber and other vulcanized polymers play an important role in the construction of a great deal of the hardware and equipment used in the Bell System. The uses range from wire and cable jackets and insulations to molded goods, such as the floor tiles in phone booths, splicing tape, underground conduit and couplings, waveguide supports, and manhole seals. Through the years more and more of the plant

equipment has been and will be buried, necessitating the development of vulcanizate compounds that can withstand the rigors of different soil environments to provide twenty to thirty years service life.

O. DeVries reported the destruction of 22 percent of the hydrocarbons of "fresh raw rubber" by fungi in two years and 30 percent in five years.[1] But one must question the purity of any sample of natural rubber (NR) and assume that the diluents therein have promoted this degree of consumption, for it has been found that most pure synthetic polymers, by themselves, are generally resistant to fungi, i.e., polymers do not serve as a source of carbon for the growth of fungi.[2,3] However, they do not inhibit their growth. For this reason, the assorted ingredients that are added in making up a useable compound must be selected with care to be sure that they are not biologically susceptible. Although individual components may be resistant, in combination with others they may be susceptible to deterioration. Therefore, many combinations must be studied to find the most resistant vulcanizates.

Soil burial tests on various designs of tape, underground drop wire, and coaxial cable and on other experimental materials were started in 1929 and continued until late 1954. The results were evaluated and new soil burial tests were proposed to investigate additional materials and structures of possible interest for Outside Plant use. For this purpose, the Bell Laboratories Rubber Research Group supplied the below-listed items which were buried in 1958 in the moist, highly acid soil of the Bainbridge Environmental Test Plot in Georgia. Matched control specimens of all samples were put into storage for future comparative testing.

(*i*) *Wire Coatings.* Specimens consisted of 22 vulcanized wire samples (Table I) using both #22 AWG electrical-grade aluminum and 0.027-inch lead- and brass-coated copper-steel wire conductors. The coatings included 10 jacket compounds utilizing 7 different rubber polymers, and 6 insulation compounds made from 3 rubbers. Several fungicides were added to one of the insulations and one of the jacket formulations. A 48-volt dc potential was applied to half of the buried specimens.

(*ii*) *Molded Goods.* Dumbbell-shaped test specimens were cut from vulcanized sheets of 7 then-current rubber molding compounds (#260–266) utilizing 5 different polymers. Additional rubber and crosslinked polyethylene (XPE) molding compounds (#290–299) were added later for a total of 17 compounds in test. The formulations for the above are listed in Table II.

(*iii*) *Adhesion Studies.* Various vulcanized rubber-to-metal bonded

specimens (#267–281) were made up using 3 different rubber compounds (Table III), 3 metals (aluminum, cold-rolled steel, and stainless steel sheet), and several proprietary bonding systems.

In 1959, crosslinked polyethylene insulated wires #485–490 (Table IV) were added to the test. Further additions of vulcanized test samples (#322–324), shown in Table V, were made when the new ethylene-propylene rubber polymers (EPM and EPDM) became available.

Duplicate specimens of most of the above materials were buried in 1960 in the dry, extremely alkaline soil of the Roswell Environmental Test Plot in New Mexico. Later additions were made in 1965.

II. VULCANIZED INSULATED WIRES

2.1 *Rubber Covered Wires*

2.1.1 *Exposure Results*

While the specimens under potential usually have shown more degradation than those without potential, essentially no significant difference in capacitance or in insulation resistance was found between the samples aged with and without the applied 48-volt dc potential. However, because of the drastic reduction of insulation resistance that developed in the buried rubber covered wires during the first year, the potential had to be removed from most of these wires. The total current drain exceeded the fuse capacity of the test area. After a year and a half, only 6 of the original 22 types of rubber coverings (Table I) could be continued in the test with an applied potential. These were compounds #305, 311, 314, 315, 317, and 321. Interestingly, only #305 contained a fungicide, while both #317 and #321 were on aluminum conductors.

Because of the generally poor condition of the samples and the deterioration in electrical properties, only the 1-kHz measurements for capacitance, conductance, and insulation resistance were performed. The nonblack butyl (IIR) insulation #312, for example, was found to be discolored and cracked after only one year in the soil. After two years of exposure, the IIR jacket #313 could not even be measured on the test equipment. Conversely, the heat and water resistant chlorosulfonated polyethylene elastomeric (CSM) jacket #314 and #321 was the one exception since the insulation resistance increased somewhat on both aluminum and copper conductors.

In the current testing program one fungicide, copper-8-quinolinolate, was found to inhibit microbiological attack to a considerable degree

TABLE I—VULCANIZED WIRE JACKET AND INSULATION COMPOUNDS

Ingredients	Compound Type	NR Ins	NR Jkt	SBR Ins	SBR Ins	SBR Ins	SBR Ins	SBR Jkt	CR Jkt	CR Jkt	CR Jkt	CR Jkt	NBR Jkt	IIR Ins	IIR Jkt	CSM Jkt	SI Jkt
	Copper-Steel Cond (Aluminum Cond)	300	301 (316)	302	303	304	305	306 (317)	307 (318)	308 (319)	309	310	311	312	313 (320)	314 (321)	315
Elastomers																	
Reclaimed Rubber (NR)			29.0														
Natural Rubber—Smoked Sheet (NR)		100.0	85.0														
Styrene-butadiene Rubber GR-S 1007 (SBR)				100.0	100.0	100.0	100.0										
Styrene-butadiene Rubber GR-S 1712 (SBR)								100.0									
Polychloroprene W (CR)									100.0	100.0	100.0	100.0					
Butadiene-acrylonitrile Copolymer 1001 (NBR)													100.0				
Isobutylene-isoprene Copolymer 035 (IIR)														100.0	100.0		
Chloro-sulfonated Polyethylene Elastomer 20 (CSM)																100.0	
Silicone Rubber 80 (SI)																	100.0
Fillers																	
Calcium Carbonate				55.0	55.0	55.0	55.0							90.0			
Zinc Oxide		67.0	25.0	5.0	5.0	5.0	5.0	5.0	3.0				5.0	5.0	5.0		
Hard Clay								30.0	40.0	40.0	40.0	40.0				60.0	
Ex. Light. Calcined Magnesium Oxide									3.0								
Easy-processing Channel (EPC) Black			27.0														
Fast-extruding Furnace (FEF) Black								25.0					60.0		50.0	10.0	
Semi-reinforcing Furnace (SRF) Black								25.0	52.0	52.0	52.0	52.0					
Reinforcers and Plasticizers																	
Mineral Rubber		47.0		50.0	50.0	50.0	50.0										
High Styrene Resin				27.0	27.0	27.0	27.0										
Hydrogenated Rosin																2.5	
Aromatic Hydrocarbon Resin																10.0	
Sulfonic Acid—Paraffin Oil			1.08														
White Petroleum Grease																3.0	
Dibutyl Phthalate													15.0				
Light Process Oil									17.86	17.86	17.86	17.86				7.0	

TABLE I—VULCANIZED WIRE JACKET AND INSULATION COMPOUNDS (Continued)

Ingredients	Compound Type	NR Ins	NR Jkt	SBR Ins	SBR Ins	SBR Ins	SBR Ins	SBR Jkt	CR Jkt	CR Jkt	CR Jkt	CR Jkt	NBR Jkt	IIR Ins	IIR Jkt	CSM Jkt	SI Jkt
	Copper-Steel Cond (Aluminum Cond)	300	301 (316)	302	303	304	305	306 (317)	307 (318)	308 (319)	309	310	311	312	313 (320)	314 (321)	315
Age Resistors																	
65 N-phenyl-beta-naphthylamine/35 dppd		1.0		0.5	0.5	0.5	0.5	3.0									
Sym. dibetanaphthyl-ppd		1.0	0.90	0.5	0.5	0.5	0.5										
Trimethyl dihydroquinoline													3.0			2.0	
N-phenyl-alpha-napthylamine			1.35														
N-phenyl-beta-napthylamine									2.0	2.0	2.0	2.0				1.0	
Nickel dibutyl dithio carbamate														1.2	1.2		
NN′-bis (1-ethyl-e-methyl pentyl) ppd																	
Paraffinic wax—Heliozone—E. I. duPont		1.0	4.5	5.0	5.0	5.0	5.0						4.0			2.0	
Paraffinic wax—Sunwax 4414-Sun Oil								3.0									
Paraffinic wax—Herron wax #24—Herron Bros.									4.0	4.0	4.0	4.0					
Paraffinic wax—AA-1177 wax—Allied Asphalt														4.8	4.8		
Paraffin wax — — —Esso									4.0	4.0	4.0	4.0					
Fungicides																	
Copper-8-quinolinolate							1.0					2.0					
N-trichloromethylthio-4-cyclohexane 1,2 dicarboximide					2.0												
Zinc dimethyl-dithio carbamate + zinc-2-mercapto benzothiazole											2.0						
Dihydroablethylammonium pentachloro-phenoxide						2.0											
Curing Agents																	
2-Mercaptobenzothiazole															1.0		
pp′-Dibenzoylquinonedioxime														6.0			
Di-ortho-tolylguanidine		0.22	0.18						0.5	0.5	0.5	0.5					
Lead monoxide				1.5	1.5	1.5	1.5	1.5							40.0		
Benzothiazole disulfide															0.5		
2-Mercaptiomidazoline									0.4	0.4	0.4	0.4					
Poly-para-dinitrosobenzene														0.4			
Red lead oxide										20.0	20.0	20.0		9.0			
2-Napthalenethiol		0.45	0.75	0.8	0.8	0.8	0.8	1.5									
Stearic Acid		1.0	—	1.0	1.0	1.0	1.0						1.0	1.5	2.0		
Sulfur		4.0	5.1	4.0	4.0	4.0	4.0	2.0	1.0	1.0	1.0	1.0	2.0	1.5	2.0		
Dipentamethylene thiuram tetrasulfide																0.5	
Tetra methyl thiuram monosulfide		0.33	0.43	0.5	0.5	0.5	0.5	0.5	0.5	0.5	0.5	0.5	0.5				
Tetra methyl thiuram disulfide															1.0		

TABLE II—VULCANIZABLE MOLDING COMPOUNDS–FORMULATIONS

Ingredients	Number / Compound	260 M210C	261 M206	262 M247	263 M226	264 M246	265 M252	266 M252A	290	291	292	293 H-60-16	294 M269	295 H-61-8 H-61-9	296 H-60-8	297 H-61-9	298 M278	299 H-64-1
Polymer																		
Natural Rubber-Smoked Sheet	(NR)	100.0																
Styrene-butadiene Rubber-1004	(SBR)		100.0								25.0							
Polychloroprene Rubber-GN	(CR)			100.0														
Butadiene-acrylonitrile Rubber-1041	(NBR)				100.0													
Butadiene-acrylonitrile Rubber-1042	(NBR)					100.0												
Isobutylene-isoprene Copolymer-218	(IIR)						100.0	100.0										
Polyethylene-DYOB	(PE)								100.0									
Polyethylene-DYNH	(PE)									100.0	75.0							
Ester Urethane Rubber-509												100.0						
Polychloroprene Rubber-WX	(CR)												100.0					
Ethylene-propylene Copolymer-60	(EPM)													100.0				
Chlorosulfonated Polyethylene-40	(CSM)														100.0			
Ethylene-propylene-diene Terpolymer-1070	(EPDM)															100.0	100.0	
Ether Urethane Rubber-C																		100.0
Fillers																		
Easy-processing Channel	(EPC) Black			20.0	50.0								25.0					
Fast-extruding Furnace	(FEF) Black					40.0											20.0	
Medium-thermal	(MT) Black								418.0	100.0	100.0	100.0	55.0	100.0	25.0		20.0	
Semi-reinforcing Furnace	(SRF) Black	47.0	45.0				50.0	50.0										40.0
High-abrasion Furnace	(HAF) Black															50.0		15.0
Hard Clay				80.0													125.0	
Plasticizers																		
Polyethylene-8406																		3.0
Pine Tar		2.0																
Light Process Oil			15.0	12.0			5.0	5.0								20.0		
Para Coumarone-indene Resin P-10					20.0													
Mineral Rubber													10.0					
Polyether-TP-90B													10.0					
Aromatic Type Oil-53																	30.0	10.0

TABLE II—VULCANIZABLE MOLDING COMPOUNDS–FORMULATIONS (Continued)

Ingredients	Number	260	261	262	263	264	265	266	290	291	292	293	294	295	296	297	298	299
	Compound	M210C	M206	M247	M226	M246	M252	M252A				H-60-16	M269	H-61-8 H-61-9	H-60-8	H-61-9	M278	H-64-1
Protectants																		
Phenyl-beta-napthylamine (PBNA)		1.0																
65%PBNA/35% Diphenyl-p-phenylenediamine				3.0									3.0					
Nickel Dibutyl Dithiocarbamate															3.0			
Paraffinic Wax Blend #1*			3.0															
Paraffinic Wax Blend #3†				4.0									3.0					
Paraffinic Wax Blend #6‡							6.0	6.0										
Vulcanizing Agents																		
Stearic Acid		3.0		0.5	1.5	1.0							0.5				1.0	
Tetramethyl Thiuram Disulfide		0.1				2.5	1.0											
2-Mercaptobenzothiazole		1.0														0.5	1.5	1.0
Zinc Oxide		5.0		5.0	5.0	5.0	5.0	5.0					5.0			5.0	5.0	
Magnesium Oxide				4.0														
Zinc Chloride 2 Benzothiazolyl Disulfide																	0.35	
Tetramethyl Thiuram Monosulfide			0.4		0.5											1.5		
Benzothiazyl Disulfide															0.5			3.0
Di-ortho-tolyguamidine Salt of Dicatechol Borate				0.25														
Piperidinium Pentamethylene Dithiocarbamate				0.3														
4,4'-Dithiodimorpholine						1.5												
Diabenzoyl-p-quinone Dioxime								3.0										
Red Lead Oxide (Pb_3O_4)								10.0										
Tetra Methyl Thiuram Disulfide													0.5					
Sulfur		3.0	2.0		1.25		1.5									1.5	2.5	1.5
Dicumyl Peroxide-R (96-99%)									4.0	4.0	4.0	4.0		4.0				
2-Mercaptiomidazoline													1.0					
Lead Monoxide-Litharge															20.0			
Dipentamethylene Thiuram Tetrasulfide															0.75			
Zinc Dimethyldithiocarbamate																	1.5	

* Heliozone—E. I. duPont
† Herron Wax #24—Herron Bros.
‡ AA-1177-20 [Wax + 20% N,N'-bis (1-ethyl-e-methyl) p-phenylene diamine-Allied Asphalt]

TABLE III—RUBBER COMPOUNDS USED IN BONDING STUDY

Ingredients	M-206	M-210C	M-204
Styrene butadiene copolymer—SBR 1004	100.0	—	—
Natural rubber—smoked sheet		100.0	—
Polychloroprene—GNA			100.0
Black—SRF	45.0	47.0	—
Black—HAF			50.0
Light process oil	15.0	—	15.0
Pine tar		2.0	—
Paraffinic wax	3.0	—	—
Zinc oxide	5.0	5.0	5.0
Stearic acid		3.0	0.5
Phenyl beta naphthylamine		1.0	1.5
Sulfur	2.0	3.0	—
Tetramethylthiuram monosulfide	0.4	—	—
Benzo thiazyl disulfide	0.4	—	—
2-Mercapto benzothiazole		1.0	—
Tetramethylthiuram disulfide		0.1	—
Magnesia—extra light calcined			4.0
Diorthotolyl guanidine salt of dipyrocatechol borate			0.4

in the styrene-butadiene rubber (SBR) insulation #305. This same fungicide offered no protection, however, to the polychloroprene (CR) jacket #310, although it has been reported as giving CR "complete protection against fungus attack."[4]

In general, the mechanical properties of the rubber wire coatings that were intact and not damaged by insects or micro-organisms were not seriously affected. The natural rubber compounds #300, 301, and 316 showed some softening and the SBRs #302–306 and 317 changed little, while most of the polychloroprenes tended to harden. The CR (#310) containing copper-8-quinolinolate fungicide, however, showed some softening. The butadiene-acrylonitrile copolymer (NBR) compound #311 hardened more than the other compounds. Its compression resistance measurement (see Appendix A) doubled in only one year. This degree of hardening was not expected.

Although the adhesion* of the wire coating to the conductor varied considerably, in general it appeared that the burial did not reduce adhesion materially. The exceptions were those wires in which the conductor had corroded and those with the blistered jackets, which

* Adhesion test—measurement of the resistance in pounds required to pull a 1-3/8 inch length of conductor free from 3/8 of an inch of insulation.

TABLE IV—CROSSLINKED POLYETHYLENE WIRE JACKETS

Ingredients	#485	#486	#487	#488	#489	#490
			Composition in Parts			
Polyethylene DYNH	100.0	100.0	100.0	100.0	100.0	100.0
Medium Color Channel Black	2.0	2.0	2.0	—	2.0	2.0
Medium Thermal Black	—	50.0	100.0	—	—	50.0
Calcium Carbonate	—	—	—	50.0	—	—
Dicumyl Peroxide—T—(90–92%)	2.5	2.5	2.5	2.5	—	—
2,5-Di-*t*-butylperoxy-2,5-Dimethyl Hexane Powder	—	—	—	—	4.0	4.0
			Extrusion Conditions			
Cylinder Temperature °F	210	210	200	230	190	260
Head Temperature °F	270	275	280	270	270	275
Worm Speed RPM	15	15	12	17	17	15
			Compression (1-inch jaw-2000 lbs)			
Original	1110	940	610	690	1030	820
Original + 2 days 212°F oven	1360	970	590	640	1250	780
8 years—New Mexico	1190	1020	619	62	1409	844
11+ years—shelf-aged control	—	—	—	721	—	—
			Mooney Scorch (320°F-small rotor at 2 rpm)			
Minimum (M)	4.4				4.2	
Time to minimum (TM)	1.0				2.4	
TM + 2 point rise	3.9				8.0	
TM + 5 point rise	5.2				12.2	
TM + 10 point rise	6.3				17.9	
TM + 35 point rise	11.5				66.0	

TABLE V—RECENT ADDITIONAL WIRES IN TEST
(Ethylene-propylene Copolymer and Diene-modified Terpolymer)

Ingredients	Compound Type	#322 EPDM Jkt	#323 EPM Jkt	#324 EPM Ins
Ethylene-propylene-diene-terpolymer (EPDM) Rubber 1040		100.0	—	—
Ethylene-propylene-copolymer (EPM) Rubber 404			100.0	100.0
Fast-extruding furnace (FEF) Black		100.0	25.0	—
High abrasion-low structure-furnace (HAF-LS) Black			50.0	—
Semi-reinforcing furnace (SRF) Black				3.0
Treated Aluminum Silicate Complex				110.0
Trimethyl Dihydroquinoline			1.0	1.0
Zinc Oxide		5.0	5.0	5.0
Naphthenic Petroleum Oil, ASTM Type 3		50.0	25.0	—
Paraffinic Petroleum Oil, ASTM Type 4				35.0
Stearic Acid		1.0	—	—
Sulfur		2.0	0.3	0.3
Dicumyl Peroxide T (90-93%)			4.25	4.25
Red Lead Oxide				3.75
Dibasic Lead Stearate				0.5
2-Mercaptobenzothiazole		2.0	—	—
50% Zinc Dimethyldithiocarbamate ±50% Tetramethylthiuramdisulfide		4.0	—	—
Tellurium Diethyldithiocarbamate		1.33	—	—
Compression Resistance (1-inch jaw, 2000 psi) after 4 years subsoil burial				
Roswell, N. M.	(alkali soil)	645	779	677
Bainbridge, Ga.	(acid soil)	663	409	260

were all specimens with the applied potential. The test showed that aluminum conductors of this type should not be buried since they corroded rapidly during exposure. Some parts of the aluminum conductors under the polychloroprene jackets #318 and #319 were completely corroded in less than a year. The above test results are given in Table VI.

Figure 1a shows a reeled length of the blistered SBR insulated wire #302A-1 and Fig. 1b is an enlargement of one of these blisters. This type of blister was common also on the A-1 samples (under potential) #303, 304, 308, and 310.[5] The copper-steel conductors under the rubber insulation of some of these were found to contain pits due to corrosion in their copper coatings. But not all blistered specimens had corrosion pits, nor did all pitted specimens have blistered insulations. Pronounced

TABLE VI—TEST RESULTS ON RUBBER COVERED WIRE AFTER ONE YEAR SOIL BURIAL AT BAINBRIDGE

Sample	Compression Resistance					Adhesion				
		After Exposure					After Exposure			
	Original	With Potential	% Change	Without Potential	% Change	Original	With Potential	% Change	Without Potential	% Change
300 NR I	1700	1475	−13.2	1385	−18.5	8.0	6.9	−13.8	2.7	−66.3
301 NR J	1785	1785	0	1850	+3.6	9.1	3.9	−57.1	4.1	−55.0
302 SBR I	1005	1010	+1.0	970	−3.5	8.0	5.0	−37.5	6.5	−18.8
303 SBR I*	870	1230	+41.4	995	+14.4	7.6	6.5	−14.5	8.9	+17.1
304 SBR I†	1040	910	−12.5	995	−4.3	4.4	3.2	−27.3	3.8	−13.6
305 SBR I§	1105	1205	+9.1	1265	+14.5	7.2	8.9	+23.6	7.0	−2.8
306 SBR J	1415	1310	−7.4	1335	−5.7	4.5	3.9	−13.3	3.7	−17.8
307 CR J	900	1370	+52.2	1265	+40.6	0.6	3.8	+533.3	2.2	+266.7
308 CR J	1105	1595	+41.3	1540	+39.4	3.8	5.7	+50.0	3.9	+2.6
309 CR J‡	1395	2005	+43.7	1775	+27.2	9.7	9.8	+1.0	7.2	−25.8
310 CR J§	1425	1110	−22.1	800	−43.9	7.5	3.8	−49.3	3.0	−60.0
311 NBR J	1360	2415	+77.6	2780	+104.4	1.5	9.0	+500.0	7.4	+393.3
312 IIR I	920	1105	+20.1	1115	+21.2	10.1	8.1	−2.0	7.4	−36.6
313 IIR J	1090	835	−23.4	1170	+7.3	6.3	—	—	12.4	+96.8
314 CSM I	980	1335	+36.2	1330	+35.7	10.2	8.0	−21.6	9.4	−7.8
315 SI —	510	540	+5.9	510	0	0	0.9		—	
316 NR J	1785	1280	−28.3	1540	−13.7		—		—	
317 SBR J	1415	1055	−25.4	—	—		—		—	
318 CR J	900	—	—	—	—		—		—	
319 CR J	1105	—	—	—	—		—		—	
320 IIR J	1090	790	−27.5	740	−32.1		—		—	
321 CSM J	980	800	−18.4	800	−18.4		—		—	

* N-trichoromethylthio-4-cyclohexane 1, 2-dicarboximide
† Dihydroabiethylammonium pentachlorophenoxide
‡ Zinc dimethyldithiocarbamate and Zinc 2-Mercaptobenzothiazole
§ Copper-8-quinolinolate
I—Insulation J—Jacket
Note: All conductors are copper except #316 through #321 which are aluminum.

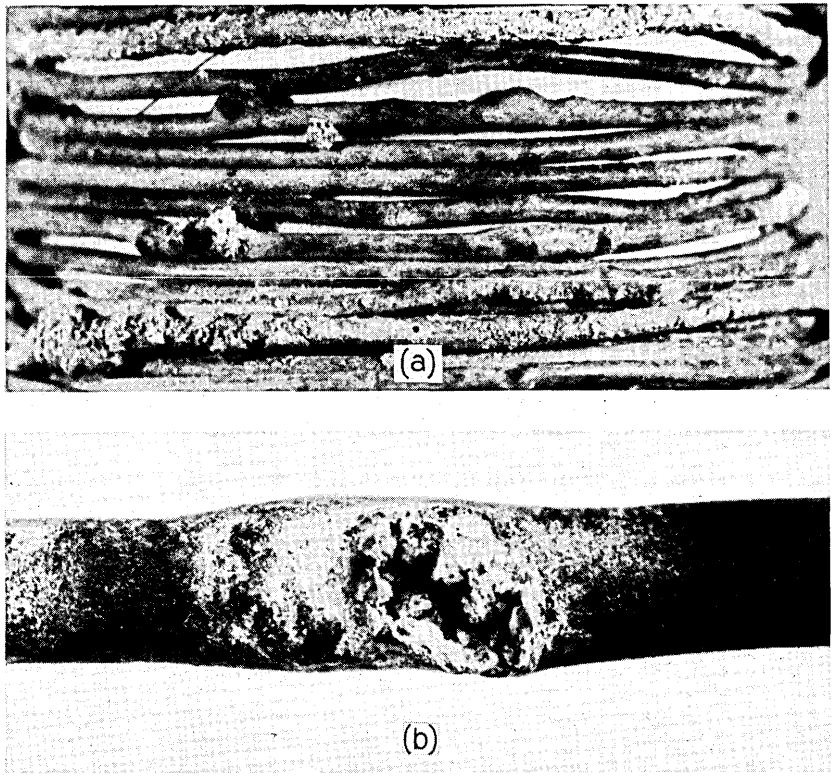

Fig. 1—(a) Blisters and surface deposits on a spool of SBR insulated wire #302A-1 after one year burial at Bainbridge. (b) Enlargement of a burst blister on this specimen.

pitting was found on the #305A-1 and #307A-1 samples and on the A-11 samples (without potential) #301, 304, 308, and 309. In general, the specimens under potential showed more degradation than those without potential and the degree of corrosion seemingly had little correlation with most of the rubber compounds tested.

2.1.2 *Discussion*

Corrosion has been defined as "a process by means of which metals undergo chemical reactions with nonmetallic elements in their environments producing chemical compounds which are either oxides or salts."[6] It has been well established that the process of corrosion is electrolytic in character.[7] A current flows between the anode and cathode areas and

the amount of corrosion is proportional to the amount of current flow.

Discrete corrosion cells appear to have been created at the blisters, possibly due to discontinuities, pinholes, foreign inclusion, or any inhomogeneities which are certain to exist[8] and thus supply a point of potential difference.[7] The rubber coatings are permeable and water accumulates under a coating in the form of the blisters providing a wet environment for the creation of an oxygen concentration cell.[9,10] R. M. Burns and W. W. Bradley have warned that an accumulation of alkali, natural or as a corrosion product, in the cathodic areas of the electrolytic cells may lessen adhesion, give rise to blistering, and cause chemical disintegration in the structure of the coating.[8]

Figure 2a is an example of a typical blister on one of polychloroprene

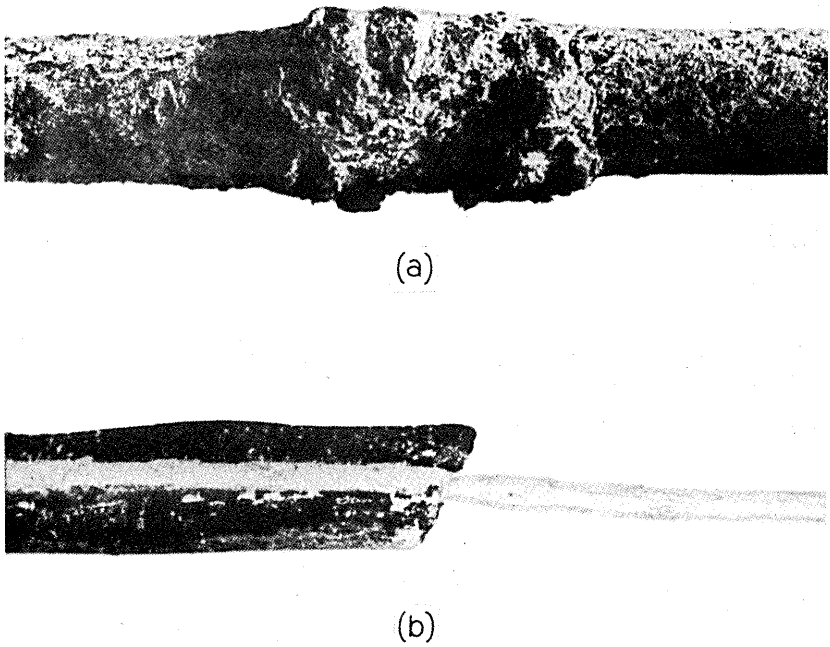

Fig. 2—(a) Typical blister on the polychloroprene jacketed aluminum wire #318A-1 after burial at Bainbridge for one year. (b) Cutaway section of one of these blisters revealing the severe corrosion of the aluminum conductor and the powdered aluminum oxide corrosion product.

jacketed aluminum wires (#318A-1) and Fig. 2b shows a cutaway section of one of these blisters which reveals the powdered aluminum oxide (Al_2O_3) corrosion product.[5] The conditions for corrosion of aluminum were so aggressive in some locations that the conductor was found to have completely corroded away leaving only the white oxide powder in its place after only a year's burial.

Aluminum is attacked by both alkalies and dilute acids (amphoteric).[7] With polychloroprene rubber, there is the possibility of the chlorination of the aluminum. Also, a high chloride content in the soil will destroy the protective oxide film and increase the conductivity of the electrolyte.[8] Additionally, the corrosion product on the surface influences the distribution of the attack, for beneath it the aluminum becomes anodic and corrodes.[11]

The loss in insulation resistance that occurred in this experiment is not necessarily a detriment in the case of the 15 jacket stocks, but it does mean that the 7 insulation compounds tested are virtually useless where soil burial is involved.

The loss in insulation resistance of buried insulated wire samples has been demonstrated before in other testing programs such as that of J. T. Blake, et al., and this loss was traced to soil fungi.[12,13] These microorganisms create micropores through the insulation which fill with water. The micropores occurred although the base hydrocarbon was stable. The fungi appear to consume the nutrient additives in the insulation, and the resultant tiny passages allow water to penetrate.

Also, the very poor performance demonstrated by the nonblack IIR insulation described above is similar to that reported by Blake, et al., for a white polychloroprene compound containing a hard clay filler.[13] They found this material to be more vulnerable to fungus attack than their black CR.

Because of the continuing trend of electrical and physical deterioration, further evaluations of the early rubber covered wires were discontinued after four years and the wires were removed from the test plots.

2.2 *Chemically Crosslinked Polyethylene Covered Wires*

Unlike the 1958 rubber covered wires, the crosslinked polyethylene wire specimens of 1959 and 1960 were left in the soil as planned. The black compounds showed no visible damage or loss in physical properties in the initial tests. Also, there seemed to be no indications of micropore formation. As can be seen in Table IV, these XPE compounds contained few additives and they did not contain plasticizers

which are usually quite susceptible to microbial degradation. Interestingly, though, after eight years the buried specimens without black (#488) were extremely brittle and resembled nonblack specimens that had undergone severe ultraviolet radiation exposure. To confirm that no UV degradation has occurred, an infrared spectrum was run on the brittle jacket by the Attenuated Total Reflectance method and it revealed a significant carbonyl absorption band but an absence of any UV-formed vinyl bands.[14] However, the specimens had the characteristic, butyric acid-like, rancid odor of oxidized polyethylene. Also, the conductor beneath the deteriorated white jacket (#488) was found to be badly corroded while the conductors under the black jackets were in excellent condition.

In addition to not containing any carbon black, the white stock was the only one that contained calcium carbonate. This deterioration was unexpected since calcium carbonate is often listed as being inert or resistant and even regarded as a protective additive.

Embrittlement and corrosion were first noted on the eight-year white specimens retrieved from the Roswell burial site. This deterioration had not been observed on the previous samples removed after only four years exposure. Although no XPE specimens had been retrieved after eight years of burial at Bainbridge, a special visual inspection was made after a little more than ten years and the same brittle condition was found.

Fortunately, small particle size channel carbon black at a concentration of less than 2 percent is evidently a very effective protectant for chemically crosslinked polyethylene under soil burial conditions. It should be noted, however, that the #487 sample with a 100-part loading (<50 percent) of the coarser medium thermal (MT) black does have some holes and chew marks.

Included in Table IV are the results of compression tests* conducted on specimens of the compound after aging for two days at 100°C. These data are of interest because they reveal how well the nonblack compound #488 withstood this type of thermal aging and yet deteriorated badly in the soil. Similarly, the control specimens of this white #488 wire that have been shelf-aged for eleven years have remained unaffected both visually and physically. The contrast between the buried and shelf-aged, white, crosslinked polyethylene specimens and the seemingly unaffected buried black specimens can be seen in Fig. 3. Although the specimens were exposed straight and unstrained, they

* See Appendix A.

Fig. 3—Chemically crosslinked polyethylene covered wires. (a) Cracked and brittle white jacket compound #488 retrieved after eight years burial in the soil at Roswell. (b) Well-preserved white jacket compound #488 after 11 + years of shelf-aging in storage at Bell Laboratories, Murray Hill, N. J. (c) Apparently unaffected 2-percent black polyethylene compound #485 retrieved after eight years burial in the soil at Roswell.

were later wrapped around a mandrel to illustrate the extreme brittleness of the buried white specimen #488.

No other reports have been found of this difference in the soil burial aging of black and white chemically crosslinked polyethylene.

Both chemical and physical change can initiate brittle failures in polyethylenes.[15] For example, oxidation mechanisms are chemical, while stress cracking and thermal embrittlement are physical. They can act singly or in concert and it was difficult to identify the cause in the soil environment. Water was present and cracking seems to have occurred.

The addition of a chemical crosslinking agent permits the relatively inexpensive use of the combination of a low molecular weight grade of polyethylene and carbon black. The chemistry of free radical production and crosslinking by dicumyl peroxide has been described by E M. Dannenburg, et al.[16]

In this exposure experiment, two different peroxide vulcanizing agents were used to produce a 30-mil-thick jacket over 20-gauge copper-weld conductors. It is now known that the 2,5-di-*t*-butylperoxy-2,5-dimethylhexane agent requires a higher temperature or slower extruder speed than the dicumyl peroxide agent. This difference is illustrated in Table IV with the Mooney Scorch Test* results for compounds #485 and #489. No allowance was made for this difference when these wires were jacketed and this probably explains the 30 percent increase in the physical test properties of the aged #489 specimens. An undercured vulcanizate often continues to cure with time and an increasing tensile strength is one indication of this.

Carbon black plays varied and important roles in the protection of

* Mooney Scorch Test—Mooney Shearing Disk Viscometer Test according to the procedure given in the 1967 Book of ASTM Standards, Part 28, D1646-63, ASTM, Phil., Pa., utilizing the small rotor at 2 rpm at 320°F.

polyolefins. It is effective as a light screen in protecting against photo-oxidation[17] and is used as a UV absorber in Bell System cables.[18] It also functions as an effective antioxidant.[19,20]

In general, the test program demonstrates the excellent resistance to degradation during soil burial of black chemically crosslinked polyethylene.

2.3 *Ethylene-Propylene Rubber Covered Wires*

Many specimens of the ethylene-propylene rubbers buried in 1965 are still in test. Coated wire specimens retrieved after four years of exposure in topsoil showed a considerable amount of insect damage, blistered jackets, and corroded conductors, but there was little or no damage in specimens buried in the subsoil. Although the subsoil sections appeared to be undamaged, there was a significant difference in the results of the physical tests conducted on specimens from the two exposure test sites (Table V). While the diene-terpolymer (EPDM) jacket specimens (#322) were apparently unaffected by the different soil and climate conditions, both the EPM (copolymer) insulation and EPM jacket formulations (#323 and #324) suffered a 50 percent greater loss in compression resistance after exposure in the acid soil than they did in the alkaline soil. This is the first rubber showing a difference in reaction to the soils of the two test sites.

III. MOLDING COMPOUNDS

The Bell System utilizes a great number of molded rubber parts. This requires the development of and experience with many types of rubber compounds. In 1958, seven then currently used rubber compounds based on natural, styrene-butadiene, polychloroprene, nitrile-butadiene, and butyl rubber polymers were put into the soil burial program. The test specimens were prepared in the form of dumbbells cut with ASTM Die C from molded sheets as per ASTM D412-62T.[21]

Three additional compounds of rigid black-loaded chemically crosslinked polyethylene were later added. In 1960, the following materials were also added:

(*i*) A polyester urethane rubber with peroxide cure;
(*ii*) An ethylene-propylene rubber with peroxide cure;
(*iii*) A black-loaded polychloroprene containing no clay;
(*iv*) A black-loaded chlorosulfonated polyethylene.

Finally, in 1964, three more "improved" compounds were placed in

the test. These consisted of two ethylene-propylene rubbers with and without clay and a black-loaded polyether urethane rubber.

A complete description of the formulation of all of these molded vulcanizates is given in Table II.

Measurements of physical properties of the original compounds were made immediately after molding. It was thus possible to compare the effects of soil burial and normal aging. The test data are presented in Table VII as tensile strength and percent elongation, while the retained percentage of these physical properties with increasing exposure time is graphically illustrated in Figs. 4 through 7. The measurements were made in accordance with ASTM D412-62T.[21]

It was unfortunate that precut dumbbells were used for testing the soil burial properties of the molding compounds because insects or rodents chewed the edges of the dumbbells. Some of these damaged specimens are shown in Figs. 8 and 9. It is now obvious that complete molded sheets should have been buried so that test specimens could have been cut from undamaged areas.

The exposure plot was sprayed with an insecticide (heptachlor) before the first samples were buried. It appears that the initial spray treatment was only effective for a few years. The damage became worse as the population became reestablished in succeeding years.

3.1 *Exposure Results*

The initial clay-loaded black polychloroprene #262 failed badly (50 percent loss in tensile strength) in less than one year due to water absorption. A second CR composition (#294) designed for soil burial with an easy processing channel (EPC) black loading and no clay showed greater resistance to deterioration. It retained its physical properties but during eight years of exposure it sustained much insect damage, particularly in New Mexico.

The compound showing the best performance in the first series of vulcanizates was #263—the high nitrile NBR with an EPC carbon black filler. Although there was some loss in elongation in New Mexico, the specimens were still in excellent condition when removed from both exposure sites after an eight-year burial. A loss in elongation was also found in the shelf-aged specimens so this did not probably result from the soil burial.

On the other hand, the nonblooming, heat resistant nitrile #264 lost about 20 to 25 percent of its original tensile strength while the elongation of the control remained fairly constant. It also had little insect damage.

TABLE VII—MOLDING COMPOUNDS–PHYSICAL TEST RESULTS

Compound	Site A-Georgia B-New Mexico	Original Tensile Strength psi	8 yr Control Tensile Strength psi	8 yr/6 inches Burial Tensile Strength psi	8 yr/18 inches Burial Tensile Strength psi	Original Elongation %	8 yr Control Elongation %	8 yr/6 inches Burial Elongation %	8 yr/18 inches Burial Elongation %
260 Natural rubber	A	3350	2490	1270	1460	490	310	160	170
Black shock mount	B	3350	2760	1310	1060	490	320	170	140
261 Styrene-butadine	A	1225	900	930	1250	410	240	230	250
Low comp. set	B	1225	1325	1240	895	410	250	220	220
262 Polychloroprene-with clay	A	2150	2080	900	1000	495	180	200	220
Cover stock	B	2150	1825	1520	1910	495	260	60	130
263 Nitrile-sulfur cure-	A	2355	2210	2200	2450	460	330	300	340
high shear	B	2355	2750	2300	2340	460	210	160	160
264 Nitrile-heat resistant-	A	3095	3180	2140	2500	320	240	180	220
non-blooming	B	3095	2750	2450	2260	320	240	210	200
265 Butyl-sulfur cure	A	2460	2040	1800	2090	795	690	590	720
	B	2460	2300	1340	1720	795	750	550	610
266 Butyl-quinoid cure	A	1350	1010	950	930	650	600	450	430
Hydrophone	B	1350	1000	880	730	650	460	300	250
290 Polyethylene	A	3310	3580	3440	3380	no elongation measurements made			—
crosslinked-black	B	3310	3700	3560	3570				
291 Polyethylene	A	2780	2790	2740	2710	no elongation measurements made			—
crosslinked-black	B	2780	2930	2780	2720				
292 Polyethylene/SBR	A	2750	2780	3130	3060	160	60	180	180
crosslinked-black	B	2750	2980	2600	3150	160	140	110	170
293 Ester Polyurethane	A	2440	(6 Yr) 2100	(2 Yr) 190*	(2 Yr) 910*	210	280	(2 Yr) 60*	(2 Yr) 150*
black loaded-peroxide	B	2440	(6 Yr) 2150	(2 Yr) 110*	(2 Yr) 330*	190	260	(2 Yr) 70*	(2 Yr) 110*
294 Polychloroprene-no clay	A	1690	1650	1510	1520	510	340	200	200
-black loaded	B	1650	1650	1200	1610	500	340	170	200
295 EPM-black loaded-	A	1390	1500	960	1260	440	410	300	350
peroxide cure	B	920	920	920	820	550	540	500	450
296 Chlorosulfonated	A	3210	3400	2140	3080	660	550	350	430
polyethylene-litharge cure	B	3080	3400	2960	2770	650	550	450	450
297 EPDM-no clay 4 Yr	A	3050	2525	2610	2570	550	410	440	450
low black-sulfur cure 4 Yr	B	3160	2810	2530	2360	690	560	480	400
8 Yr	B	3160	2400	2100	2140	690	520	380	380
298 EPDM-clay loaded- 4 Yr	A	1930	1600	1190	1610	800	620	580	680
black-sulfur cure 4 Yr	B	1600	1590	1500	1400	770	600	660	680
299 Ether polyurethane 4 Yr	A	3400	3175	3160	3150	530	420	440	450
black loaded-sulfur 4 Yr cure	B	3120	3280	2820	2970	530	450	440	480

* Samples untestable (0) after 4 years exposure

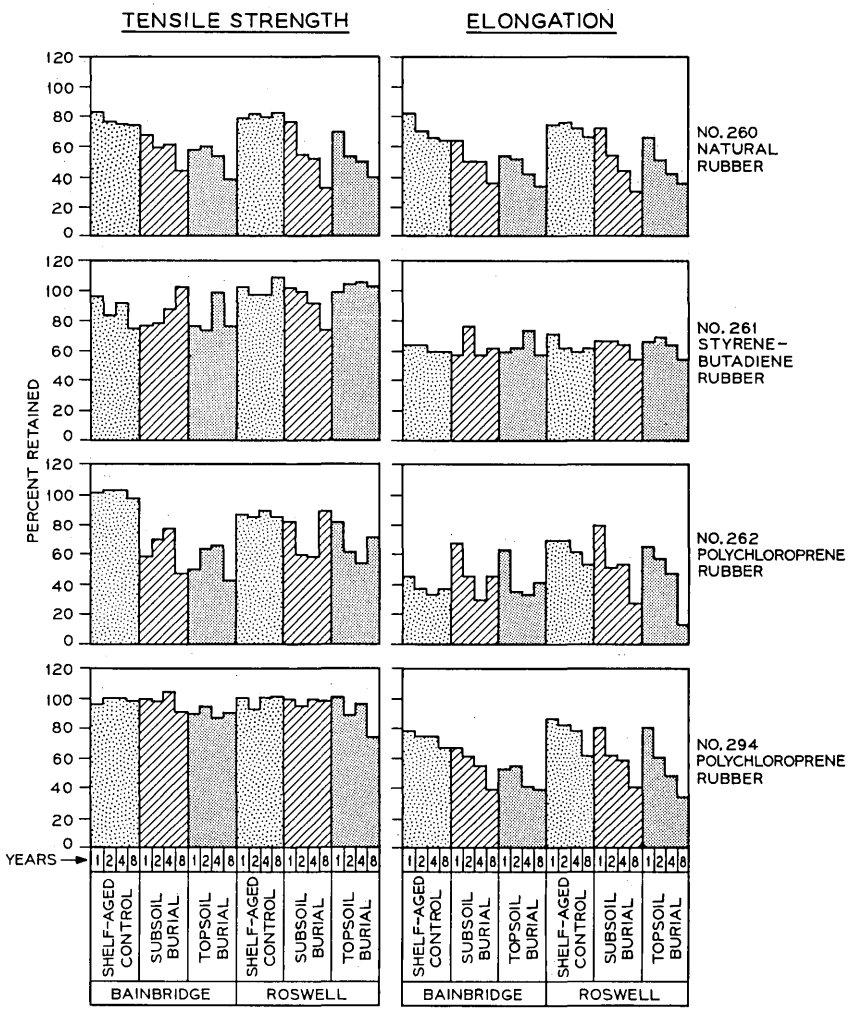

Fig. 4—Buried molding compounds (#260–262, 294)–percentage of retained tensile strength and elongation versus time of soil burial.

The IIR formulations #265 and 266 were designed for use as hydrophone diaphragms and involve different curing systems. The sulfur cure in #265 was found to corrode any contacting metal parts so a quinoid cure was provided in #266. Both butyls retained their physical properties fairly well (see Figure 5), but suffered considerable insect damage, particularly in New Mexico. Thus the test values vary greatly.

The EPM and CSM rubber stocks (#295, 296) appear to be better than many of the earlier vulcanizates but not as good as the sulfur cured nitrile #263. Also, the high-resilience NR shock mount compound #260 did not behave as well as the low-compression set SBR #261 which was only slightly affected.

As in the case of the vulcanized wire coatings, all of the black, chem-

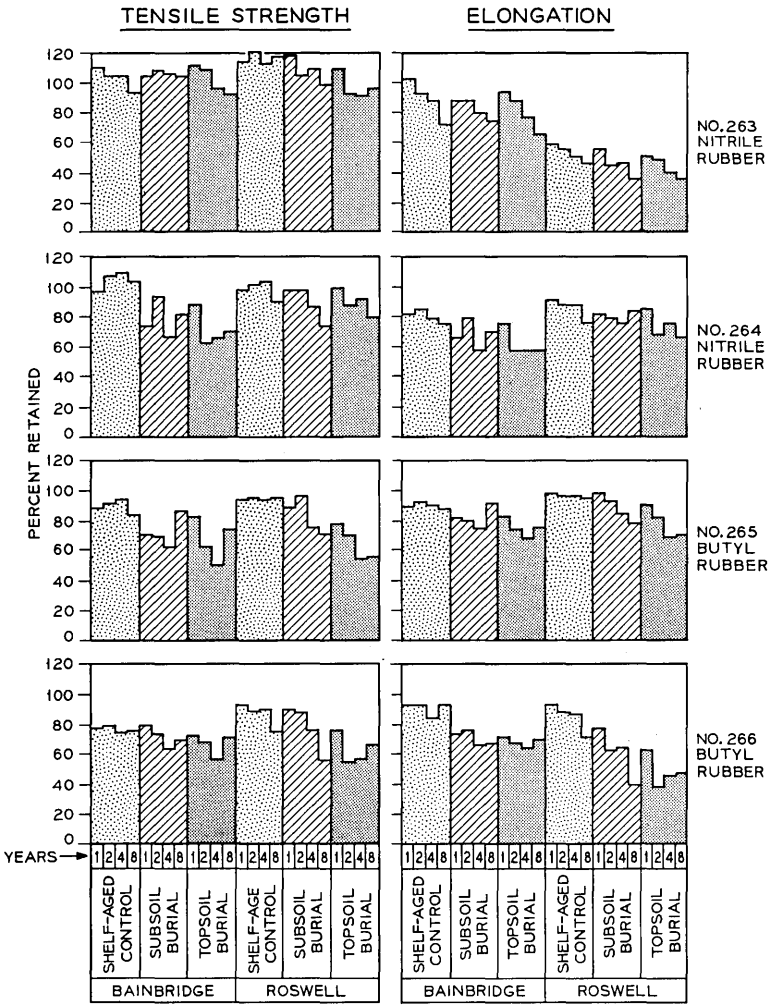

Fig. 5—Buried molding compounds (#263–266)–percentage of retained tensile strength and elongation versus time of soil burial.

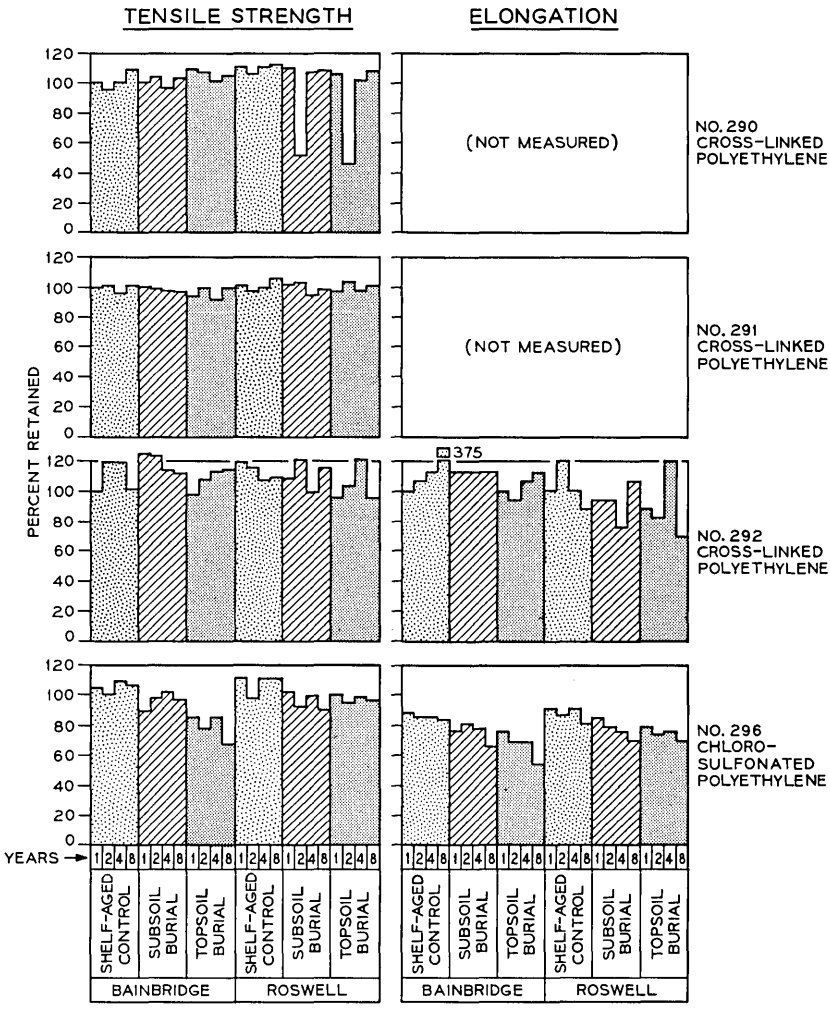

Fig. 6—Buried molding compounds (#290–292, 296)–percentage of retained tensile strength and elongation versus time of soil burial.

ically crosslinked polyethylene molded samples #290–292 appear to be unaffected by soil exposure and are being continued in the burial program.

This burial program has clearly demonstrated that the polyester urethane vulcanizate (#293) was biologically susceptible and subject to hydrolysis. This was evident after only one year of burial, for the #293

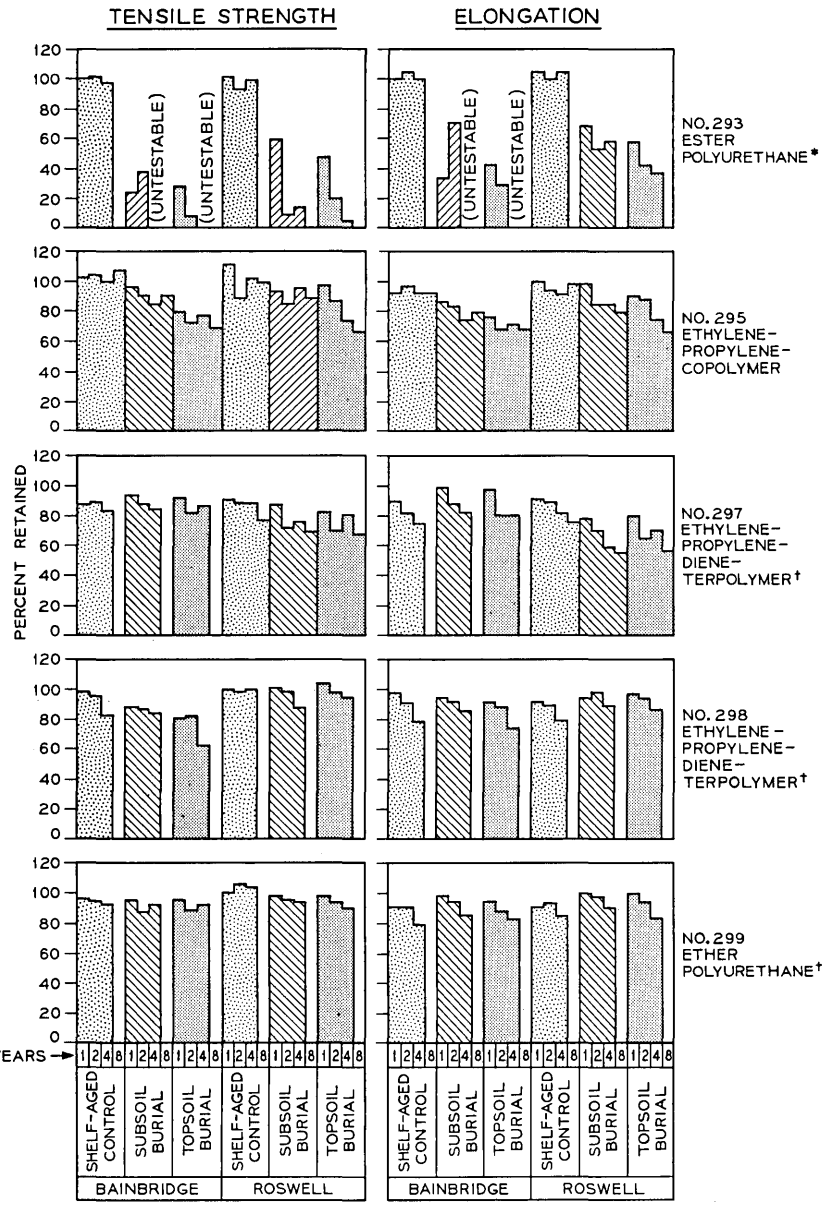

*-AFTER 4 YEARS ALL OF THE BURIED SPECIMENS COULD NOT BE TESTED
†-EIGHT YEAR DATA NOT YET AVAILABLE

Fig. 7—Buried molding compounds (#293, 295, 297–299)–percentage of retained tensile strength and elongation versus time of soil burial.

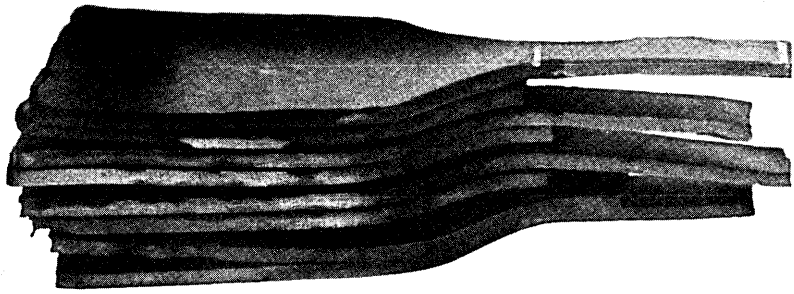

Fig. 8—Insect damaged edges of rubber dumbbell test specimens after four years burial at Roswell.

specimens already had deep cracks. Degradation was so severe that specimens could not be retrieved and tested after six years of exposure. In contrast, the polyether urethane compound (#299) was virtually unaffected by soil burial.

Figure 10 displays one more phenomenon involving the ester polyurethane sample that has occurred in the exposure test. The remains

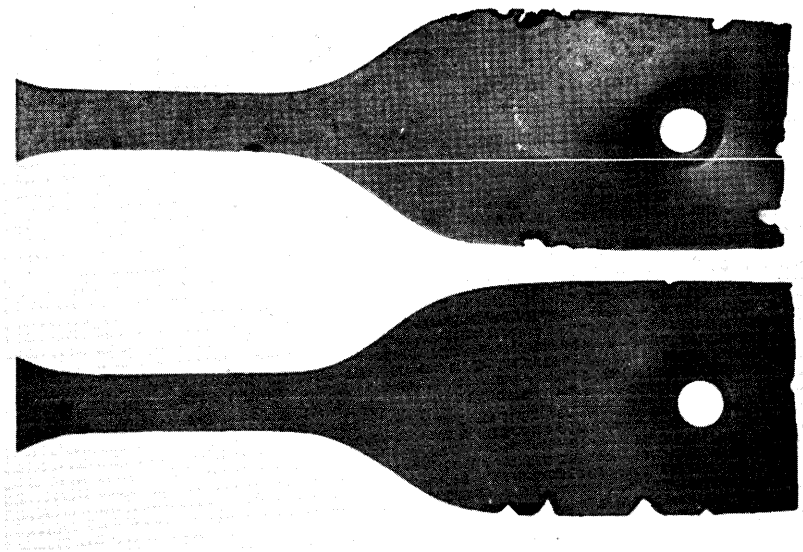

Fig. 9—Insect damaged specimens of butyl molding compounds #265 and #266 after four years burial at Roswell.

Fig. 10—A mixed pile of tested specimens of #293 polyester urethane from four years shelf-aging and four years burial at Roswell which have been in storage together for five years. Generally, the buried specimens were brittle and the shelf-aged were tacky, but where they have been in contact with each other, the shelf-aged controls were found to have liquified.

of the four-year shelf-aged control specimens and those that were retrieved after four years burial at Roswell were stored together after they had been tested. When examined after five years of storage, the burial specimens were found to be brittle and the controls to be tacky. But wherever they had been in contact with each other, the controls had liquified as is illustrated by the shiny wet areas in the photograph. In this same period of time, the remaining untested control specimens in this experiment are also getting moist and approaching this liquid state without contact with any other specimens.

The last three compounds in this program—two EPDMs with and without clay, #297, 298, and the sulfur-cured polyether urethane #299 represent four-year exposure data. Some losses in physical properties are indicated, particularly in elongation for #297 and #298. The #299 polyurethane also shows a very slight loss, as did the shelf-aged controls. None of the three suffered any insect damage.

To summarize the ranking of the better molding compounds for

soil burial purposes, the black-loaded, chemically crosslinked polyethylenes are most resistant, followed in succession by the EPC black, high nitrile NBR #263, the black polychloroprene without clay #294, and finally the low-compression set SBR #261.

Since there has been little change during the first four years of exposure as contrasted with the earlier rubbers, with additional exposure time the polyether urethane compound #299 may also prove to be satisfactory for soil burial uses. But the polyester urethane elastomer should not be buried because its hydrolyzes badly. The 60-percent loss in tensile and elongation sustained by the natural rubbers makes them also a poor choice for use in the soil.

3.2 *Discussion*

A number of other reports on the effect of water on urethane vulcanizates appeared after the above samples were prepared. R. J. Athey[22] reported that water absorbed by a urethane vulcanizate produces two effects, a reversible plasticization and an irreversible degradation. Hydrolytic degradation of the polymer chain was found to cause a permanent reduction in the properties of the vulcanizate. The functional groups present on the chain, e.g., urethane, urea, or ester groups, are hydrolyzed, resulting in chain scission, loss of branching or crosslinking, and a decrease in molecular weight.

The susceptibility of the ester urethanes to degradation by water arises from the relative ease of hydrolysis of the ester group.[23] B. S. Biggs has reported on the ease of polyester hydrolysis. He found that hydrolysis is accelerated by high temperature and catalyzed by acids and alkalies.[24] Many polymers of this class are stable only when kept neutral and he felt that this has been the main barrier to their greater commercial utilization. W. Cooper, et al., also found that polyester urethanes are less resistant to dilute acid and confirmed that acidic exposure conditions will catalyze degradation.[23]

Practically the same pattern of deterioration was observed in a U. S. Government exposure test of these two types of urethane elastomers.[25] In this study, samples were exposed in the Canal Zone and Kentucky—environments of high humidity—and after one- to two-year service periods the polyester had become tar-like and unfit for further use, while the polyester vulcanizates were not adversely affected. Microbial attack was found along with the hydrolysis. This work also indicated that additions of a polycarbodiimide and pentachlorophenol retarded chain scission and microbial attack, respectively.

It should be noted that there are some "anti-oxidants" now available

which are purported to improve the stability and retard the effects of hydrolysis on elastomeric vulcanizates containing ester groups.

Interestingly, a Russian study reported a nitrile rubber (butadiene-acrylonitrile copolymer), containing 15 percent acrylonitrile, tested with natural and butyl rubbers, that was affected by microorganisms, while the other synthetic rubbers in the program did not develop mold.[26] In this same study, all "carbon black vulcanizates" were found resistant to the action of microorganisms. The individual compound ingredients studied, nonblack fillers (kaolin and whiting) and carbon blacks, were also found to resist the action of microorganisms. There are many other ingredients in a typical rubber compound which individually or in combination could affect the resistance of a vulcanizate to degradation and a great deal more selective testing needs to be done.

Uncrosslinked polyethylene (PE) suffers a rapid loss of ductility and a sharp increase in brittle point with the incorporation of increasing loadings of carbon black; but the introduction of crosslinks allows considerable quantities of black to be added without sacrifice in brittle point.[16] In fact, yield point, ductility, elasticity, and tensile properties are improved, while problems of environmental stress cracking are minimized. The creation of the #290 molding compound with its 400 percent loading of medium thermal furnace (MT) black was only possible because of the peroxide vulcanization. Increased elongation or more elastic properties can be provided by including a rubbery polymer in the formulation as was done in compound #292.

IV. ADHESION STUDIES

Many pieces of equipment in the Bell System require the permanent vulcanized bonding of molded rubber to metal as part of their construction. These composite articles involve a variety of different rubbers and metals. Since much of this equipment will be located underground in the future, samples were prepared for soil burial testing. These samples included a number of combinations of three different rubber compounds, three metals, and several proprietary bonding systems.

The test specimens consisted of rubber laminates composed of a piece of vulcanized rubber, approximately 1/8 inch thick by 1 inch by 3 inches with a 1/2-inch section on one end free of bonding agent. The rubber was bonded to the prepared surface of a similar sized sheet metal strip to provide a peel test specimen. These test specimens were mounted on polyethylene tubes in the conventional manner. A peel test supplies some rough, but valuable information despite its recent critics.[27]

Figure 11 illustrates the comparative pull test used in this program. If the bond is weak, an adhesion failure occurs and no rubber is left on the metal. If the rubber is weak, a cohesion failure occurs and it tears leaving a major portion of the rubber adhering to the metal. Strong bonds and strong rubbers are very difficult to pull apart.

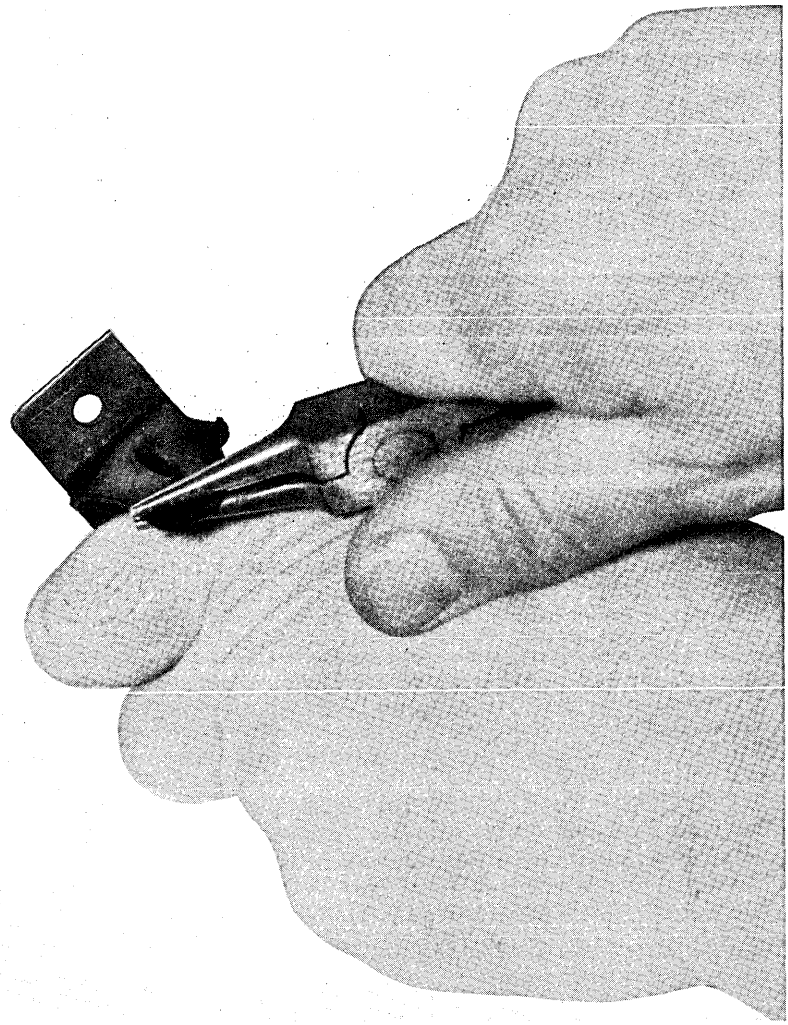

Fig. 11—Hand-peel test used to determine the strength of rubber-to-metal bond. Specimen is #275-SBR compound M-206 bonded to stainless steel with the Chemlok 201 plus Chemlok 220 system—after retrieval from Bainbridge.

The three metals utilized in the construction of the samples were Type AA 2024-0 aluminum, Type SAE 1010-1015 cold-rolled steel, and Type AISI 430 stainless steel.

The three elastomeric vulcanizates tested were a styrene-butadiene rubber stock in seven metal-adhesive-rubber combinations, a polychloroprene rubber compound in six composites, and a natural rubber mixture which was used as part of two stainless steel laminates. The complete formulations are described in Table III.

Bonding agents are most often solutions or dispersions of specially compounded polymers in organic solvents. The bonding systems tested in this experiment included several adhesives designated commercially as "Ty-ply", made by the Marbon Chemical Division of Borg-Warner Corporation, and another series called "Chemlok" supplied by the Hughson Chemical Company, a division of Lord Manufacturing Company, Erie, Pennsylvania.

Although the cold-rolled steel and copper-bearing aluminum alloy are susceptible to significant corrosion, they were included in this study because of their ease of bonding and their convenience in checking the interfacial reactions. After six years of burial, these tests were discontinued.

Figure 12 shows a number of specimens retrieved after burial for one year in Bainbridge. The visibly corroded specimens in the photograph are aluminum and cold-rolled steel, while the shiny specimens are the #269 and #272 samples made with stainless steel. The A-1 specimens are from the 6-inch topsoil region and the A-6 items are from the subsoil.

The very severe corrosion of the untreated aluminum which occurred in the soil has destroyed the bonds of all five of the aluminum burial laminates shown in Fig. 13. In the polychloroprene aluminum specimens #279 (Fig. 14) the corrosion seems heavier at the rubber-metal interface than on the outside, indicating possible corrosion due to differential aeration and accelerated by chloride contaminants.[8]

Bacteria may have also been a cause for they can initiate or promote soil corrosion by producing corrosive substances, by the creation of a corrosive environment through establishment of oxygen concentration cells, or by their consumption of hydrogen which may affect corrosion by depolarizing cathodic reactions.[28]

Usually corrosion leads to bond failure, but among the retrieved specimens from Georgia there were two noteworthy exceptions. The laminates made with the Ty-Ply 3640 and with the combined Chemlok 201 and 220 adhesives maintained good bonds to the cold-rolled steel

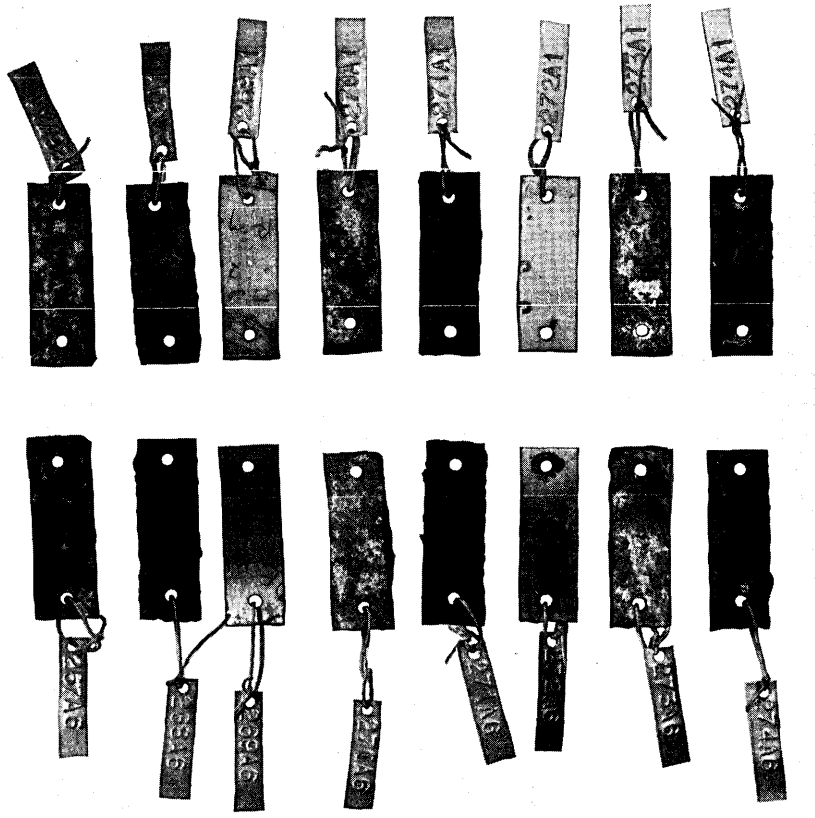

Fig. 12—Rubber-to-metal bonded laminate specimens after one year burial at Bainbridge. The A-1 specimens were buried in the topsoil, and the A-6 specimens were in the subsoil. Samples #269 and #272 are bonds to stainless steel while the corroded remainder are either cold-rolled steel or aluminum.

despite the corrosion. Duplicate specimens have, however, weakened in New Mexico and in general the damage in this alkaline soil seemed to be more severe than in the acidic Georgia soil, especially in the subsoil (A-6 specimens).

Specimens #280 were the only composites tested that involved polychloroprene bonded to cold-rolled steel. The bonding agent was Ty-Ply UP. On the #280 shelf-aged controls the bond remained strong but there was appreciable rust on the exposed metal surfaces of both control specimens. The bond of the buried specimens of this composite, however, was quite weak and had appreciable interfacial corrosion

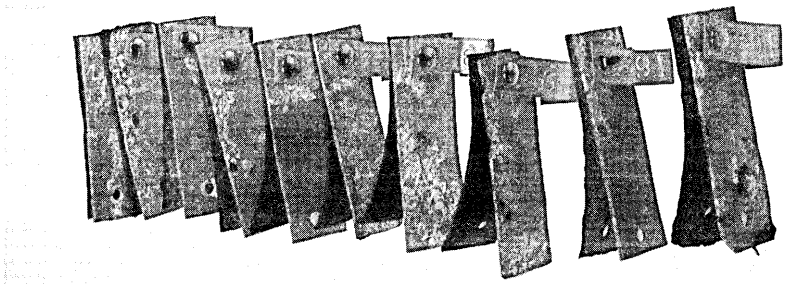

Fig. 13—Specimens of the five rubber-to-aluminum bonded combinations retrieved from two depths after four years soil burial exposure at Roswell. All bonds have failed due to severe corrosion.

after only one year. It is possible that the CR rubber compound itself may contribute to the rusting of cold-rolled steel as indicated by similar laboratory tests with rubber molds of cold-rolled steel. In fact, polychloroprene has been reported to cause pitting through chromium platings on steel molds.[29] Similarly, plain steel molds are not usually used when working with other halogen-containing polymers such as PVC. In addition, the presence of carbon black was found to increase the galvanic current between adhesive and metal which causes a progressive destruction of the bond.[29]

Table VIII lists all of the components of the individual laminate samples and the results of eight years burial compared with shelf-aged controls. None of the rubber-to-metal bonded control specimens have suffered adhesion failures and nearly all are still in excellent condition.

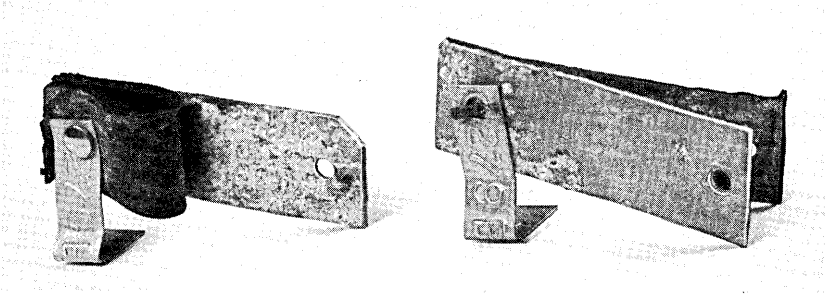

Fig. 14—Heavier corrosion at the interface of the polychloroprene-to-aluminum bond than on the exposed side of the metal strip.

TABLE VIII—RUBBER-TO-METAL BONDS–OBSERVATIONS AFTER SOIL BURIAL RETRIEVAL

Sample & Site	Rubber	Metal	Adhesive System	Observations*
267 A	CR	Alum.	Ty-Ply S	4 yrs, rubber strong, severe corrosion, bond weak
B				6 yrs, little bond, heavy corrosion
268 A	SBR	Steel	Ty-Ply 3640	4 yrs, rubber OK, heavy rust, bond excellent
B				6 yrs, heavy rust, weak bond and rubber
269 A	CR	St. Steel	Ty-Ply S	8 yrs, bond and rubber—excellent
B				8 yrs, bond and rubber—excellent
270 A	CR	Alum.	Ty-Ply UP	4 yrs, rubber strong, heavy corrosion, no bond
B				6 yrs, rubber strong, heavy corrosion, no bond
271 A	SBR	Steel	Ty-Ply UP + Ty-Ply RC	4 yrs, rubber weak, heavy rust, bond excellent
B				6 yrs, rubber tender, heavy rust, bond good
272 A	NR	St. Steel	Ty-Ply UP + Ty-Ply RC	8 yrs, bond good, rubber weakening
B				8 yrs, (no sample exposed)
273 A	SBR	Alum.	Chemlok 201 + Chemlok 220	4 yrs, rubber good, some corrosion, bond fair
B				6 yrs, rubber good, heavy corrosion, no bond
274 A	SBR	Steel	Chemlok 201 + Chemlok 220	4 yrs, rubber good, heavy rust, bond strong
B				6 yrs, rubber tender, heavy rust, bond fair
275 A	SBR	St. Steel	Chemlok 201 + Chemlok 220	8 yrs, bond good, rubber weakening
B				8 yrs, bond fair, rubber strong
276 A	SBR	Alum.	Chemlok 220	4 yrs, rubber weak, bad corrosion, no bond
B				6 yrs, rubber strong, heavy corrosion, no bond
277 A	SBR	Steel	Chemlok 220	4 yrs, rubber weak, heavy rust, bond strong
B				6 yrs, rubber fair, heavy rust, bond fair
278 A	NR	St. Steel	Chemlok 220	8 yrs, bond excellent, rubber weakening
B				8 yrs, bond and rubber good
279 A	CR	Alum.	Chemlok 220	4 yrs, rubber strong, corrosion, bond weak
B				6 yrs, rubber strong, heavy rust, bond weak
280 A	CR	Steel	Ty-Ply UP	4 yrs, rubber strong, heavy rust, bond weak
B				6 yrs, rubber strong, heavy rust, little bond
281 A	CR	St. Steel	Chemlok 220	8 yrs, bond and rubber—excellent
B				8 yrs, bond fair—rubber strong

* The only 8-year samples still in burial test are Nos. 269, 272, 275, 278, 281; all others have been removed from test.
A—Bainbridge, Georgia B—Roswell, New Mexico St. Steel—Stainless Steel Alum.—Aluminum
SBR—Styrene-Butadiene NR—Natural CR—Chloroprene

The strength of the #270 control sample, consisting of a Ty-Ply UP bond of polychloroprene to aluminum, was significantly reduced.

The stainless steel laminates were the only ones that had not corroded after eight years of soil burial. When the test samples were prepared in 1958, stainless steel was a very difficult material to bond to rubber. It required some very careful preparation, skillful techniques, and luck. Today, however, with the newer bonding materials, stainless steel is no longer a problem to bond.

In the case of the SBR compound, only the combination Chemlok 201 and Chemlok 220 adhesive system gave a bond to stainless steel that was considered to be good enough to test and these specimens constituted the #275 series. They were bonded in January 1958 and, when examined in February 1960, the bonds in both the controls and the buried specimens seemed excellent.

Based on eight years of exposure, it is clear that if a strong bond is made to stainless steel initially, it will last in a soil medium for the life of the rubber.* In terms of the adhesion test, the polychloroprene bonds are giving spotty results and the natural rubber is getting quite weak. The SBR compound might have performed better had it contained an antioxidant. A number of other good rubber formulations for buried uses may be found among the series of rubber molding compounds described in Section III of this paper. New bonding systems are available and need to be tested for despite technological advances, adhesive compounding still remains primarily an art rather than a science.

All of the proprietary adhesive systems used in this program provided strong and lasting bonds as long as the metal did not corrode and the rubber did not deteriorate. Two specimens even maintained some adhesion to corroded metals.

V. ACKNOWLEDGMENTS

An exposure program, covering a span of years such as this, inevitably results in changes in the identity of the participants. I would like to express my indebtedness, thanks, and appreciation to two grand old men—now retired—Eric L. Dias who did the initial wire coating work and Caleb M. Hill for the molding and bonding preparation. Their encouragement, support, and advice have been wonderful.

---

* See Appendix B.

APPENDIX A

Compression Test[30,31]

The Compression Testing Machine was developed at Bell Laboratories with the cooperation of the H. L. Scott Company. It was designed for the evaluation of rubber compounds in the form of insulation on solid wire and it measures the compressive force required to cause the conductor to cut through the insulation. In the test, a 2-inch length of insulated wire was compressed between a pair of steel blocks with parallel plane surfaces. As the rubber on the wire was compressed, it assumed an elliptical form. The layer of rubber between the conductor and the jaws became thinner as the pressure increased until rupture occurred. Compression resistance was automatically recorded as a numerical value of the load in pounds. This test apparatus and procedure have become a standard in the wire and cable industry.

A recent joint effort between R. F. Westover of Bell Laboratories and Scott Testers, Inc., has produced a modernization of the load weighing and recording systems for the Compression Machine manufactured by Scott. This improvement increased the reliability and accuracy of results, reduced testing time, and extended the application of the machine to the highly expanded or foam forms of insulation.

APPENDIX B

Rubber-to-Stainless-Steel Bonds and Salt Water[32]

William H. Lockwood has found that rubber-to-stainless-steel bonds will fail quickly in an environment containing salt water if the steel has not been properly treated initially. For with even the best of adhesives, the usual sand blasting of the steel prior to bonding is insufficient and leads to this failure. However, a hydrochloric acid treatment of the steel will result in long-lasting bonds.

REFERENCES

1. DeVries, O., "The Destruction of the Hydrocarbon of Raw Rubber by Fungi," Chem. Abstr., *22* (Oct. 20, 1928), p. 4006.
2. Brown, Alfred E., "The Problem of Fungal Growth," Mod. Plastics, *23*, No. 8 (April 1946), pp. 189–256.
3. Greathouse, G. A., "Effect of Microorganisms on Rubber Degradation," Rubber Age, *63* (1948), pp. 337–338.
4. Ritzinger, B. B., "Fungus Resistance of Neoprene and Effect of Compounding and Use of Fungicides," Rubber Plastic Age, *40*, No. 10 (1959), pp. 1067–1069.
5. Alvino, W. M., Bell Laboratories, unpublished work (1962).
6. Burns, R. M., "Mechanisms of Corrosion Process," ASTM Bull., No. 126 (Jan. 1944), pp. 17–20.

7. Burns, R. M., "The Corrosion of Metals-I.," B.S.T.J., *15*, No. 1 (Jan. 1936), pp. 20–38.
8. Burns, R. M., and Bradley, W. W., *Protective Coatings for Metals*, Third Edition, ACS Mono. No. 163, New York: Reinhold Publishing Corp., 1967.
9. Vernon, W. H. J., "Second Experimental Report to the Atmospheric Corrosion Research Committee," Part I, Sec. VII, Trans. Faraday Soc., *23* (1927), pp. 159–165.
10. Burns, R. M., "The Corrosion of Metals-II.," B.S.T.J., *15*, No. 4 (Oct. 1936), pp. 603–625.
11. Keller, F., and Edwards, J. D., "The Behavior of Oxide Films on Aluminum," *Pittsburgh International Conference on Surface Reactions*, Pittsburgh, Pa.: Corrosion Publishing Co., 1948, pp. 202–212.
12. Blake, John T., Kitchen, Doland W., and Pratt, Orison S., "Failures of Rubber Insulation Caused by Soil Microorganisms," Trans. Amer. Inst. Elec. Eng., *69* part 2 (1950), pp. 748–755.
13. Blake, John T. Kitchen, Donald W., and Pratt, Orison S., "The Microbiological Deterioration of Rubber Insulation," Trans. Amer. Inst. Elec. Eng., *72* part 3 (1953), pp. 321–328.
14. Winslow, F. H., Matreyek, W., and Trozzolo, A. M., "Weathering of Polyethylene," Polym. Preprints, Amer. Chem. Soc., Div. Polym. Chem., *10*, No. 2 (Sept. 1969), pp. 1271–1280.
15. Heiss, J. H., and Lanza, V. L., "The Thermal Embrittlement of Stressed Polyethylene," Wire and Wire Products, *33*, No. 10 (Oct. 1958), pp. 1182–1187, 1285.
16. Dannenberg, E. M., Jordan, M. E., and Cole, H. M., "Peroxide Crosslinked Carbon Black Polyethylene Compositions," J. Poly. Sci., *31*, No. 122 (Aug. 1958), pp. 127–153.
17. Maibauer, A. E., and Myers, C. S., "Polyethylenes," Trans. Electrochem. Soc., *90* (1946), pp. 341–360.
18. Ambrose, John F., "Pigments in Polymer Materials," Bell Labs. Rec., *35* (July 1957), pp. 246–250.
19. Hawkins, W. L., Hansen, R. H., Matreyek, W., and Winslow, F. H., "The Effect of Carbon Black on Thermal Antioxidants for Polyethylene," J. Appl. Polymer Sci., *1* (1959), pp. 37–42.
20. Hawkins, W. L., Worthington, Mrs. M. A., and Winslow, F. H., "The Role of Carbon Black in the Thermal Oxidation of Polylefins," *Proc. Fourth Conf. on Carbon*, New York: Pergamon Press, 1960.
21. American Society For Testing and Materials, "Standard Methods of Tension Testing of Vulcanized Rubber," D412-62T *ASTM Standards* (1964), part 28.
22. Athey, Robert J., "Stability of Plastics," Rubber Age, *96*, No. 5 (Feb. 1965), pp. 705–712.
23. Cooper, W., Pearson, R. W., and Darke, S., "Isocyanate Reactions and the Structure of Polyurethane," Ind. Chemist, *36*, No. 421 (1960), pp. 121–126.
24. Biggs, B. S., "Deterioration of Organic Polymers," B.S.T.J., *30*, No. 2 (Oct. 1951), pp. 1078–1102.
25. Testroet, Frank B., "Performance of Urethane Vulcanizates in Environments of High Humidity," U. S. Gov. Res. Rep. *39*, 11, S26 (1964), AD-422028, Rock Island Arsenal Lab., Ill.: Rep. 63-2808, 1963, 38 pp.
26. Petnujova, A., and Zanova, V., "Influence of Composition on the Biological Degradation of Rubber Articles," Soviet Rubber Tech., *19*, No. 2 (July 1960), pp. 16–17.
27. Pickup, B., and Weatherstone, E., "Some Factors Influencing the Bonding of Rubber to Metal," J.I.R.I., *3*, No. 6 (Dec. 1969), pp. 254–261.
28. Lichtenstein, S., "Corrosion by Microbes, " Instrum. Contr. Syst., *41*, No. 2 (Feb. 1968), p. 99.
29. Buchen, S., *Rubber to Metal Bonding*, London: Crosby Lockwood and Sons Ltd., 1959, pp. 111–112.
30. Hippensteel, Claude L., "A New Mechanical Test for Rubber Insulation," Ind. Eng. Chem., *18* (April 1926), pp. 409–411.
31. Hippensteel, Claude L., "New Rubber Compression Testing Machine," Bell Lab. Rec., *5*, No. 5 (Jan. 1928), pp. 153–155.
32. Lockwood, William H., Bell Laboratories, unpublished work (1963).

Copyright © 1972 American Telephone and Telegraph Company
THE BELL SYSTEM TECHNICAL JOURNAL
Vol. 51, No. 1, January, 1972
Printed in U.S.A.

Soil Burial Tests:

Effect of Soil Burial Exposure on the Properties of Adhesives and Pressure-Sensitive Tapes

By D. W. DAHRINGER

(Manuscript received August 26, 1971)

The effects of long-term soil burial on some physical properties of adhesive bonded test specimens and pressure-sensitive adhesive tapes are presented. Changes in these measured properties are discussed and interpreted in terms of typical material characteristics. Additionally, the engineering implications of these changes are explored. Such implications include:

(i) Adhesive bonding appears to be a satisfactory means of fastening structures together for direct soil burial; however, care must be exercised to insure proper joint design and bonding procedures.

(ii) Both rubber and vinyl pressure-sensitive tapes provide sufficient retention of properties for prolonged underground service, but glass cloth and aluminum backed tape should be used only for temporary service.

I. INTRODUCTION

Included in the Bell System study of direct soil burial effects on the properties of material for telephone plant were a number of adhesives and pressure-sensitive adhesive tapes.

The 1950s and 1960s were a period of significant growth for adhesives technology, as witnessed by the number and diversity of products, applications, and publications related to the field. Few, if any, applications for buried adhesively bonded structures existed at the beginning of this program, but developments in that direction were easily predictable.

General usage of adhesives by the Bell System was initially cautious because of insufficient data and inadequate tests for evaluating

durability and reliability of bonded assemblies. However, with the development of better test methods and greater understanding of environmental deterioration, telephone applications of adhesives have increased manyfold.

Pressure-sensitive adhesive tapes have enjoyed a very rapid increase in usage within the Bell System. Many applications can be categorized as electrical insulations, such as splice protection, but more and more uses are being classed as mechanical holding, such as packaging, nameplate mounting, coil wrapping, duct sealing, leak stoppers, surface protectors, etc. All of the tapes selected for this program had been used for some form of cable splicing where outdoor exposure would be encountered. With the emphasis on buried plant, additional testing of tapes under direct soil burial was considered advisable.

Since the fields of structural adhesive bonding and tapes are quite diverse in chemistry as well as application and testing, they will be discussed separately.

II. ADHESIVES

2.1 *Description of Adhesives Tested*

2.1.1 *Types of Material*

The adhesives tested in this program were evaluated as prepared lap shear joints, with either glass fiber laminate or stainless steel substrates. A total of 25 different sample types were prepared and subjected to the two soil environments (topsoil and subsoil) at Roswell, New Mexico, and Bainbridge, Georgia.[1] The adhesives included epoxy (both simple formulation and proprietary), modified phenolics, and a polysulfide rubber.

2.1.2 *Expected Service Life*

Most adhesives are expected to have service lives greater than the structures that they bond, which is typically twenty to forty years in the Bell System. The determination of service life of an adhesive becomes a complex problem since, in addition to the bulk adhesive, there are the substrates and the very critical interfaces all of which are part of the adhesive joint and subject to environmental degradation. Attack at an interface may indicate that the substrate was not properly cleaned or prepared instead of that the adhesive was not resistant to the environment. This condition will be demonstrated in the discussion of test results. Other factors contributing to the service life

of an adhesive joint besides environment and surface preparation include the joint design, stress levels (both static and dynamic), stress mode, and the adhesive application and curing conditions.

2.2 *Test Methods*

2.2.1 *General*

The test method selected for the evaluation of the adhesives in this study was the lap shear test* detailed in ASTM D1002.[2] This method is reasonably simple, convenient, inexpensive, and adaptable to a large variety of data-generating modifications. Briefly, two substrates are bonded together as shown in Fig. 1, then the tensile force per unit

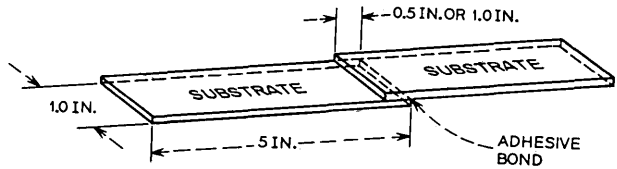

Fig. 1—Overlap shear test specimen.

area necessary to rupture that joint is measured with a suitable testing machine.

Test results can be influenced by a number of factors other than adhesive formulation. Some of these are listed in Table I. In this study, as many of the variables as possible relating to the specimen preparation and testing were held constant.

2.2.2 *Substrates*

Two substrates were selected for this program, a glass fiber laminate† and Type 302 stainless steel. The bases for selecting these two substrates were the attractive economics associated with glass fiber laminates for underground structures and the traditional corrosion resistance of the stainless steel.

2.2.3 *Sample Preparation*

Since the cleaning and preparation of the substrates is one of the most important steps in the adhesive bonding process, particular

* Also known as "overlap shear" and "tensile shear" test.
† Per ASTM D1532.

TABLE I—SOME VARIABLES AFFECTING LAP SHEAR TEST RESULTS

Length and width of overlap
Thickness of adhesive
Modulus of substrate
Modulus of adhesive
Surface preparation of substrate
Rate of testing
Curing conditions
Ambient conditions

care was taken to guarantee the uniformity of the samples. The glass fiber substrates were 1-inch × 5-inch specimens cut, using a diamond saw blade, from 1/8-inch-thick sheets. These substrates, prepared by process A in Table II, were then bonded with a 1-inch overlap. The stainless steel substrates were blanked 5 inches long from flat wire stock 1 inch wide × 0.062 inch thick. These substrates were prepared by procedure B, C, or D of Table II and bonded with a 1/2-inch overlap.

2.2.4 *Sample Testing*

After the desired burial duration and removal of the bonded samples from the two burial levels* at the two test plots, all of the samples were washed with tap water and visually inspected. The samples were then conditioned for 30 days at 95°F and 90 percent relative humidity prior to testing.

2.2.5 *Materials*

The adhesives used to bond the glass fiber laminate substrates are described in Table III. Reference numbers (171 to 181) were carried through the program and continued here for organizational purposes. Seven of these adhesives contain proprietary materials whose contents are not freely disclosed by the manufacturers and therefore they will be described in general terms. Table IV contains the information on adhesives used to bond the stainless steel substrates with #191 to 196 used in the initial phase and #197 to 204 in the second phase.

Most of the adhesives in this study were based on epoxy resins which were formulated with appropriate curing agents, modifiers, fillers, flexibilizers, etc. Several excellent texts[3-5] are available which offer comprehensive studies on the chemistry of epoxies and their curing mechanisms and should be referred to for additional information.

* Topsoil and subsoil, 6 inches and 18 inches below the surface respectively.

Cured epoxy resins, generally, because of their chemical structure, are quite resistant to chemical attack and, presumably, also biological attack. It would be expected that most of the conventional epoxy systems in the study would perform very well, unless a substrate problem occurred (as with both the glass fiber laminates and the initial group of stainless steel specimens).

The phenolic adhesives #179, 180, 194, and 195 are based on heat-curable phenolic resins compounded with either thermoplastic, such as poly (vinyl formal), or elastomeric polymers, such as nitrile rubber.

TABLE II—PREBOND TREATMENTS FOR LAP SHEAR SAMPLES

A
For Glass Fiber Laminate Only
1. Sandblast.
2. Trichlorethylene wipe prior to bonding.
B
For Stainless Steel
1. Vapor degrease.
2. Immerse in solution, 2.62% sodium metasilicate, 0.26% Triton X200 (Rohm & Haas) in deionized water.
3. Rinse in 150°F deionized water.
4. Rinse in cold deionized water.
5. Dry at 150°F.
C
For Stainless Steel
1. Vapor degrease.
2. Immerse in solution, 10% trisodium phosphate, 3.6% Triton X200, 86.4% water for 15 minutes at 150°F.
3. Rinse on hot water.
4. Rinse in distilled water.
5. Blow dry with oil-free air.
D
For Stainless Steel
1. Vapor degrease.
2. Immerse 15 minutes in 37% (by volume) concentrated hydrochloric acid in water at room temperature.
3. Rinse in cold water.
4. Rinse in distilled water.
5. Blow dry with oil-free air.

TABLE III—ADHESIVE SYSTEMS FOR GLASS FIBER SUBSTRATES

Reference Number	Adhesive Description	Surface* Preparation	Cure Cycle
171	Liquid DGEBA epoxy resin plus 8 phr† diethylaminopropylamine	A	2 hrs 165°F
172	Liquid DGEBA epoxy resin plus 20 phr liquid aromatic primary amine blend (m-Phenylenediamine/ methylenedianiline)	A	1 hr 250°F
173	Liquid DGEBA epoxy resin plus 7 phr proprietary curing agent plus 50 phr high-viscosity polyamide resin	A	4 hrs 175°F
174	Proprietary, two-part, nominally room temperature curing, modified DGEBA epoxy-based adhesive. Mix ratio 100:13 pbw	A	2 hrs 165°F
175	Liquid DGEBA epoxy resin plus 54 phr polyamide resin	A	1 hr 250°F
176	Diluent modified liquid DGEBA epoxy blend plus 50 phr liquid polysulfide polymer plus 22.5 phr tris (dimethylaminomethyl) phenol	A	1 hr 250°F
177	Proprietary, two-part aluminum metal filled, nominally room temperature curing, epoxy repair kit	A	1-1/2 hrs 160°F
178	Proprietary, paste, modified DGEBA epoxy based formulation plus 6 phr diethylaminopropylamine	A	1 hr 165°F plus 1 hr 225°F
179	Proprietary poly (vinyl formal)-modified phenolic tape	A	30 min 325°F
180	Proprietary nitrile rubber-modified phenolic solution	A	1 hr 180°F 3/4 hr 325°F
181	Proprietary resorcinol-formaldehyde	A	1 hr 165°F

* Table II
† Parts per hundred parts resin by weight

These ingredients are usually compounded in a solution for coating onto the substrates prior to drying and curing, but may also be available in film form. Some of these formulations have been used successfully for many years in such applications as brake lining bonding and aircraft honeycomb panel bonding. The resorcinol-formaldehyde adhesive (#181) is known for its extremely durable performance in marine plywood.[6] Its chemistry is similar to a phenolic (novolac) which requires a hardener for thermosetting. This type of adhesive performs best on porous or coreactive materials.

Polysulfide polymers are generally used as sealants with some adhesive properties, as in #203, and as flexibilizers for epoxy systems as in #176 and #202. As sealants, polysulfide rubbers have gained a reputation for excellent chemical, thermal, and weather resistance.

TABLE IV—ADHESIVE SYSTEMS FOR STAINLESS STEEL SUBTRATES

Reference Number	Adhesive Description	Surface Preparation*	Cure Cycle
	Initial Phase		
191	Proprietary, paste, modified DGEBA epoxy based formulation plus 6 phr† diethylaminopropylamine	B	4-1/2 hr 200°F
192	Proprietary, paste, modified DGEBA epoxy based formulation plus 6 phr diethylaminopropylamine (same material as #178)	B	4-1/2 hr 200°F
193	Proprietary, two-part aluminum metal filled, nominally room temperature curing epoxy repair kit (same material as #177)	C	2 hr 165°F
194	Proprietary poly (vinyl formal)-modified phenolic tape (same material as #179) plus primer solution	B	1 hr 225°F plus 1 hr 325°F
195	Proprietary poly (vinyl butyral)-modified phenolic film plus primer solution	B	1 hr 225°F plus 1-1/2 hr 300°F
196	Liquid diluent modified DGEBA epoxy resin plus 100 phr liquid polyamide plus 40 phr of a proprietary mineral filler	C	1 hr 250°F
	Second Phase		
197	Proprietary, one-part, high viscosity, modified-epoxy adhesive	D	1 hr 350°F
198	Proprietary, one-part, thixotropic, modified-epoxy adhesive similar to #197	D	1 hr 350°F
199	Proprietary, high-temperature-resistant, modified-epoxy adhesive film with fabric carrier	D	1 hr 350°F
200	Proprietary, highly metal-filled, two-part (100 to 9 mix ratio), low viscosity adhesive	D	3 hr 180°F plus 3 hr 250°F
201	Liquid DGEBA epoxy resin plus 20 phr liquid aromatic primary amine blend same as #172	D	2 hr 250°F
202	Liquid DGEBA epoxy resin plus 15 phr liquid aromatic primary amine blend plus 40 phr liquid polysulfide polymer	D	2 hr 250°F
203	Proprietary black polysulfide paste compound plus 12 phr lead dioxide curing agent	D	2 hr 140°F
204	Proprietary, one-part, paste, high-temperature-resistant, aluminum filled, modified DGEBA epoxy	D	2 hr 350°F

* Table II
† Parts per hundred parts resin by weight

2.3 *Results and Discussion*

2.3.1 *Glass Fiber Substrates*

The test results obtained on the bonded glass fiber specimens were essentially independent of the adhesive, except for the sample bonded with the resorcinol-formaldehyde adhesive (#181). With all of the other adhesives, and at every aging and conditioning sequence, the adhesive joint did not fail during testing. The failures occurred between the first and second layers of glass mat in one of the substrates and over the joint area, then proceeding to break across the glass mat just beyond the end of the overlap. In actuality, then, the values obtained measure only the interlaminar shear strength plus the tensile strength of a single glass ply of the substrate. Figure 2 is a plot of the test results obtained at the various aging conditions for one of the adhesive systems. All of the systems followed this pattern with a maximum deviation from this plot of about 10 percent for any value except for sample #181. These deviations, although within the range expected for this type of failure, show another anticipated trend in that the more flexible (tough) adhesive formulations tend toward the higher end of the spectrum while the more brittle formulations fall at the lower end. This is an indication of the ability of flexible adhesives to distribute stresses on rigid or friable substrates more evenly than brittle adhesives. The anomalously high values shown for the four-year Roswell specimens were typical of each system and have not been explained.

The specimens of #181 resorcinol-formaldehyde adhesive were the

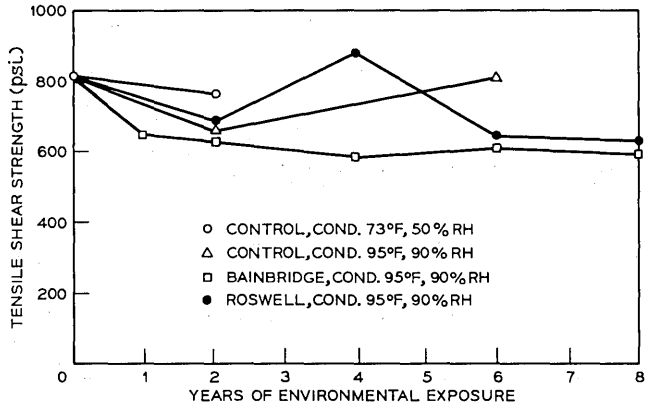

Fig. 2—Tensile shear strength of typical adhesive bonded glass fiber test specimens vs years of environmental exposure.

only ones in this group to exhibit failure apparently at the adhesive interface, and at values less than half the typical values shown in the plot. This type of adhesive is mainly used for waterproof wood bonding, but it has very high shrinkage on cure and is normally considered too brittle for most nonporous substrates (nylons and acrylics being notable exceptions).

Since laminate failure occurred in all other cases, the conclusion may be drawn from Fig. 2 that the adhesives were not severely attacked by the environment. It also indicates that sandblasting of the glass fiber laminate substrate is a viable surface preparation method. The glass fiber laminates themselves exhibit a mild deterioration in strength characteristics, but that apparently levels off with minimum additional changes. Further information on the effects of soil burial on structural laminates is presented in a companion article by T. H. Klein.[7] There was no significant difference between the specimens buried in the topsoil and those in the subsoil, nor between those at the two burial sites.

2.3.2 *Stainless Steel Substrates*

The initial group of bonded stainless steel specimens for this program proved to be seriously deficient in surface preparation. Figure 3 shows

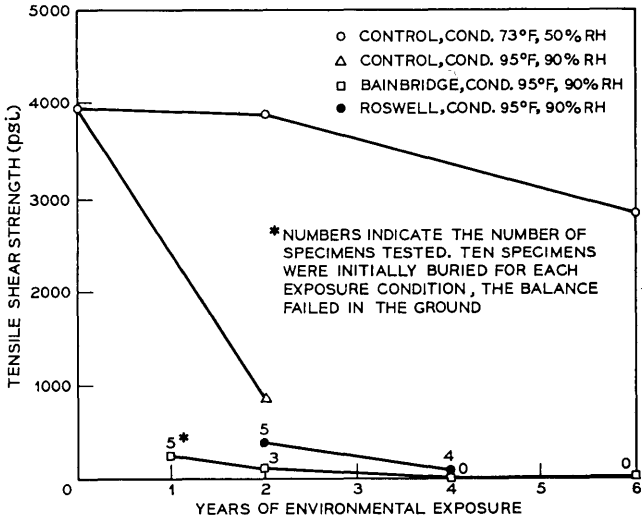

Fig. 3—Tensile shear strength of typical adhesive bonded stainless steel test specimens #191 to 196 vs years of environmental exposure.

the test results of Adhesive #191 and is typical of all the samples in this category. The initial lap shear values range from 3000 to 6000 psi and show losses of from 25 to 60 percent after six years of indoor storage and 30 days of laboratory conditioning (73°F, 50-percent RH) prior to testing. Additional specimens stored indoors for only two years but conditioned at 95°F and 90-percent RH for 30 days before testing exhibited losses in lap shear strength between 75 and 100 percent of the corresponding standard lab-conditioned specimens. Since all of the buried specimens were subject to the latter treatment prior to testing, poor results were obtained. Approximately 65 percent of the Bainbridge and 85 percent of the Roswell specimens had failed in the ground prior to testing. Of those samples that survived burial, the test results with only a few exceptions were under 1000 psi, and mostly under 500 psi. The significant decrease in lap shear strength for all of the specimens exposed to humidity versus similar but dry specimens is an indication that neither surface preparation (B or C) of the stainless steel substrates was optimum. Additionally, three of the adhesives in this group were also included in the glass fiber laminate series where no similar humidity-related degradation was noted.

Because of the poor performance of this group of specimens, and the concurrent development of the improved prebond surface preparations for stainless steel, the early (#191 to 196) portion of the burial program was terminated after six years, and a new group of stainless steel bonded specimens prepared. Newer adhesives were substituted in the

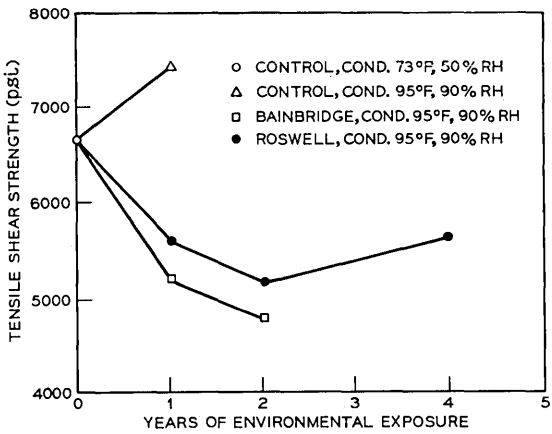

Fig. 4—Tensile shear strength of #197 adhesive bonded stainless steel test specimens vs years of environmental exposure.

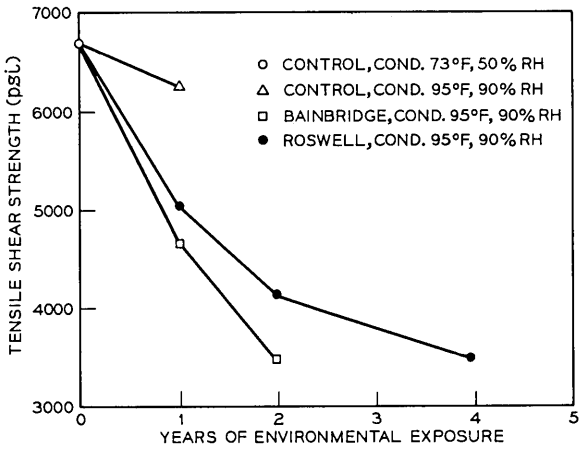

Fig. 5—Tensile shear strength of #198 adhesive bonded stainless steel test specimens vs years of environmental exposure.

second phase of the program to take advantage of advancing technology and, in the case of the polysulfide rubber, to provide specific application related information.

Figures 4 to 11 are plots of the available test data on the performance of the second group of stainless steel bonded joints (samples #197 to 204). At the time of this writing, only one- and two-year Bainbridge and one-, two-, and four-year Roswell data were available. Test results for subsoil and topsoil specimens were essentially identical and were combined for the data analysis. Figure 4 shows the joint strength decreasing some 25 percent for Bainbridge and about 20 percent for Roswell over one and two years, while the shelf control increased about 15 percent the first year. The major portion of the loss in strength of the buried specimens is in the first year, while Roswell shows a mild recovery of its four-year specimens.

Figure 5 shows losses at two years of 40 and 50 percent for Roswell and Bainbridge respectively, with only slight indications of change in slope. The four-year Roswell specimen does indicate a tapering off in the loss of joint strength. The one-year shelf control also shows a slight decrease in strength compared to the original values. Very surprising is the difference between #197 and #198 which are made by the same manufacturer and to the same formulation, except for the inclusion of a small amount of a filler to impart thixotropic properties to #198.

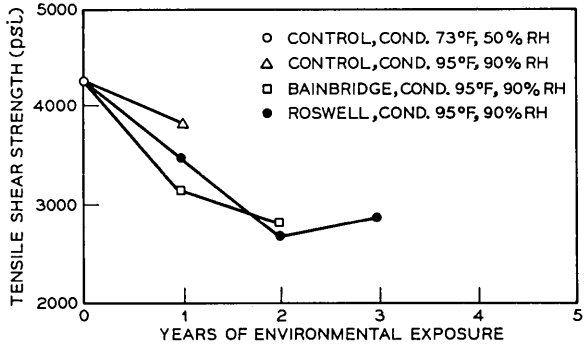

Fig. 6—Tensile shear strength of #199 adhesive bonded stainless steel test specimens vs years of environmental exposure.

Adhesive systems #199 and #200, shown in Figs. 6 and 7, exhibit general behavior patterns similar to #197 and #198 with about 25 to 35 percent decrease in joint strength after two years burial and some indication of leveling off.

Adhesive systems #201 and #202 (Figs. 8 and 9) show the effects of soil burial on two adhesive systems having equivalent bases, but incorporating a liquid polysulfide flexibilizer in #202. The initial and one-year laboratory controls of the flexibilized system are about double those of the unmodified adhesive. The unmodified adhesive exhibits a moderate decline in joint strength as a result of the soil burial, while the flexibilized adhesive loses all of its initial advantage within the first year, then parallels the unmodified system.

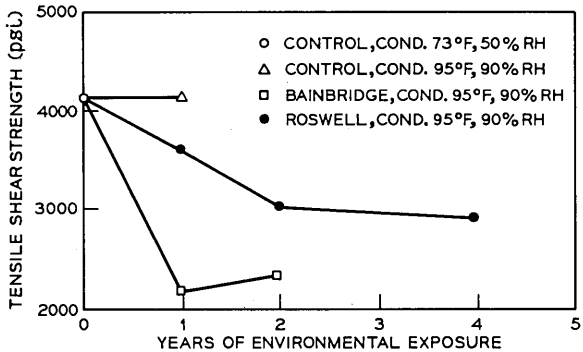

Fig. 7—Tensile shear strength of #200 adhesive bonded stainless steel test specimens vs years of environmental exposure.

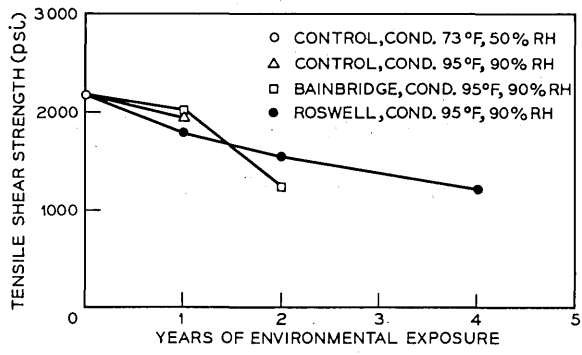

Fig. 8—Tensile shear strenght of #201 adhesive bonded stainless steel test specimens vs years of environmental exposure.

Figure 10 illustrates a pattern similar to most of the epoxy systems under test in that a gradual decrease in joint strength is found with soil burial.

The one non-epoxy system in the second group of adhesives with stainless steel substrates is shown in Fig. 11. This two-part polysulfide rubber, which is considerably lower in strength than the epoxy system,

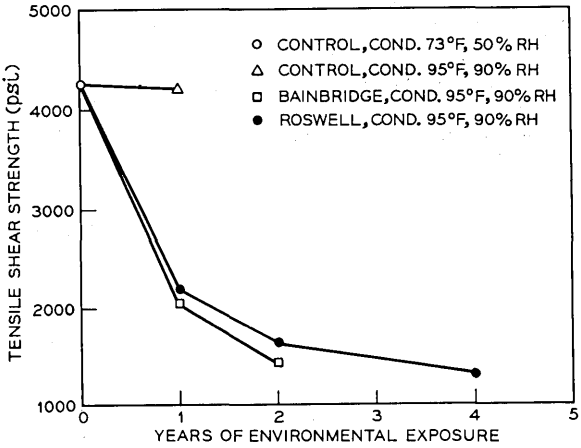

Fig. 9—Tensile shear strength of #202 adhesive bonded stainless steel test specimens vs years of environmental exposure.

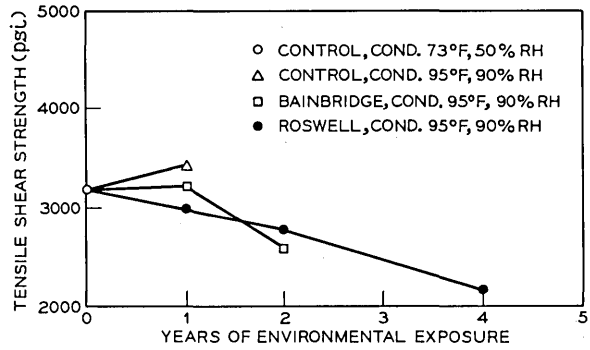

Fig. 10—Tensile shear strength of #204 adhesive bonded stainless steel test specimens vs years of environmental exposure.

actually shows a slight tendency toward increased joint strengths as a result of burial.

The changes in joint strength of the variety of buried epoxy adhesive bonded stainless steel specimens do not provide complete insight into the mechanism(s) of deterioration involved; however, some useful observations can be made. In most cases, the buried samples show significantly lower values than the one-year shelf control, indicating a definite degradation caused by the earth environment. Humidity or moisture effects during pretest conditioning can be ignored since all of the specimens and controls were exposed to the same 30-day, 95°F, 90-percent RH. Also apparent is a tendency for Bainbridge to be a harsher environment than Roswell. Because of the absence of fugitive adhesive components, the rate of joint strength loss in this group of samples does not appear to indicate a biological type degradation of the epoxy adhesives, since one might expect a more rapid and complete

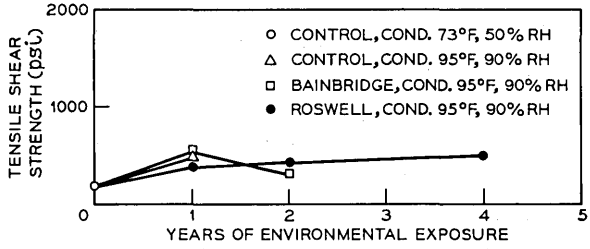

Fig. 11—Tensile shear strength of #203 adhesive bonded stainless steel test specimens vs years of environmental exposure.

failure of the specimens or, at least, no indications of leveling off. The significant difference in the behavior of #197 and #198 is indicative of a chemical attack on the filler which is probably a mineral type material. Conversely, #200 and #204 both contain metal (aluminum) fillers and neither of these exhibits the large decrease in strength experienced by #198. Of particular interest is the behavior of #201 and #202, which fits a pattern most easily explained by the leaching of unreacted polysulfide polymer that was acting only as a plasticizer. It may indicate that the typical epoxy chain extension and subsequent crosslinking caused by polysulfide/amine combinations may not occur with primary aromatic amines when cured at 250°F. This would leave the polysulfide as an unreacted and fugitive plasticizer. Additional shelf-aging data may confirm this when they become available.

A mechanism which may be controlling the degradation of the epoxy stainless steel systems is either a slow soil-chemical attack on the epoxy base resin or possibly a chemical attack at the metal/adhesive interface.

Little can be said about the polysulfide rubber system from only tensile shear data; however, one would expect that a crosslinking reaction was taking place while it was buried and that other changes such as lower elongation and increased hardness would also result.

2.4 *Engineering Implications of Data*

It is apparent, from the data presented, that adhesives can provide useful service under soil burial conditions. Most epoxy and modified-phenolic systems appear to offer adhesive qualities superior to the interlaminar shear strength of glass fiber laminates even after eight years of unstressed burial. The experiments indicate that abrasion is a satisfactory surface preparation for these laminates, and that it is possible to design joints which would be suitable for buried telephone plant applications.

The bonding of stainless steel for direct soil burial also appears to be a viable technique provided adequate care is taken in the surface preparation of the substrates. Deterioration of the ultimate load-bearing capability is experienced, with indications of continued declines after four years; however, the strength levels of some systems are well above typical requirements for bonded structures and they would be expected to perform satisfactorily with proper joint design. It must be emphasized that the data presented are the ultimate strengths after environmental conditioning without external loads. It has been shown[8,9] that the failure of some adhesive bonded test joints under moderate

static stress was hastened by the presence of high humidity. Additionally, most practical joint designs incur a combination of static and dynamic loading which experience has shown to be a more severe condition than static loading alone. Appropriate joint designs would take account of these factors.

III. PRESSURE-SENSITIVE TAPES

3.1 *Description of Tapes Tested*

3.1.1 *Types of Material*

Four types of tape (three pressure-sensitive adhesive and one composite rubber) were included in the soil burial program. All of the tapes were commercial products purchased under a Bell System specification and in general use at that time. The pressure-sensitive adhesive tapes included samples with vinyl, aluminum, and glass fabric backing, while the rubber tape was composed of a layer of vulcanized rubber coated with a layer of tacky, unvulcanized rubber. A more complete description of the four tapes is provided in Table V.

3.1.2 *Expected Service Life*

A variety of factors (approximately equivalent to the number of different applications) govern the expected service life of a pressure-sensitive tape.

The specification grade of vinyl tape included in this program is intended for use in splicing plastic-sheathed cables. The author would expect a service life of perhaps twenty years in buried environment; however, other applications have been noted where vinyl tapes become unsatisfactory in much shorter periods.

The glass tape is intended to serve as a mechanical reinforcement

TABLE V—PRESSURE-SENSITIVE ADHESIVE TAPE CHARACTERISTICS

Characteristic	Vinyl Tape	Glass Tape	Aluminum Tape	Rubber Tape
Overall thickness, inch	0.009–0.011	0.006–0.008	0.004–0.005	0.045–0.050
Backing	Plasticized vinyl	Glass cloth	0.003-inch aluminum foil	0.015-inch vulcanized rubber
Adhesive type	Rubber-resin	Rubber-resin	Rubber-resin	Unvulcanized rubber

in making gastight cable sheath closures. Very long service life (20–40 years) would be expected because of the stability of the glass, provided the installation did not permit unraveling due to adhesive failure.

The aluminum tape is intended to provide a mechanical reinforcement and a moisture barrier for cable sheath closures and should have a service life similar to the glass tape above, provided the thin aluminum backing is either adequately protected, or is not in direct contact with either a strongly acid or alkaline soil.

The rubber tape is used for splicing station wire, distributing wire, and cables. Its service life would be expected to run 10–20 years depending on atmosphere conditions, particularly ozone concentration.

3.2 *Materials*

3.2.1 *Tapes*

Pressure-sensitive adhesive tape can be described generally as a flexible backing material which has been coated with a tacky adhesive. Figure 12 shows a sectional view of a tape including features that may be optional for some tapes.

The four types of tape used in this program are all proprietary with respect to their specific composition and formulations. The tapes were purchased against a Bell System specification which controls certain use and quality requirements, thus allowing the manufacturer con-

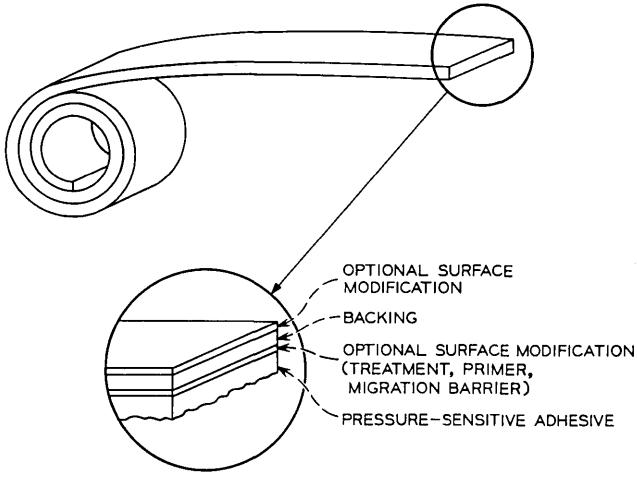

Fig. 12—Section through pressure-sensitive tape.

siderable formulating flexibility. Samples used in the Bainbridge burial were from different manufacturing runs from those used in the Roswell experiments, while the vinyl tape and the glass tape samples were obtained from different manufacturers.

3.2.2 *Backing*

The backing material of a tape is the major contributor to the physical properties of a tape and, because it is that part of a tape usually exposed to an environment, is most likely to experience considerable changes.

The vinyl tape uses a fairly soft or highly plasticized vinyl sheet for its backing. The vinyl formulation would typically consist of poly (vinyl chloride) resin, one or more plasticizers (mostly monomeric), stabilizers, coloring agents, fillers, and processing aids. Two mechanisms of deterioration exist: one is the loss of plasticizer through volatilization, extraction, or migration, and the other is dehydrochlorination due to the natural thermal instability of the vinyl resin. The stabilizers minimize deterioration by reacting with the HCl formed until they are all used up, at which point the degradation becomes very rapid, since it is catalyzed by the presence of free HCl.

The glass cloth used in the glass tape would normally be considered quite stable to most environments; however, the sizing or surface lubricant which reduces abrasion damage may be subject to chemical or biological attack. Damage to the aluminum foil backing would be expected to be exclusively chemical and reflect itself as a decrease in strength. The rubber backing would be expected to undergo change, but the type of the change would depend on the specific interaction taking place, e.g., oxidation, crosslinking, chain scission, etc.

3.2.3 *Adhesives*

The adhesives used on pressure-sensitive tapes are generally based on a rubber (either natural or synthetic) that has been compounded with a variety of modifiers such as stabilizers, tackifiers, antioxidants, curing agents, colorants, reinforcing agents, fillers, extenders, etc. In thin layers, the adhesives are usually applied as emulsions or from solvent solution; in greater thicknesses they may be calendered onto the backing. Degradation of the adhesive layer by a soil environment would be expected to proceed slowly, unless the backing were attacked rapidly to provide access to the adhesive or if some component were readily leached by surface water.

3.3 *Test Methods*

3.3.1 *General*

Physical property tests for pressure-sensitive tapes are generally oriented toward either the adhesive or the backing even though there can be a significant interplay. In this program, tensile properties of the backing and peel adhesion of the adhesives were used to determine the effects of soil burial. All of the tapes were tested for tensile strength while the two extensible tapes were also tested for elongation and "modulus" (load) at 50-percent elongation for the vinyl and at 200-percent elongation for the rubber. The significance of the "modulus" number is an indication of the force necessary to provide a common degree of application stretch; however, when measured after soil burial the data provide an indication of embrittlement.

"Adhesion" was measured as a T-peel test of one adhesive tape to the back of another piece of the same tape. This procedure had the advantage of minimizing data scatter caused by difficulties in obtaining uniformly clean surfaces for peel test.

3.3.2 *Sample Preparation*

Individual test specimens were prepared for both the peel and tensile tests prior to soil burial. The tensile specimen was made by laminating two strips of tape together (adhesive to adhesive) and then die cutting the required dumbbell specimen.* Tensile strength, elongation, and "modulus" were all determined from these specimens, if applicable.

The specimens for peel testing were prepared by applying a strip of tape to a hard surface, applying a second strip on top of the first, then trimming to a 3/4 inch width. The exposed adhesive face was covered with 0.001-inch polyethylene film to protect it from the soil. One end of the specimen was separated for 2 inches to allow gripping by the testing machine.

3.3.3 *Sample Testing*

All tape testing was conducted on an Instron Testing Machine under the conditions shown in Table VI. The values for tensile properties are expressed in terms of pounds per inch of width, and the adhesion as ounces per inch of width.

---

* ASTM D412 Die C.

TABLE VI—TAPE TESTING PARAMETERS

Material Type	Tensile Tests		Adhesion Tests	
	Crosshead Speed in/min	Full Scale lbs load	Crosshead Speed in/min	Full Scale lbs load
Vinyl	12	20	12	2
Aluminum	0.02	20	12	2
Glass	12	50	12	2
Rubber	20	20	12	5

3.4 *Results and Discussion*

3.4.1 *Vinyl Tape*

Figure 13 shows graphically the changes in the four test values obtained on the vinyl tape as a function of aging time. The six lines in each graph represent indoor storage and burial in both topsoil and subsoil for the samples used in the two exposure locations.

Neither of the two samples of vinyl tape shows very large changes in its physical properties; however, subtle differences can be detected which follow distinct patterns. In the tensile strength area, we see that the Bainbridge specimens experience very little decrease while the control shows about a 15-percent increase. The Roswell specimens show a slight decrease with very little difference between top soil and subsoil specimens while the control shows about a 10-percent decrease. Elongations decreased significantly for the Bainbridge samples, including the shelf-aged control, while the two buried Roswell samples decreased less but mainly after two years of burial. The unusual result in this group was the control for the Roswell samples which showed an increase in elongation of almost 25 percent after two years.

The Roswell control actually fits a pattern of increase in plasticizer content since the tensile strength and "modulus" decreased and the elongation increased. This, however, is not the typical behavior of a plasticized vinyl, which tends to lose plasticizer on aging and follows the pattern of all the other specimens, e.g., tensile and modulus increase with elongation decrease.

The modulus changes show very close parallels for all three aging conditions of the Bainbridge specimen and the two buried Roswell specimens. It appears that the Roswell control specimen was inadvertently allowed to absorb plasticizer, either from another plasticized vinyl or from an accidental spill.

The two manufacturers' samples show adhesion values which are unaffected by the burial environment, since extremely close alignment of values occurred between topsoil, subsoil, and control for each sample over the period of the test. The absolute values for the Roswell sample showed increased adhesion values of almost 25 percent while the other sample decreased by a similar amount. The increase in adhesion values might be a result of the increase in backing modulus or stiffness plus, perhaps, a very slight crosslinking in the adhesive and a small contribution from a phenomenon known as "building tack." Building tack is a time-dependent function of the adhesive's ability to wet out a surface completely. Most pressure-sensitive adhesives will achieve 99 percent of their building tack in from 1 to 7 days. The fact that

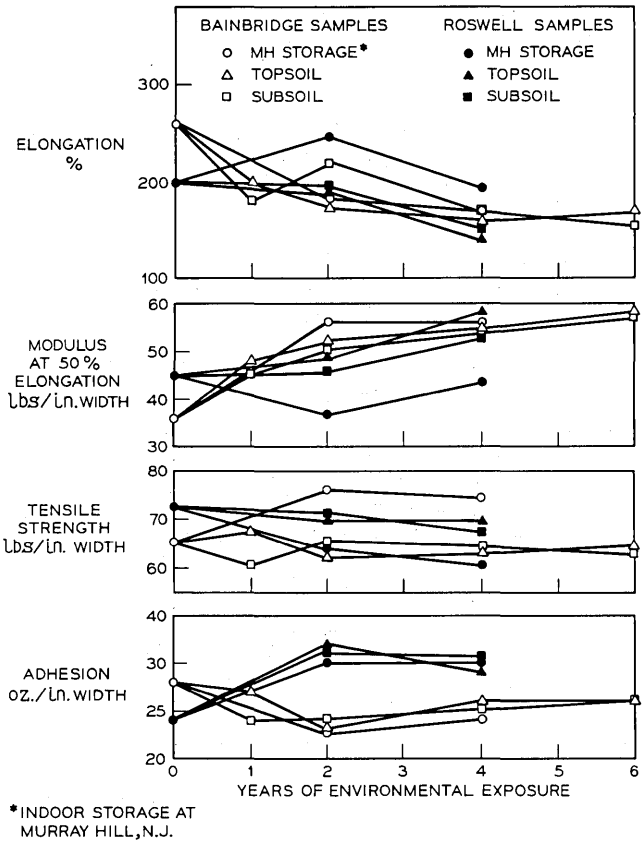

Fig. 13—Vinyl tape test results vs years of environmental exposure.

the sample from Bainbridge showed decreases in adhesion, despite significant increases in stiffness of the backing, shows that the adhesive is being degraded. This may take the form of oxidative degradation, beyond the stage of mild crosslinking, or plasticizer migration where the adhesive absorbs plasticizer from the backing and becomes soft and stringy with a much lower cohesive strength.

3.4.2 *Glass Tape*

The test results from the glass tape evaluation are shown in Fig. 14. In general, it can be seen that not only soil burial but also shelf aging had a marked effect on the tensile strength and adhesion values of the glass tape. Also shown is the difference in aging pattern at the two

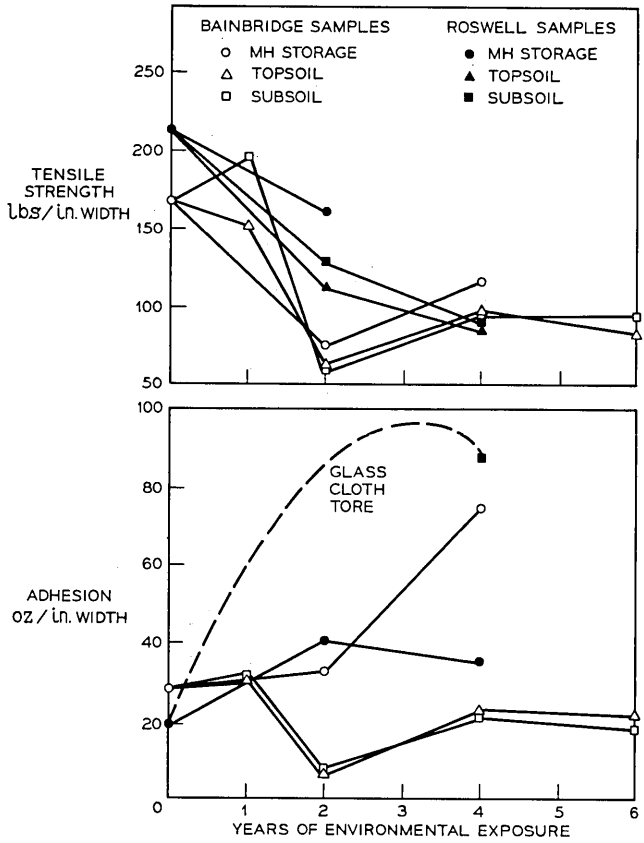

Fig. 14—Glass tape test results vs years of environmental exposure.

burial sites, but since different manufacturers' products were used at each location, it may be difficult to draw useful conclusions.

The specimens buried at Roswell showed a significant and steady decrease in tensile strength for both topsoil and subsoil conditions. Two-year shelf aging also produced a significant decrease in tensile strength, but less than the buried specimens. The specimens buried at Bainbridge were somewhat more erratic in their tensile strength values, e.g., the one-year subsoil specimens were actually higher than the original test value, while the two-year specimens were very low and four- and six-year specimens were higher in value than the two-year specimens.

Adhesion values are also erratic, e.g., the Roswell shelf-aged control doubled in two years while the glass tore in the buried specimens before the adhesive failed. After four years, a value of 88 oz/in of width was obtained on the subsoil buried specimens, or over four times the unaged value. The topsoil specimens tore before adhesive failure, presumably at values above the 88 oz/in which was sustained by the subsoil specimens. The shelf-aged Roswell control exhibited a slight decrease after six years versus four years. The Bainbridge adhesion specimens behaved the opposite of the Roswell specimens. The shelf-aged control underwent very little change at two years, then rose rapidly to more than double the initial value at four years. Topsoil and subsoil buried specimens virtually overlapped each other in test values with the two-year specimens falling significantly out of line with an otherwise very gradual decrease.

The general performance of the glass tape is indicative of several important changes taking place. The glass backing itself is losing strength in both manufacturers' products. Presumably this is due to the sizing's loss of effectiveness in preventing mechanical (abrasion) damage to the glass fibers. The adhesive, on the other hand, shows significant differences for the two manufacturers. The Roswell samples show rapid crosslinking at ambient temperature conditions (limited shelf life) followed by a degradation of mechanical properties probably due to oxidation and embrittlement. The Bainbridge samples show a slower initial room temperature thermosetting rate followed by a very rapid one. The thermosetting rate was inhibited for the buried specimens, but sufficient data are not available to determine if the lower soil temperature or the soil chemistry was the inhibiting factor.

3.4.3 *Aluminum Tape*

Figure 15 shows the test results for the aluminum tape. Samples buried at Roswell showed very little difference in tensile strength from

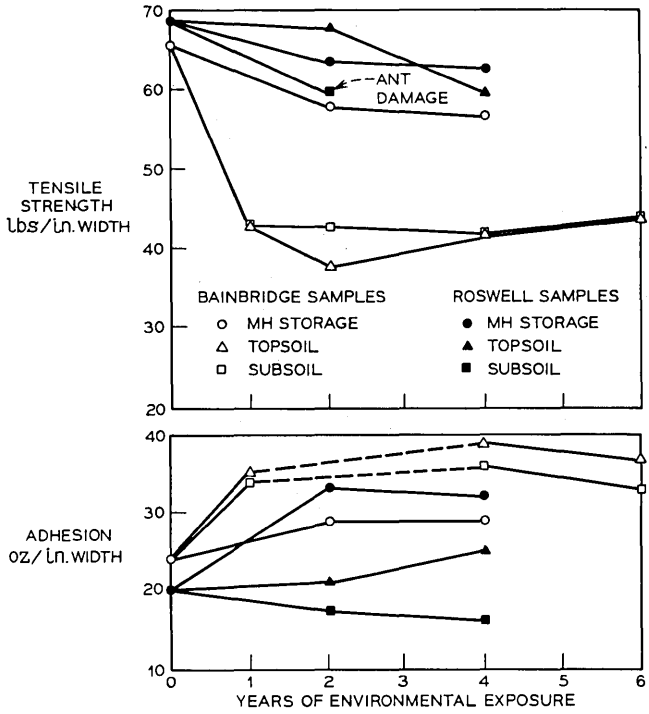

Fig. 15—Aluminum tape test results vs years of environmental exposure.

the control (shelf-aged) specimen up to four years, except that the four-year subsoil specimens showed ant damage and were not tested. The first-year specimens buried at Bainbridge were approximately 30 percent below the initial values and continued considerably below the control after subsequent periods. It is apparent that the acid condition of the Bainbridge soil had at least an initial corrosive effect on the aluminum backing, whereas the mildly alkaline Roswell did not.

Adhesion values for the Roswell samples remained relatively constant, the subsoil specimens showing a slight decrease, and the topsoil specimen a slight increase over the control. The two- and four-year shelf-aged specimens both exhibited a large increase over the initial value. The Bainbridge results, except at two years, are considerably higher than the Roswell specimens and their own shelf-aged controls. The Bainbridge shelf-aged control did not exhibit the same magnitude of increase in adhesion as shown by the Roswell control. This can be attributed to differences in the adhesive coating and its concentration of cross-

linking agents or to the possibility of an inordinate delay in obtaining the initial test results, which would have allowed the building tack factor time to increase the initial value.

3.4.4 *Rubber Tape*

Figure 16 illustrates the test results obtained on shelf-aged and buried specimens of rubber tape. It should be remembered that the rubber tape is much thicker than a regular tape (0.045 inch with 2/3 unvulcanized white rubber and 1/3 of vulcanized dark rubber). All original and shelf-aged specimens exhibited very little change except for adhesion.

Significant changes occurred in the buried specimens mainly over the first period of test. Values for the topsoil and subsoil specimens

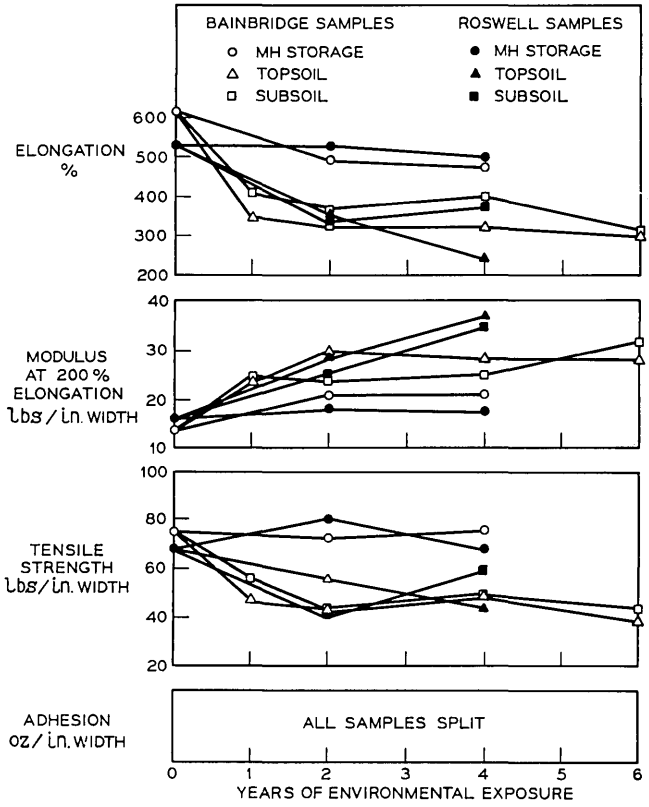

Fig. 16—Rubber tape test results vs years of environmental exposure.

were very close indicating little dependence on the depth of burial. Losses of up to 45 percent in elongation and 40 percent in tensile strength and gains of about 100 percent in modulus could be attributed to the soil burial. Adhesion values were not plotted because of the nature of the tape and the fact that after the initial tests all readings were no longer adhesion but tear in the white rubber at values in the range of 200 oz/in of width.

The deterioration in physical properties of the rubber tape is most likely due to biochemical attack causing oxidation and embrittlement of both the vulcanized and unvulcanized portions of the tape.

3.5 *Engineering Implications Of Data*

The test methods for the soil burial program on tapes were chosen so as to learn as much about the properties of the tape as possible. It is now appropriate to discuss these changes in properties in terms of the performance of a tape in a typical use context.

A vinyl tape installed properly over a cable or conduit for soil burial would be expected to cause no problem based on the findings of this study. The changes in elongation capability and the increased stiffness of the backing would not have a functional bearing on the cable, nor would it cause the tape to cease performance of its function. It would indicate that a tape exposed to the environment would not be suitable for reuse were it to be removed.

The glass tape shows characteristics which would be of concern for other than temporary applications. In particular, the rapid deterioration of tensile strength and the erratic adhesion performance are undesirable, especially since the glass tape would be used on high-stress applications. This could mean that even the slightest movement or differential expansion of an underground cable could cause a loss in adhesion or an actual tensile break.

The aluminum tape ages well under burial conditions but exhibited some attack in the more acid soil of Bainbridge. It is assumed that adequate protection of the thin aluminum backing (by overcoating with a barrier material) would retard the corrosion in both strong acid and alkaline soils. The main purpose of the tape as a moisture barrier would then remain in effect.

The rubber tape, although degraded by soil burial, should still provide reasonable service. The amount of deterioration is insufficient to cause a mechanical failure since adequate amounts of elongation and tensile strength remain after long exposure to soil environments.

IV. ACKNOWLEDGMENTS

The author would like to express his appreciation for the efforts of D. J. Maccia and the late J. D. Cummings in collecting the test data.

REFERENCES

1. Connolly, R. A., "Soil Burial of Materials and Structures," B.S.T.J., this issue, pp. 1–21.
2. *ASTM—Standards Book 16*, Philadelphia: American Society For Testing and Materials, 1970.
3. Skeist, I., *Epoxy Resins*, New York: Reinhold Publishing Corp., 1964.
4. Lee, H., and Neville, K., *Epoxy Resins*, New York: McGraw-Hill, 1957.
5. Lee, H., and Neville, K., *Handbook of Epoxy Resins*, New York: McGraw-Hill, 1967.
6. Bruno, E. J., *Adhesives in Modern Manufacturing*, Dearborn, Michigan: Society of Manufacturing Engineers, 1970, p. 8.
7. Klein, T. H., "Effect of Soil Burial Exposure on the Properties of Structural Grade Reinforced Plastic Laminates," B.S.T.J., this issue, pp. 51–62.
8. Rider, D. K., "Adhesives Engineering," Trans. N. Y. Acad. Sci., Series II, *29*, No. 6 (1967), pp. 711–721.
9. Sharpe, L. H., "Some Aspects of the Permanence of Adhesive Joints," Appl. Polym. Symposia, *3*, (1966), pp. 353–359.

Copyright © 1972 American Telephone and Telegraph Company
THE BELL SYSTEM TECHNICAL JOURNAL
Vol. 51, No. 1, January, 1972
Printed in U.S.A.

Soil Burial Tests:

Trends in Material Behavior After Eight Years of Soil Exposure

By R. A. CONNOLLY

(Manuscript received December 8, 1971)

The preceding papers have presented detailed coverage of soil burial effects on specific classes of organic materials. This paper summarizes some of the trends which have emerged in the eight years of soil exposure in both acid and alkaline soil:

(*i*) *High-density and black crosslinked polyethylenes, rigid PVCs, acrylics, polycarbonates, acetates, fluorocarbons, styrene polyesters, unfilled epoxy, neoprene without clay, and sulfur-cured nitrile rubber have been essentially unaffected.*

(*ii*) *Insect attack is confined to the soft forms of materials such as cellulosics, rubbers, and thermoplastics, specifically low-density polyethylene and certain plasticized poly(vinyl chloride) samples. All cast resins, structural laminates, and hard thermosetting plastics have been completely free of insect attack.*

(*iii*) *With both plastics and elastomers, significant losses in tensile strength are almost always accompanied by large decreases in insulation resistance.*

(*iv*) *Some plastic materials tend to increase in tensile strength due to the loss of constituents while some lose strength because of chemical breakdown. The reinforced thermosetting materials decrease in strength because of moisture penetration along the resin-fiber bond.*

(*v*) *Of the plasticized PVC wire insulations, the materials with trioctyl and octyl diphenyl phosphate, and dioctyl adipate blend, have shown significant increases in modulus indicative of plasticizer loss due to leaching and/or microbial consumption.*

(*vi*) *Unless there is chemical breakdown or biological damage, the strength losses of all molded plastics and many elastomers appear to level off, after four years of exposure, at about 25–45 percent.*

(*vii*) *Epoxy and phenolic adhesives for bonding reinforced polyester laminates were not severely attacked but rather laminate failure occurred in all cases. In contrast to this, bonds to stainless steel generally decreased in a straight-line relationship.*

(*viii*) *There has been no appreciable effect of 6-inch versus 18-inch depth on materials performance and no significant consistent difference between the two plots.*

I. INTRODUCTION

It is difficult to pick out trends from the data discussed in the preceding papers but there are some trends that may aid design engineers in developing longer lasting structures for buried plant. The effects are categorized for discussion as follows:

(*i*) Moisture/property
(*ii*) Biological
(*iii*) Site and depth of burial

These effects also are shown in Table I.[1] The numbers in this table, however, are not exclusive (i.e., some materials may be affected in more than one way) and therefore are not additive.

II. MOISTURE/PROPERTY CHANGE

A minimum of one-third of the materials in any one class in Table I (except the adhesives and thermoplastics) has shown a significant property change (arbitrarily chosen as $\geqq$ 25 percent) due to chemical or moisture influences. For instance, the effects of soil burial on the insulation resistance of certain elastomers and thermoplastics and thermosetting plastics is shown in Table II. The plastic materials that have markedly changed are the cellulosics, polyamide type 6, melamine glass, styrene polyester glass, alkyd glass, the silica-filled styrene-butadiene copolymer, and all the elastomers except the natural rubber jacket. With the exception of the cellulosic esters, the polyamides which can undergo hydrolysis, and possibly the styrene materials, the dc resistance of thermoplastic compounds has not been affected by soil burial. In contrast to this, it is very apparent that all the thermosetting materials, phenolics, diallyl phthalates, melamine, styrene polyester glass, alkyd and styrene-butadiene glass, which can absorb considerable

TABLE I—FACTORS FOUND TO CAUSE DEGRADATION OF PLASTIC AND ELASTOMERIC MATERIALS

Class of Materials	Number of Materials	Affected by			Materials in Categories							
			Site		Moisture/Property*		Microorganisms†		Rodents		Insects	
		Depth	Ga	NM	No. Affected	% Affected	No. Affected	% Affected	No. Affected	% Affected	No. Affected	% Affected
Tensile Bar or Sheet												
Thermoplastic	28	No	No	No	7	25	3	13	1	4	13(0)	46
Thermosets	10	No	No	No	3	33	0	0	0	0	0	0
Casting Resins	3	No	No	No	1	33	0	0	0	0	0	0
Rubber	17	No	No	No	8	47	9	53	0	0	10(2)	59
Pressure Sensitive Tapes	4	No	Yes	No	3	75	1	25	0	0	1(0)	25
Plastic Insulation												
Polyethylene	18	No	No	No	7	39	0	0	0	0	17(6)	94
Poly (Vinyl Chloride)	15	No	No	No	5	33	8	53	0	0	12(2)	87
Rubber	18	—	—	—	11	61	15	83	0	0	15(11)	83
Reinforced Plastic Laminates												
Structural Grade	20	No	No	No	12	60	0	0	0	0	0	0
Electrical Grade	23	No	No	Yes	23	100	2	8	0	0	2(1)	8
Adhesives	15	No	No	No	0	0	0	0	0	0	0	0

* Based on mechanical or electrical changes $\geqq 25\%$.
† Based on known susceptibility.
( ) Destroyed.

TABLE II—DC INSULATION RESISTANCE OF PLASTICS AND ELASTOMERS

Materials	Years of Exposure	Orders of Magnitude of Change			
		1	2	4	8
Thermoplastics					
Cellulosics (4)*		0	0	2	½
Styrenes (2)		½	1½	½	½
Acrylics (3)		0	0	1	0
Polyolefins (2)		0	0	0	0
Poly (Vinyl Chloride) (2)		0	0	0	0
Polycarbonate (1)		0	0	0	0
Acetals (2)		0	0	0	0
Fluorocarbon Polymers (2)		0	0	0	0
Polyamides (2)		2	2	2	2
Thermosets					
Phenolics (4)		1½	1	½	1
Diallyl Phthalates (2)		1	2	½	1
Melamine, Glass (1)		3	3	2	3
Styrene Polyester, Glass (1)		3	3	3	
Alkyd, Glass (1)		2	2	3	
Styrene-Butadiene Copolymer (1)		3	4	4	
Elastomers					
Natural Rubber Insulation		−5			
Natural Rubber Jacket		−0			
SBR Insulation (3)		−½			
SBR Jacket		−2½			
Neoprene Jacket, Type W, MgO		−2½			
Neoprene Jacket, Type W, red lead cure		−2½			
Neoprene Jacket, Type W, with red lead cure and zinc salt of dimethyl dithiocarbamic and zinc salt of 2 mercaptohenzo thiozole		−3			
Butyl Rubber Insulation		−3½			
Chloro-Sulfonated Polyethylene		+½			
Silicone Rubber		−6			

* Number of different formulations in the group.

amounts of water by wicking, for example, have lost significant dc insulation resistance. In line with these trends, Fig. 1 shows the tensile strength changes of some of the poorer materials. In a soil environment, the thermoplastic materials that do show significant changes tend to increase in strength due to loss of plasticizers, lubricants, etc. The cellulosics may contain dibutyl sebacate which has shown a tendency to leach from the material. The thermosetting materials which have reinforcing material in the form of particulate or fibrous fillers, etc., lose tensile strength due to water absorption along the interface of the matrix and reinforcing material. It appears that most of the materials that have shown large losses in dc resistance have also shown large losses in tensile

strength. No material lost significant tensile strength that did not also show a large insulation resistance loss.

Another rather pronounced trend shown in Fig. 1 is that the tensile strength losses appear to have leveled off between the fourth and eighth years. Of course, the long-term trend will be better defined after the 16-year inspections in 1974 and 1976.

The insulation resistance of the elastomer insulated or jacketed wires exposed for only one year at Bainbridge was generally poor. As shown in Table II, natural rubber insulation, SBR jacket, all the neoprenes (with and without fungicides), butyl rubber, and silicone rubber failed badly after only one year. Table III lists the range of tensile strength losses for 17 elastomers and, as with the plastic materials, no significantly large change in tensile strength occurred without an accompanying large drop in insulation resistance. A plot of the tensile data is shown in Fig. 2 and, as with the plastic tensile data, appears to be leveling off in some materials. The exceptions, of course, are the ester-based polyurethanes which failed completely between the second and

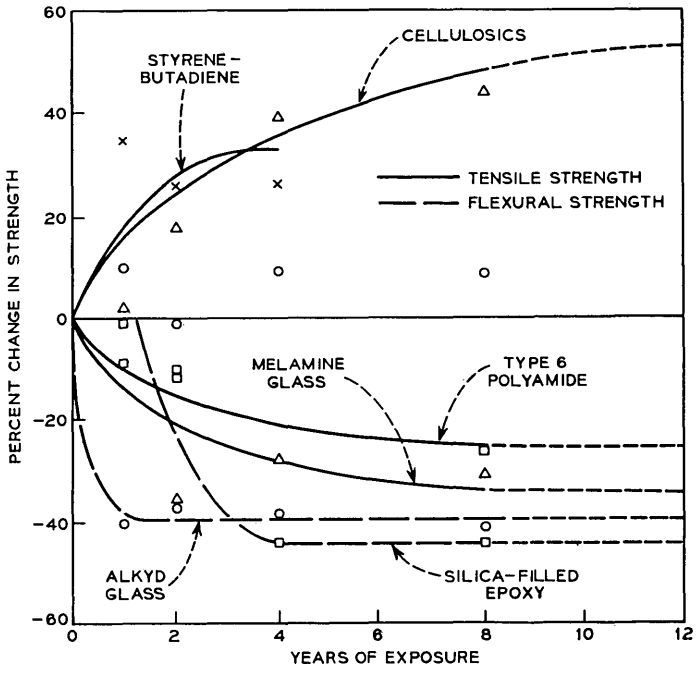

Fig. 1—Strength changes of plastic materials versus soil exposure time.

TABLE III—TENSILE STRENGTH REDUCTIONS IN ELASTOMERIC COMPOUNDS AFTER UP TO EIGHT YEARS OF SOIL BURIAL EXPOSURE

Material	Tensile Strength Loss −%				
	+15–0	1–15	16–25	26–50	>51
Natural Rubber, black					√
Styrene-Butadiene Copolymer			√		
Polychloroprene, with clay					√
Polychloroprene, no clay, black		√			
Nitrile Rubber, sulfur cure	√				
Nitrile Rubber, heat resistant			√		
Butyl Rubber, sulfur cure				√	
Butyl Rubber, quinoid cure				√	
Polyethylene, low density, crosslinked, black	√				
Polyethylene, crosslinked, black		√			
Polyethylene SBR, crosslinked, black	√				
Polyurethane, ester based, black					√
Polyurethane, ether based, black, sulfur cure		√			
Ethylene Propylene Copolymer, peroxide cure, black			√		
Chloro-Sulfonated Polyethylene			√		
Ethylene Propylene Terpolymer, sulfur cure				√	
Ethylene Propylene Terpolymer, sulfur cure, clay loaded, black				√	

fourth years and natural rubber which appears to be steadily decreasing.

Unfortunately, not all of the elastomeric materials tested for tensile strength retention were evaluated for insulation resistance. However, the tensile data for natural rubber, neoprene loaded with clay, ester-based polyurethane, and butyl rubber are in complete agreement with the insulation resistance data.

Of the 23 types of electrical-grade laminates based on phenolic, melamine, silicone, epoxy, and polyester resins each suffers a large decrease in insulation resistance, which may be as high as 90 percent, while showing only moderate decrease in flexural strength. Since these materials are thin and contain some form of reinforcing, the

effects of water have been magnified. These materials are clearly not suitable for direct soil burial.

Structural-grade epoxy and polyester type laminates exhibit the same degree of mechanical degradation and after eight years maintained 65 to 70 percent of their initial flexural strength. The laminates with fiber glass cloth reinforcement retained 80 to 85 percent of their strength and have superior resistance to soil burial than all the other methods of reinforcement (such as chopped strand mat which lost 40 to 45 percent of its strength).

The epoxy and phenolic type adhesives for bonding polyester-based laminates performed well since laminate failure occurred in all cases between the first and second layers of glass mat. This, of course, meant that what was being measured was the interlaminar shear strength plus the tensile strength of a single ply of the substrate. The results indicate that these adhesives were not severely attacked by these environments. Even with good surface treatments, epoxy-bonded stainless steel shear lap specimens continue to lose their ultimate load bearing capacity with time. However, since the initial strength levels are well above typical requirements, they would be expected to perform satisfactorily with proper joint design.

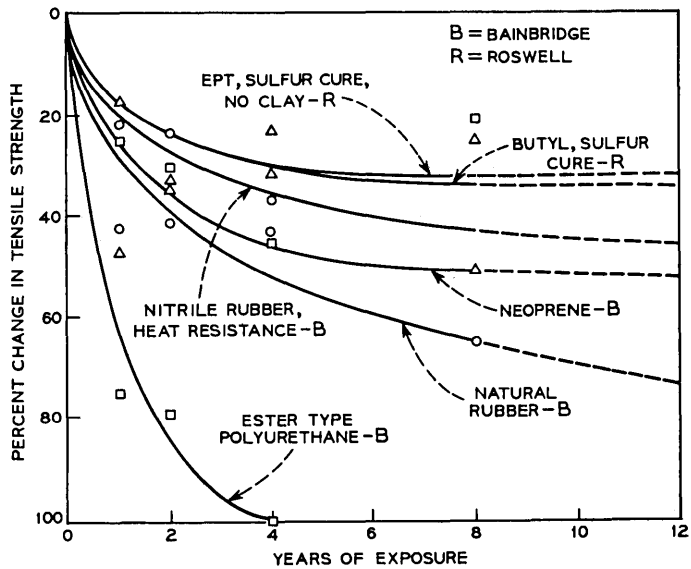

Fig. 2—Tensile strength changes of elastomeric materials versus soil exposure time.

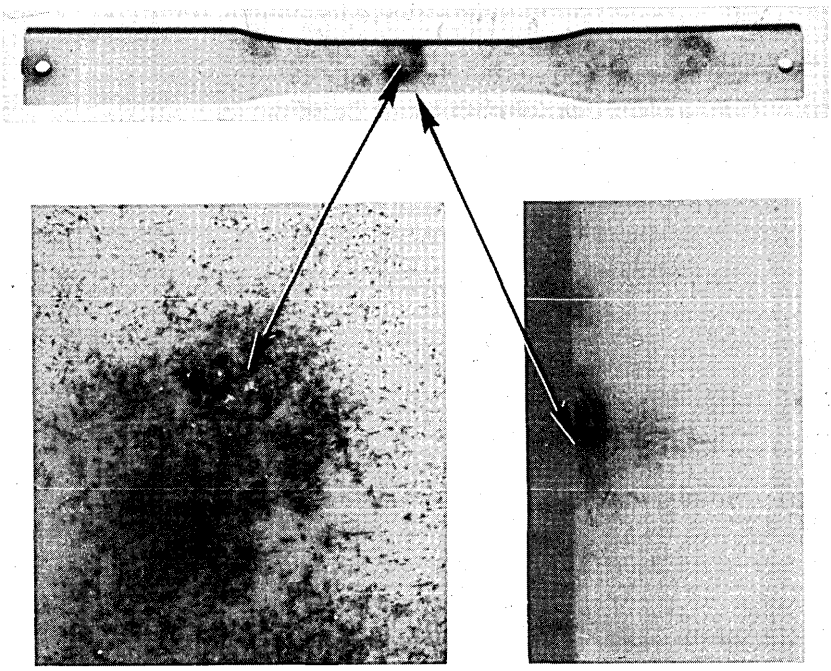

Fig. 3—Ester-based polyurethane with pronounced fungal attack.

Of the four adhesively backed tapes evaluated in this program, both the vinyl and rubber types have maintained sufficient strength after up to eight years and should continue to do so while the glass type has shown large losses in tensile strength and erratic adhesion and the aluminum tape has been damaged by corrosion. These last two are therefore not recommended for direct soil burial, except for short-duration applications.

III. BIOLOGICAL PROPERTY CHANGE

The results of this program to date generally support the work in the literature relating to biological damage.

Table I also shows the materials affected by fungi. The best example of this is the molded ester-based polyurethane which, after two years in Roswell, showed considerable surface fungal growth. This growth can be seen on Fig. 3 in the form of black discoloration. A closer examination shows penetration over half-way through the sample. Interest-

ingly, the tensile strength of this material had not been significantly reduced after two years, but after four years there was a loss of 26 percent. In the future, if the fungal attack continues as expected, the strength and other properties will continue to be degraded significantly.[2] Another good example is the wood flour filled phenolplastic tensile sample which, after eight years of exposure, showed a dimpled surface (Fig. 4). Initially, these samples had a resin-rich surface with essentially no wood flour exposed. With the absorption of water, the thin surface layer of resin fractured due to expansion and the wood flour was exposed to the environment. Subsequently, decay started and resulted in the white mycellia shown in Fig. 4.

With respect to insect damage, the results in this study are in agreement with those of Flateau,[3] and Gay and Wetherly.[4] The former has found over a 1- to 20-year period in Australia that rigid PVC, high-density polyethylene, and polyesters are highly resistant while natural rubbers, polyurethane, and plasticized PVC, cellulose acetate, and the

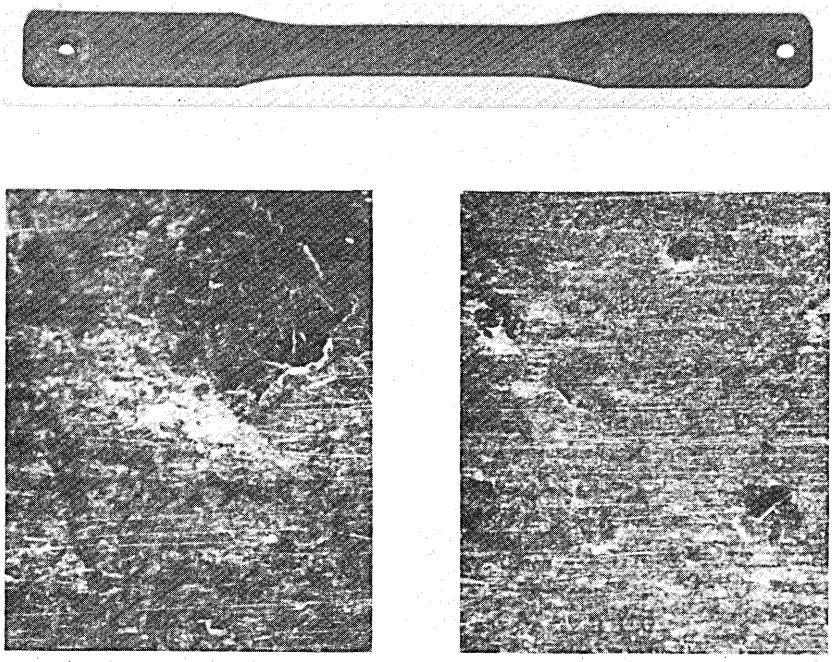

Fig. 4—Phenolplastic (one-step, wood flour) after eight years of exposure showing dimpling of the surface. Enlargement on the right shows several dimples and the one on the left shows the cracked resin and white fungal growth.

synthetic rubbers are moderately resistant to nonresistant materials, Gay and Wetherly report that few plastic materials in common use are immune to attack while materials such as plasticized PVC, polyethylene, and cellulose are liable to severe damage. Figure 5 shows the edge type

Fig. 5—Clay-loaded neoprene illustrating insect attack at edges (3/4X) and typical tufted appearance (25X).

of insect damage observed on many samples. The tufted pattern is typical.

Table I shows that about 32 percent of those samples with insect attack (does not include any casting resins or plastic reinforced laminates) failed. If the total number of materials is considered, 20 percent failed because of insects. Failure in the case of the insulated conductors means exposing bare metal while in the case of the tensile samples it means chewing completely through the sample.

Although other studies[5–8] have demonstrated that thermoplastic and elastomeric materials are susceptible to rodent damage, essentially none occurred in this program. This is due to the low population density of the animals at the test sites and the lack of the long horizontal trenches made in cable laying that tend to attract rodents. Consequently, from the design standpoint, the data in Refs. 5–8 probably provide the more reliable information with regard to animal damage.

The observations of Berk, et al.,[9] show that certain plasticizers are susceptible to fungal attack. Their findings are supported by those of the U. S. Office of Scientific Research and Development[10] which has also reported heavy fungal growth in some materials. Selected phthalates trimellitates as well as blends of nitrile rubber may be expected to give adequate service in the soil. It appears that the plasticizer loss rate in these materials has leveled off or even slightly decreased. This suggests, with these particular plasticizers, either that microbial attack is not a major contributor to degradation or that they must migrate to the surface before microbial degradation can begin.

IV. EFFECT OF SITE AND DEPTH OF BURIAL

Although the chemistry of the two plots is markedly different, with very few exceptions no significant difference in materials behavior occurred during the eight years of exposure. However, it should be recognized that the averaging and grouping of materials tends somewhat to obscure the effects of soil burial on individual materials. Even so, some clear-cut changes did occur. For instance, the phenolic, melamine, silicone, epoxy, and polyester electrical-grade reinforced plastic laminates suffered more in the alkaline environment of Roswell than in the Georgia exposure. Direct soil burial of these laminates is not expected nor were they specifically designed for this environment. The aluminum pressure-sensitive tape corroded in the acid environment but was essentially unaffected in the mildly alkaline New Mexico soil. This is typical behavior for aluminum.

The effect of depth of burial, 6 inches and 18 inches, was virtually undetectable. In view of the rather small depth difference of 12 inches, this is not difficult to accept, especially since the site difference, which is much greater, also had little effect. This, however, does not mean that with some soils there may not be a difference; for example, soils with a high water table, etc., or different soil profiles.

V. CONCLUSIONS

Based on up to eight years of soil exposure, the following trends can be identified with respect to the performance of plastic and elastomeric materials:

(*i*) The materials that have been essentially unaffected by soil burial to date include high-density and crosslinked polyethylenes, rigid PVCs, acrylics, polycarbonates, acetals, fluorocarbon polymers, neoprene without clay, styrene-polyester and unfilled epoxy, and sulfur-cured nitrile rubber.

(*ii*) Insect attack is confined to the softer materials such as cellulosics, rubbers, and thermoplastics, specifically low-density polyethylene and certain plasticized poly(vinyl chloride) samples. All cast resins, structural laminates, and thermosetting plastics have been completely free of insect attack.

(*iii*) There has been no significant rodent attack on these materials or their supporting polyethylene tubes. This is mainly attributable to the low population density of these animals in the test areas.

(*iv*) With both plastics and elastomers significant losses in tensile strength are almost always accompanied by large decreases in insulation resistance.

(*v*) Some thermoplastic materials tend to increase in tensile strength due to the loss of constituents such as plasticizers, which results in embrittlement, while the reinforced materials decrease because of the moisture migration along the resin-fiber bond.

(*vi*) Of the plasticized PVC wire insulations, the compounds containing trioctyl and octyl diphenyl phosphate, dioctyl adipate blend, tricresyl phosphate, or dioctyl phosphate have shown significant increases in modulus, indicative of plasticizer loss due to leaching and or fungal consumption.

(*vii*) Nearly all elastomers exhibited large losses in insulation resistance while natural rubber, butyl rubber, clay-loaded

neoprene, ester-based polyurethane, and the sulfur-cured ethylene propylene terpolymers with and without clay exhibited tensile losses of greater than 25 percent.

(*viii*) The strength losses of all plastics appear to level off after four years of exposure at about 25 to 45 percent. This also seems to be true of the elastomers except for those materials shown to fail in soil environment.

(*ix*) There has been no appreciable effect of the 6-inch versus 18-inch depth on materials performance nor a significant consistent difference between the two test plots.

VI. ACKNOWLEDGMENTS

This summary is based on the preceding papers by R. J. Miner, J. B. DeCoste, G. H. Bebbington, D. W. Dahringer, F. X. Ventrice, T. H. Klein, and T. K. Kwei and their cooperation is acknowledged with appreciation.

REFERENCES

1. Connolly, R. A., "Soil Burial of Materials and Structures," presented at the Second International Biodeterioration Symposium, Lunteren, The Netherlands, September 18, 1971.
2. Greathouse, G. A., editor, and Wessel, C. J., joint editor, *Deterioration of Materials: Causes and Preventative Techniques*, New York: Reinhold, 1954, p. 835.
3. Flatau, G., "Protection of Telephone Cables from Attack by Insects," presented at the Fifteenth Annual Wire and Cable Symposium, December 7–9, 1966, 18 pages.
4. Gay, F. J., and Wetherly, A. H., *Laboratory Studies of Termite Resistance, V*, "The Termite Resistance of Plastics," Division of Entomology Technical Paper No. 10, Commonwealth Scientific and Industrial Research Organization, Melbourne, Australia, 1969, 49 pages.
5. Blain, R., "Gopher Protection of Buried Cable Plant," Telephony, April 24, 1965, pp. 12, 46, 48, 98.
6. Connolly, R. A., and Landstrom, R. E., "Gopher Damage to Buried Cable Materials," Materials Research and Standards, *9*, No. 12, 1969.
7. Kirk, J. D., Brooks, R. C., and Saul, D. G., "Progress and Pitfalls of Rural Buried Plant," Telephone Engineering and Management, April 15, 1970, pp. 64–67.
8. Howard, W. E., "Tests of Pocket Gophers Gnawing Electric Cables," Journal of Wildlife Management, *17*, 1953, pp. 296–300.
9. Berk, S., Erbert, H., and Teitell, L., "Utilization of Plasticizers and Related Organic Compounds by Fungi," Ind. Eng. Chem., *49*, July 1957, pp. 1115–1124.
10. U. S. Office of Scientific Research and Development, National Defense Research Committee, Tropical Deterioration Administrative Committee, *The Problem of Fungal Growth of Synthetic Resins, Plastics, and Plasticizers*, Report No. 6007, October 1945.

Copyright © 1972 American Telephone and Telegraph Company
THE BELL SYSTEM TECHNICAL JOURNAL
Vol. 51, No. 1, January, 1972
Printed in U.S.A.

Waiting Time Jitter

By D. L. DUTTWEILER

(Manuscript received July 15, 1971)

Waiting time jitter is a low-frequency phase jitter introduced whenever asynchronous digital signals are synchronized for multiplexing by pulse stuffing. It contains arbitrarily low frequency components and cannot be completely removed from the demultiplexed signals.

In this paper the spectrum of waiting time jitter is derived, and supporting experimentally recorded waiting time jitter spectra are presented.

A question of much engineering interest is at what rate waiting time jitter accumulates in a chain of multiplexer-demultiplexer pairs. A calculation based on the theoretical waiting time jitter spectrum shows that under reasonable conditions the rate at which the rms amplitude of the accumulated waiting time jitter grows is no greater than the square root of the number of multiplexer-demultiplexer pairs. Experimental data consistent with this upper bound are given.

I. INTRODUCTION

When a number of lower speed digital signals are to be time division multiplexed to form a higher speed signal, it is necessary that the lower speed signals all be synchronous. If the sources of these signals are remote, this synchronization will be difficult to achieve.

One way of achieving it is to distribute timing information from a master clock to the local clocks at the sources of the lower speed digital signals. In many situations, however, using a master clock and synchronizing the entire digital communication network is either not possible or not economically desirable.

An alternative method of achieving synchronization is to use pulse stuffing synchronization.[1,2] The pulse stuffing synchronization scheme is reviewed in the next section. Basically, the idea is to bring the symbol rates of each of the incoming lines up to some common rate just before multiplexing by inserting dummy pulses. After demultiplexing, the dummy pulses are removed and each of the signals retimed to smooth out the gaps.

The retiming can never be done perfectly. There is always a phase jitter present on the demultiplexed signals. In Sections III and IV the spectrum of this degrading jitter is derived. Its accumulation in chains of multiplexer-demultiplexer pairs is studied in Section VI.

II. PULSE STUFFING SYNCHRONIZATION

It is convenient to review pulse stuffing synchronization by describing the operation of a particular system. Since our experimental data were taken on the M12 multiplex, we have chosen this system to describe.[3] The reader should have no difficulty generalizing to other systems. The few details of the operation of the M12 that are essential for our discussion will be reviewed where necessary.

The M12 is designed to multiplex four asynchronous DS-1 digital signals (nominally 1.544 Mb/s) into a DS-2 bit stream (nominally 6.312 Mb/s).[4] For each of the four DS-1 digital data streams there is associated circuitry in the M12 designed to insert dummy pulses and bring its symbol rate up to a common one.

A block diagram of one of these synchronizers is shown in Figure 1.

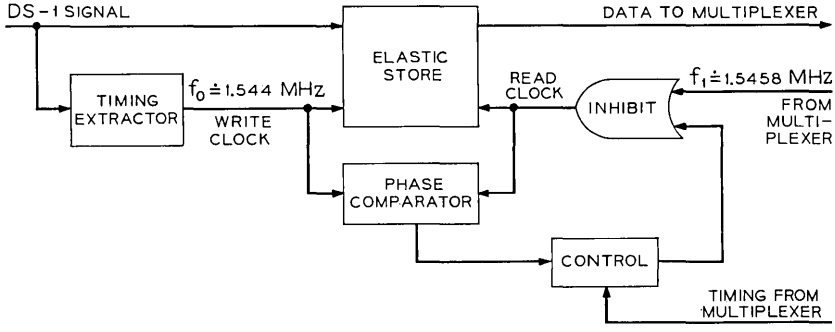

Fig. 1—A block diagram of one of the four synchronizers in an M12.

The data is written into the elastic store under the influence of the write clock, and read out under the influence of the read clock. The write clock is derived from the DS-1 signal. Its frequency (nominally 1.544 MHz) will be denoted by f_0 and its period, by $t_0 = 1/f_0$.*

The clocking signal at the input to the inhibit gate is derived from

* In making these definitions it is being tacitly assumed that there is no jitter on the write clock. This assumption will not always be reasonable since there may be jitter on the DS-1 signal from which it is derived. The effects of this jitter are studied in Section V.

a local clock. It is identical except for constant phase offsets with the corresponding clocking signals in the other three synchronizers. Thus, the data read out of the four synchronizers can be multiplexed by interleaving with no difficulty.

The pulses on the clocking signal at the input to the inhibit gate are normally separated by four DS-2 time slots. Every twelfth pulse is separated from its successor by five DS-2 time slots to allow framing and control pulses to be inserted onto the DS-2 signal. The average frequency of this clocking signal will be denoted by f_1 and its average period by $t_1 = 1/f_1$. Nominally,

$$f_1 = (12/49) \cdot 6.312 = 1.5458 \text{ MHz}.$$

For the remainder of this paper, the jitter on this clocking signal will be neglected, and it will be approximated as an unjittered clocking signal with frequency f_1.*

By design the frequency f_1 is greater than f_0. If all the pulses at the input to the inhibit gate were allowed to pass through, the read clock would eventually overtake the write clock. Since it is necessary to write before reading, some pulses must be inhibited.

The inhibiting of pulses is done by the phase comparator and associated control circuitry. The output of the phase comparator, $\phi_S(t)$, is the phase difference between the read and write clocks (or, equivalently, the jitter on the output data stream of the synchronizer). The control circuitry monitors $\phi_S(t)$ and as soon as possible after $\phi_S(t)$ crosses some predetermined threshold Λ inhibits a clocking pulse, or, as it is more commonly phrased, stuffs a (data) pulse.

A typical graph of $\phi_S(t)$ is shown in Figure 2. By convention $\phi_S(t)$ is defined as positive if the read clock precedes the write clock. This seemingly backwards definition gives $\phi_S(t)$ positive slope and negative jumps as seems to be traditional.[5,6] Since the write clock must always precede the read clock, the threshold Λ must be set so that $\phi_S(t)$ is always negative.

The positive slope of $\phi_S(t)$ at nonjump times reflects the fact that in the absence of inhibit pulses the read clock is gradually overtaking the write clock. Whenever a pulse is stuffed, $\phi_S(t)$ drops by one slot (by definition one slot equals t_1 seconds). Stuffing does not occur as soon as $\phi_S(t)$ crosses the threshold. It is necessary to wait until a stuffing

* The techniques of Section V could be used to remove this assumption also. It is not particularly interesting to do so, however, since little error results from making it. The jitter being neglected is systematic and of relatively high frequency. It is easily removed at the demultiplexer.

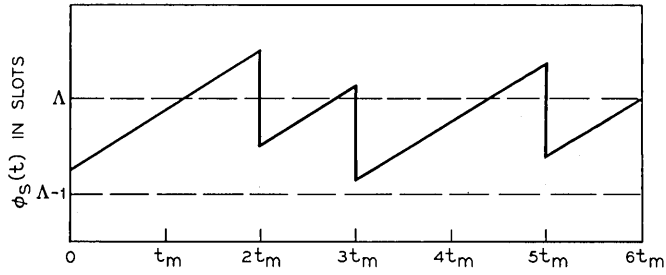

Fig. 2—A typical graph of the output of the phase comparator.

opportunity occurs. These opportunities, which are fixed by M12 format considerations, occur at regular intervals 1176 DS-2 time slots apart. Let t_m denote this interval. Then,

$$t_m = 1176 \cdot (12/49)\ t_1$$
$$= 288\ t_1\ .$$

The maximum possible stuffing rate is $f_m = 1/t_m$. In the M12

$$f_m = 6.312/1176 \text{ MHz}$$
$$= 5.367 \text{ kHz}.$$

The actual average rate at which pulses are being stuffed is $f_s = f_1 - f_0$. The stuffing ratio

$$\rho = f_s/f_m\ ,$$

which must be between 0 and 1, is a critical parameter. Nominally, in the M12

$$\rho = f_s/f_m = (f_1 - f_0)/f_m$$
$$= \frac{(12/49) \cdot 6.312 - 1.544}{6.312/1176}$$
$$= 0.3346,$$

or slightly more than 1/3.

It will be convenient for the remainder of this paper to measure time in stuffing opportunities and frequency in cycles per stuffing opportunity. All numerical values for times and frequencies given from here on are to be assumed to have these units unless other units are explicitly stated. Conversion to seconds and Hertz is easy through

the relations

$$1 \text{ stuffing opportunity} = 0.186 \text{ ms}$$

and

$$1 \text{ cycle per stuffing opportunity} = 5.367 \text{ kHz}.$$

It has been traditional to consider $\phi_S(t)$ as being the sum of two jitter waveforms—the first being stuffing jitter and the second waiting time jitter. Stuffing jitter is defined as the jitter that would be present if stuffing could occur on demand, and waiting time jitter is usually defined as the low-frequency jitter present in $\phi_S(t)$ because in actuality there is a "waiting time" between stuff demand and stuff execution. Since these definitions are hard to make precise, we shall not attempt to make any such distinctions and shall merely call $\phi_S(t)$ the waiting time jitter waveform.

After each of the four DS-1 signals is synchronized, it is multiplexed with the other three, transmitted over an appropriate facility and demultiplexed by an M12. Stuffed pulses on each of the lines are removed in an associated desynchronizer.

A block diagram of a desynchronizer is shown in Figure 3. Information telling the demultiplexer where stuffs have been made is carried on the DS-2 signal along with the data. Thus, it is possible for the write clock in the desynchonizer to exactly duplicate the read clock in the synchronizer. It has gaps where stuffs were made.

The read clock on the elastic store in the desynchronizer is obtained from a voltage controlled oscillator (VCO). The output of the phase comparator, which is proportional to the phase difference between the read and write clocks, is filtered and fed back to the VCO in such a way as to keep the read clock from overtaking or falling too far behind the write clock.

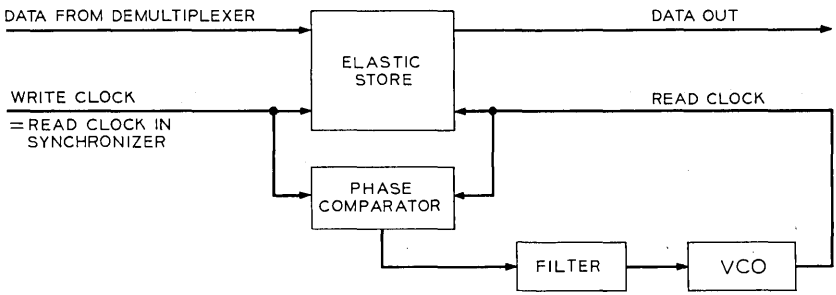

Fig. 3—A block diagram of one of the four desynchronizers in an M12.

The desynchronizer acts as a phase-locked loop and smooths the gaps created by stuffing pulses. Ideally, the output of the desynchronizer would be identical with the input to the synchronizer. Unfortunately, all phase-locked loops have a low-pass nature and some low-frequency jitter degrades the output.

Let $\phi_D(t)$ denote this jitter. Then

$$\phi_D(t) = h(t)*\phi_S(t),$$

where $h(t)$ is the overall transfer function of the phase-locked loop in the desynchronizer and * denotes convolution. In the M12 $h(t)$ falls off at 12 dB per octave after cutoff at about 0.12 cycle per stuffing opportunity (644 Hz).*

Often $\phi_S(t)$ and $\phi_D(t)$ are both called waiting time jitter (distinguishable only by context). To avoid any confusion, we shall only call $\phi_S(t)$ waiting time jitter and shall always call $\phi_D(t)$ filtered waiting time jitter.

Because of the low-pass nature of $h(t)$, the low-frequency components of waiting time jitter are present in filtered waiting time jitter and degrade the demultiplexed signal. It is not difficult to demonstrate that it is quite possible for $\phi_S(t)$ to contain significant low-frequency power. In Figure 4a, $\phi_S(t)$ is drawn assuming $\rho = 1/2$. The lowest frequency component in this waveform is at the relatively high frequency of 1/2 cycle per stuffing opportunity. But, it is unrealistic to assume $\rho = 1/2$ exactly. Figures 4b and 4c show $\phi_S(t)$ for ρ slightly greater than 1/2 and ρ slightly less than 1/2. In both cases there is a strong low-frequency envelope. In general, whenever ρ is close to a simple rational number (a rational number with a small denominator), but not exactly equal to it, $\phi_S(t)$ will have appreciable low-frequency power.

This idea is developed in papers by Kozuka[5] and Matsuura, Kozuka, and Yuki[6]. Formulas are given for the peak-to-peak amplitude of the low-frequency envelope present on the waveform $\phi_S(t)$ when ρ is close to, but not exactly equal to, a simple rational number. Questions arise, however, as to how close is close enough and how the trade off between approximation accuracy and simpler rational numbers is to be made (for example, should 0.45^+ be considered close to 1/2 or to 9/20?).

An alternate approach is to calculate the power spectrum of waiting time jitter as we do in the next section.

---

* The M12 has been recently redesigned and now has a lower cutoff frequency.

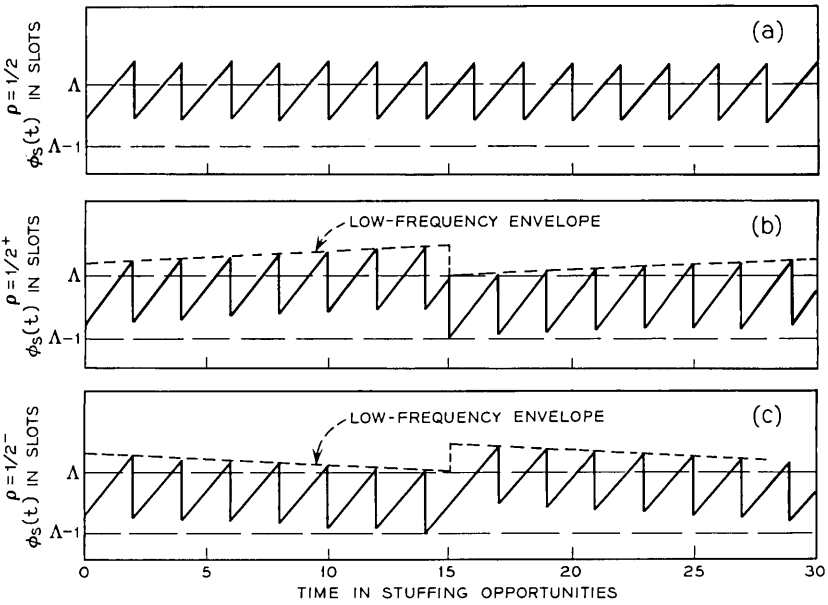

Fig. 4—In the upper portion of this figure ρ equals 1/2 exactly, and there are no low-frequency components in $\Phi_S(t)$. In the other portions of this figure ρ is close but not exactly equal to 1/2, and there are strong low-frequency components.

III. THE SPECTRUM OF WAITING TIME JITTER

3.1 *Theoretical*

In Appendix A the power spectrum $S_S(f)$ of $\phi_S(t)$ is calculated. Briefly, the procedure used is to (*i*) find an equation describing waiting time jitter waveforms, (*ii*) introduce initial condition random variables into this equation in such a way that a stationary ensemble of waiting time jitter waveforms is defined, (*iii*) compute the covariance of the waiting time jitter random process, and (*iv*) Fourier transform this covariance to obtain the power spectrum $S_S(f)$.

It is possible to find the power spectrum of waiting time jitter without using random process theory. A procedure similar to one used by Iwerson[7] to find the spectrum of quantizing noise in a delta modulator with unequal positive and negative step sizes could be used. (The similarity of the underlying mathematics in these two at first seemingly unrelated problems is remarkable.) Our method of finding the spectrum (that is, via random processes) does not require any approximations. The method used by Iwerson requires approximating pulses by delta

functions. This approximation is unimportant for his problem, but of more consequence in the waiting time jitter problem. A further advantage of proceeding via random process theory is that the arguments needed are somewhat simpler and more concise, especially those that are given in Appendix B of this paper (corresponding with those in Appendix D of the paper by Iwerson).

The result of Appendix A is (remember, frequency is being measured in cycles per stuffing opportunity)

$$S_S(f) = \operatorname{sinc}^2 f \cdot Q(f) + \sum_{n=1}^{\infty} \left(\frac{\rho}{2\pi n}\right)^2 (\delta(f - n) + \delta(f + n)), \tag{1}$$

where

$$\operatorname{sinc} f = \frac{\sin \pi f}{\pi f},$$

$$Q(f) = \sum_{n=1}^{\infty} \left(\frac{1}{2\pi n}\right)^2 (\operatorname{rep} \delta(f - \rho n) + \operatorname{rep} \delta(f + \rho n)), \tag{2}$$

$$\operatorname{rep} X(f) = \sum_{k=-\infty}^{\infty} X(f - k) \quad \text{for any function} \quad X(f),$$

and $\delta(\cdot)$ is the Dirac delta function. It is convenient to define

$$S_{S,A}(f) = \operatorname{sinc}^2 f \cdot Q(f) \tag{3}$$

and

$$S_{S,B}(f) = \sum_{n=1}^{\infty} \left(\frac{\rho}{2\pi n}\right)^2 (\delta(f - n) + \delta(f - n)). \tag{4}$$

With this notation

$$S_S(f) = S_{S,A}(f) + S_{S,B}(f).$$

Graphs of $\operatorname{sinc}^2 f$, $Q(f)$, and $S_{S,B}(f)$ are given in Figure 5. Only the lines associated with the first, second, and third terms of the defining sum for $Q(f)$ are shown in the graph of $Q(f)$. The lines labeled 1^- are lines introduced by

$$\left(\frac{1}{2\pi \cdot 1}\right)^2 \operatorname{rep} \delta(f - \rho \cdot 1).$$

Lines labeled 1^+ are lines introduced by

$$\left(\frac{1}{2\pi \cdot 1}\right)^2 \operatorname{rep} \delta(f + \rho \cdot 1).$$

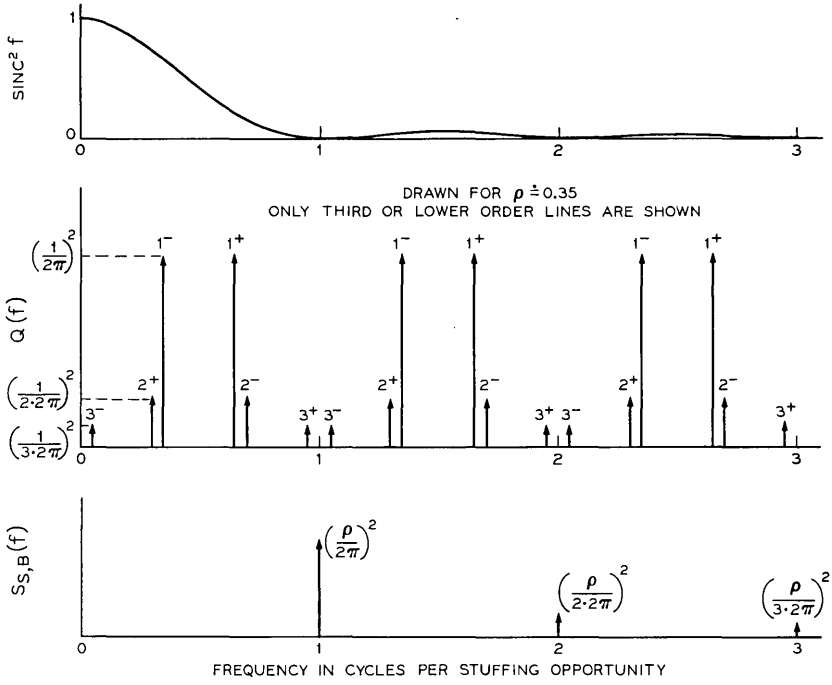

Fig. 5—The components of the spectrum of waiting time jitter.

In general, n^--lines and n^+-lines are lines introduced by

$$\left(\frac{1}{2\pi n}\right)^2 \text{rep } \delta(f - \rho n)$$

and

$$\left(\frac{1}{2\pi n}\right)^2 \text{rep } \delta(f + \rho n)$$

respectively. This notational scheme is similar to the one used by Iwerson.

The interesting information about the spectrum $S_S(f)$ is carried by $Q(f)$. $S_{S,B}(f)$ contains only relatively high-frequency components. The function $\text{sinc}^2 f$ is just an envelope. The low-frequency content of $S_S(f)$ is determined by ρ through $Q(f)$.

If ρ is irrational, none of the spectral lines will coincide. When ρ is rational, the spectral lines do eventually coincide and it is possible

to replace the infinite sum in the defining equation for $Q(f)$ by a finite sum. Iwerson shows that if $\rho = p/q$ where p and q are relatively prime,

$$Q(f) = \frac{1}{4q^2} \sum_{n=1}^{q-1} \csc^2\left(\frac{n}{q}\pi\right) \operatorname{rep} \delta\left(f - \frac{pn}{q}\right) + \frac{1}{12q^2} \operatorname{rep} \delta(f). \quad (5)$$

3.2 *Experimental*

The spectra of waiting time jitter waveforms produced by an M12 were recorded for a number of stuffing ratios. Three representative spectra are shown in Figures 6, 7, and 8. The stuffing ratios in these three figures are respectively 0.186, 0.372, and 0.333. The stuffing ratio was varied by varying the DS-1 symbol rate.

The vertical dB scale on the graphs is only approximate. In addition, no attempt was made to have 0 dB correspond to any particular amount of jitter power, and therefore, readings taken from it are only relative.

In Figures 6 and 7 the stuffing ratio is not close to any simple rational number and the spectral lines are all distinct. To record Figure 8, the stuffing ratio was set as close as possible to 1/3. The expected coincidence of lines is quite apparent.

The weak line at about 0.08 cycle per stuffing opportunity in Figure 8 is not present in the theoretical spectrum. Its origin can be traced to an improper (only in the sense that it deviates from the usual model) functioning of the synchronizer in the M12. This improper functioning,

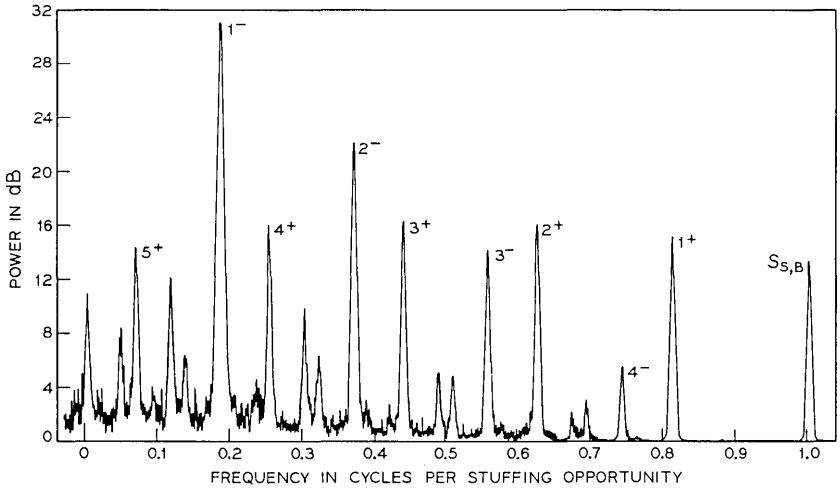

Fig. 6—An experimental waiting time jitter spectrum with $\rho = 0.186$.

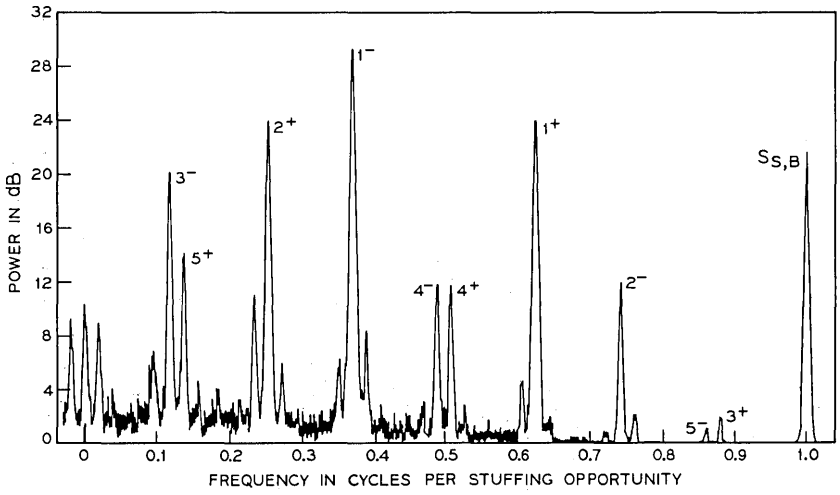

Fig. 7—An experimental waiting time jitter spectrum with $\rho = 0.372$.

termed multiple stuffing, is also apparent when looking at oscilloscope traces of waiting time jitter waveforms. Occasionally stuffs will be made when they quite obviously should not be (for instance, twice in a row with $\rho < 1/2$). The actual M12 used to record the spectra of Figures 6, 7, and 8 was an experimental model having an asynchronous

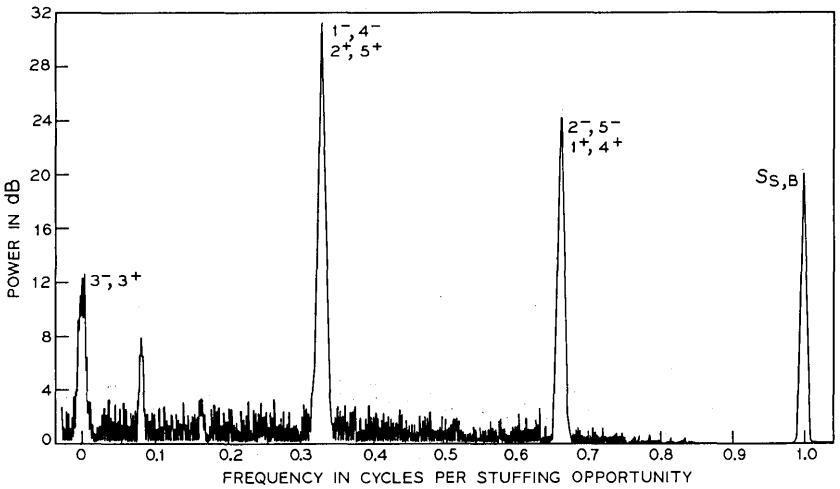

Fig. 8—An experimental waiting time jitter spectrum with $\rho = 0.333$.

delay line[8] elastic store rather than the usual commutator type (see page 617 of Ref. 4). It was used because it exhibited slightly less multiple stuffing.

In Tables I, II, and III the powers of the lines in the experimental and theoretical waiting time jitter spectra are tabulated for the stuffing ratios 0.186, 0.372, and 0.333 respectively. To obtain the theoretical powers listed in Tables I and II, equation (2) for $Q(f)$ was used. The rational stuffing ratio formula (5) for $Q(f)$ was used in computing the theoretical powers listed in Table III.

The entries in the columns headed uncorrected experimental power were simply read off Figures 6, 7, and 8. For ease of comparison corrected experimental powers are also listed. These entries were obtained by multiplying the corresponding uncorrected powers by 0.817 (to correct the vertical scaling) and subtracting 42.0 (to add an absolute reference). The constants 0.817 and 42.0 were chosen by a least squares procedure.

The differences between the theoretical and corrected experimental powers are listed in the last column of Tables I, II, and III. The agreement is to within 0.5 dB except in a few cases where discrepancies are easily explained in terms of the low frequency and small amplitude limitations of the spectrum analyzer.

IV. THE RMS AMPLITUDE OF FILTERED WAITING TIME JITTER

4.1 *Theoretical*

Since

$$\phi_D(t) = h(t)*\phi_S(t),$$

TABLE I—SPECTRAL LINE POWERS FOR $\rho = 0.186$

Line	Normalized Frequency	Power (dB)			
		Theoretical	Experimental Uncorrected	Experimental Corrected	Difference
1^-	0.186	−16.5	31.0	−16.6	−0.1
2^-	0.372	−24.1	22.3	−23.7	0.4
3^-	0.558	−30.5	14.1	−30.4	0.1
4^-	0.744	−38.2	5.6	−37.4	0.8
5^-	0.930	−52.5	—	—	—
1^+	0.814	−29.3	15.2	−29.5	−0.2
2^+	0.628	−28.6	16.1	−28.8	−0.2
3^+	0.442	−28.5	16.3	−28.6	−0.1
4^+	0.256	−29.0	15.8	−29.0	0.0
5^+	0.070	−30.0	14.3	−30.3	−0.3
$S_{S,B}$	1.000	−30.6	13.5	−30.9	−0.3

TABLE II—SPECTRAL LINE POWERS FOR $\rho = 0.372$

Line	Normalized Frequency	Power (dB)			
		Theoretical	Experimental Uncorrected	Experimental Corrected	Difference
1^-	0.372	−18.0	29.4	−17.9	0.1
2^-	0.744	−32.2	11.8	−32.3	−0.1
3^-	0.116	−25.7	20.1	−25.5	0.2
4^-	0.488	−31.8	11.8	−32.3	−0.5
5^-	0.860	−46.0	1.2	−41.0	5.0
1^+	0.628	−22.6	24.0	−22.4	0.2
2^+	0.256	−22.9	23.8	−22.5	0.4
3^+	0.884	−43.3	2.0	−40.3	3.0
4^+	0.512	−32.1	11.6	−32.5	−0.4
5^+	0.140	−30.2	14.0	−30.5	−0.3
$S_{S,B}$	1.000	−24.6	21.3	−24.6	0.0

the spectrum $S_D(f)$ of filtered waiting time jitter is given by

$$S_D(f) = |H(f)|^2 S_S(f)$$

where $H(f)$ is the Fourier transform of $h(t)$, that is,

$$H(f) = \mathfrak{F}\{h(t)\} = \int_{-\infty}^{\infty} h(t)e^{-j2\pi ft}\,dt.$$

Only the low frequency components of $S_S(f)$ will not be significantly attenuated by $|H(f)|^2$.

The power $P_D(\rho)$ in $\phi_D(t)$ (that is, the rms amplitude squared of $\phi_D(t)$) is given by

$$\begin{aligned} P_D(\rho) &= \int_{-\infty}^{\infty} S_D(f)\,df \\ &= \int_{-\infty}^{\infty} |H(f)|^2 S_S(f)\,df \\ &= \int_{-\infty}^{\infty} |H(f)|^2 S_{S,A}(f)\,df + \int_{-\infty}^{\infty} |H(f)|^2 S_{S,B}(f)\,df \\ &\triangleq P_{D,A}(\rho) + P_{D,B}(\rho). \end{aligned}$$

Typically, $h(t)$ cuts off at frequencies much smaller than 1 cycle per stuffing opportunity where the lowest frequency spectral line in $S_{S,B}(f)$ is located, and, therefore, $P_{D,B}(\rho)$ is quite small in comparison to $P_{D,A}(\rho)$. Since $P_{D,A}(\rho)$ is symmetric about 1/2 (that is, $P_{D,A}(\rho) = P_{D,A}(1 - \rho)$), it is to be expected that $P_D(\rho)$ will be essentially symmetric also.

TABLE III—SPECTRAL LINE POWERS FOR $\rho = 0.333$

Line	Normalized Frequency	Power (dB)			
		Theoretical	Experimental Uncorrected	Experimental Corrected	Difference
$1^-, 2^+, 4^-, 5^+, \cdots$	0.333	−16.0	31.4	−16.3	− 0.3
$1^+, 2^-, 4^+, 5^-, \cdots$	0.667	−22.0	24.2	−22.2	− 0.2
$3^-, 3^+, 6^-, 6^+, \cdots$	0.000	−20.3	12.6	−31.7	−11.4
$S_{S,B}$	1.000	−25.5	20.2	−25.5	0.0

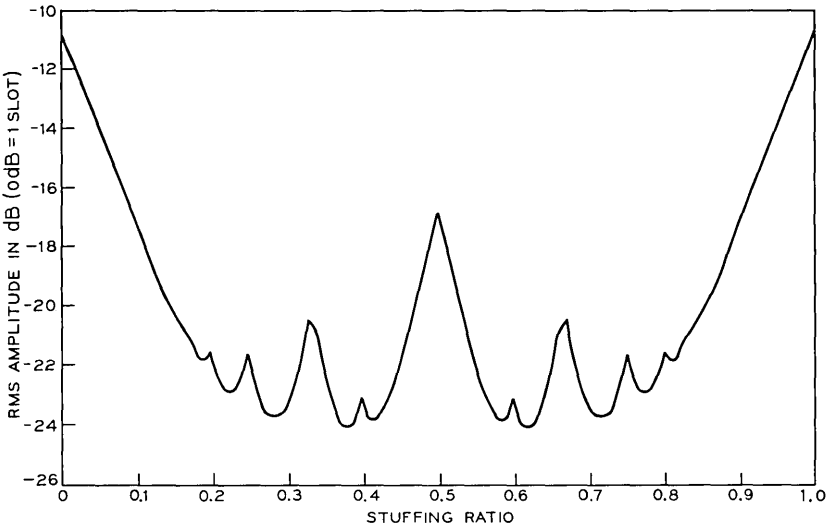

Fig. 9—A theoretical graph of the rms amplitude of filtered waiting time jitter as a function of ρ with $H(f)$ assumed to have a double pole at 0.12 cycle per stuffing opportunity.

A computer program was written to plot $P_D(\rho)$ for various filter transfer functions $H(f)$. Two sample graphs appear in Figures 9 and 10. The assumed transfer functions were respectively

$$H(f) = \left(\frac{0.12}{jf + 0.12}\right)^2$$

and

$$H(f) = \left(\frac{0.06}{jf + 0.06}\right)^2.$$

The first transfer function is a good approximation to that of the filter in the M12*. The cutoff frequency of the second transfer function is 1/2 that of the first. In both graphs the predicted symmetry is quite apparent as are the expected peaks at rational stuffing ratios. The peaking is more pronounced with the sharper filter.

For both filters there appears to be significant benefit to be gained by choosing ρ intelligently. Actually, as will be discussed more fully in Subsection 5.2, this conclusion is misleading because the effect of jitter on the input DS-1 signal has not been considered.

* As noted in a previous footnote, the phase-locked loop in the M12 has been recently redesigned and now has a lower cutoff.

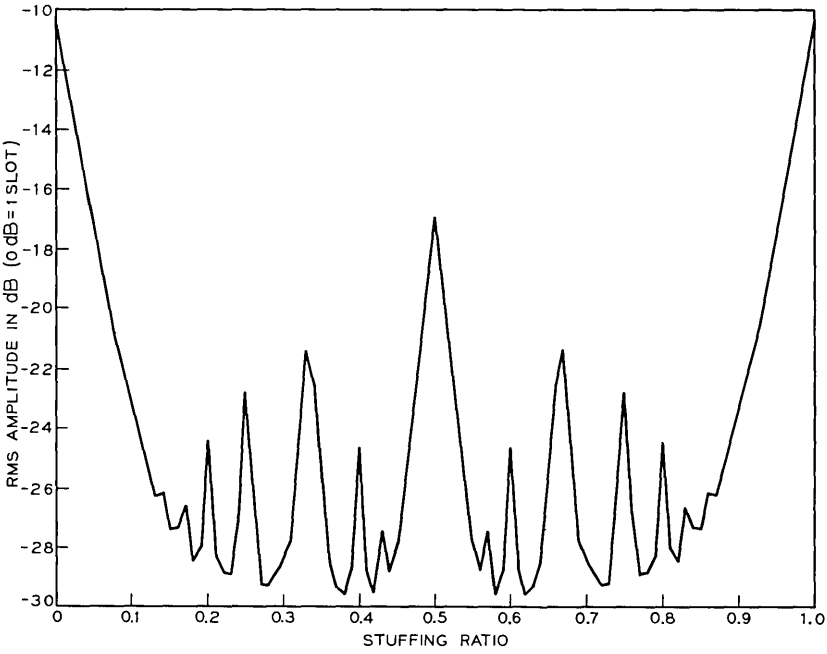

Fig. 10—A theoretical graph of the rms amplitude of filtered waiting time jitter as a function of ρ with $H(f)$ assumed to have a double pole at 0.06 cycle per stuffing opportunity.

4.2 *Experimental*

An experimental recording of $P_D(\rho)$ versus ρ for $\rho \in [0, 1]$ appears in Figure 11. As in the experimental spectra of Figures 6, 7, and 8 the dB scale is only approximate and relative. With this fact taken into account, the agreement with Figure 9 is good.

The vertical lines at the tops of the peaks are caused by the low-frequency cutoff of the true rms voltmeter used in making Figure 11. The unit used cutoff at 10^{-4} cycle per stuffing opportunity (0.5 Hz).

V. INPUT JITTER

5.1 *Generalized Spectrum*

It is possible to generalize the spectrum derivation of Appendix A to allow for jitter already present on the signal at the input to the synchronizer. This jitter will indeed usually be present. If the signal at the input to the synchronizer is coming from a moderately sized T1 line, it will be degraded by significant repeater jitter.[9-11] In addition,

it will be degraded by filtered waiting time jitter if it has already passed through a syndes (synchronizer-desynchronizer pair).

Let $\phi_I(t)$ denote the jitter on the signal at the input to the synchronizer and $\phi_S(t)$ and $\phi_D(t)$ again denote the jitters on the outputs of the synchronizer and desynchronizer. All of these jitters will be assumed to be defined with respect to an unjittered reference signal and to be positive if their associated signals are ahead of it. In Section III the output of the phase comparator and the jitter on the output of the synchronizer were identical, and we denoted them both by $\phi_S(t)$. When there is input jitter, these two jitters are no longer identical and a new symbol must be introduced for one of them. We have chosen to still call the jitter on the output of the synchronizer $\phi_S(t)$. The symbol $\phi_{SPC}(t)$ will be used for the output of the synchronizer's phase comparator. We have

$$\phi_{SPC}(t) = \phi_S(t) - \phi_I(t).$$

In Appendix B it is shown that with input jitter accounted for the spectrum of waiting time jitter is given by

$$\begin{aligned} S_S(f) &= \operatorname{sinc}^2 f \cdot \hat{Q}(f) + \sum_{n=1}^{\infty} \left(\frac{\rho}{2\pi n}\right)^2 (\delta(f-n) + \delta(f+n)) \\ &\qquad + \operatorname{sinc}^2 f \cdot \operatorname{rep} S_I(f) \\ &\triangleq S_{S,A}(f) \quad + S_{S,B}(f) \quad + S_{S,C}(f), \end{aligned} \tag{6}$$

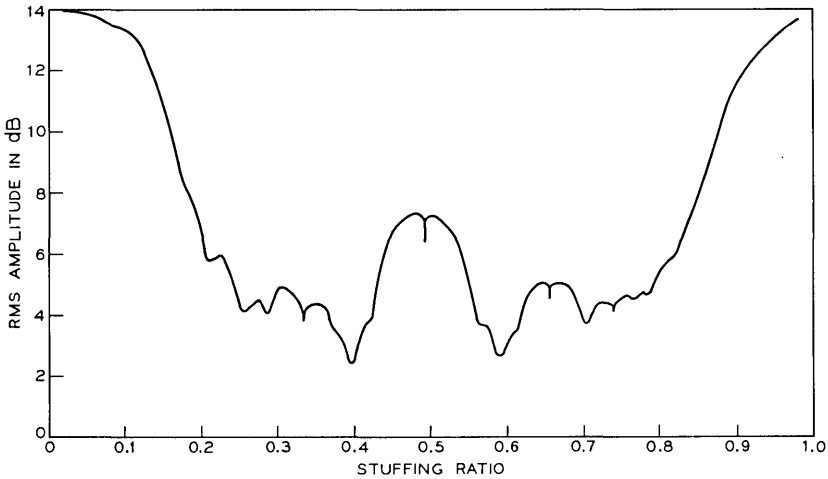

Fig. 11—An experimental graph of the rms amplitude of filtered waiting time jitter as a function of ρ.

where

$$\hat{Q}(f) = \sum_{n=1}^{\infty} \left(\frac{1}{2\pi n}\right)^2 (\text{rep } Z_n(f - n\rho) + \text{rep } Z_n(f + n\rho)) \tag{7}$$

$$Z_n(f) = \mathfrak{F}\{z_n(t)\}$$

$$= \int_{-\infty}^{\infty} z_n(t) e^{-j2\pi ft}\, dt,$$

$$z_n(t) = E\{\exp\{-j2\pi n(\phi_I(t) - \phi_I(0))\}\},$$

$S_I(f)$ is the spectrum of the input jitter, and E denotes expectation.

The input jitter $\phi_I(t)$ will usually only have significant power in frequencies that are quite small in comparison to 1 cycle per stuffing opportunity. When this is the case, the approximation (see Figure 12)

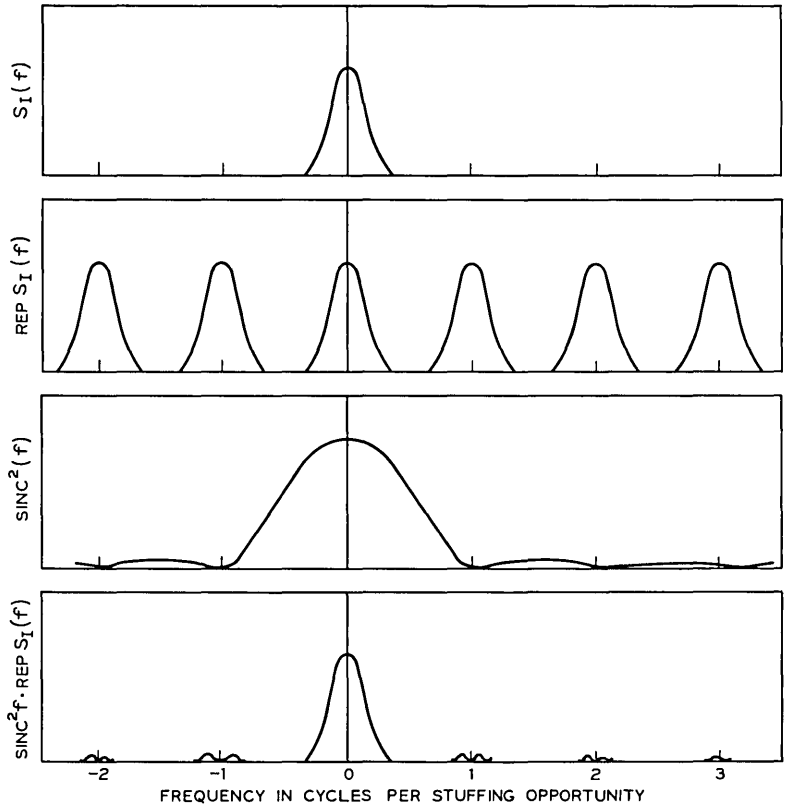

Fig. 12—Approximating $\text{sinc}^2 f \cdot \text{rep } S_I(f)$ by $S_I(f)$.

$$\operatorname{sinc}^2 f \cdot \operatorname{rep} S_I(f) \doteq \operatorname{sinc}^2 f \cdot S_I(f)$$
$$\doteq S_I(f)$$

can be used to simplify (6) to

$$S_S(f) \doteq \operatorname{sinc}^2 f \cdot \hat{Q}(f) + \sum_{n=1}^{\infty} \left(\frac{\rho}{2\pi n}\right)^2 (\delta(f-n) + \delta(f+n)) + S_I(f). \quad (8)$$

The input jitter makes its presence felt in two ways. The first way is simply in the appearance of the feedthrough term $S_I(f)$ (or, more precisely, $\operatorname{sinc}^2 f \cdot \operatorname{rep} S_I(f)$). The second way is in the smearing of spectral lines. The function $\hat{Q}(f)$ has the same functional form as $Q(f)$, but the envelope functions $Z_n(f)$ replace impulses.

The envelope functions $Z_n(f)$ are difficult to compute in general. Evaluating them requires evaluating the same type expressions that must be evaluated to find the spectrum of exponentially modulated carriers. This latter problem has been a traditionally difficult one. Exact evaluations for the special cases of Gaussian input jitter and sinusoidal input jitter and approximate evaluations for small amplitude input jitter are possible.

5.1.1 *Gaussian Input Jitter*

If $\phi_I(t)$ is Gaussian with zero mean and covariance $C_I(t)$, then the random variable $\phi_I(t) - \phi_I(0)$ is Gaussian with zero mean and covariance $2(C_I(0) - C_I(t))$. By the well known formula for the characteristic function of a Gaussian random variable,

$$z_n(t) = E\{\exp\{-j2\pi n(\phi_I(t) - \phi_I(0))\}\}$$
$$= \exp\{-(2\pi n)^2(C_I(0) - C_I(t))\}.$$

Using the infinite series expansion for the exponential function, we have

$$z_n(t) = \exp\{-(2\pi n)^2 C_I(0)\} \exp\{(2\pi n)^2 C_I(t)\}$$
$$= \exp\{-(2\pi n)^2 C_I(0)\} \sum_{k=0}^{\infty} \frac{(2\pi n)^{2k}}{k!} C_I^k(t).$$

Therefore,

$$Z_n(f) = \mathfrak{F}\{z_n(t)\}$$
$$= \exp\{-(2\pi n)^2 C_I(0)\} \sum_{k=0}^{\infty} \frac{(2\pi n)^{2k}}{k!} \mathfrak{F}\{C_I^k(t)\}.$$
$$= \exp\{-(2\pi n)^2 C_I(0)\}\, \delta(f)$$
$$+ \exp\{-(2\pi n)^2 C_I(0)\} \sum_{k=1}^{\infty} \frac{(2\pi n)^{2k}}{k!} \underbrace{S_I(f) * \cdots * S_I(f)}_{k \text{ terms}}. \quad (9)$$

The envelope $Z_n(f)$ is composed of an impulse at the origin (the carrier line in exponential modulation theory) and an infinite sum of kth order convolutions of the input jitter spectrum with itself.

5.1.2 *Sinusoidal Input Jitter*

If the input jitter is sinusoidal, exact results are also possible. Sinusoidal input jitter can be modeled by the random process

$$\phi_I(t) = \beta \sin (2\pi Ft + \theta),$$

where β and F are constants and θ is a random variable distributed uniformly on $[0, 2\pi)$. [Introducing θ is necessary to randomize the epoch and make $\phi_I(\cdot)$ stationary.]

By direct substitution,

$$\begin{aligned} z_n(t) &= E\{\exp\{-j2\pi n(\phi_I(t) - \phi_I(0))\}\} \\ &= E\{\exp\{-j2\pi n\beta \sin (2\pi Ft + \theta)\} \exp\{j2\pi n\beta \sin \theta\}\} \\ &= E\{\exp\{j2\pi n\beta \sin (-2\pi Ft - \theta)\} \exp\{j2\pi n\beta \sin \theta\}\}. \end{aligned}$$

Using the expansion

$$e^{j\lambda \sin x} = \sum_{k=-\infty}^{\infty} J_k(\lambda) e^{jkx},$$

where the $J_k(\lambda)$ are Bessel functions of the first kind (see, for example, equation 7.53 of Ref. 12) in this equation, we have

$$\begin{aligned} z_n(t) &= E\left\{\sum_{k=-\infty}^{\infty} J_k(2\pi n\beta) e^{-ik(2\pi Ft+\theta)} \cdot \sum_{l=-\infty}^{\infty} J_l(2\pi n\beta) e^{il\theta}\right\} \\ &= \sum_{k,l=-\infty}^{\infty} J_k(2\pi n\beta) J_l(2\pi n\beta) e^{-ik2\pi Ft} E\{e^{i(l-k)\theta}\} \\ &= \sum_{k=-\infty}^{\infty} J_k^2(2\pi n\beta) e^{-ik2\pi Ft}. \end{aligned}$$

Therefore,

$$Z_n(f) = \sum_{k=-\infty}^{\infty} J_k^2(2\pi n\beta)\ \delta(f + kF). \tag{10}$$

The transform $Z_n(f)$ consists of a string of impulses stretching from $-\infty$ to $+\infty$ and separated from each other by F cycles per stuffing opportunity.

5.1.3 *Small Signal Approximations*

Small signal approximations for the $Z_n(f)$ can be derived easily using the power series expansion for an exponential function. We have

$$\begin{aligned} z_n(t) &= E\{\exp\{-j2\pi n(\phi_I(t) - \phi_I(0))\}\} \\ &= 1 - j2\pi n E\{\phi_I(t) - \phi_I(0)\} \\ &\quad + \frac{1}{2!}(-j2\pi n)^2 E\{(\phi_I(t) - \phi_I(0))^2\} + \cdots \\ &= 1 - \tfrac{1}{2}(2\pi n)^2 E\{(\phi_I(t) - \phi_I(0))^2\} + \cdots \\ &= 1 - (2\pi n)^2(C_I(0) - C_I(t)) + \cdots, \end{aligned}$$

and

$$\begin{aligned} Z_n(f) &= \mathfrak{F}[z_n(t)] \\ &= \delta(f) - (2\pi n)^2(C_I(0)\ \delta(f) - S_I(f)) + \cdots. \end{aligned} \tag{11}$$

If n and the input jitter are small enough, it will be reasonable to approximate $Z_n(f)$ by the first few terms of this expansion.

The simplest such approximation is

$$Z_n(f) \doteq \delta(f). \tag{12}$$

Taking one more term gives the better approximation

$$\begin{aligned} Z_n(f) &\doteq \delta(f) - (2\pi n)^2(C_I(0)\ \delta(f) - S_I(f)) \\ &= (1 - (2\pi n)^2 C_I(0))\ \delta(f) + (2\pi n)^2 S_I(f). \end{aligned} \tag{13}$$

Both of these approximations have the desirable property of preserving total power.

The power in the term $(2\pi n)^2 S_I(f)$ can be used as a guide for determining which of these approximations (if either) is reasonable. For all n, the total power in $Z_n(f)$ is 1. If

$$(2\pi n)^2 \int_{-\infty}^{\infty} S_I(f)\, df \triangleq (2\pi n)^2 P_I$$

is very small in comparison to one (say < 0.01), the approximation

$$Z_n(f) \doteq \delta(f)$$

will be adequate. For moderate power (say $0.01 < (2\pi n)^2 P_I < 0.1$), the second approximation will still be reasonable.

For a given input jitter power, either of these approximations is better for small n than large. For weak input jitter

$$Z_n(f) \doteq \delta(f)$$

will be reasonable for small n, but not for large. Thus, the effect of weak input jitter is to smear the high order n-lines. [The feedthrough

term will be negligible because if $Z_n(f) \doteq \delta(f)$ is reasonable for even small n, $\text{sinc}^2 f \cdot \text{rep}\, S_I(f)$ will be negligible in comparison to $\text{sinc}^2 f \cdot \hat{Q}(f)$].

5.2 *Filtered Waiting Time Jitter Power with Gaussian Input Jitter*

When the effect of input jitter is considered, the power in filtered waiting time jitter is again given by

$$P_D(\rho) = \int_{-\infty}^{\infty} | H(f) |^2 S_S(f)\, df,$$

but with $S_S(f)$ as defined by equation (6). Let $P_{D,A}(\rho)$, $P_{D,B}(\rho)$, and $P_{D,C}$ denote the components of $P_D(\rho)$ due to $S_{S,A}(f)$, $S_{S,B}(f)$, and $S_{S,C}(f)$ respectively. The power $P_{D,C}$ is a constant independent of ρ. If

$$\text{sinc}^2 f \cdot \text{rep}\, S_I(f) \doteq S_I(f),$$

then

$$P_{D,C} \doteq \int_{-\infty}^{\infty} | H(f) |^2 S_I(f)\, df,$$

which is the power of the jitter that would be present at the output of the syndes (synchronizer-desynchronizer pair) if its only effect were to filter the input jitter. The jitter power added to the bit stream by pulse stuffing is to within this approximation

$$\Delta P_D(\rho) = P_{D,A}(\rho) + P_{D,B}(\rho).$$

Computer-drawn graphs of $\Delta P_D(\rho)$ for Gaussian input jitter appear in Figures 13 through 16. The transfer function $H(f)$ was assumed to equal that of Figure 9 for Figures 13 and 15 and that of Figure 10 for Figures 14 and 16. For Figures 13 and 14

$$S_I(f) = \frac{1}{2\pi}\left(\frac{1}{10}\right)^2 \frac{0.2}{(0.1)^2 + f^2},$$

and for Figures 15 and 16

$$S_I(f) = \frac{1}{2\pi}\left(\frac{1}{4}\right)^2 \frac{0.2}{(0.1)^2 + f^2}.$$

Both of these spectra are RC with a cutoff at 0.1 cycle per stuffing opportunity. The rms amplitude of the jitter of the first is 1/10 slot, and of the second, 1/4 slot. The first jitter spectrum is felt to be representative of what will typically be encountered in the field.

A comparison of Figures 9, 13, and 15 and of Figures 10, 14, and 16 shows that the effect of input jitter is to erode the peaks and valleys

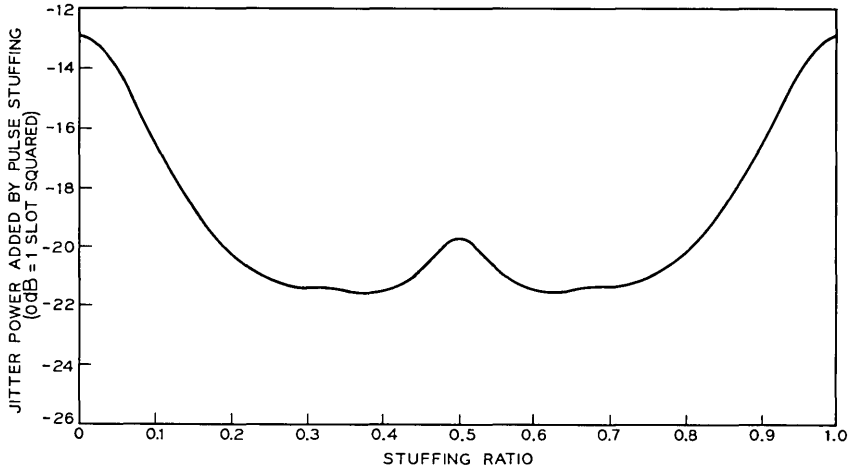

Fig. 13—A theoretical graph of the jitter power added by pulse stuffing as a function of ρ. The jitter on the input to the syndes is assumed to be Gaussian with an rms amplitude of 1/10 slot and an RC spectrum with a corner frequency of 0.1 cycle per stuffing opportunity. The transfer function $H(f)$ is assumed to have a double pole at 0.12 cycle per stuffing opportunity.

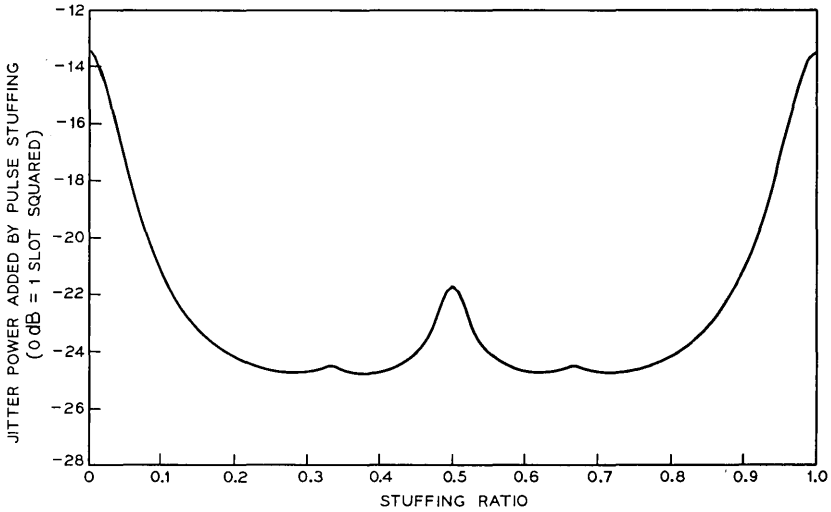

Fig. 14—A theoretical graph of the jitter power added by pulse stuffing as a function of ρ. The jitter on the input to the syndes is assumed to be Gaussian with an rms amplitude of 1/10 slot and an RC spectrum with a corner frequency of 0.1 cycle per stuffing opportunity. The transfer function $H(f)$ is assumed to have a double pole at 0.06 cycle per stuffing opportunity.

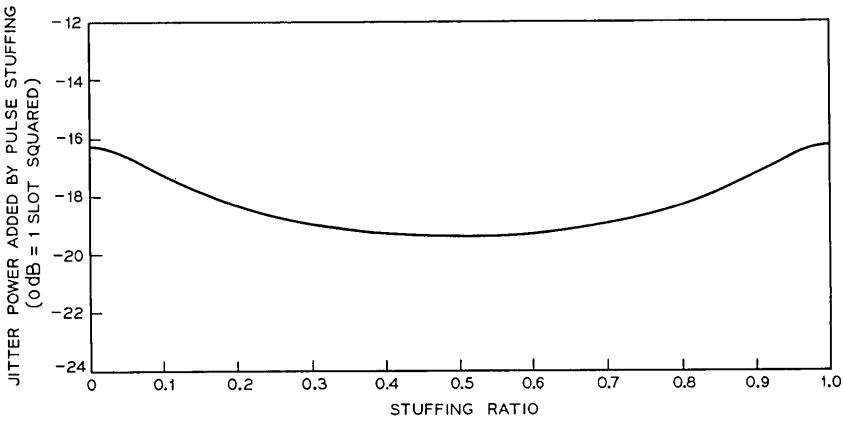

Fig. 15—A theoretical graph of the jitter power added by pulse stuffing as a function of ρ. The jitter on the input to the syndes is assumed to be Gaussian with an rms amplitude of 1/4 slot and an RC spectrum with a corner frequency of 0.1 cycle per stuffing opportunity. The transfer function $H(f)$ is assumed to have a double pole at 0.12 cycle per stuffing opportunity.

of the no input jitter graphs. It is felt that this erosion will occur for almost all input jitter and not just for Gaussian input jitter with a spectrum of the above form. Thus, the choice of ρ is not so critical as it appears to be in Figures 9 and 10 when, as is usually the case, input jitter is not negligible. Notice, however, that even with non-negligible input jitter, there is still an advantage in using a narrow phase-locked loop. The graphs of Figures 14 and 16 are typically 3 dB below those of Figures 13 and 15.

5.3 *A Bound on the Power in Filtered Waiting Time Jitter*

By neglecting the effect of the filter in the desynchronizer, it is possible to obtain a simple bound on the power in filtered waiting time jitter. This bound is quite weak, but will be useful in the next section to bound the accumulation rate of filtered waiting time jitter in chains of syndes.

Let

$$H_{\max} = \max_{f \in (-\infty, \infty)} | H(f) |.$$

Then

$$P_D \leqq H_{\max}^2 P_S$$

where

$$\begin{aligned} P_S &= \int_{-\infty}^{\infty} S_S(f)\, df \\ &= \int_{-\infty}^{\infty} S_{S,A}(f)\, df + \int_{-\infty}^{\infty} S_{S,B}(f)\, df + \int_{-\infty}^{\infty} S_{S,C}(f)\, df \\ &\triangleq P_{S,A} + P_{S,A} + P_{S,C} \,. \end{aligned}$$

From equations (32), (31), and (33) of Appendix B

$$P_{S,A} = 1/12,$$

$$P_{S,B} = \rho^2/12 \leqq 1/12,$$

and

$$P_{S,C} = P_I \,,$$

where P_I is the input jitter power. Therefore

$$P_D \leqq H_{\max}^2(1/6 + P_I). \tag{14}$$

If there is no peaking,

$$H_{\max} = H(0) = 1$$

and

$$P_D \leqq 1/6 + P_I \,. \tag{15}$$

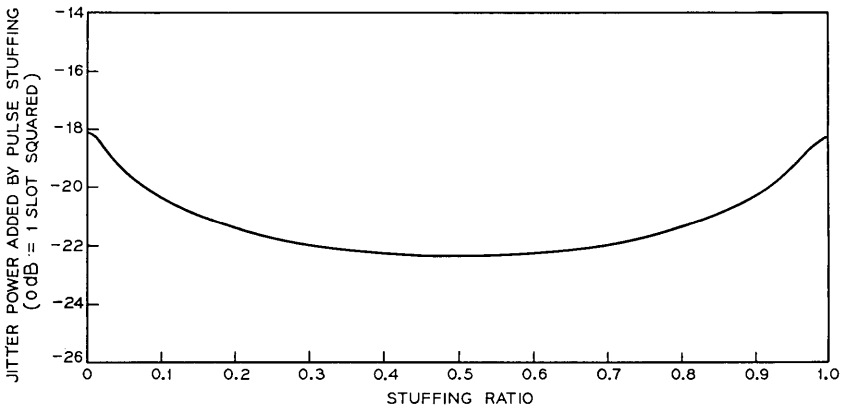

Fig. 16—A theoretical graph of the jitter power added by pulse stuffing as a function of ρ. The jitter on the input to the syndes is assumed to be Gaussian with an rms amplitude of 1/4 slot and an RC spectrum with a corner frequency of 0.1 cycle per stuffing opportunity. The transfer function $H(f)$ is assumed to have a double pole at 0.06 cycle per stuffing opportunity.

VI. WAITING TIME JITTER ACCUMULATION

6.1 *Theoretical Bound*

A question of much engineering interest is how fast filtered waiting time jitter accumulates in tandem connections of syndes. Although the bound (15) is quite weak, it does guarantee that when there is no peaking in any of the transfer functions of the desynchronizers in the chain, the rms amplitude of the jitter on the output of the Nth syndes is no greater than $\sqrt{N/6}$,* and thus that the rate of accumulation of filtered waiting time jitter is no faster than $\sqrt{N}$. Notice that to obtain this bound on the growth rate, it was not necessary to assume the stuffing ratios at each of the synchronizers identical nor the transfer functions of each of the desynchronizers identical.

6.2 *Experimental Data*

The power of the filtered waiting time jitter at the output of a chain of M12 syndes was measured for chain lengths N of 1, 2, 4, 8, and 16 and six different stuffing ratios. The recorded powers are listed in Table IV and plotted in Figure 17.

The upper bound†

$$P_{D,N} \leqq N/6$$

is plotted for comparison in each of the six graphs. The bound is typically about 15 dB above the data. No data are inconsistent with it.

The other line plotted in each of the graphs is

$$P_{D,N} = NP^*_{D,1} , \tag{16}$$

where $P^*_{D,1}$ is the theoretical power in filtered waiting time jitter from just one syndes. The values used for $P^*_{D,1}$ were taken from the computer program that produced the graph of Figure 9 and are listed in Table IV for convenience. This line was plotted because it seems to be a reasonable empirical approximation to the data.

The fact that $P_{D,2} < P_{D,1}$ for low stuffing ratios is rather surprising. We do not have a completely satisfactory explanation. For the stuffing ratios where this decrease in power occurs, the 1^--lines and 1^+-lines

---

* It is of course being tacitly assumed here that the input to the first syndes is jitter free and that no other jitters (such as repeater jitter) are being introduced along the chain. A bound including the effects of other jitters could easily be obtained from (15) also.

† There is about 0.15 dB peaking in the phase-locked loop of an M12 so we should strictly be using a bound based on (14) rather than (15). For this slight amount of peaking and the chain lengths considered here, the difference is negligible.

TABLE IV—ACCUMULATION DATA

Stuffing Ratio	Jitter Powers in dB (0 dB = 1 Slot Squared)					
	Theoretical	Experimental				
ρ	N = 1	N = 1	N = 2	N = 4	N = 8	N = 16
0.018	−11.8	−10.9	−13.1	−10.0	− 6.1	− 2.2
0.092	−17.3	−14.8	−20.7	−17.1	− 9.5	− 5.7
0.167	−21.5	−20.7	−18.4	−19.0	−16.8	−10.3
0.241	−22.9	−21.8	−19.6	−16.8	−12.8	− 6.6
0.316	−22.6	−20.5	−15.2	−14.9	−11.7	− 9.1
0.391	−24.5	−20.7	−19.8	−15.6	−12.5	− 9.6

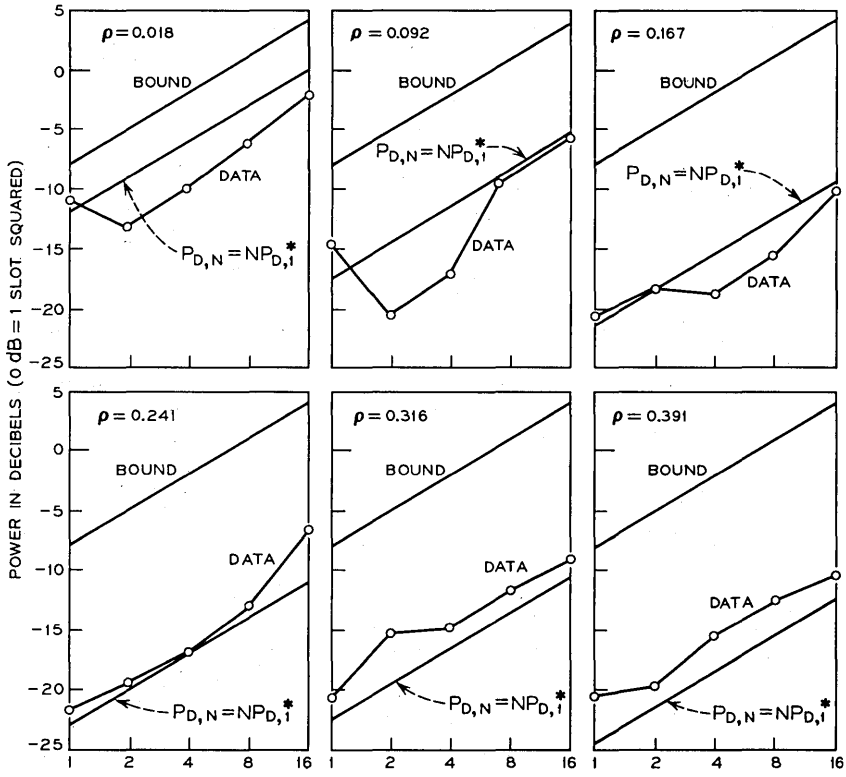

Fig. 17—Experimental accumulation data as a function of log N.

of $\hat{Q}(f)$ are within the passband of $H(f)$. It is felt that an explanation lies partly in the fact that $Z_1(f)$ may (and the approximation of Subsection 5.1.3 suggests it will) throw much of the power in these lines out of the passband of $H(f)$. If this idea is pursued and calculations made, however, it appears that while this phenomenon helps, it cannot be solely responsible. Multiple stuffing may possibly have played a role here also.

VII. SUMMARY

Expressions giving the spectrum of waiting time jitter both when there is and is not significant input jitter have been found. Using these theoretical expressions, graphs of the jitter power added by pulse stuffing versus the stuffing ratio have been drawn. These graphs indicate that when there is no input jitter there is much to be gained by intelligently choosing the stuffing ratio, but that with a typical amount of input jitter present, much of the advantage is lost.

Bounds on the power in filtered waiting time jitter have been found, and it has been shown that when there is no peaking in the desynchronizers of a chain of syndes, the rms amplitude of filtered waiting time jitter accumulates at a rate no faster than the square root of the number of syndes in the chain.

VIII. ACKNOWLEDGMENTS

This paper could not have been written without the assistance of M. R. Aaron, who introduced the author to the waiting time jitter problem, assembled a collection of waiting time jitter references, and contributed greatly through informal discussions. He was the first to notice the applicability of the work of J. E. Iwerson to the waiting time jitter problem. In addition the author is grateful to the M12 multiplex group for assisting in making the laboratory measurements. In particular, A. A. Geigel was most helpful in explaining the operation and circuitry of the M12 multiplex and in collecting the test equipment needed.

APPENDIX A

In this appendix the spectrum $S_S(f)$ of $\phi_S(t)$ is calculated. As noted previously, the procedure used will be to (*i*) write an equation describing waiting time jitter waveforms, (*ii*) introduce initial condition random variables into this equation in such a way that a stationary ensemble

of waiting time jitter waveforms is defined, (*iii*) compute the covariance of the waiting time jitter random process, and (*iv*) Fourier transform this covariance to obtain the power spectrum.

Let $[\cdot]$ denote the greatest integer function, that is, let

$$[x] = \begin{cases} \vdots & \vdots \\ -1, & -1 \leqq x < 0 \\ 0, & 0 \leqq x < 1. \\ 1, & 1 \leqq x < 2 \\ \vdots & \vdots \end{cases}$$

In Figure 18 a waiting time jitter waveform is drawn assuming stuffing opportunities occur at integer times and that just after stuffing at time $t = 0$, $\phi_S(\cdot)$ equals $\Lambda - 1$. With the aid of the greatest integer function an equation describing the waveform of Figure 18 can be written. It is

$$\phi_S(t) = (\Lambda - 1) + \rho t - [\rho[t]]. \tag{17}$$

Obtaining this equation is the key step in finding the spectrum of waiting time jitter. The constant term $\Lambda - 1$ is needed to make $\phi_S(0) = \Lambda - 1$. The second term ρt generates the linearly increasing portion of the waveform $\phi_S(t)$. Stuffs are made by $[\rho[t]]$. The reader should convince himself that this nesting of greatest integer functions puts stuffs in the proper locations.

Equation (17) defines $\phi_S(\cdot)$ at a stuffing time to be equal to its value just after a stuff has been made if one is to be made. In other words, it makes the function $\phi_S(\cdot)$ continuous from the right. This convention

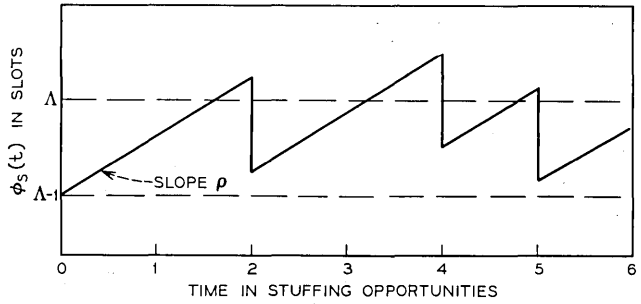

Fig. 18—A waiting time jitter waveform starting at $\Lambda - 1$ at time $t = 0$.

is as good as any. For the purposes here it makes little difference how $\phi_S(\cdot)$ is defined at switching times.

A waiting time jitter waveform drawn at random from a stationary ensemble of waiting time jitter waveforms (see Figure 19) will not in general (in fact almost surely will not) have stuffing opportunities coming at integer times. Define the random variable τ as how long before time $t = 0$ a stuffing opportunity last occurred. Over the ensemble τ will be distributed uniformly on the interval [0, 1).

Define the random variable ζ as by how much $\phi_S(\cdot)$ exceeded $\Lambda - 1$ at time $t = -\tau^+$ (see Figure 19). The random variable ζ must exist in the interval [0, 1). It cannot be less than 0 because $\phi_S(\cdot)$ never is less than $(\Lambda - 1)$. It must be less than 1 because if $\phi_S(\cdot)$ exceeds Λ just before the stuffing opportunity at time $t = -\tau$, a stuff will be

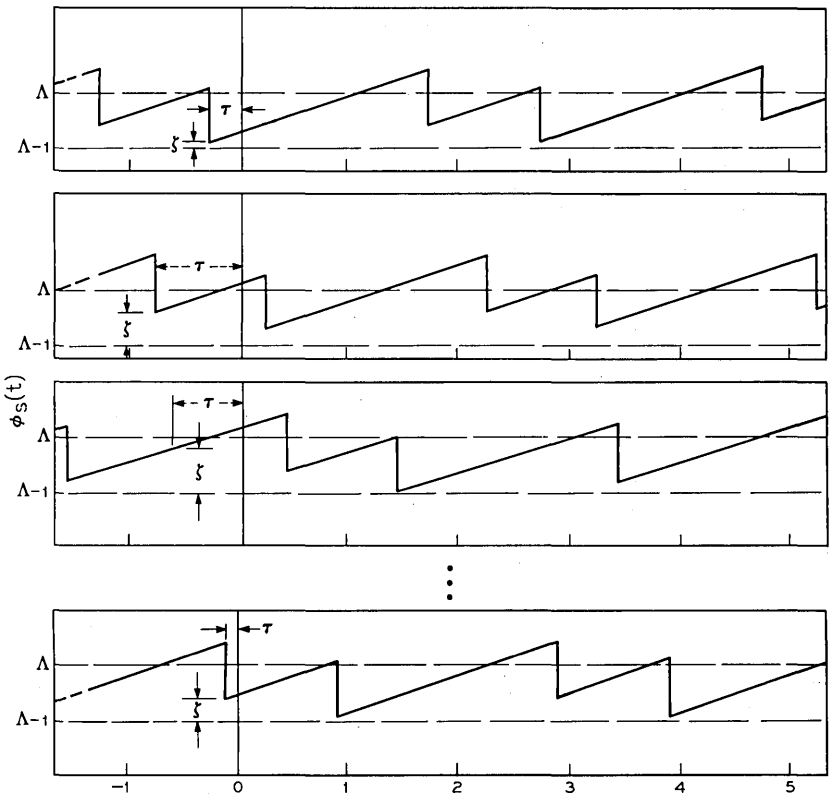

Fig. 19—An ensemble of waiting time jitter waveforms.

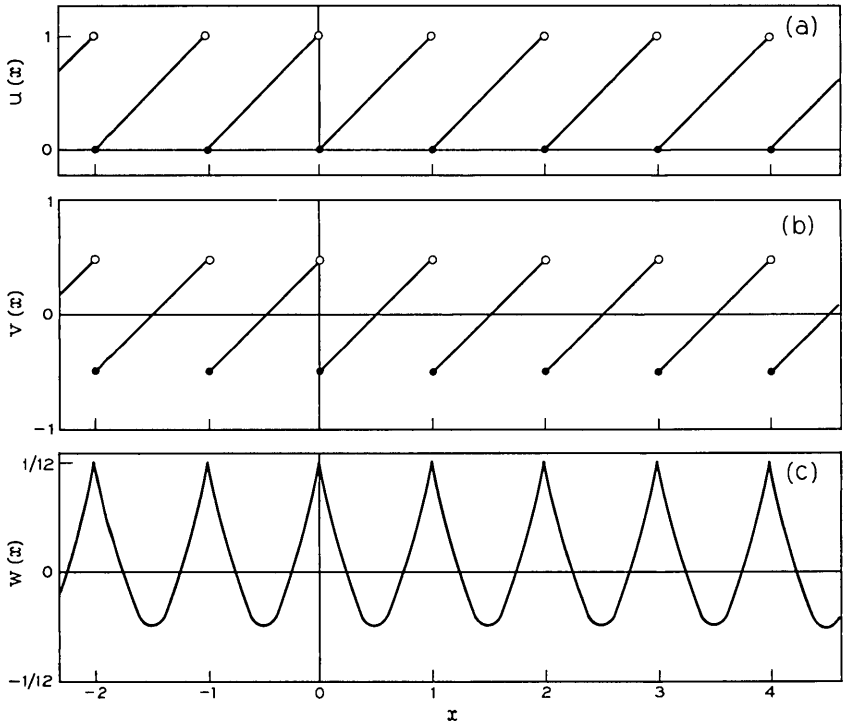

Fig. 20—Graphs of the functions $u(x)$, $v(x)$, and $w(x)$.

made. Over the stationary ensemble, ζ will be independent of τ and distributed uniformly over [0, 1).

A modified version of equation (17) that allows for nonzero ζ and τ is

$$\phi_S(t) = (\Lambda - 1) + \zeta + \rho(t + \tau) - [\zeta + \rho[t + \tau]]. \tag{18}$$

Define (see Figure 20a)

$$\begin{aligned} u(x) &= x - [x] \\ &= x \bmod 1. \end{aligned}$$

An equation equivalent to (18) is

$$\phi_S(t) = (\Lambda - 1) + u(\zeta + \rho[t + \tau]) + \rho u(t + \tau). \tag{19}$$

The next step in the procedure is to find the covariance of the random process $\phi_S(\cdot)$. By definition the covariance $C_S(t)$ of $\phi_S(\cdot)$ is given by

$$C_S(t) = E\{(\phi_S(s + t) - \mu_S)(\phi_S(s) - \mu_S)\},$$

where

$$\mu_S = E\{\phi_S(t)\}$$

and E denotes expectation.

The mean μ_S is not difficult to evaluate. We have

$$\begin{aligned}\mu_S &= E\{\phi_S(0)\}\\ &= E\{(\Lambda - 1) + u(\zeta + \rho[\tau]) + \rho u(\tau)\}\\ &= E\{(\Lambda - 1) + u(\zeta) + \rho u(\tau)\}\\ &= \Lambda - 1 + 1/2 + \rho/2.\end{aligned}$$

Define (see Figure 20b)

$$v(x) = u(x) - 1/2.$$

Then, for all t

$$\phi_S(t) - \mu_S = v(\zeta + \rho[t + \tau]) + \rho v(t + \tau). \tag{20}$$

Returning to the evaluation of $C_S(t)$, we have

$$\begin{aligned}C_S(t) &= E\{(\phi_S(t) - \mu_S)(\phi_S(0) - \mu_S)\}\\ &= E\{v(\zeta + \rho[t + \tau])v(\zeta + \rho[\tau])\} + E\{v(\zeta + \rho[t + \tau])\rho v(\tau)\}\\ &\quad + E\{\rho v(t + \tau)v(\zeta + \rho[\tau])\} + E\{\rho v(t + \tau)\rho v(\tau)\}\\ &= E\{v(\zeta + \rho[t + \tau])v(\zeta)\} + E\{v(\zeta + \rho[t + \tau])\rho v(\tau)\}\\ &\quad + E\{\rho v(t + \tau)v(\zeta)\} + E\{\rho v(t + \tau)\rho v(\tau)\}.\end{aligned}$$

The second and third terms in this expansion (cross covariances) are zero. Indeed,

$$\begin{aligned}E\{v(\zeta + \rho[t + \tau])\rho v(\tau)\} &= \rho E\{E\{v(\zeta + \rho[t + \tau])v(\tau) \mid \tau\}\}\\ &= \rho E\{v(\tau)E\{v(\zeta + \rho[t + \tau]) \mid \tau\}\}\\ &= \rho E\{v(\tau)\cdot 0\}\\ &= 0\end{aligned}$$

and

$$\begin{aligned}E\{\rho v(t + \tau)v(\zeta)\} &= \rho E\{E\{v(t + \tau)v(\zeta) \mid \tau\}\}\\ &= \rho E\{v(t + \tau)E\{v(\zeta) \mid \tau\}\}\\ &= \rho E\{v(t + \tau)E\{v(\zeta)\}\}\\ &= E\{v(t + \tau)\cdot 0\}\\ &= 0.\end{aligned}$$

The fact that

$$E\{v(\zeta + \rho[t + \tau]) \mid \tau\} = 0$$

follows once it is observed that $v(\cdot)$ is periodic with period 1 and that the integral of $v(\cdot)$ over any unit length interval is zero. Therefore,

$$C_S(t) = C_{S,A}(t) + C_{S,B}(t),$$

where

$$C_{S,A}(t) = E\{v(\zeta + \rho[t + \tau])v(\zeta)\}$$

and

$$C_{S,B}(t) = \rho^2 E\{v(t + \tau)v(\tau)\}.$$

The covariance $C_{S,B}(t)$ is the easier to evaluate. We have

$$\begin{aligned}
\rho^{-2}C_{S,B}(t) &= E\{v(t + \tau)v(\tau)\} \\
&= \int_0^1 v(t + \tau)v(\tau)\, d\tau \\
&= \int_0^1 v(t + \tau)(\tau - 1/2)\, d\tau \\
&= \int_0^{1-u(t)} (v(t) + \tau)(\tau - 1/2)\, d\tau \\
&\quad + \int_{1-u(t)}^1 (v(t) + \tau - 1)(\tau - 1/2)\, d\tau \\
&= \int_0^1 (v(t) + \tau)(\tau - 1/2)\, d\tau - \int_{1-u(t)}^1 (\tau - 1/2)\, d\tau \\
&= \int_0^1 \tau(\tau - 1/2)\, d\tau - \int_{1-u(t)}^1 (\tau - 1/2)\, d\tau \\
&= 1/12 - (1/2)u(t)(1 - u(t)).
\end{aligned}$$

Define

$$w(t) = 1/12 - (1/2)u(t)(1 - u(t)).$$

Then,

$$C_{S,B}(t) = \rho^2 w(t). \tag{21}$$

A graph of $w(t)$ appears in Figure 20c.

Turning to the calculation of $C_{S,A}(t)$, we have

$$\begin{aligned}
C_{S,A}(t) &= E\{v(\zeta + \rho[t + \tau])v(\zeta)\} \\
&= E\{E\{v(\zeta + \rho[t + \tau])v(\zeta) \mid \tau\}\}.
\end{aligned}$$

The same manipulations that were used to find an expression for $C_{S,B}(t)$ show

$$E\{v(\zeta + \rho[t + \tau])v(\zeta) \mid \tau\} = w(\rho[t + \tau]).$$

Therefore,

$$\begin{aligned} C_{S,A}(t) &= E\{w(\rho[t + \tau])\} \\ &= \int_0^1 w(\rho[t + \tau]\, d\tau \\ &= \int_0^{1-u(t)} w(\rho[t])\, d\tau + \int_{1-u(t)}^1 w(\rho[t + 1])\, d\tau \\ &= (1 - u(t))w(\rho[t]) + u(t)w(\rho[t + 1]). \end{aligned} \tag{22}$$

A typical graph of $C_{S,A}(t)$ is shown in Figure 21.

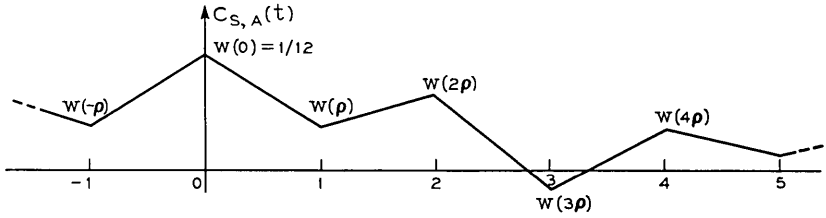

Fig. 21—The covariance $C_{S,A}(t)$.

It is convenient before calculating $S_S(f)$ to mention an equivalent formula for $C_{S,A}(t)$. Define

$$A(t) = \begin{cases} 1 - |\, t\,|, & |\, t\,| \leqq 1 \\ 0, & |\, t\,| > 1 \end{cases}.$$

Then (see Figure 21),

$$C_{S,A}(t) = \sum_{n=-\infty}^{\infty} w(\rho n)A(t - n) \tag{23}$$

$$= A(t) * (w(\rho t) \cdot \text{rep } \delta(t)) \tag{24}$$

where $*$ denotes convolution and for any function $X(f)$

$$\text{rep } X(f) = \sum_{k=-\infty}^{\infty} X(f - k).$$

The Fourier transform of $C_S(t)$ is the spectrum of $\phi_S(t)$. As a matter

of definition

$$\begin{aligned} S_S(f) &= \mathfrak{F}\{C_S(t)\} \\ &= \mathfrak{F}\{C_{S,A}(t)\} + \mathfrak{F}\{C_{S,B}(t)\} \\ &= S_{S,A}(f) + S_{S,B}(f). \end{aligned}$$

The transform $S_{S,B}(f)$ is the easier to take. The function $w(\cdot)$ is periodic with period 1 and has zero mean. Thus, it has the Fourier series expansion

$$w(x) = \sum_{\substack{n=-\infty \\ n\neq 0}}^{\infty} c_n e^{j2\pi nx}$$

where for $n = \pm 1, \pm 2, \cdots$

$$\begin{aligned} c_n &= \int_0^1 w(x)e^{-j2\pi nx}\,dx \\ &= \int_0^1 (1/12 - (1/2)u(x)(1 - u(x)))e^{-j2\pi nx}\,dx \\ &= -(1/2)\int_0^1 u(x)(1 - u(x))e^{-j2\pi nx}\,dx \\ &= -(1/2)\int_0^1 x(1 - x)e^{-j2\pi nx}\,dx \\ &= (2\pi n)^{-2}. \end{aligned}$$

Therefore,

$$\begin{aligned} S_{S,B}(f) &= \mathfrak{F}\{C_{S,B}(t)\} \\ &= \mathfrak{F}\{\rho^2 w(t)\} \\ &= \mathfrak{F}\left\{\rho^2 \sum_{\substack{n=-\infty \\ n\neq 0}}^{\infty} \left(\frac{1}{2\pi n}\right)^2 e^{j2\pi nt}\right\} \\ &= \rho^2 \sum_{\substack{n=-\infty \\ n\neq 0}}^{\infty} \left(\frac{1}{2\pi n}\right)^2 \mathfrak{F}\{e^{j2\pi nt}\} \\ &= \rho^2 \sum_{\substack{n=-\infty \\ n\neq 0}}^{\infty} \left(\frac{1}{2\pi n}\right)^2 \delta(f - n) \\ &= \rho^2 \sum_{n=1}^{\infty} \left(\frac{1}{2\pi n}\right)^2 (\delta(f - n) + \delta(f + n)). \end{aligned} \tag{25}$$

$S_{S,A}(f)$ is only slightly more difficult to compute. Using equation (24) for $C_{S,A}(t)$, we have

$$\begin{aligned} S_{S,A}(f) &= \mathfrak{F}\{C_{S,A}(t)\} \\ &= \mathfrak{F}\{A(t)*(w(\rho t)\cdot \text{rep } \delta(t))\} \\ &= \mathfrak{F}\{A(t)\}\cdot\mathfrak{F}\{w(\rho t)\cdot \text{rep } \delta(t)\} \\ &= \mathfrak{F}\{A(t)\}\cdot(\mathfrak{F}\{w(\rho t)\}*\mathfrak{F}\{\text{rep } \delta(t)\}). \end{aligned}$$

The evaluations

$$\mathfrak{F}\{A(t)\} = \frac{\sin^2 \pi f}{(\pi f)^2} \triangleq \text{sinc}^2 f$$

and

$$\mathfrak{F}\{\text{rep } \delta(t)\} = \text{rep } \delta(f)$$

can be found in most Fourier transform tables. Proceeding as in the evaluation of $S_{S,B}(f)$, we have

$$\begin{aligned} \mathfrak{F}\{w(\rho t)\} &= \mathfrak{F}\left\{\sum_{\substack{n=-\infty \\ n\neq 0}}^{\infty} \left(\frac{1}{2\pi n}\right)^2 e^{j2\pi n\rho t}\right\} \\ &= \sum_{\substack{n=-\infty \\ n\neq 0}}^{\infty} \left(\frac{1}{2\pi n}\right)^2 \mathfrak{F}\{e^{j2\pi n\rho t}\} \\ &= \sum_{\substack{n=-\infty \\ n\neq 0}}^{\infty} \left(\frac{1}{2\pi n}\right)^2 \delta(f - n\rho) \\ &= \sum_{n=1}^{\infty} \left(\frac{1}{2\pi n}\right)^2 (\delta(f - n\rho) + \delta(f + n\rho)). \end{aligned}$$

Assembling these three evaluations, we obtain

$$S_{S,A}(f) = \text{sinc}^2 f\cdot Q(f), \tag{26}$$

where

$$\begin{aligned} Q(f) &= \text{rep } \delta(f)* \sum_{n=1}^{\infty} \left(\frac{1}{2\pi n}\right)^2 (\delta(f - n\rho) + (f + n\rho)) \\ &= \sum_{n=1}^{\infty} \left(\frac{1}{2\pi n}\right)^2 (\text{rep } \delta(f - n\rho) + \text{rep } \delta(f + n\rho)). \end{aligned} \tag{27}$$

APPENDIX B

In this appendix the arguments of the previous appendix are generalized to allow for input jitter. Rather than trying to write an equation

for $\phi_S(t)$ directly, it is easier to first write an equation for $\phi_{SPC}(t)$.

With the jitter sign convention of Section V, the instantaneous frequency of the signal at the input to the synchronizer is $f_0 + \dot{\phi}_I(t)$ and the instantaneous stuffing ratio is $\rho - \dot{\phi}_I(t)$. As in Appendix A, let Λ denote the stuffing threshold, let τ be a random variable denoting how long before time $t = 0$ a stuffing opportunity occurs, and let ζ be a random variable denoting how far above $\Lambda - 1$, $\phi_{SPC}(\cdot)$ was just after the stuffing opportunity at time $t = -\tau$. The random variables ζ and τ will again be independent and distributed uniformly on [0, 1). If there were no stuffing, $\phi_{SPC}(t)$ would evolve as

$$\phi_{SPC}(t) = (\Lambda - 1) + \zeta + \int_{-\tau}^{t} (\rho - \dot{\phi}_I(s))\, ds. \tag{28}$$

In actuality there is stuffing, and at every stuffing opportunity a pulse is stuffed if $\phi_{SPC}(t)$ is greater than Λ at that time. An equation describing $\phi_{SPC}(t)$ when stuffing is taking place is*

$$\begin{aligned}\phi_{SPC}(t) &= (\Lambda - 1) + \zeta + \int_{-\tau}^{t} (\rho - \dot{\phi}_I(s))\, ds \\ &\quad - [\zeta + \int_{-\tau}^{[t+\tau]-\tau} (\rho - \dot{\phi}_I(s))\, ds] \\ &= (\Lambda - 1) + \zeta + \rho(t + \tau) - \phi_I(t) + \phi_I(-\tau) \\ &\quad - [\zeta + \rho[t + \tau] - \phi_I([t + \tau] - \tau) + \phi_I(-\tau)]. \end{aligned} \tag{29}$$

A more convenient form for (29) can be obtained by again introducing the function $u(\cdot)$. It is

$$\begin{aligned}\Phi_{SPC}(t) &= (\Lambda - 1) + u(\zeta + \rho[t + \tau] + \phi_I(-\tau) - \phi_I([t + \tau] - \tau)) \\ &\quad + \rho u(t + \tau) + \phi_I([t + \tau] - \tau) - \phi_I(t).\end{aligned}$$

Since

$$\phi_S(t) = \phi_{SPC}(t) + \phi_I(t),$$

* Actually, this equation stuffs more than one time slot if the waveform $\phi_{SPC}(t)$ immediately before a stuffing opportunity has not only increased to a value above Λ, but is also above $\Lambda + 1$ (see Figure 22). A related problem arises if $\phi_{SPC}(t)$ immediately before stuffing is below $\Lambda - 1$ (see Figure 23). The first situation will not occur if the sum of ρ and the negative of the maximum possible negative change of $\phi_I(t)$ in one time slot is less than 1. The second situation will not occur if ρ minus the maximum possible positive change of $\phi_I(t)$ in one time slot is greater than zero. In other words, the model will not deviate from actuality if ρ is not close to 0 or 1 and $\phi_I(t)$ is a low-frequency jitter. These conditions are reasonable and will be assumed to be met.

we have

$$\phi_S(t) = (\Lambda - 1) + u(\zeta + \rho[t + \tau] - \phi_I([t + \tau] - \tau) + \phi_I(-\tau)) + \rho u(t + \tau) + \phi_I([t + \tau] - \tau).$$

The mean μ_S of $\phi_S(t)$ is not difficult to compute. The integral of $u(x)$ over any unit length interval is $1/2$, and therefore

$$E\{\rho u(t + \tau)\} = \rho/2.$$

Similarly,

$$\begin{aligned} &E\{u(\zeta + \rho[t + \tau] - \phi_I([t + \tau] - \tau) + \phi_I(-\tau))\} \\ &\quad = E\{E\{u(\zeta + \rho[t + \tau] - \phi_I([t + \tau] - \tau) + \phi_I(-\tau)) \mid \tau, \phi_I(\cdot)\}\} \\ &\quad = E\{1/2\} \\ &\quad = 1/2. \end{aligned}$$

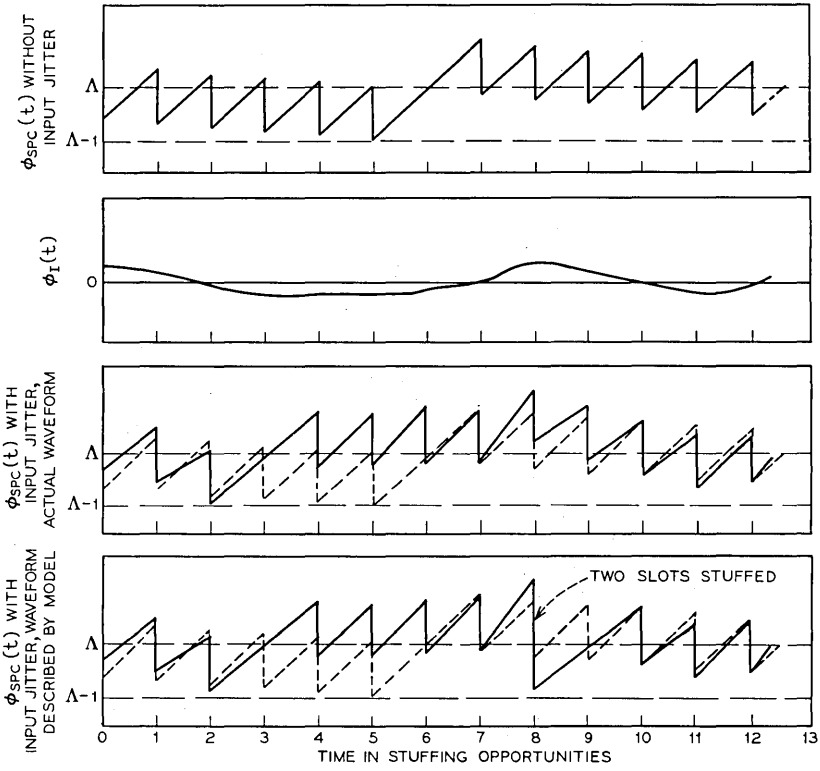

Fig. 22—Deviation of the model from actuality when $\rho = 1^-$.

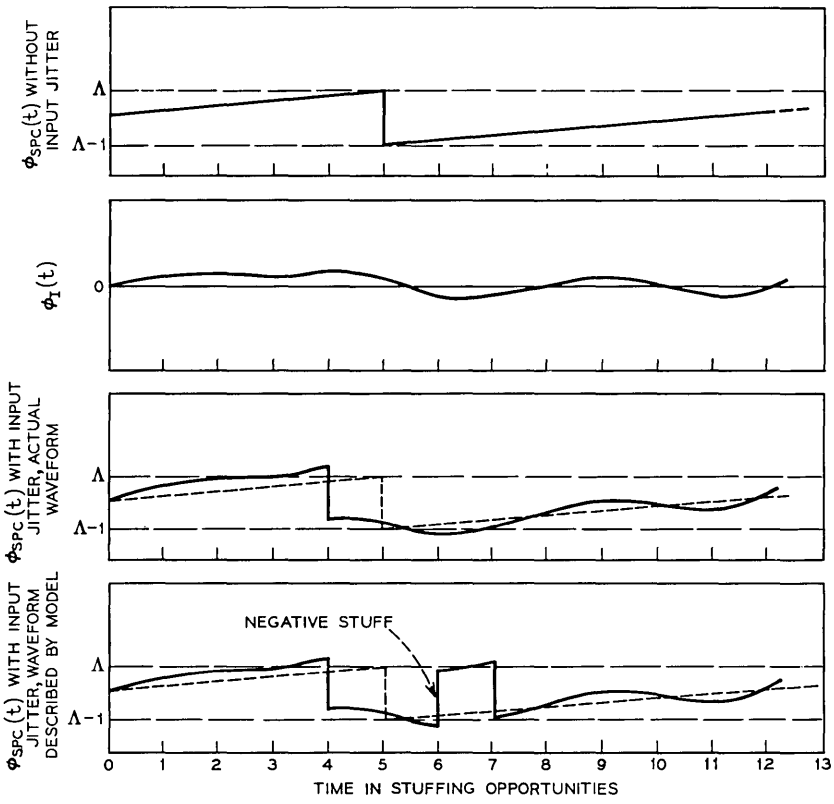

Fig. 23—Deviation of the model from actuality when $\rho = 1^+$.

Therefore,

$$\mu_S = 1/2 + \rho/2$$

and

$$\phi_S(t) - \mu_S = v(\zeta + \rho[t + \tau] - \phi_I([t + \tau] - \tau) + \phi_I(-\tau)) + \rho v(t + \tau) + (\phi_I([t + \tau] - \tau) - \mu_I) \quad (30)$$

where

$$\mu_I = E\{\phi_I(t)\}.$$

The three terms in this equation for $\phi_S(t) - \mu_S$ are easily shown to be uncorrelated. Thus,

$$\begin{aligned} C_S(t) &= E\{(\phi_S(t) - \mu_S)(\phi_S(0) - \mu_S)\} \\ &= E\{v(\zeta + \rho[t + \tau] - \phi_I([t + \tau] - \tau) + \phi_I(-\tau))v(\zeta)\} \\ &\quad + E\{\rho v(t + \tau)\rho v(\tau)]\} \\ &\quad + E\{(\phi_I([t + \tau] - \tau) - \mu_I)(\phi_I(-\tau) - \mu_I)\} \\ &\triangleq C_{S,A}(t) \\ &\quad + C_{S,B}(t) \\ &\quad + C_{S,C}(t). \end{aligned}$$

From Appendix A we have

$$\begin{aligned} C_{S,B}(t) &= E\{\rho^2 v(t + \tau)v(\tau)\} \\ &= \rho^2 w(t) \end{aligned} \tag{31}$$

where

$$w(t) = 1/12 - (1/2)u(t)(1 - u(t)).$$

The evaluation of $C_{S,A}(t)$ is similar to the evaluation of the corresponding term in Appendix A. We have

$$\begin{aligned} &C_{S,A}(t) \\ &= E\{v(\zeta + \rho[t + \tau] - \phi_I([t + \tau] - \tau) + \phi_I(-\tau))v(\zeta)\} \\ &= E\{E\{v(\zeta + \rho[t + \tau] - \phi_I([t + \tau] - \tau) + \phi_I(-\tau))v(\zeta) \mid \tau, \phi_I(\cdot)\}\} \\ &= E\{w(\rho[t + \tau] - \phi_I([t + \tau] - \tau) + \phi_I(-\tau))\}. \end{aligned}$$

Since $\phi_I(t)$ is assumed stationary,

$$\begin{aligned} C_{S,A}(t) &= E\{w(\rho[t + \tau] - \phi_I([t + \tau]) + \phi_I(0))\} \\ &= E\{E\{w(\rho[t + \tau] - \phi_I([t + \tau]) + \phi_I(0)) \mid \phi_I(\cdot)\}\} \\ &= (1 - u(t))E\{w(\rho[t] - \phi_I([t]) + \phi_I(0))\} \\ &\quad + u(t)E\{w(\rho[t + 1] - \phi_I([t + 1]) + \phi_I(0))\} \\ &= A(t)*(r(t)\cdot \text{rep } \delta(t)), \end{aligned} \tag{32}$$

where

$$r(t) = E\{w(\rho t - \phi_I(t) + \phi_I(0))\}.$$

Turning to the final term, we have again using the stationarity of $\phi_I(t)$

$$\begin{aligned} C_{S,C}(t) &= E\{(\phi_I([t+\tau]) - \mu_I)(\phi_I(0) - \mu_I)\} \\ &= E\{E\{(\phi_I([t+\tau]) - \mu_I)(\phi_I(0) - \mu_I) \mid \phi_I(\cdot)\}\} \\ &= (1 - u(t))E\{(\phi_I([t]) - \mu_I)(\phi_I(0) - \mu_I)\} \\ &\quad + u(t)E\{(\phi_I([t+1]) - \mu_I)(\phi_I(0) - \mu_I)\} \\ &= A(t)*(E\{(\phi_I(t) - \mu_I)(\phi_I(0) - \mu_I)\}\cdot \text{rep } \delta(t)) \\ &= A(t)*(C_I(t)\cdot \text{rep } \delta(t)). \end{aligned} \tag{33}$$

The spectrum $S_S(f)$ of the random process $\phi_S(t)$ is the Fourier transform of $C_S(t)$. Let $S_{S,A}(f)$, $S_{S,B}(f)$, and $S_{S,C}(f)$ denote the Fourier transforms of $C_{S,A}(t)$, $C_{S,B}(t)$, and $C_{S,C}(t)$. From Appendix A

$$\begin{aligned} S_{S,B}(t) &= \mathfrak{F}\{C_{S,B}(t)\} \\ &= \sum_{n=1}^{\infty} \left(\frac{\rho}{2\pi n}\right)^2 (\delta(f-n) + \delta(f+n)). \end{aligned} \tag{34}$$

The next easiest Fourier transform to take is that giving $S_{S,C}(f)$. We have

$$\begin{aligned} S_{S,C}(f) &= \mathfrak{F}\{C_{S,C}(t)\} \\ &= \mathfrak{F}\{A(t)*(C_I(t)\cdot \text{rep } \delta(t))\} \\ &= \mathfrak{F}\{A(t)\}\cdot(\mathfrak{F}\{C_I(t)\}*\mathfrak{F}\{\text{rep } \delta(t)\}) \\ &= \text{sinc}^2 f\cdot(S_I(f)* \text{ rep } \delta(f)) \\ &= \text{sinc}^2 f\cdot \text{rep } S_I(f). \end{aligned} \tag{35}$$

The evaluation of $S_{S,A}(f)$ is the most difficult. We have

$$\begin{aligned} S_{S,A}(f) &= \mathfrak{F}\{C_{S,A}(t)\} \\ &= \mathfrak{F}\{A(t)*(r(t)\cdot \text{rep } \delta(t))\} \\ &= \mathfrak{F}\{A(t)\}\cdot \mathfrak{F}\{r(t)\cdot \text{rep } \delta(t)\} \\ &= \text{sinc}^2 f\cdot \hat{Q}(f), \end{aligned}$$

where

$$\begin{aligned} \hat{Q}(f) &= \mathfrak{F}\{r(t)\cdot \text{rep } \delta(t)\} \\ &= \mathfrak{F}\{r(t)\}* \text{ rep } \delta(f). \end{aligned}$$

The periodic function $w(x)$ has the Fourier series expansion (see Appendix A)

$$w(x) = \sum_{\substack{n=-\infty \\ n=0}}^{\infty} \left(\frac{1}{2\pi n}\right)^2 e^{j2\pi nx}.$$

Therefore,

$$\begin{aligned}
\mathfrak{F}\{r(t)\} &= \sum_{\substack{n=-\infty \\ n\neq 0}}^{\infty} \left(\frac{1}{2\pi n}\right)^2 \mathfrak{F}\{E\{\exp\{j2\pi n(\rho t - \phi_I(t) + \phi_I(0))\}\}\} \\
&= \sum_{\substack{n=-\infty \\ n\neq 0}}^{\infty} \left(\frac{1}{2\pi n}\right)^2 \delta(f - \rho n) * \mathfrak{F}\{E\{\exp\{-j2\pi n(\phi_I(t) - \phi_I(0))\}\}\} \\
&= \sum_{\substack{n=-\infty \\ n\neq 0}}^{\infty} \left(\frac{1}{2\pi n}\right)^2 \delta(f - \rho n) * Z_N(f) \\
&= \sum_{\substack{n=-\infty \\ n\neq 0}}^{\infty} \left(\frac{1}{2\pi n}\right)^2 Z_n(f - \rho n) \qquad (36)
\end{aligned}$$

where

$$Z_n(f) = \mathfrak{F}\{z_n(t)\}$$

and

$$z_n(t) = E\{\exp\{-j2\pi n(\phi_I(t) - \phi_I(0))\}\}.$$

It is convenient to obtain another form for equation (36). Clearly,

$$\begin{aligned}
z_{-n}(t) &= E\{\exp\{-j2\pi(-n)(\phi_I(t) - \phi_I(0))\}\} \\
&= E\{\exp\{-j2\pi n(\phi_I(0) - \phi_I(t))\}\}.
\end{aligned}$$

Since $\phi_I(\cdot)$ is stationary,

$$\begin{aligned}
z_{-n}(t) &= E\{\exp\{-j2\pi n(\phi_I(-t) - \phi_I(0))\}\} \\
&= z_n(-t).
\end{aligned}$$

Therefore,

$$\begin{aligned}
Z_{-n}(f) &\triangleq \mathfrak{F}\{z_{-n}(t)\} \\
&= \int_{-\infty}^{\infty} z_{-n}(t) e^{-j2\pi ft}\, dt \\
&= \int_{-\infty}^{\infty} z_n(-t) e^{-j2\pi ft}\, dt \\
&= \int_{-\infty}^{\infty} z_n(t) e^{-j2\pi(-f)t}\, dt \\
&= Z_n(-f).
\end{aligned}$$

Using this last relation in equation (36), we have

$$\mathfrak{F}\{r(t)\} = \sum_{n=1}^{\infty} \left(\frac{1}{2\pi n}\right)^2 (Z_n(f - \rho n) + Z_{-n}(f + \rho n))$$

$$= \sum_{n=1}^{\infty} \left(\frac{1}{2\pi n}\right)^2 (Z_n(f - \rho n) + Z_n(-f - \rho n)).$$

Therefore,

$$\hat{Q}(f) = \text{rep } \delta(f) * \sum_{n=1}^{\infty} \left(\frac{1}{2\pi n}\right)^2 (Z_n(f - \rho n) + Z_n(-f - \rho n))$$

$$= \sum_{n=1}^{\infty} \left(\frac{1}{2\pi n}\right)^2 (\text{rep } Z_n(f - \rho n) + \text{rep } Z_n(-f - \rho n)). \quad (37)$$

In summary,

$$S_S(f) = \text{sinc}^2 f \cdot \hat{Q}(f)$$

$$+ \sum_{n=1}^{\infty} \left(\frac{\rho}{2\pi n}\right)^2 (\delta(f - n) + \delta(f + n)) + \text{sinc}^2 f \cdot \text{rep } S_I(f) \quad (38)$$

where $\hat{Q}(f)$ is as above.

REFERENCES

1. Mayo, J. S., "Experimental 224 Mb/s PCM Terminals," B.S.T.J., *44*, No. 9, part 2 (November 1965), pp. 1813–1841.
2. Witt, F. J., "An Experimental 224 Mb/s Digital Multiplexer-Demultiplexer Using Pulse Stuffing Synchronization," B.S.T.J., *44*, No. 9, part 2, (November 1965), pp. 1843–1885.
3. Bruce, R. A., "A 1.5 to 6 Megabit Digital Multiplex Employing Pulse Stuffing," IEEE Int. Conf. on Commun., (June 1969), pp. 34–1 to 34–7.
4. Bell Laboratories Staff, *Transmission Systems for Communications*, Western Electric Company, Winston-Salem, North Carolina, 1970.
5. Kozuka, S., "Phase Controlled Oscillator for Pulse Stuffing Synchronization System," Review of the Electrical Communication Laboratory, *17*, Numbers 5-6, (May-June, 1969), pp. 376–387.
6. Matsuura, Y., Kozuka, S., and Yuki, K., "Jitter Characteristics of Pulse Stuffing Synchronization," IEEE Int. Conf. on Commun., (June 1968), pp. 259–264.
7. Iwerson, J. E., "Calculated Quantizing Noise of Single-Integration Delta-Modulation Coders," B.S.T.J., *48*, No. 7, part 3, (September 1969), pp. 2359–2389.
8. Kitamura, Z., K. Terada, and K. Asada, "Asynchronous Logical Delay Line for Elastic Stores," Electronics and Communications in Japan, *50*, (November 1967), pp. 90–99.
9. Bennett, W. R., "Statistics of Regenerative Digital Transmission," B.S.T.J., *37*, No. 6, part 2, (November 1958), pp. 1501–1542.
10. Rowe, H. E., "Timing in a Long Chain of Regenerative Binary Repeaters," B.S.T.J., *37*, No. 6, part 2, (November 1958), pp. 1543–1598.
11. Byrne, C. J., B. J. Karafin, and D. B. Robinson, Jr., "Systematic Jitter in a Chain of Digital Regenerators," B.S.T.J., *42*, No. 6, part 3, (November 1963), pp. 2679–2714.
12. Panter, P. F., *Modulation, Noise, and Spectral Analysis*, New York: McGraw-Hill, 1965.

Copyright © 1972 American Telephone and Telegraph Company
THE BELL SYSTEM TECHNICAL JOURNAL
Vol. 51, No. 1, January, 1972
Printed in U.S.A.

Coupled Line Equations with Random Coupling

By J. A. MORRISON and J. McKENNA

(Manuscript received August 23, 1971)

The coupled line equations for two modes traveling in the same direction are considered. The covariances of the mode transfer functions are calculated in the case of random coupling. Exact results are obtained when the coupling is a function of a finite state Markov chain, and also when the coupling is white noise. Perturbation results are obtained in the case of weak, zero mean, wide sense stationary coupling. It is also shown that perturbation results are valid in the case of strong coupling, if the correlation length is short.

I. INTRODUCTION

We consider the coupled line equations for two modes traveling in the forward direction,[1]

$$\begin{aligned} \frac{dI_0}{dz} + \Gamma_0 I_0(z) &= jc(z)I_1(z), \\ \frac{dI_1}{dz} + \Gamma_1 I_1(z) &= jc(z)I_0(z), \end{aligned} \tag{1}$$

subject to the initial conditions

$$I_0(0) = i_0 , \; I_1(0) = i_1 . \tag{2}$$

The time dependence $\exp(2\pi jft)$ has been suppressed. Here $c(z)$ is the real coupling coefficient, which we take to be a random function of z, and the loss and phase constants are

$$\Gamma_0 = \alpha_0 + j\beta_0 , \; \Gamma_1 = \alpha_1 + j\beta_1 . \tag{3}$$

These equations provide an approximate description of a variety of physical systems[2,3,4] such as optical fibers[5,6] and metal waveguides.[7,8] Typically, with the choice $i_0 = 1$, $i_1 = 0$, $I_0(z)$ represents a desired mode launched at $z = 0$, and $I_1(z)$ an undesired spurious mode.

Rowe and Young[1,9] have studied these equations with $c(z)$ taken to be white noise. When $c(z)$ is white noise, equations (1) are symbolic, and Rowe and Young interpret them by a limiting process, and with the aid of a matrix technique obtain exact expressions for the means and covariance functions of the solutions. With the aid of these solutions they studied pulse distortion caused by the coupling, and provide additional verification of Personick's[10] interesting result that in some cases *increasing* the random coupling can improve the impulse response.

This article has three main purposes. The *first* is to show that there is another class of stochastic coupling coefficients for which the means and covariances of the solutions of (1) can be calculated exactly. These involve Markov processes which can assume only a finite number of values. We set up the equations satisfied by the covariance functions and means for a general coupling of this type in Section II, and solve them in a special case in Section III.

The *second* purpose of this paper is to show, with the use of Ito integrals and the Ito calculus, that the interpretation of equations (1) by Rowe and Young when $c(z)$ is white noise is consistent with the interpretation due to Stratonovich.[11] This is the subject matter of Section IV.

The *third* purpose is to apply a perturbation technique developed by Papanicolaou and Keller[12] to the coupled line equations. It is shown that this method can be applied not only to the case of weak coupling, but also to the case of strong coupling if the correlation length is short. This is the subject of Section V.

In the remainder of Section I, we define the quantities of interest, introduce notation, and discuss some of the previously mentioned points at greater length.

The differential loss and phase constants are given by

$$\Delta\Gamma = \Gamma_0 - \Gamma_1 = \Delta\alpha + j\Delta\beta. \tag{4}$$

We write the coupling coefficient in the form

$$c(z) = CN(z), \tag{5}$$

where $N(z)$ is dimensionless. Following Rowe and Young[1,9] we assume that $\Delta\alpha$ is independent of the frequency f, but that $\Delta\beta$ and C are odd functions of f. We further assume that C is an odd function of $\Delta\beta$. Also, let

$$g_0(z, \Delta\beta) = e^{\Gamma_0 z} I_0(z),\ g_1(z, \Delta\beta) = e^{\Gamma_0 z} I_1(z). \tag{6}$$

Note that our $g_0(z, \Delta\beta)$ corresponds to Rowe and Young's $G_0(z)$ and

our $g_1(z, \Delta\beta)$ to their $\mathbf{G}_1(z)$. Then, from (1), (4), and (5),

$$\begin{aligned} \frac{dg_0}{dz} &= jC(\Delta\beta)N(z)g_1(z, \Delta\beta) \\ \frac{dg_1}{dz} &= \Delta\Gamma g_1(z, \Delta\beta) + jC(\Delta\beta)N(z)g_0(z, \Delta\beta), \end{aligned} \tag{7}$$

with initial conditions

$$g_0(0, \Delta\beta) = i_0 , \quad g_1(0, \Delta\beta) = i_1 . \tag{8}$$

Now define the correlation functions

$$R_{k\ell}(z) = \langle g_k(z, \Delta\beta + \sigma)g_\ell^*(z, \Delta\beta)\rangle, \quad (k, \ell = 0, 1), \tag{9}$$

where * denotes complex conjugate and $\langle\ \rangle$ denotes stochastic average. Rowe and Young[1,9] have calculated $R_{k\ell}(z)$ exactly for the case of white noise coupling, with spectral density D_0 ,

$$\langle N(z)N(\zeta)\rangle = D_0\delta(z - \zeta), \tag{10}$$

in the case of initial values $i_0 = 1$ and $i_1 = 0$, corresponding to the signal and spurious modes respectively. They have also calculated the average of the squared envelope of the impulse response, which involves a double integral with respect to $\Delta\beta$ and σ of $R_{00}(z)$. The calculation was exact for frequency-independent coupling[1] (i.e., $C = c_0$ sgn $\Delta\beta$), and approximate for moderate fractional bandwidths for frequency-dependent coupling.[9]

In this paper we will be concerned with the calculation of $R_{k\ell}(z)$ only, and will not consider the time domain statistics. We note that the average powers in the two modes are given by

$$P_0(z) = e^{-2\alpha_0 z}R_{00}(z)\,|_{\sigma=0}, \quad P_1(z) = e^{-2\alpha_0 z}R_{11}(z)\,|_{\sigma=0}. \tag{11}$$

We first consider the case

$$N(z) = F(M(z), z), \tag{12}$$

where $M(z)$ is a finite state Markov chain[13] which has, in general, a nonstationary transition mechanism. Using the results of a paper by Morrison,[14] we obtain a system of ordinary differential equations, with prescribed initial conditions, for calculating $R_{k\ell}(z)$. If the process $M(z)$ has a stationary transition mechanism, and F is a function of $M(z)$ alone, these equations have constant coefficients. In the particular case in which $N(z) = T(z)$, where $T(z)$ is the random telegraph process,[15] we obtain the Laplace transforms of $R_{k\ell}$ explicitly.

Next we investigate the case of white noise coupling by means of the Ito calculus.[16] This approach differs from that used by Rowe and Young,[1,9] who consider the line as the limit of discrete sections, of vanishing length, of uncoupled ideal lines, with discrete mode converters at the end of each section. The quantities $R_{k\ell}(z)$ are calculated exactly for white noise coupling, in agreement with the results of Rowe and Young.[1,9]

Finally, we turn to the asymptotic calculation, for long lines, of the quantities $R_{k\ell}(z)$, in the case of weak coupling, weak attenuation, and narrow fractional bandwidth. The coupling is assumed to have zero mean and to be wide sense stationary, so that $c(z)$ is given by (5), where

$$\langle N(z)\rangle = 0, \quad \langle N(z)N(\zeta)\rangle = \rho(z - \zeta). \tag{13}$$

The asymptotic equations for $R_{k\ell}(z)$ are determined, first for the nonresonance case, and then for the resonance case, in which the differential phase constant is small. There is an alternate interpretation of the resonance case, for which the correlation length is short. It turns out that for white noise coupling (which has zero correlation length), corresponding to (10), the asymptotic equations for $R_{00}(z)$ and $R_{11}(z)$ are exact, in both the nonresonance and resonance cases, and those for $R_{01}(z)$ and $R_{10}(z)$ are exact in the resonance case.

II. MARKOV CHAIN COUPLING

We begin by writing down the equations satisfied by the quantities

$$r_{k\ell}(z) = g_k(z, \Delta\beta + \sigma)g_\ell^*(z, \Delta\beta), \quad (k, \ell = 0, 1). \tag{14}$$

Let

$$C_0 = C(\Delta\beta), \quad C_\sigma = C(\Delta\beta + \sigma). \tag{15}$$

Then, from (4) and (7), for sufficiently smooth $N(z)$, it follows that

$$\frac{dr_{00}}{dz} = jN(z)(C_\sigma r_{10} - C_0 r_{01}), \tag{16}$$

$$\frac{dr_{01}}{dz} = jN(z)(C_\sigma r_{11} - C_0 r_{00}) + \Delta\Gamma^* r_{01}\ , \tag{17}$$

$$\frac{dr_{10}}{dz} = jN(z)(C_\sigma r_{00} - C_0 r_{11}) + (\Delta\Gamma + j\sigma)r_{10}\ , \tag{18}$$

$$\frac{dr_{11}}{dz} = jN(z)(C_\sigma r_{01} - C_0 r_{10}) + (\Delta\Gamma^* + \Delta\Gamma + j\sigma)r_{11}\ . \tag{19}$$

These equations do not hold when $N(z)$ is white noise, as will be discussed later. From (8) the initial conditions are

$$r_{k\ell}(0) = i_k i_\ell^*, \quad (k, \ell = 0, 1). \tag{20}$$

We now consider the case of coupling corresponding to (12), and first state some properties of the finite state Markov chain.[13] The sample functions $M(z)$ are defined on the half line $0 \leqq z < \infty$, have right-continuous paths, and can take on only a finite number N of distinct values $a_p (p = 1, \cdots, N)$. An initial probability distribution is given:

$$\mathrm{X}_p = \text{Prob } \{M(0) = a_p\}, \quad (p = 1, \cdots, N), \tag{21}$$

where $\mathrm{X}_p > 0$ and

$$\sum_{p=1}^{N} \mathrm{X}_p = 1. \tag{22}$$

The transition probabilities are defined, for $0 \leqq x \leqq y$, by

$$P_{pq}(x, y) = \text{Prob } \{M(y) = a_q \mid M(x) = a_p\}, \quad (p, q = 1, \cdots, N). \tag{23}$$

We consider only those processes which can be defined by means of a continuous, bounded infinitesimal generator. Thus, we assume given an $N \times N$ matrix function

$$\boldsymbol{\tau}(z) = (\tau_{pq}(z)), \tag{24}$$

satisfying the conditions

$$\tau_{pq}(z) \geqq 0, \quad p \neq q, \quad \tau_{pp}(z) \leqq 0, \quad (p, q = 1, \cdots, N), \tag{25}$$

and

$$\sum_{q=1}^{N} \tau_{pq}(z) = 0, \qquad (p = 1, \cdots, N). \tag{26}$$

Then[13], for $\delta z \to 0 +$, $(p, q = 1, \cdots, N)$,

$$P_{pp}(z, z + \delta z) = 1 + \tau_{pp}(z)\, \delta z + \mathrm{o}(\delta z), \tag{27}$$

$$P_{pq}(z, z + \delta z) = \tau_{pq}(z)\, \delta z + \mathrm{o}(\delta z), \qquad p \neq q. \tag{28}$$

If the matrix $\boldsymbol{\tau}$ is constant then the process $M(z)$ is said to have a stationary transition mechanism.

Stochastic matrix differential equations of the form

$$\frac{d\mathbf{W}}{dz} = \mathbf{A}(M(z), z)\mathbf{W}(z), \qquad \mathbf{W}(0) = \boldsymbol{\gamma}[M(0)], \tag{29}$$

where $\mathbf{W}$ and $\boldsymbol{\gamma}$ are $n \times m$ matrices, and $\mathbf{A}$ is an $n \times n$ matrix, have been considered by Morrison.[14] Equations were obtained for calculating the stochastic average $\langle \mathbf{W}(z) \rangle$, in the case that $\mathbf{A}$ and $\boldsymbol{\gamma}$ are real, but it is easily verified that these equations are still valid for complex valued $\mathbf{A}$ and $\boldsymbol{\gamma}$. This may be shown by writing the system (29) in real form, and then combining in complex form the equations for calculating the stochastic averages of the real and imaginary parts of $\mathbf{W}(z)$.

Let $\mathbf{E}_N$ denote the row vector with all N elements equal to 1, and let

$$\mathrm{X} = (\mathrm{X}_1 , \cdots , \mathrm{X}_N) \tag{30}$$

be the row vector of initial probabilities given by (21). Note, from (22) and (26), that

$$\mathbf{E}_N \mathrm{X}^t = 1, \quad \mathbf{E}_N \boldsymbol{\tau}^t(z) \equiv \mathbf{0}, \tag{31}$$

where t denotes transpose. Let

$$\langle r_{k\ell}(z) \rangle_p = \langle r_{k\ell}(z) \mid M(z) = a_p \rangle \text{ Prob } \{M(z) = a_p\}, \tag{32}$$

$(k, \ell = 0, 1)$, $(p = 1, \cdots , N)$, and introduce the column vectors

$$\mathbf{R}_{k\ell}(z) = \text{col } (\langle r_{k\ell}(z) \rangle_1 , \cdots , \langle r_{k\ell}(z) \rangle_N), \quad (k, \ell = 0, 1). \tag{33}$$

Then, from (9) and (14),

$$R_{k\ell}(z) = \langle r_{k\ell}(z) \rangle = \mathbf{E}_N \mathbf{R}_{k\ell}(z), \quad (k, \ell = 0, 1). \tag{34}$$

We define the $N \times N$ diagonal matrix $\mathbf{D}(z)$ by

$$\mathbf{D}(z) = \text{diag } [F(a_p , z)], \tag{35}$$

and denote the unit matrix of order N by $\mathbf{I}_N$. Then, for the system (16) through (19), with $N(z)$ given by (12), it is found that[14]

$$\frac{d\mathbf{R}_{00}}{dz} = j\mathbf{D}(z)(C_\sigma \mathbf{R}_{10} - C_0 \mathbf{R}_{01}) + \boldsymbol{\tau}^t(z)\mathbf{R}_{00} , \tag{36}$$

$$\frac{d\mathbf{R}_{01}}{dz} = j\mathbf{D}(z)(C_\sigma \mathbf{R}_{11} - C_0 \mathbf{R}_{00}) + [\Delta\Gamma^* \mathbf{I}_N + \boldsymbol{\tau}^t(z)]\mathbf{R}_{01} , \tag{37}$$

$$\frac{d\mathbf{R}_{10}}{dz} = j\mathbf{D}(z)(C_\sigma \mathbf{R}_{00} - C_0 \mathbf{R}_{11}) + [(\Delta\Gamma + j\sigma)\mathbf{I}_N + \boldsymbol{\tau}^t(z)]\mathbf{R}_{10} , \tag{38}$$

$$\frac{d\mathbf{R}_{11}}{dz} = j\mathbf{D}(z)(C_\sigma \mathbf{R}_{01} - C_0 \mathbf{R}_{10}) + [(\Delta\Gamma^* + \Delta\Gamma + j\sigma)\mathbf{I}_N + \boldsymbol{\tau}^t(z)]\mathbf{R}_{11} . \tag{39}$$

From (20), (21), (30), (32) and (33), the initial conditions are

$$\mathbf{R}_{k\ell}(0) = i_k i_\ell^* \mathrm{X}^t, \quad (k, \ell = 0, 1). \tag{40}$$

If the process $M(z)$ has a stationary transition mechanism, and if the coupling coefficient (5) depends on z through $M(z)$ only, then the differential equations (36) through (39) have constant coefficients. We consider a particular example of this in more detail in the next section.

III. RANDOM TELEGRAPH COUPLING

We now consider the particular case when $N(z) = T(z)$, the random telegraph process,[15] which is one of the simplest finite state Markov chains. It is an ensemble of square wave functions $\{T(z)\}$, such that each sample function $T(z)$ can assume only the values ± 1. For fixed z, a sample function chosen at random will equal $+1$ or -1 with equal probability. The probability $p(n, z)$ of a given sample function changing sign n times in an interval of length z is given by the Poisson process

$$p(n, z) = \frac{(bz)^n}{n!} e^{-bz}, \qquad (n = 0, 1, 2, \cdots), \tag{41}$$

where b is the average number of changes per unit length. The process $T(z)$ has zero mean and is wide sense stationary,

$$\langle T(z) \rangle = 0, \quad \langle T(z)T(\zeta) \rangle = \exp \{-2b \mid z - \zeta \mid \}. \tag{42}$$

The states of the process $T(z)$ are $a_1 = 1$ and $a_2 = -1$, and the vector of initial probabilities is

$$\mathrm{X} = (\tfrac{1}{2}, \tfrac{1}{2}) = \tfrac{1}{2}\mathbf{E}_2 = \tfrac{1}{2}\mathbf{E}. \tag{43}$$

The process has a stationary transition mechanism, with infinitesimal generator

$$\boldsymbol{\tau} = \begin{bmatrix} -b & b \\ b & -b \end{bmatrix} = \boldsymbol{\tau}^t. \tag{44}$$

Since $N(z) = T(z)$, we have, from (12),

$$F(a_p, z) = a_p = (-1)^{p-1}, \quad (p = 1, 2). \tag{45}$$

Hence, from (35),

$$\mathbf{D} = \begin{bmatrix} 1 & 0 \\ 0 & -1 \end{bmatrix}. \tag{46}$$

Note that

$$\mathbf{D}^2 = \mathbf{I}_2 = \mathbf{I}, \quad \mathbf{E}\boldsymbol{\tau}^t = \mathbf{0}, \quad \mathbf{ED}\boldsymbol{\tau}^t = -2b\mathbf{ED}. \tag{47}$$

Let

$$Q_{k\ell}(z) = \mathbf{EDR}_{k\ell}(z), \quad (k, \ell = 0, 1). \tag{48}$$

Then, multiplying equations (36) and (39) by **E**, and equations (37) and (38) by **ED**, we obtain, from (34), (47), and (48),

$$\frac{dR_{00}}{dz} = j(C_\sigma Q_{10} - C_0 Q_{01}), \tag{49}$$

$$\frac{dR_{11}}{dz} = j(C_\sigma Q_{01} - C_0 Q_{10}) + (\Delta\Gamma^* + \Delta\Gamma + j\sigma)R_{11}\ , \tag{50}$$

and

$$\frac{dQ_{01}}{dz} = j(C_\sigma R_{11} - C_0 R_{00}) + (\Delta\Gamma^* - 2b)Q_{01}\ , \tag{51}$$

$$\frac{dQ_{10}}{dz} = j(C_\sigma R_{00} - C_0 R_{11}) + (\Delta\Gamma + j\sigma - 2b)Q_{10}\ . \tag{52}$$

Similarly, multiplying equations (37) and (38) by **E**, and equations (36) and (39) by **ED**, we obtain

$$\frac{dR_{01}}{dz} = j(C_\sigma Q_{11} - C_0 Q_{00}) + \Delta\Gamma^* R_{01}\ , \tag{53}$$

$$\frac{dR_{10}}{dz} = j(C_\sigma Q_{00} - C_0 Q_{11}) + (\Delta\Gamma + j\sigma)R_{10}\ , \tag{54}$$

and

$$\frac{dQ_{00}}{dz} = j(C_\sigma R_{10} - C_0 R_{01}) - 2bQ_{00}\ , \tag{55}$$

$$\frac{dQ_{11}}{dz} = j(C_\sigma R_{01} - C_0 R_{10}) + (\Delta\Gamma^* + \Delta\Gamma + j\sigma - 2b)Q_{11}\ . \tag{56}$$

From (34), (40), (43), (46) and (48), the initial conditions are

$$R_{k\ell}(0) = i_k i_\ell^*\ , \quad Q_{k\ell}(0) = 0, \quad (k, \ell = 0, 1). \tag{57}$$

Equations (49) through (56), subject to (57), are solved by means of Laplace transforms in Appendix A. The Laplace transforms $\hat{R}_{00}(s)$ and $\hat{R}_{11}(s)$ of $R_{00}(z)$ and $R_{11}(z)$ are given by (128) and (129), where $\Delta(s)$ is given by (130), and d_1 , d_2 and η are defined in (125). Note that d_1 and d_2 are linear in the Laplace transform parameter s. Thus $\Delta(s)$ is a quartic in s, and we denote the roots of $\Delta(s) = 0$ by $s_k = s_k(\Delta\beta, \sigma)$, $k = 1, 2, 3, 4$. Inversion of the Laplace transforms in (128)

and (129) leads to

$$R_{00}(z) = \sum_{k=1}^{4} A_{0k}(\Delta\beta, \sigma) \exp [s_k(\Delta\beta, \sigma)z] \tag{58}$$

and

$$R_{11}(z) = \sum_{k=1}^{4} A_{1k}(\Delta\beta, \sigma) \exp [s_k(\Delta\beta, \sigma)z], \tag{59}$$

the coefficients A_{0k} and A_{1k} being the residues at $s = s_k$ of the expressions in (128) and (129) respectively.

Similarly, the Laplace transforms $\hat{R}_{01}(s)$ and $\hat{R}_{10}(s)$ of $R_{01}(z)$ and $R_{10}(z)$ are given by (138) and (139), where $E(s)$ is given by (140), and e_1 and e_2 are defined in (135). Note that e_1 and e_2 are linear in s, so that $E(s)$ is a quartic in s. We denote the roots of $E(s) = 0$ by $\mu_k = \mu_k(\Delta\beta, \sigma)$, $k = 1, 2, 3, 4$. Inversion of the Laplace transforms in (138) and (139) leads to

$$R_{01}(z) = \sum_{k=1}^{4} B_{0k}(\Delta\beta, \sigma) \exp [\mu_k(\Delta\beta, \sigma)z], \tag{60}$$

and

$$R_{10}(z) = \sum_{k=1}^{4} B_{1k}(\Delta\beta, \sigma) \exp [\mu_k(\Delta\beta, \sigma)z], \tag{61}$$

the coefficients B_{0k} and B_{1k} being the residues at $s = \mu_k$ of the expressions in (138) and (139) respectively.

IV. WHITE NOISE COUPLING

In this section we investigate the case of white noise coupling, corresponding to (5) and (10), by means of the Ito calculus. We begin by considering the vector equation

$$\frac{d\mathbf{u}}{dz} = \mathbf{A}\mathbf{u} + \mathbf{B}\mathbf{u}\xi(z), \tag{62}$$

where $\mathbf{A}$ and $\mathbf{B}$ are constant matrices, and $\xi(z)$ is Gaussian white noise, with zero mean and spectral density 1. According to Wonham,[17] the Ito differential equation corresponding to (62) is

$$d\mathbf{u} = (\mathbf{A} + \tfrac{1}{2}\mathbf{B}^2)\mathbf{u}dz + \mathbf{B}\mathbf{u}dw, \tag{63}$$

where w is a Wiener process. The result is stated for real equations, but it may be verified that it holds for complex $\mathbf{A}$, $\mathbf{B}$ and $\mathbf{u}$, by considering the equations for the real and imaginary parts.

The integral equation corresponding to (63) is

$$\mathbf{u}(z) = \mathbf{u}(0) + (\mathbf{A} + \tfrac{1}{2}\mathbf{B}^2) \int_0^z \mathbf{u}(\zeta)\, d\zeta + \mathbf{B} \int_0^z \mathbf{u}(\zeta)\, dw(\zeta). \tag{64}$$

The second integral in (64) is an Ito integral, and it has the property that its stochastic average is zero.[18] Thus,

$$\langle \mathbf{u}(z) \rangle = \langle \mathbf{u}(0) \rangle + (\mathbf{A} + \tfrac{1}{2}\mathbf{B}^2) \int_0^z \langle \mathbf{u}(\zeta) \rangle\, d\zeta, \tag{65}$$

or, in differential form,

$$\frac{d}{dz} \langle \mathbf{u}(z) \rangle = (\mathbf{A} + \tfrac{1}{2}\mathbf{B}^2) \langle \mathbf{u}(z) \rangle. \tag{66}$$

We will also make use of the Ito calculus for the product of differentials,[16] namely

$$(dw)^2 = dz, \quad dwdz = 0, \quad (dz)^2 = 0. \tag{67}$$

We now consider the line equations for white noise coupling, so that, from (5) and (10),

$$c(z) = C\sqrt{D_0}\, \xi(z). \tag{68}$$

Hence, from (1), (62), and (66),

$$\frac{d}{dz} \langle I_0(z) \rangle = -(\Gamma_0 + \tfrac{1}{2}C^2 D_0) \langle I_0(z) \rangle, \tag{69}$$

and

$$\frac{d}{dz} \langle I_1(z) \rangle = -(\Gamma_1 + \tfrac{1}{2}C^2 D_0) \langle I_1(z) \rangle. \tag{70}$$

These equations agree with those obtained by Rowe and Young.[1,9] From (2), (69), and (70),

$$\langle I_\ell(z) \rangle = i_\ell \exp\left[-(\Gamma_\ell + \tfrac{1}{2}C^2 D_0)z\right], \quad (\ell = 0, 1). \tag{71}$$

Also, from (5), (7), (62), (63), and (68),

$$\begin{aligned} dg_0 &= -\tfrac{1}{2}C^2 D_0 g_0\, dz + jC\sqrt{D_0}\, g_1\, dw, \\ dg_1 &= (\Delta\Gamma - \tfrac{1}{2}C^2 D_0) g_1\, dz + jC\sqrt{D_0}\, g_0\, dw. \end{aligned} \tag{72}$$

But, from (14),

$$\begin{aligned} dr_{k\ell}(z) = {} & dg_k(z, \Delta\beta + \sigma) g_\ell^*(z, \Delta\beta) + g_k(z, \Delta\beta + \sigma)\, dg_\ell^*(z, \Delta\beta) \\ & + dg_k(z, \Delta\beta + \sigma)\, dg_\ell^*(z, \Delta\beta). \end{aligned} \tag{73}$$

Hence, from (4), (14), (15), (72), and (73), making use of the relationships in (67),

$$dr_{00} = D_0[C_0C_\sigma r_{11} - \tfrac{1}{2}(C_0^2 + C_\sigma^2)r_{00}]\,dz + j\sqrt{D_0}\,(C_\sigma r_{10} - C_0 r_{01})\,dw, \tag{74}$$

$$dr_{01} = [\Delta\Gamma^* - \tfrac{1}{2}(C_0^2 + C_\sigma^2)D_0]r_{01}\,dz + C_0C_\sigma D_0 r_{10}\,dz + j\sqrt{D_0}\,(C_\sigma r_{11} - C_0 r_{00})\,dw, \tag{75}$$

$$dr_{10} = [(\Delta\Gamma + j\sigma) - \tfrac{1}{2}(C_0^2 + C_\sigma^2)D_0]r_{10}\,dz + C_0C_\sigma D_0 r_{01}\,dz + j\sqrt{D_0}\,(C_\sigma r_{00} - C_0 r_{11})\,dw, \tag{76}$$

$$dr_{11} = [(\Delta\Gamma^* + \Delta\Gamma + j\sigma) - \tfrac{1}{2}(C_0^2 + C_\sigma^2)D_0]r_{11}\,dz + C_0C_\sigma D_0 r_{00}\,dz + j\sqrt{D_0}\,(C_\sigma r_{01} - C_0 r_{10})\,dw. \tag{77}$$

From (9), (14), (63), and (66), it follows that

$$\frac{dR_{00}}{dz} = -\tfrac{1}{2}(C_0^2 + C_\sigma^2)D_0R_{00} + C_0C_\sigma D_0R_{11}\ , \tag{78}$$

$$\frac{dR_{11}}{dz} = C_0C_\sigma D_0R_{00} + [(\Delta\Gamma^* + \Delta\Gamma + j\sigma) - \tfrac{1}{2}(C_0^2 + C_\sigma^2)D_0]R_{11}\ , \tag{79}$$

and

$$\frac{dR_{01}}{dz} = [\Delta\Gamma^* - \tfrac{1}{2}(C_0^2 + C_\sigma^2)D_0]R_{01} + C_0C_\sigma D_0R_{10} \tag{80}$$

$$\frac{dR_{10}}{dz} = C_0C_\sigma D_0R_{01} + [(\Delta\Gamma + j\sigma) - \tfrac{1}{2}(C_0^2 + C_\sigma^2)D_0]R_{10}\ . \tag{81}$$

These equations for R_{kl} are consistent with those obtained by Rowe and Young.[1,9] The initial conditions are given by (57), and the solutions of (78) through (81) are easy to write down. The characteristic roots corresponding to (78) and (79) are, from (4),

$$\lambda = (\Delta\alpha + \tfrac{1}{2}j\sigma) - \tfrac{1}{2}(C_0^2 + C_\sigma^2)D_0 \pm [C_0^2C_\sigma^2D_0^2 + (\Delta\alpha + \tfrac{1}{2}j\sigma)^2]^{\frac{1}{2}}, \tag{82}$$

and those corresponding to (80) and (81) are

$$\lambda = (\Delta\alpha + \tfrac{1}{2}j\sigma) - \tfrac{1}{2}(C_0^2 + C_\sigma^2)D_0 \pm [C_0^2C_\sigma^2D_0^2 - (\Delta\beta + \tfrac{1}{2}\sigma)^2]^{\frac{1}{2}}. \tag{83}$$

We now return to the random telegraph coupling and consider a case where the coupling is large but has a short correlation length. We define the correlation length of the random telegraph process to be

$$\ell_c = \frac{1}{2b}\ , \tag{84}$$

which is just the separation at which the covariance drops to $1/e$ of its peak value. This also agrees with a more general definition of the correlation length of a wide sense stationary process, due to C. L. Mallows:[19]

$$\ell_c = \lim_{\Omega\to\infty} \left\{ 2\pi \int_{-\Omega}^{\Omega} |\ \mathcal{S}(\omega)\ |^2\, d\omega \Big/ \left| \int_{-\Omega}^{\Omega} \mathcal{S}(\omega)\, d\omega \right|^2 \right\}, \tag{85}$$

where $\mathcal{S}(\omega)$ is the spectral density function. We set

$$C_0 = \sqrt{bS_0}\,, \qquad C_\sigma = \sqrt{bS_\sigma}\,. \tag{86}$$

If we substitute (86) into the expression (130) for $\Delta(s)$, and (140) for $E(s)$, as $b \to \infty$, $\Delta(s)$ has the roots

$$s = (\Delta\alpha + \tfrac{1}{2}j\sigma) - \tfrac{1}{2}(S_0 + S_\sigma) \pm [(\Delta\alpha + \tfrac{1}{2}j\sigma)^2 + S_0S_\sigma]^{\frac{1}{2}} + 0\left(\frac{1}{b}\right), \tag{87}$$

$$s = -2b + (\Delta\alpha + \tfrac{1}{2}j\sigma) + \tfrac{1}{2}(S_0 + S_\sigma) \pm [S_0S_\sigma - (\Delta\beta + \tfrac{1}{2}\sigma)^2]^{\frac{1}{2}} + 0\left(\frac{1}{b}\right), \tag{88}$$

and $E(s)$ has the roots

$$\mu = (\Delta\alpha + \tfrac{1}{2}j\sigma) - \tfrac{1}{2}(S_0 + S_\sigma) \pm [S_0S_\sigma - (\Delta\beta + \tfrac{1}{2}\sigma)^2]^{\frac{1}{2}} + 0\left(\frac{1}{b}\right), \tag{89}$$

$$\mu = -2b + (\Delta\alpha + \tfrac{1}{2}j\sigma) + \tfrac{1}{2}(S_0 + S_\sigma) \pm [S_0S_\sigma + (\Delta\alpha + \tfrac{1}{2}j\sigma)^2]^{\frac{1}{2}} + 0\left(\frac{1}{b}\right). \tag{90}$$

With the aid of (87) through (90), it is straightforward to calculate $\lim_{b\to\infty} R_{k\ell}(z)$, $(k, \ell = 0, 1)$. These limits are just the corresponding expressions for white noise coupling, if in the expressions for white noise we set

$$C_0^2 D_0 = S_0\,, \quad C_\sigma^2 D_0 = S_\sigma\,. \tag{91}$$

But (91) is consistent with (86), in view of (10), since

$$\int_{-\infty}^{\infty} \langle T(z + \zeta)T(\zeta)\rangle\, dz = \frac{1}{b}\,, \tag{92}$$

from (42).

VI. PERTURBATION THEORY

We now assume the random coupling is described by a zero mean, wide sense stationary process $N(z)$, with an autocorrelation function

satisfying (102), but which is otherwise arbitrary. We assume in addition that there is a characteristic length ℓ, e.g., the correlation length ℓ_c, and an ϵ, $0 < \epsilon \ll 1$, such that

$$C_0\ell = 0(\epsilon), \quad C_\sigma\ell = 0(\epsilon), \quad \Delta\alpha\ell = 0(\epsilon^2), \quad \sigma\ell = 0(\epsilon^2), \tag{93}$$

and in the first instance

$$\Delta\beta\ell = 0(1). \tag{94}$$

This can best be described as a case with weak coupling, weak attenuation, and narrow fractional bandwidth.

We consider the asymptotic calculation of $R_{k\ell}(z)$ for small ϵ. The asymptotic results are valid for $z/\ell = 0(1/\epsilon^2)$. We begin by stating, in a form which will suffice for our present purposes, some results of Papanicolaou and Keller[12] on stochastic differential equations.

Thus, consider the linear vector stochastic differential equation

$$\frac{d\mathbf{w}}{dz} = [\epsilon\mathbf{A}_1(z) + \epsilon^2\mathbf{A}_2]w(z), \qquad \mathbf{w}(0) = \mathbf{w}_0\,, \tag{95}$$

where $\mathbf{A}_1(z)$ is a randon matrix with zero mean,

$$\langle\mathbf{A}_1(z)\rangle \equiv 0, \tag{96}$$

$\mathbf{A}_2$ is a constant nonstochastic matrix, and $\mathbf{w}_0$ is a nonstochastic vector. Define

$$\overline{\mathbf{A}_1\mathbf{A}_1} = \lim_{Z\to\infty}\left[\frac{1}{Z}\int_0^Z\int_0^z \langle\mathbf{A}_1(z)\mathbf{A}_1(\zeta)\rangle\, d\zeta\, dz\right]. \tag{97}$$

Then asymptotically, for $0 < \epsilon \ll 1$,

$$\frac{d}{dz}\langle\mathbf{w}(z)\rangle \approx \epsilon^2(\overline{\mathbf{A}_1\mathbf{A}_1} + \mathbf{A}_2)\langle\mathbf{w}(z)\rangle, \qquad \langle\mathbf{w}(0)\rangle = \mathbf{w}_0\,. \tag{98}$$

We now apply the above result to equations (16) through (19) for $r_{k\ell}(z)$, subject to the assumptions (93) and (94), where $\Delta\Gamma$ is given by (4). Thus, we let

$$\mathbf{w} = (r_{00}\,, r_{11}\,, e^{j\Delta\beta z}r_{01}\,, e^{-j\Delta\beta z}r_{10})^t, \tag{99}$$

where t denotes transpose. Then,

$$\epsilon\mathbf{A}_1(z) = jN(z)\begin{bmatrix} 0 & 0 & -C_0e^{-j\Delta\beta z} & C_\sigma e^{j\Delta\beta z} \\ 0 & 0 & C_\sigma e^{-j\Delta\beta z} & -C_0e^{j\Delta\beta z} \\ -C_0e^{j\Delta\beta z} & C_\sigma e^{j\Delta\beta z} & 0 & 0 \\ C_\sigma e^{-j\Delta\beta z} & -C_0e^{-j\Delta\beta z} & 0 & 0 \end{bmatrix}, \tag{100}$$

and

$$\epsilon^2 \mathbf{A}_2 = \begin{bmatrix} 0 & 0 & 0 & 0 \\ 0 & (2\Delta\alpha + j\sigma) & 0 & 0 \\ 0 & 0 & \Delta\alpha & 0 \\ 0 & 0 & 0 & (\Delta\alpha + j\sigma) \end{bmatrix}. \tag{101}$$

Note that $\mathbf{A}_1(z)$ as given by (100) satisfies (96), by virtue of (13). The calculation of $\overline{\mathbf{A}_1\mathbf{A}_1}$, defined by (97), is carried out in Appendix B, under the assumption that

$$\lim_{Z\to\infty} \left[\frac{1}{Z}\int_0^Z \zeta \mid \rho(\zeta) \mid d\zeta\right] = 0, \tag{102}$$

where $\rho(\zeta)$ is given by (13). Let

$$S(\omega) = \int_0^\infty e^{j\omega\zeta}\rho(\zeta)\, d\zeta. \tag{103}$$

Since, from (9) and (14), $R_{k\ell}(z) = \langle r_{k\ell}(z)\rangle$, it follows from (98), (99), (101), (148), and (149) that, asymptotically,

$$\frac{dR_{00}}{dz} \approx -[C_0^2 S(-\Delta\beta) + C_\sigma^2 S(\Delta\beta)]R_{00} + C_0 C_\sigma[S(\Delta\beta) + S(-\Delta\beta)]R_{11}\,, \tag{104}$$

$$\frac{dR_{11}}{dz} \approx C_0 C_\sigma[S(\Delta\beta) + S(-\Delta\beta)]R_{00} + [(2\Delta\alpha + j\sigma) - C_0^2 S(\Delta\beta) - C_\sigma^2 S(-\Delta\beta)]R_{11}\,, \tag{105}$$

and, from (150), that

$$\frac{dR_{01}}{dz} \approx [(\Delta\alpha - j\Delta\beta) - (C_0^2 + C_\sigma^2)S(\Delta\beta)]R_{01}\,, \tag{106}$$

$$\frac{dR_{10}}{dz} \approx [(\Delta\alpha + j\Delta\beta + j\sigma) - (C_0^2 + C_\sigma^2)S(-\Delta\beta)]R_{10}\,. \tag{107}$$

The initial conditions are given by (57).

Now,

$$\int_0^\infty \cos(\omega\zeta)\ \delta(\zeta)\, d\zeta = \frac{1}{2}\int_{-\infty}^\infty \cos(\omega\zeta)\ \delta(\zeta)\, d\zeta = \tfrac{1}{2}, \tag{108}$$

$$\int_0^\infty \sin(\omega\zeta)\ \delta(\zeta)\, d\zeta = 0.$$

Hence, from (103), for $\rho(\zeta) = D_0\delta(\zeta)$ we have $S(\omega) \equiv 1/2(D_0)$. Note that the asymptotic equations (104) and (105) for R_{00} and R_{11} are, in fact, exact for white noise, as is seen from (4), (78) and (79). However, from (57), (106) and (107), for $S(\omega) = 1/2(D_0)$, we have asymptotically

$$R_{01}(z) \approx i_0 i_1^* \exp\{[\Delta\Gamma^* - \tfrac{1}{2}(C_0^2 + C_\sigma^2)D_0]z\}, \tag{109}$$

$$R_{10}(z) \approx i_1 i_0^* \exp\{[(\Delta\Gamma + j\sigma) - \tfrac{1}{2}(C_0^2 + C_\sigma^2)D_0]z\}. \tag{110}$$

It is readily verified that these results are asymptotically consistent for $0 \leqq z/\ell \leqq 0(1/\epsilon^2)$, to lowest order in ϵ, with the exact equations (80) and (81) for white noise, under the assumptions in (93) and (94). The characteristic roots corresponding to (80) and (81) are, from (83),

$$\lambda = \pm j(\Delta\beta + \tfrac{1}{2}\sigma) + (\Delta\alpha + \tfrac{1}{2}j\sigma) - \tfrac{1}{2}(C_0^2 + C_\sigma^2)D_0 + \frac{0(\epsilon^4)}{\ell}. \tag{111}$$

The above results are valid under the assumptions (93) and (94). Suppose now that instead of (94) we have

$$(\Delta\beta)\ell = 0(\epsilon^2), \tag{112}$$

which we refer to as the resonance case. Note if we set $b = b_0/\epsilon^2$ and $\ell = \ell_c = 1/2b$, the correlation length, the random telegraph case considered at the end of Section IV is a special example of this resonance case. The resonance case can thus correspond to large coupling, moderate attenuation and fractional bandwidth, and small correlation length. Corresponding to (16) through (19), we take

$$\mathbf{w} = (r_{00}, r_{11}, r_{01}, r_{10})^t, \tag{113}$$

so that, from (93), (95), and (112), we now have

$$\epsilon\mathbf{A}_1(z) = jN(z)\begin{bmatrix} 0 & 0 & -C_0 & C_\sigma \\ 0 & 0 & C_\sigma & -C_0 \\ -C_0 & C_\sigma & 0 & 0 \\ C_\sigma & -C_0 & 0 & 0 \end{bmatrix}, \tag{114}$$

and

$$\epsilon^2\mathbf{A}_2 = \begin{bmatrix} 0 & 0 & 0 & 0 \\ 0 & (\Delta\Gamma^* + \Delta\Gamma + j\sigma) & 0 & 0 \\ 0 & 0 & \Delta\Gamma^* & 0 \\ 0 & 0 & 0 & (\Delta\Gamma + j\sigma) \end{bmatrix}. \tag{115}$$

Note that $\mathbf{A}_1(z)$ as given by (114) satisfies (96), by virtue of (13). The calculation of $\overline{\mathbf{A}_1\mathbf{A}_1}$, defined by (97), is carried out in Appendix B. It follows from (98), (113), (115), (152), and (153), with $R_{k\ell}(z) = \langle r_{k\ell}(z) \rangle$, that asymptotically

$$\frac{dR_{00}}{dz} \approx -(C_0^2 + C_\sigma^2)S(0)R_{00} + 2C_0C_\sigma S(0)R_{11}\,, \tag{116}$$

$$\frac{dR_{11}}{dz} \approx 2C_0C_\sigma S(0)R_{00} + [(\Delta\Gamma^* + \Delta\Gamma + j\sigma) - (C_0^2 + C_\sigma^2)S(0)]R_{11}\,, \tag{117}$$

and

$$\frac{dR_{01}}{dz} \approx [\Delta\Gamma^* - (C_0^2 + C_\sigma^2)S(0)]R_{01} + 2C_0C_\sigma S(0)R_{10}\,, \tag{118}$$

$$\frac{dR_{10}}{dz} \approx 2C_0C_\sigma S(0)R_{01} + [(\Delta\Gamma + j\sigma) - (C_0^2 + C_\sigma^2)S(0)]R_{10}\,. \tag{119}$$

Thus, in the resonance case, the asymptotic equations (116) through (119) for $R_{k\ell}(z)$, $(k, \ell = 0, 1)$, are exact for white noise, for which $S(0) = 1/2(D_0)$, as is seen from (78) through (81).

APPENDIX A

We here solve equations (49) through (56), subject to the initial conditions (57). The Laplace transform of $F(z)$ is

$$\hat{F}(s) = \int_0^\infty e^{-sz}F(z)\,dz. \tag{120}$$

Taking the Laplace transforms of equations (49) through (52), and using (57), one finds that

$$s\hat{R}_{00} + jC_0\hat{Q}_{01} - jC_\sigma\hat{Q}_{10} = i_0i_0^*, \tag{121}$$

$$(s - \Delta\Gamma^* - \Delta\Gamma - j\sigma)\hat{R}_{11} - jC_\sigma\hat{Q}_{01} + jC_0\hat{Q}_{10} = i_1i_1^*, \tag{122}$$

and

$$(s + 2b - \Delta\Gamma^*)\hat{Q}_{01} = jC_\sigma\hat{R}_{11} - jC_0\hat{R}_{00}\,, \tag{123}$$

$$(s + 2b - \Delta\Gamma - j\sigma)\hat{Q}_{10} = jC_\sigma\hat{R}_{00} - jC_0\hat{R}_{11}\,. \tag{124}$$

Let

$$d_1 = s + 2b - \Delta\Gamma^*, \quad d_2 = s + 2b - \Delta\Gamma - j\sigma,$$

$$\eta = 2\Delta\alpha + j\sigma. \tag{125}$$

Then, substituting for $\hat{Q}_{01}$ and $\hat{Q}_{10}$ from (123) and (124) into (121)

and (122), it follows that

$$\left(s + \frac{C_0^2}{d_1} + \frac{C_\sigma^2}{d_2}\right)\hat{R}_{00} - C_0C_\sigma\left(\frac{1}{d_1} + \frac{1}{d_2}\right)\hat{R}_{11} = i_0i_0^*, \tag{126}$$

$$-C_0C_\sigma\left(\frac{1}{d_1} + \frac{1}{d_2}\right)\hat{R}_{00} + \left(s - \eta + \frac{C_0^2}{d_2} + \frac{C_\sigma^2}{d_1}\right)\hat{R}_{11} = i_1i_1^*. \tag{127}$$

Hence

$$\hat{R}_{00} = \{[(s - \eta)\, d_1\, d_2 + C_0^2\, d_1 + C_\sigma^2\, d_2]i_0i_0^* + C_0C_\sigma(d_1 + d_2)i_1i_1^*\}/\Delta(s), \tag{128}$$

$$\hat{R}_{11} = \{C_0C_\sigma(d_1 + d_2)i_0i_0^* + (s\, d_1\, d_2 + C_0^2\, d_2 + C_\sigma^2\, d_1)i_1i_1^*\}/\Delta(s), \tag{129}$$

where

$$\Delta(s) \equiv [s(s - \eta)\, d_1\, d_2 + (C_0^2 + C_\sigma^2)s(d_1 + d_2) - \eta(C_\sigma^2\, d_1 + C_0^2\, d_2) + (C_\sigma^2 - C_0^2)^2]. \tag{130}$$

Similarly, taking the Laplace transforms of equations (53) through (56), and using (57),

$$(s - \Delta\Gamma^*)\hat{R}_{01} + jC_0\hat{Q}_{00} - jC_\sigma\hat{Q}_{11} = i_0i_1^*, \tag{131}$$

$$(s - \Delta\Gamma - j\sigma)\hat{R}_{10} - jC_\sigma\hat{Q}_{00} + jC_0\hat{Q}_{11} = i_1i_0^*, \tag{132}$$

and

$$(s + 2b)\hat{Q}_{00} = jC_\sigma\hat{R}_{10} - jC_0\hat{R}_{01}, \tag{133}$$

$$(s + 2b - \eta)\hat{Q}_{11} = jC_\sigma\hat{R}_{01} - jC_0\hat{R}_{10}, \tag{134}$$

where η is defined in (125). Let

$$e_1 = s + 2b, \quad e_2 = s + 2b - \eta. \tag{135}$$

Then, substituting for $\hat{Q}_{00}$ and $\hat{Q}_{11}$ from (133) and (134) into (131) and (132),

$$\left(s - \Delta\Gamma^* + \frac{C_0^2}{e_1} + \frac{C_\sigma^2}{e_2}\right)\hat{R}_{01} - C_0C_\sigma\left(\frac{1}{e_1} + \frac{1}{e_2}\right)\hat{R}_{10} = i_0i_1^*, \tag{136}$$

$$-C_0C_\sigma\left(\frac{1}{e_1} + \frac{1}{e_2}\right)\hat{R}_{01} + \left(s - \Delta\Gamma - j\sigma + \frac{C_0^2}{e_2} + \frac{C_\sigma^2}{e_1}\right)\hat{R}_{10} = i_1i_0^*. \tag{137}$$

From (136) and (137) it follows that

$$\hat{R}_{01} = \{[(s - \Delta\Gamma - j\sigma)e_1e_2 + C_0^2e_1 + C_\sigma^2e_2]i_0i_1^* + C_0C_\sigma(e_1 + e_2)i_1i_0^*\}/E(s), \tag{138}$$

and

$$\hat{R}_{10} = \{C_0C_\sigma(e_1 + e_2)i_0i_1^* + [(s - \Delta\Gamma^*)e_1e_2 + C_0^2e_2 + C_\sigma^2e_1]i_1i_0^*\}/E(s), \tag{139}$$

where

$$\begin{aligned} E(s) \equiv\ & (s - \Delta\Gamma - j\sigma)(s - \Delta\Gamma^*)e_1e_2 + (C_0^2 + C_\sigma^2)s(e_1 + e_2) \\ & - [C_0^2\Delta\Gamma^* + C_\sigma^2(\Delta\Gamma + j\sigma)]e_1 - [C_0^2(\Delta\Gamma + j\sigma) + C_\sigma^2\Delta\Gamma^*]e_2 \\ & + (C_\sigma^2 - C_0^2)^2. \end{aligned} \tag{140}$$

APPENDIX B

We here carry out the calculation of $\overline{\mathbf{A}_1\mathbf{A}_1}$, defined by (97). Corresponding to (100) we have, from (13),

$$\epsilon^2\langle \mathbf{A}_1(z)\mathbf{A}_1(\zeta)\rangle = -\rho(z - \zeta)\begin{bmatrix} \mathbf{F} & \mathbf{0} \\ \mathbf{0} & \mathbf{G} \end{bmatrix}, \tag{141}$$

where

$$\mathbf{F} = \begin{bmatrix} [C_0^2e^{-j\Delta\beta(z-\zeta)} + C_\sigma^2e^{j\Delta\beta(z-\zeta)}] & -2C_0C_\sigma\cos\Delta\beta(z - \zeta) \\ -2C_0C_\sigma\cos\Delta\beta(z - \zeta) & [C_0^2e^{j\Delta\beta(z-\zeta)} + C_\sigma^2e^{-j\Delta\beta(z-\zeta)}] \end{bmatrix}, \tag{142}$$

and

$$\mathbf{G} = \begin{bmatrix} (C_0^2 + C_\sigma^2)e^{j\Delta\beta(z-\zeta)} & -2C_0C_\sigma e^{j\Delta\beta(z+\zeta)} \\ -2C_0C_\sigma e^{-j\Delta\beta(z+\zeta)} & (C_0^2 + C_\sigma^2)e^{-j\Delta\beta(z-\zeta)} \end{bmatrix}. \tag{143}$$

Now,

$$\begin{aligned} & \int_0^Z \int_0^z e^{j\omega(z-\zeta)}\rho(z - \zeta)\, d\zeta\, dz \\ & \qquad = \int_0^Z \int_0^z e^{j\omega\zeta}\rho(\zeta)\, d\zeta\, dz = \int_0^Z (Z - \zeta)e^{j\omega\zeta}\rho(\zeta)\, d\zeta. \end{aligned} \tag{144}$$

Hence, for real ω, from (102) and (103),

$$\lim_{Z\to\infty}\left[\frac{1}{Z}\int_0^Z \int_0^z e^{j\omega(z-\zeta)}\rho(z - \zeta)\, d\zeta\, dz\right] = S(\omega). \tag{145}$$

Also,

$$\begin{aligned} \int_0^Z \int_0^z e^{j\omega(z+\zeta)}\rho(z - \zeta)\, d\zeta\, dz &= \int_0^Z e^{2j\omega z}\int_0^z e^{-j\omega\zeta}\rho(\zeta)\, d\zeta\, dz \\ &= \frac{1}{2j\omega}\int_0^Z (e^{2j\omega Z}e^{-j\omega\zeta} - e^{j\omega\zeta})\rho(\zeta)\, d\zeta. \end{aligned} \tag{146}$$

Hence, for real $\omega \neq 0$,

$$\lim_{Z\to\infty}\left[\frac{1}{Z}\int_0^Z\int_0^z e^{j\omega(z+\zeta)}\rho(z-\zeta)\,d\zeta\,dz\right] = 0. \tag{147}$$

Thus, from (97), (141) through (143), (145), and (147),

$$\epsilon^2\overline{\mathbf{A}_1\mathbf{A}_1} = \begin{bmatrix}\mathbf{X}(\Delta\beta) & \mathbf{0}\\ \mathbf{0} & \mathbf{Y}(\Delta\beta)\end{bmatrix}, \qquad (\Delta\beta)\ell = 0(1), \tag{148}$$

where

$$\mathbf{X}(\Delta\beta) = \begin{bmatrix}-[C_0^2S(-\Delta\beta) + C_\sigma^2S(\Delta\beta)] & C_0C_\sigma[S(\Delta\beta) + S(-\Delta\beta)]\\ C_0C_\sigma[S(\Delta\beta) + S(-\Delta\beta)] & -[C_0^2S(\Delta\beta) + C_\sigma^2S(-\Delta\beta)]\end{bmatrix}, \tag{149}$$

and

$$\mathbf{Y}(\Delta\beta) = (C_0^2 + C_\sigma^2)\begin{bmatrix}S(\Delta\beta) & 0\\ 0 & S(-\Delta\beta)\end{bmatrix}. \tag{150}$$

Now consider $\mathbf{A}_1(z)$ as given by (114). Then, from (13),

$$\epsilon^2\langle\mathbf{A}_1(z)\mathbf{A}_1(\zeta)\rangle = -\rho(z-\zeta)\begin{bmatrix}\mathbf{H} & \mathbf{0}\\ \mathbf{0} & \mathbf{H}\end{bmatrix}, \tag{151}$$

where

$$\mathbf{H} = \begin{bmatrix}(C_0^2 + C_\sigma^2) & -2C_0C_\sigma\\ -2C_0C_\sigma & (C_0^2 + C_\sigma^2)\end{bmatrix}. \tag{152}$$

Hence, from (97), (145), (151), and (152),

$$\epsilon^2\overline{\mathbf{A}_1\mathbf{A}_1} = -S(0)\begin{bmatrix}\mathbf{H} & \mathbf{0}\\ \mathbf{0} & \mathbf{H}\end{bmatrix}, \qquad (\Delta\beta)\ell = 0(\epsilon^2). \tag{153}$$

Note, from (148) and (150), the nonuniform behavior of $\epsilon^2\overline{\mathbf{A}_1\mathbf{A}_1}$ in the neighborhood of resonance, which arises from the discontinuity of the limit in (147) at $\omega = 0$.

REFERENCES

1. Rowe, H. E. and Young, D. T., "Transmission Distortion in Multi-Mode Random Waveguides," IEEE Trans. on Microwave Theory and Techniques, to be published.
2. Miller, S. E., "Coupled Wave Theory and Waveguide Applications," B.S.T.J., *33*, No. 3, part 1 (May 1954), pp. 661–720.
3. Schelkunoff, S. A., "Conversion of Maxwell's Equations into Generalized Telegraphist's Equations," B.S.T.J., *34*, No. 5, part 2 (September 1955), pp. 995–1043.

4. Louisell, W. H., *Coupled Mode and Parametric Electronics*, New York: John Wiley and Sons, 1960.
5. Jones, A. L., "Coupling of Optical Fibers and Scattering in Fiber," J. Opt. Soc. Amer., *55*, No. 3 (March 1965), pp. 261–271.
6. Marcuse, D., "Mode Conversion Caused by Surface Imperfections of a Dielectric Slab Waveguide," B.S.T.J., *48*, No. 10, part 3 (December 1969), pp. 3187–3215.
7. Miller, S. E., "Waveguide as a Communication Medium," B.S.T.J., *33*, No. 6, part 2 (November 1954), pp. 1209–1265.
8. Rowe, H. E. and Warters, W. D., "Transmission in Multimode Waveguide with Random Imperfections," B.S.T.J., *41*, No. 3, part 2 (May 1962), pp. 1031–1170.
9. Young, D. T. and Rowe, H. E., "Optimum Coupling for Random Guides with Frequency-Dependent Coupling," IEEE Trans. on Microwave Theory and Techniques, to be published.
10. Personick, S. D., "Time Dispersion in Dielectric Waveguides," B.S.T.J., *50*, No. 3 (March 1971), pp. 843–859.
11. Wonham, W. M., "Random Differential Equations in Control Theory," in *Probabilistic Methods in Applied Mathematics, 2* Edited by A. T. Bharucha-Reid, New York: Academic Press, 1970, pp. 139–142.
12. Papanicolaou, G. C. and Keller, J. B., "Stochastic Differential Equations with Applications to Random Harmonic Oscillators and Wave Propagation in Random Media," SIAM J. Appl. Math., *21*, No. 2 (September 1971), pp. 287–305.
13. Doob, J. L., *Stochastic Processes*, New York: John Wiley and Sons, 1953, pp. 235–255.
14. Morrison, J. A., "Moments and Correlation Functions of Solutions of Some Stochastic Matrix Differential Equations," J. Math Phys., to be published.
15. Blanc-Lapierre, A. and Fortet, R., *Theory of Random Functions*, New York: Gordon and Breach, 1965, *1*, p. 161.
16. McKean, H. P., Jr., *Stochastic Integrals*, New York: Academic Press, 1969, p. 33.
17. Wonham, W. M., "Optimal Stationary Control of a Linear System with State-Dependent Noise," SIAM J. Control, *5*, No. 3 (August 1967), pp. 486–500.
18. Doob, J. L, op. cit., p. 437.
19. Mallows, C. L., private communication.

Copyright © 1972 American Telephone and Telegraph Company
THE BELL SYSTEM TECHNICAL JOURNAL
Vol. 51, No. 1, January, 1972
Printed in U.S.A.

Derivation of Coupled Power Equations

By D. MARCUSE

(Manuscript received August 6, 1971)

The modes of a multimode dielectric waveguide are coupled by imperfections of the waveguide structure. The propagation of the coupled modes is described by coupled wave equations involving the wave amplitudes. If the coupling functions are random variables the interaction between the modes can be described more easily by coupled power equations. The derivation of the coupled power equations from the coupled wave equations is accomplished with the help of perturbation theory.

I. INTRODUCTION

The interaction of the modes of a multimode waveguide can be described by coupled wave equations.[1,2,3] The coupling between the waves is caused by imperfections of the waveguide structure. These imperfections are either deviations of the refractive index from the index distribution of the perfect waveguide or they are departures of the waveguide geometry from its nominal value. Changes of the core diameter of an optical fiber causes coupling between the guided modes and also coupling of the guided modes to the radiation modes.

Solutions of the coupled wave equations are hard to obtain for many modes since not only the wave amplitudes but also their relative phases enter into the description.

In most problems of practical interest the coupling coefficient is a random function of distance and only the exchange of power between the modes is of interest. A description of this problem in terms of coupled wave equations yields more information (phase information) than is required and consequently is quite complicated. One might expect intuitively that a description in terms of power exchange between the modes should exist.[4] If it were permissible to add power instead of amplitude one would be tempted to write down power rate equations that account for the incremental loss of power of one mode in terms of the power that is transferred per unit length from this mode to all the other guided modes while an increase in power can be expressed

by the power that is transferred per unit length from all the other modes to the mode under consideration. Coupled power equations for two modes have been derived from the coupled wave equations that admit just this intuitive kind of interpretation.[5] Our derivation of the coupled power equations from the coupled wave equations is not mathematically rigorous. It is based on ideas of perturbation theory and on the assumption that the coupling coefficients can be described by correlation functions with Gaussian shape. No attempt has been made to solve the difficult problem of estimating the accuracy of the approximate theory.

II. COUPLED WAVE EQUATIONS

Many problems of coupling between the modes of multimode waveguides or the coupling between several different transmission lines can be expressed in terms of coupled wave equations[1,2,3]

$$\frac{\partial a_\nu}{\partial z} = \sum_{\mu=1}^{N} c_{\nu\mu} a_\mu \, . \tag{1}$$

The amplitude of the νth mode is a_ν ; $c_{\nu\mu}$ is the coupling coefficient that describes the interaction between mode μ and ν. The diagonal elements of the matrix of coupling coefficients represent the propagation constants of the modes

$$c_{\nu\nu} = -i\beta_\nu \, . \tag{2}$$

The system of equations (1) is the starting point of our discussion. In the absence of loss, power must be conserved. We thus require

$$\frac{\partial}{\partial z} \sum_{\nu=1}^{N} | \, a_\nu \, |^2 = 0. \tag{3}$$

With the help of (1) we obtain

$$\frac{d}{dz} \sum_{\nu=1}^{N} a_\nu a_\nu^* = \sum_{\nu=1}^{N} \left(a_\nu \frac{da_\nu^*}{dz} + a_\nu^* \frac{da_\nu}{dz} \right) = \sum_{\nu=1}^{N} \sum_{\mu=1}^{N} (c_{\nu\mu}^* + c_{\mu\nu}) a_\nu a_\mu^* \, . \tag{4}$$

The asterisk indicates complex conjugation. In order to write the last part of (4) in its indicated form the ν and μ labels of the second term had to be interchanged. Since (4) must vanish for any possible choice of the amplitude coefficients (which at any point along the line can be chosen arbitrarily by means of initial conditions) we obtain the following condition for the coupling coefficients.

$$c_{\nu\mu}^* = -c_{\mu\nu} \, . \tag{5}$$

It is advantageous to separate the rapidly varying z-dependent part exp $(-i\beta_\nu z)$ from the wave amplitudes by the relation

$$a_\nu = A_\nu e^{-i\beta_\nu z}. \tag{6}$$

The coupled wave equations now assume the form

$$\frac{dA_\nu}{dz} = \sum_{\mu \neq \nu} c_{\nu\mu} A_\mu e^{i\Delta\beta_{\nu\mu} z}, \tag{7}$$

with the abbreviation

$$\Delta\beta_{\nu\mu} = \beta_\nu - \beta_\mu . \tag{8}$$

It follows from this definition that

$$\Delta\beta_{\nu\sigma} + \Delta\beta_{\sigma\mu} = \Delta\beta_{\nu\mu} . \tag{9}$$

III. DERIVATION OF COUPLED POWER EQUATIONS

The coupling coefficients are functions of the z coordinate that measures distance along the waveguide axis. In metallic as well as dielectric waveguides the coupling coefficients assume the form

$$c_{\nu\mu} = K_{\nu\mu} f(z). \tag{10}$$

$K_{\nu\mu}$ is independent of z. The function $f(z)$ often describes the actual shape of the deformed waveguide boundary or the bent waveguide axis. From (5) we obtain the condition

$$K^*_{\nu\mu} = -K_{\mu\nu} . \tag{11}$$

The function $f(z)$ is supposed to be a stationary random variable whose correlation function is assumed to be Gaussian

$$\langle f(z) f(z - u) \rangle = \sigma^2 e^{-(u/D)^2}. \tag{12}$$

σ^2 is the variance and D is the correlation length of $f(z)$. Since we aim at deriving coupled power equations we use the fact that the average power carried by each mode is

$$P_\nu = \langle \mid a_\nu \mid^2 \rangle = \langle \mid A_\nu \mid^2 \rangle. \tag{13}$$

The symbol $\langle\ \rangle$ indicates an ensemble average. From (7) and (13) we obtain

$$\begin{aligned} \frac{dP_\nu}{dz} &= \left\langle A^*_\nu \frac{dA_\nu}{dz} \right\rangle + \left\langle A_\nu \frac{dA^*_\nu}{dz} \right\rangle \\ &= \sum_{\mu \neq \nu} \{ K_{\nu\mu} \langle f(z) A^*_\nu A_\mu \rangle e^{i\Delta\beta_{\nu\mu} z} + K^*_{\nu\mu} \langle f(z) A_\nu A^*_\mu \rangle e^{-i\Delta\beta_{\nu\mu} z} \}. \end{aligned} \tag{14}$$

Let us assume that the waveguide begins at $z = 0$. At a point z sufficiently close to $z = 0$ we obtain the following approximate solution of the wave equations (7)

$$A_\nu(z) = A_\nu(0) + \sum_{\rho \neq \nu}^{N} A_\rho(0) K_{\nu\rho} \int_0^z f(x) e^{i\Delta\beta_{\nu\rho}x}\, dx. \tag{15}$$

The solution of the wave equations (15) is based on first-order perturbation theory. It applies if the coupling is sufficiently weak or if z is chosen sufficiently small so that $A_\rho(z)$ is only slightly different from $A_\rho(0)$. The input values $A_\rho(0)$ are not subject to statistical fluctuations; their value is thus identical with their average value. Neglecting terms of higher than second order in $K_{\nu\mu}$ we obtain by substitution of (15) into (14)

$$\frac{dP_\nu}{dz} = \sum_{\mu \neq \nu} \left\{ \sum_{\rho \neq \nu} K_{\nu\mu} K^*_{\nu\rho} A^*_\rho(0) A_\mu(0) \int_0^z \langle f(z) f(x) \rangle e^{i(\Delta\beta_{\nu\mu}z - \Delta\beta_{\nu\rho}x)}\, dx \right.$$
$$\left. + \sum_{\rho \neq \mu} K_{\nu\mu} K_{\mu\rho} A^*_\nu(0) A_\rho(0) \int_0^z \langle f(z) f(x) \rangle e^{i(\Delta\beta_{\nu\mu}z + \Delta\beta_{\mu\rho}x)}\, dx + \text{c.c.} \right\}. \tag{16}$$

Terms proportional to the first power of $K_{\nu\mu}$ are absent from (16) since

$$\langle f(z) \rangle = 0. \tag{17}$$

The abbreviation "c.c." indicates additional terms that are the complex conjugate of the terms shown in (16).

Using (12) and the relation

$$\Delta\beta_{\mu\rho} = -\Delta\beta_{\rho\mu}\,, \tag{18}$$

we can write

$$\int_0^z \langle f(z) f(x) \rangle e^{i(\Delta\beta_{\nu\mu}z + \Delta\beta_{\mu\rho}x)}\, dx = \sigma^2 e^{i(\Delta\beta_{\nu\mu} - \Delta\beta_{\rho\mu})z} \int_0^z e^{-(u/D)^2} e^{i\Delta\beta_{\rho\mu}u}\, du. \tag{19}$$

We must now assume that $z \gg D$ requiring simultaneously that σ^2 is sufficiently small so that (15) is a good approximation. We can then write

$$\int_0^z e^{-(u/D)^2} e^{i\Delta\beta_{\rho\mu}u}\, du = \int_0^\infty e^{-(u/D)^2} e^{i\Delta\beta_{\rho\mu}u}\, du$$
$$= \tfrac{1}{2}\sqrt{\pi}\, D e^{-[(D/2)\Delta\beta_{\rho\mu}]^2} + iF(D, \Delta\beta_{\rho\mu}). \tag{20}$$

The function $F(D, \Delta\beta_{\rho\mu})$ is real and independent of z. It is thus clear that the expression in (19) depends on z only through the factor $\exp [i(\beta_\nu - \beta_\rho)z]$. Oscillatory terms do not contribute appreciably to the right-hand side of the differential equation (16). This fact becomes apparent if we integrate (16) with respect to z. The functions $A_\nu(z)$ are slowly varying compared to the oscillatory terms. Integrals over sine and cosine functions contribute very little compared to integrals over slowly varying functions. This consideration allows us to neglect the oscillatory terms in favor of the nonoscillatory terms. We thus consider only the term (19) with $\beta_\nu = \beta_\rho$. In an exactly analogous manner we obtain also

$$\int_0^z \langle f(z)f(x)\rangle e^{i(\Delta\beta_{\nu\mu}z - \Delta\beta_{\nu\rho}x)}\, dx$$

$$= \sigma^2 e^{i(\Delta\beta_{\nu\mu} - \Delta\beta_{\nu\rho})z} \int_0^z e^{-(u/D)^2} e^{i\Delta\beta_{\nu\rho}u}\, du$$

$$= \sigma^2[\tfrac{1}{2}\sqrt{\pi}\, D e^{-[(D/2)\Delta\beta_{\nu\rho}]^2} + iF(D, \Delta\beta_{\nu\rho})]e^{i(\beta_\rho - \beta_\mu)z}. \quad (21)$$

By the above argument, that only nonoscillatory terms contribute to the differential equation (16), we keep only the term with $\beta_\rho = \beta_\mu$. Equation (16) now assumes the form

$$\frac{dP_\nu(z)}{dz} = \sigma^2 \sum_{\mu \neq \nu} \Big\{ [K_{\nu\mu}K^*_{\nu\mu}A_\mu(0)A^*_\mu(0) + K_{\nu\mu}K_{\mu\nu}A_\nu(0)A^*_\nu(0)]$$

$$\cdot \left[\frac{\sqrt{\pi}}{2} D e^{-[(D/2)(\beta_\nu - \beta_\mu)]^2} + iF(D, \Delta\beta_{\nu\mu}) \right] + \text{c.c.} \Big\}. \quad (22)$$

Because of our assumption that the coupling is sufficiently weak so that the wave amplitudes do not change very much over the distance z we replace $A_\mu(0)$ with $A_\mu(z)$ and obtain from (22) with the help of (11) and (13)

$$\frac{dP_\nu(z)}{dz} = \sqrt{\pi}\, \sigma^2 D \sum_{\mu=1}^{N} |K_{\nu\mu}|^2 e^{-[(D/2)(\beta_\nu - \beta_\mu)]^2} (P_\mu(z) - P_\nu(z)). \quad (23)$$

The complex conjugate terms cause the imaginary part of (22) to disappear.

Our derivation of equation (23) provides us with the derivative of the power of the ν-th mode essentially at $z = 0$. However, we could have followed the same procedure by assuming that the wave amplitudes or the power carried by each mode was given at some point z' and could have calculated the power derivative at some adjacent point

$z' + \Delta z$. With the assumption of weak coupling we would then have obtained the derivative of the power of the νth mode at an arbitrary point z' along the waveguide in terms of the power in all the other modes at (or near) that same point. In a strict sense, the procedure just described contains the flaw that the wave amplitudes $A_\nu(z')$ are statistical quantities. At $z = 0$ we used the fact that the wave amplitudes could be arbitrarily but definitely prescribed to take $A_\nu(0)$ out of the ensemble average. This cannot be done if we replace $A_\nu(0)$ with $A_\nu(z')$. However, we can use the following device to escape from this dilemma. Instead of considering the full ensemble of waveguides we select subensembles in such a way that within each subensemble the wave amplitudes $A_\nu(z')$ have the same complex value (within a certain prescribed narrow range). Our derivation of (23) then holds for each member of the subensemble. By regrouping the full ensemble into subensembles in such a way that the amplitudes $A_\nu(z')$ within each subensemble are all very nearly identical we find that equation (23) holds for each of the subensembles. We now average (23) over the subensembles and obtain an equation, equal in form to (23), that applies to the average power of the full ensemble. (See Appendix.)

For a given value of the rms deviation σ, (23) is obviously more accurate for smaller values of the correlation length D. For $D \to 0$ the length of guide needed for an approximate solution of the wave equations shrinks to zero and the only approximation left in our derivation consists in neglecting the oscillatory terms in (16). For finite values of D we must impose a restriction on the allowed values of σ. Let K^2 and P indicate the maximum values of $|K_{\nu\mu}|^2$ and $|P_\mu - P_\nu|$ while $\Delta\beta$ indicates the smallest value of $\beta_\nu - \beta_\mu$. Equation (23) yields the inequality

$$\frac{dP_\nu}{dz} \leqq \sqrt{\pi}\,\sigma^2 DNK^2 P e^{-[(D/2)\Delta\beta]^2}. \tag{24}$$

N is the number of guided modes in the waveguide. According to our approximate derivation we had to require that P_ν change only slightly over a distance in the order of the correlation length D. We integrate (24) over a distance κD with κ being a number close to but larger than unity and obtain

$$\frac{P_\nu(z + \kappa D) - P_\nu(z)}{P} \leqq \kappa\sqrt{\pi}\,\sigma^2 D^2 NK^2 e^{-[(D/2)\Delta\beta]^2}. \tag{25}$$

Since the right-hand side of (25) must be much smaller than unity in order for our approximate derivation of (23) to be valid we obtain the following inequality for the square of the rms deviation

$$\sigma^2 \ll \frac{e^{[(D/2)\Delta\beta]^2}}{\sqrt{\pi}\,\kappa D^2 N K^2}. \tag{26}$$

We have found the interesting result that the approximate coupled power equations hold for large values of σ not only in the limit of very small D but also in the limit of very large D. The minimum value of the right-hand side of (26) as a function of D is obtained for

$$D = \frac{2}{\Delta\beta}, \tag{27}$$

which is the least favorable correlation length in terms of the validity of the coupled power equations. The inequality (26) with D given by (27) becomes

$$\sigma^2 \ll \frac{e(\Delta\beta)^2}{4\sqrt{\pi}\,\kappa N K^2}. \tag{28}$$

If σ^2 remains below the value given by the inequality (28) the coupled power equations hold for all values of D.

We have assumed so far that the waveguide modes suffer no loss. This assumption is an idealization that can easily be extended to the more general case. The waveguide modes do not only suffer heat losses but also lose power by radiation. In fact the same mechanism that causes coupling between the guided modes also causes coupling to the radiation field so that losses are inevitable if the modes are coupled. If mode ν suffers the power loss α_ν we obtain the coupled power equations in the presence of loss in the obvious form†

$$\frac{dP_\nu}{dz} = -\alpha_\nu P_\nu + \sqrt{\pi}\,\sigma^2 D \sum_{\mu=1}^{N} |K_{\nu\mu}|^2 e^{-[(D/2)(\beta_\nu-\beta_\mu)]^2}(P_\mu - P_\nu). \tag{29}$$

Equation (29) has a simple intuitive interpretation. The decrease of power per unit length in mode ν is caused by the loss of power $\alpha_\nu P_\nu$ per unit length to heat and radiation, by an outflow of power to all the other modes indicated by the index μ, and finally there is an influx of power from all the other modes to mode ν that tends to offset the power loss.

IV. CONCLUSIONS

For randomly coupled waves the coupled wave equations can be transformed into coupled power equations. In this paper we derived

† The assumption of a Gaussian correlation function (12) is not essential for our derivation. In general $\sqrt{\pi}\,\sigma^2 D \exp\{-[(D/2)(\beta_\nu - \beta_\mu)]^2\}$ can be replaced by the Fourier transform of the correlation function $\langle f(z)f(z-u)\rangle$.

the coupled power equations for the special case of coupling coefficients that can be expressed as the product of a constant term times a function $f(z)$ that is independent of the mode labels. We further assumed that the correlation function of the coupling coefficients have Gaussian shape. The derivation of the coupled power equations from the coupled wave equations is based on perturbation theory. The coupled power equations are thus only approximately valid. An inequality was derived that limits the allowable values of the rms deviation σ of the coupling function $f(z)$. The coupled power equations are easier to use than the coupled wave equations since the coefficient matrix of the coupled power equations is constant, real, and symmetric so that the theory of symmetric matrices can be used for their solution.

The accuracy of our approximate derivation of the coupled power equations is not known.

APPENDIX

It is the purpose of the argument involving the subensembles to prove that we can use in (16)

$$\langle A_\rho^*(z')A_\mu(z')f(z' + \Delta z)f(z' + z + \Delta z)\rangle$$
$$= \langle A_\rho^*(z')A_\mu(z')\rangle\langle f(z' + \Delta z)f(z' + z + \Delta z)\rangle. \quad (30)$$

We abbreviate the product of the wave amplitudes by x and the product of f with itself by y and write (30) in the simplified form

$$\langle xy\rangle = \langle x\rangle\langle y\rangle. \quad (31)$$

To show that (31) holds we introduce the probability W_i of finding any member of the full ensemble, the probability P_j of finding a particular subensemble and finally the conditional probability $p_{i,j}$ of finding the member i of the full ensemble in the subensemble j. These three probabilities are related by the equation

$$W_i = p_{i,j}P_j . \quad (32)$$

We can now write the ensemble average in the form

$$\langle xy\rangle = \sum_i W_i x_i y_i = \sum_i p_{i,j}P_i x_i y_i . \quad (33)$$

The sum over the full ensemble can now be rearranged to be extended first over a particular subensemble (this sum is indicated by a prime on the summation sign) followed by a sum over all the subensembles

$$\langle xy \rangle = \sum_j P_j \sum_i{}' p_{i,j} x_i y_i \ . \tag{34}$$

The subensembles were selected on the basis that x_i was constant (or nearly so) in any given one of them. We can thus take x_i out of the sum over the members of each subensemble and obtain

$$\langle xy \rangle = \sum_j x_j P_j \langle y \rangle_j \ . \tag{35}$$

The symbol $\langle \ \rangle_j$ indicates an ensemble average over the members of the jth subensemble. The subensembles were selected such that members with equal amplitude values are grouped together in each subensemble. This grouping does not affect the function $f(z)$. The average of y over the subensemble should thus be identical to an average of y over the full ensemble. We assume

$$\langle y \rangle_j = \langle y \rangle, \tag{36}$$

and obtain from (35) the desired result

$$\langle xy \rangle = \langle x \rangle \langle y \rangle. \tag{37}$$

REFERENCES

1. Miller, S. E., "Coupled Wave Theory and Waveguide Applications," B.S.T.J., *33*, No. 3 (May 1954), pp. 661–719.
2. Johnson, C. C., *Field and Wave Electrodynamics*, New York: McGraw Hill, 1965.
3. Marcuse, D., "Mode Conversion Caused by Surface Imperfections of a Dielectric Slab Waveguide," B.S.T.J., *48*, No. 10 (December 1969), pp. 3187–3215.
4. Personick, S. D., "Time Dispersion in Dielectric Waveguides," B.S.T.J., *50*, No. 3 (March 1971), pp. 843–859.
5. Rowe, H. E., and Young, D. T., "Transmission Distortion in Multimode Random Waveguides," to be published in IEEE Trans. on Microwave Theory and Techniques.

Copyright © 1972 American Telephone and Telegraph Company
THE BELL SYSTEM TECHNICAL JOURNAL
Vol. 51, No. 1, January, 1972
Printed in U.S.A.

Buffering of Data Generated by the Coding of Moving Images

By J. O. LIMB

(Manuscript received August 20, 1971)

Data are generated at a fairly uneven rate when video telephone signals are coded by transmitting only the parts of the picture that change from frame to frame. Complete smoothing of these data is impracticable because of the size of the required buffer. Obviously, even a small buffer provides some advantage however. The object of this paper is to explore the relation between buffer requirements and channel rate under varying experimental conditions.

The study was made by recording three minutes of data (covering a range of action) on a digital computer and simulating buffer behavior for various channel rates and operating conditions.

With little or no buffering, a large rate is necessary. As the size of the buffer is increased, the required channel rate typically decreases quite rapidly until the buffer is large enough to smooth the data over an entire field. Beyond this point there is relatively little improvement until the buffer is large enough to smooth the data generated by a moving user from one movement to the next.

At times data are generated at a faster rate than can be handled by the buffer-channel combination. Reduction of the rate of data generation during these periods can be controlled either by using the amount of activity in the picture as a control or by using the state of the buffer as a control. Both methods have distinctly different effects on the buffer-size versus channel-rate curve. The two modes of control can be effectively combined in developing a successful control strategy.

The buffer size required to achieve within-field smoothing can be reduced dramatically if the data within the field are not taken in the order in which these data are generated but instead are interleaved in a systematic manner; this is because of the nonuniform rate of data generation within a field.

I. INTRODUCTION

Although most coding schemes for pictures have considered only a single frame at a time, it has long been realized that if only the changes

between frames were transmitted the average bit rate could be reduced significantly.[1,2] For *Picturephone*® service this is particularly true because most of the time the person using a *Picturephone* set sits quite still or only moves his mouth. However, extreme movement can occur when a camera is panned, when a user leans forward to adjust the controls, or when he stands up and moves out of the field of the camera. In such instances the amount of movement can exceed even that which would be expected in movies or broadcast television. But even if such extremes were unimportant, it would still be necessary to buffer the data generated during normal human movement in order to take advantage of the large reduction in average bit rate which occurs when one transmits only those parts of the picture which change.

Movements exceeding one second in duration are probably not unusual during videotelephone use. To smooth the peaks in data generated during such movement would require a large buffer, capable of storing a significant fraction of the data generated during the movement. Even if buffers were cost-free items, it would probably not be feasible to smooth, completely, the flood of data generated during movement because of the delay introduced into the signal path by the buffer. (The maximum round-trip delay that can be tolerated in a conversation is between one-half second and one second.[3])

J. C. Candy, et al., describe experiments with a frame-to-frame buffered coder operating with feedback control to reduce the accuracy (both spatial and amplitude) with which the picture elements are reproduced.[4] They use a 67,000-bit buffer and assume a 2-megabit/second channel. The algorithm for selecting those points to be transmitted differs from the one used in this study and will affect the results somewhat.

The object of this study is to explore the relation between channel-rate and buffer requirements and to determine how much smoothing the buffer can achieve. The effects of two different buffer control techniques for reducing the spatial resolution in moving areas are compared and the saving in buffer capacity, using a technique of interleaving data (which in effect uses the frame memory of a coder to obtain some smoothing), is investigated.

II. DESIGN OF EXPERIMENT

There is currently no adequate statistical model to describe the movements of videotelephone users. If there were, transforming this to a data rate and then obtaining overflow statistics for the buffer

would still be a difficult task. Therefore we studied buffering by simulation.

A repeatable source of data is a necessity if required buffer sizes are to be computed and compared for many channel rates and under different conditions. This precludes the use of a live subject for each experiment, since variations between runs could mask the effect being studied. We would like to have recorded several minutes of a typical videotelephone signal in binary form but this would have required much more storage than was available. Instead the signal was recorded in a reduced data form which could still yield the necessary information for the study. This is described more fully below.

The picture was divided into moving and stationary areas using a moving area detector.[5] A typical segmentation is shown in Fig. 1. For each horizontal line in the picture two measurements were made to represent quantitatively the moving (or changing) area. First, the elements falling in the moving area were counted; second, the number of moving area segments was counted. These two figures were each represented as 8-bit numbers, packed into one word, transmitted to the computer, and stored on a digital disk pack. Knowing these two numbers, we can calculate the number of bits generated per line by many different coding schemes. Buffer simuations can then be performed by incrementing a counter (each line) with the data generated during the line, and then decrementing the counter by the amount the channel transmits during the line.

In calculating the buffer requirements for a particular channel rate the only important variable is the ratio between the number of bits used to transmit information about the address of each segment and the number of bits used to transmit the amplitude of each pel (picture element) within the segment. For example, if 16 bits are used to denote each segment and 4 bits are used to denote the amplitude of each pel within a segment, the ratio is 4. If we have the buffer-size versus channel-rate curve for this allocation of bits and want to find the curve for a coding scheme which allocates 32 bits to each segment and 8 bits to each pel within the segment, we need only halve the scales of the axes. Most results have been obtained assuming 16 bits per segment and 4 bits per element. The 16 bits allocated to each segment can be distributed in many ways. For example, 8 bits can be used for a starting address, 4 bits for an error-correcting code, and 4 bits for a terminating code. Or, the 16 bits can be used just for a starting address and a stopping address. The 4-bit amplitude code can be used for an element difference code or a frame difference code. Of course, the actual allocation

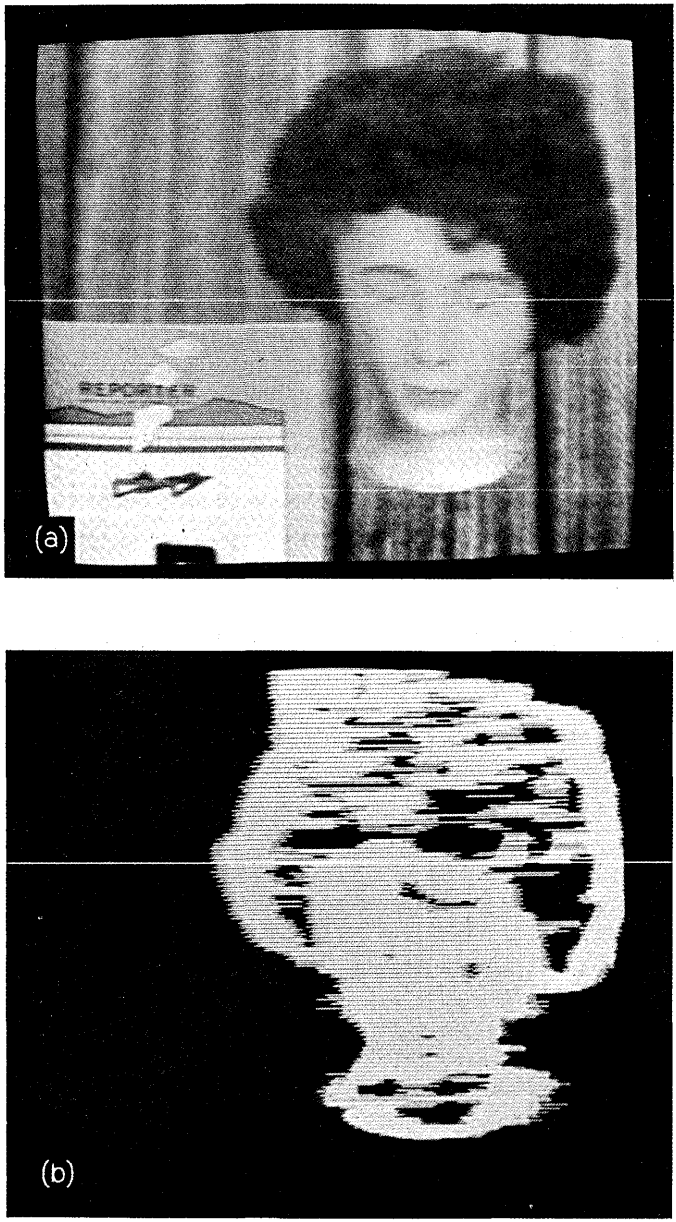

Fig. 1—(a) Picture showing moving head against stationary background; (b) Flags showing area deemed moving.

of bits is rather immaterial as far as a buffer study is concerned. Bookkeeping bits which occur every line, such as synchronization words and some forms of forced replenishment, were not explicitly incorporated in the simulations. These can be simply incorporated by modifying the channel rate to take these factors into account. Incrementing the buffer at a line rate rather than at an element rate makes little difference when we are interested in studying the smoothing that takes place over a frame and from frame-to-frame rather than over a line.

A rather basic assumption in comparing the buffer requirements of various schemes is that the operation of the movement detector does not change with the type of processing that is done (e.g., subsampling). This is almost true of the 2-dimensional movement detector that was used, and further sophistication in the design of movement detectors should make them even less sensitive to the type of coding employed. In any event the required buffer size is not strongly dependent on the segmentation criterion used because during periods of rapid movement when the buffer is most likely to be full it is quite easy to pick out the moving area.

2.1. *Recording of Data*

An RCA vidicon camera was used having a signal format roughly equal to that used in *Picturephone* service: 248 elements and 271 lines with 24 blanked elements in the line and 16 blanked lines in the frame; a 30-Hz frame rate with a 2-to-1 interlace. The signal was fed to a 7-bit quantizer via a 1-MHz low-pass filter. The frame difference signal was formed by subtracting the frame delayed signal from the undelayed signal. The difference signal was then fed to the movement detector which decided whether a point belonged to either the moving area or the stationary area. In order to make a decision the movement detector examined the frame-difference threshold signal of a block of 24 samples: 8 from the line being coded, 8 from the line above, and 8 from the line below. The frame-difference threshold signal is unity for those samples whose magnitude, as compared with the previous frame, changed by more than a threshold value; otherwise it is zero. In our experiment the threshold was set at 3/128ths of the peak signal value. The movement detector will change from the stationary to the moving mode when 8 or more of the 24 samples currently being evaluated have a frame-difference threshold signal of value 1. The movement detector will change back to the stationary mode when two or less of the 24 samples have a frame-difference threshold signal of value 1. Thus the decision is hysteretic, and, consequently, the movement

detector yields a reasonably contiguous moving area (see Fig. 1). If a stored signal is updated in only the segmented area then the resulting picture is of reasonable quality.

Just over three minutes of data were recorded. During the first minute (inactive data sample) the subject was asked to talk naturally but quietly, keeping his head and body relatively still. During the second minute (medium activity data sample) the activity was increased with the subject making occasional hand movements and more pronounced head movements. The subject was most active during the third minute (active data sample) making exaggerated head movements and hand movements but no large body movements such as standing or moving out of the field of view. Some characteristics of the data are given in Table I.

The statistics shown in Table I are (*i*) the mean value, (*ii*) the value which was exceeded only 1 percent of the time, and (*iii*) the maximum value. The mean number of segments in a line increased from less than 1 to 1.5 as the activity increased from inactive to active. The number of pels in the segmented area increased proportionately more — from 18 to 75. The small increase in the average number of segments is probably caused by short segments combining to form a single longer segment as the amount of movement increases. The maximum value and the 99-percent value do not show such a marked increase with movement as does the mean. Notice, however, that the maximum value of the number of pels for the active data cannot increase further, since it is equal to the number of pels in a line.

For the coding techniques in which we were interested, the required buffer size was more dependent on that portion of the data used for describing amplitudes of pels than that portion used for positioning

TABLE I—MEAN, 99% VALUE, AND MAXIMUM OF THE NUMBER OF MOVING AREA SEGMENTS AND PELS IN A LINE.

	Inactive		Medium		Active	
	Seg.	Pel	Seg.	Pel	Seg.	Pel
Mean rate per line	0.7	17.6	1.3	44	1.5	75
99% value per line	3.0	100	4.0	122	5.0	183
Maximum rate per line	7.0	119			9.0	224

segments. This does not necessarily mean, however, that the segmenting criterion should be changed so as to decrease the number of pels at the expense of increasing the number of segments. Such a policy could lead to an increase in the overall data rate since the reduction in data rate due to the decrease in the number of pels to be transmitted could be more than offset by the increase in data rate due to the increased number of segments. The segmenting criterion which gives the minimum buffer requirement will depend on other factors such as whether or not subsampling[4] is used, what buffer control,[5] if any, is employed, and so on. Thus, at this early stage we have simply demanded that the segmenting give a reasonably contiguous coverage of the moving area, leaving the fine tuning until the basic structure of the coder is known.

III. RESULTS

Figure 2 shows a number of results relating required buffer size to channel rate. The channel rate is specified in bits-per-line. Thus a channel rate of 1 bit per pel corresponds to a channel rate of 224 bits

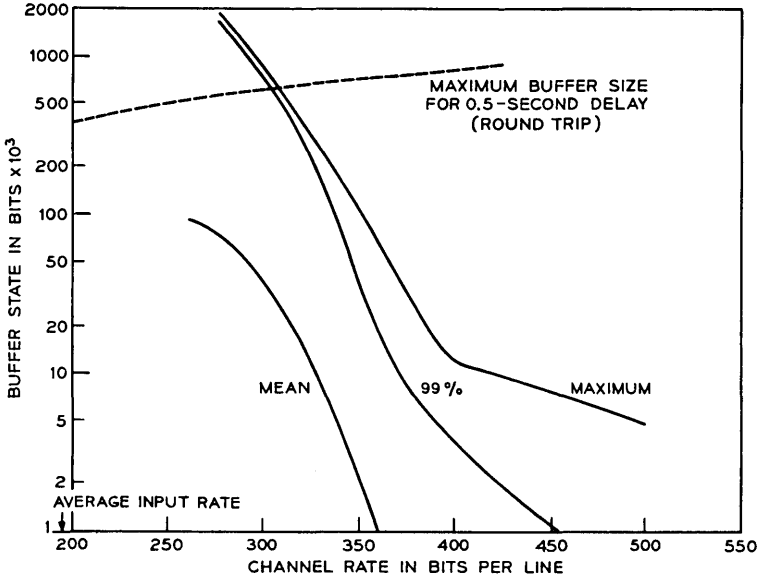

Fig. 2—Channel rate vs buffer state for medium activity data. Curves are for maximum buffer state, 99-percent point (1 percent overflow), and mean buffer state.

per line, excluding line address and line synchronizing bits. The simulations assume no data are generated or transmitted during the vertical blanking interval. This period can be used for the transmission of periodic data such as forced picture updating.[4]

The buffer size is specified in kilobits and plotted on a logarithmic scale to accommodate a large range of values. The term "state of the buffer" will be used to mean the fullness of the buffer at a particular instant. "Capacity of the buffer" will be used to denote the number of bits the buffer can store before overflow occurs. In this study the buffer was always large enough so that, for the channel rates used, the buffer never overflowed and hence may be regarded as infinite. Three statistics of buffer state were measured: (*i*) the mean, (*ii*) the buffer state which was exceeded only one percent of the time, and (*iii*) the maximum buffer state.

It is difficult to decide what measure of buffer state is appropriate in determining the capacity required for a buffer in a real system. The 99-percent point would probably result in too frequent buffer overflow although, of course, it depends critically on what actually happens to the received picture when the buffer does overflow. Note that using the 99-percent curve would result in less frequent overflow of a finite buffer than of an infinite buffer* since a finite buffer will cease to overflow as soon as the data generation rate falls below the channel rate. However, it may be a while before meaningful data can again be transmitted after overflow has occurred.

Conversely, the maximum buffer state is severe as a measure of practical buffer requirement because overflow would never occur. However, if the buffer in a working system were to overflow just once every minute (this curve was obtained for a 1-minute sample), then overflow would probably be too frequent. In the results that follow, the maximum buffer state is the measure that is most generally used as an indication of buffer capacity requirement.

The one-way signal delay through the send and receive buffer is assumed to be

$$\Delta = \text{buffer capacity/channel rate.} \tag{1}$$

Thus, if the round-trip delay, 2Δ, is to be kept less than 0.5 second then the send buffer and the receive buffer must each have a capacity

* Of course an infinite buffer, strictly speaking, will never overflow; however, we regard overflow as occurring whenever the simulated buffer size is exceeded. An infinite buffer continues to operate normally after the simulated buffer size is exceeded.

less than that given by the dotted limiting curve [derived from equation (1)] of Fig. 2.

The curves of Fig. 2 have two distinguishing features:

(*i*) A sharp change in slope at high channel rates.
(*ii*) A gradual turnover of the curves at lower channel rates.

This is most apparent in the maximum buffer-state curve. The change in slope, at the far right of each curve, is the point at which the buffer ceases to smooth over a whole field and we hypothesize that the upper change in slope is the point at which the buffer ceases to smooth significantly between one movement of the user and the next. The curves obtained from data interleaving (see later) provide evidence relating the "rightmost" change in slope (elbow) to the transition from intrafield to field-to-field smoothing.

Regarding the upper change in slope, we can calculate approximately the number of frames stored in the buffer during periods of peak data generation in the following manner: about 325,000 bits are generated per frame when the subject is active. If only 70,600 bits are transmitted per frame (275 bits per line) then the buffer has to hold about 255,000 bits for the frame, and if the buffer were full (1.4 million bits) then about 5-1/2 frames of active data would be stored in the buffer. The difference in data generation rate between two frames, five frames apart, is probably sufficient to explain the change in slope of the curves for large buffers.

From the elbow of the maximum buffer state curve to where the curve turns over at the top the slope is very steep. In reducing the channel rate from 400 bits per line to 300 bits per line the buffer size increases from 15,000 bits to 830,000 bits, an increase of 55 times. Thus, the elbow seems a suitable compromise for an operating point, enabling one to obtain the advantages of within-field smoothing for a reasonable buffer size. Of course, the actual operating point that is chosen will be a measure of economics, balancing the cost of the channel against the cost of the buffer.*

3.1. *Relation Between Activity and Buffer Requirements*

The maximum buffer state is plotted as a function of channel rate in Fig. 3 for the first, second, and third minutes of recorded data. It is assumed that each pel in the segmented area is specified with

* Or if the channel costs are relatively high the operating point will be determined by the maximum tolerable signal delay.

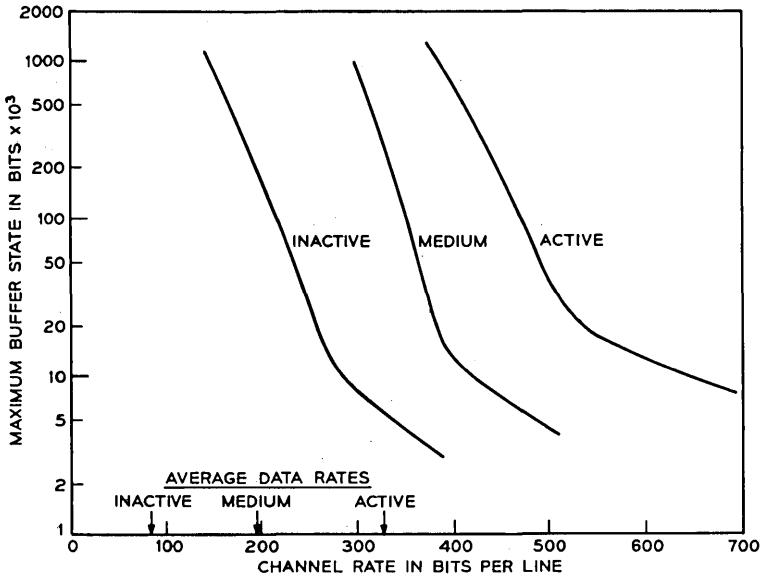

Fig. 3—Channel rate vs buffer state for three different amounts of activity in the data sample. The lower elbow moves upward and to the right as the amount of activity increases.

4 bits and each segment is specified with 16 bits. The average rates are again shown by arrows on the abscissa.

The active sequence has more than four times the average data rate of the inactive sequence, while the average data rate of the sequence having medium activity falls roughly midway between the other two. These three curves have much the same shape with the same pronounced elbow. As the amount of activity decreases, the slope of the segment to the right of the elbow becomes steeper and the position of the elbow shifts downward. This increase in the slope of the curve below the elbow is probably attributable to the fact that for inactive data human movements are shorter in duration and the segmented areas are less clumped than in active data, making smoothing within a field less profitable. Thus larger benefits are obtained with smaller buffers (below 10^3 bits) leading to smaller benefits as the channel rate is reduced to approach the elbow point in the curve.

A coder should be capable of handling the data generated during the active data sample with only occasional overflow since this type of movement could easily be encountered in practice. Thus, if we have a buffer of 50,000 bits, a channel rate of 490 bits per line would be

required, according to the curve, for active data. To determine what the buffer is buying us in this instance, compare this with the data rate required by a simple in-frame coder which transmits 4 bits for each picture point. The picture quality of the two schemes would certainly be comparable but the required channel rate for the simple in-frame scheme would be 890 bits per line. Thus, simple frame-to-frame coding with a 50,000-bit buffer in this instance has enabled us to almost halve the required channel-rate.

3.2. *Change of Buffer Requirements as Segment-to-Data Ratio Varies*

The curve labeled (16, 4) in Fig. 4 indicates the maximum buffer-state versus the channel-rate for the medium activity data sample (also shown in Figs. 2 and 3). If all conditions are left the same except for the number of bits used to denote the amplitude of each data point, which is reduced from 4 bits to 2 bits, then the curve labeled (16, 2) results. To compare these curves assume that we have a 50K-bit buffer and determine what channel-rate will just fill this buffer. For the

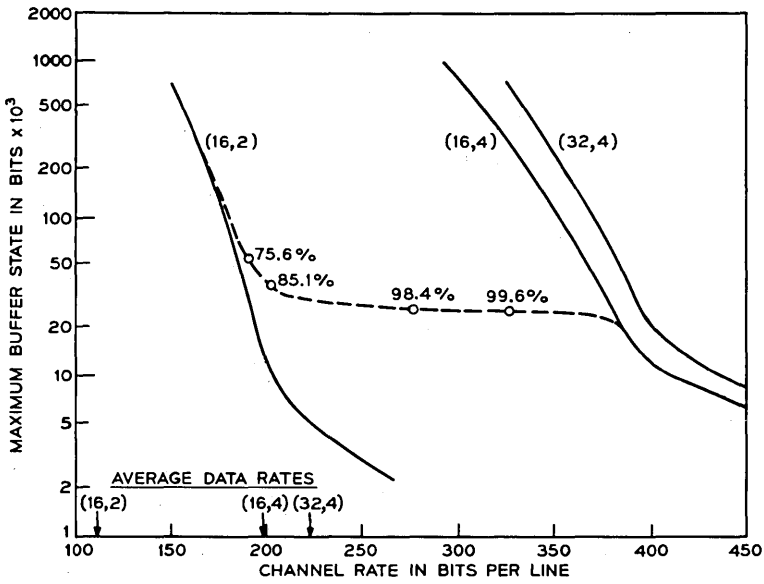

Fig. 4—Channel rate vs buffer state for the medium activity data sample as (*i*) the number of bits/pel required to code the picture is halved (16,2) and (*ii*) the number of bits to code a segment is doubled (32,4) relative to the normal coding (16,4). Also shown is the effect of subsampling when the buffer state exceeds 25,000 bits. Percentage points show time spent in full-resolution mode.

(16, 4) curve the rate is 367 bits per line and for the (16, 2) curve the rate is 185 bits per line, a reduction by almost half (0.504). This is not too surprising in that the average data generation rate is reduced by nearly half (0.556), and reflects the fact that the part of the generated data which specifies the segments is but a small fraction of the total data generated [12 percent for the (16, 4) case].

If, on the other hand, we double the bits used to specify each segment from 16 to 32 the curve labeled (32, 4) results, and as we would expect gives a negligible increase in channel rate for a given buffer capacity (4.6 percent). Consequently, it may prove well worthwhile to transmit additional error protective bits with each segment in an effort to limit the degrading effects of channel errors.

3.3 *Buffer Feedback*

One method for reducing the required buffer size is to use some form of feedback so that when the buffer exceeds a certain capacity the accuracy with which the data is coded is reduced. This may be either a reduction in the accuracy with which the amplitude of the data is specified (reduction in contrast resolution) or a reduction in the number of picture points transmitted (reduction in spatial resolution).[5] The form of the reduction in resolution is not particularly important for this simulation, but we have found that reducing the spatial resolution by a factor of two in moving areas has very little effect on the picture quality.[4,5,6]

The dotted curve in Fig. 4 indicates what happens when feedback from the buffer is used to halve the number of samples transmitted in the segmented area (or alternatively, to halve the number of bits used to specify the amplitude of each element within the moving area). In this case a barrier was put at 25,000 bits; whenever the buffer state exceeded this amount the bit rate assigned to elements within the segmented area was halved. The figure shows rather dramatically how the curve first follows the (16, 4) curve until the buffer state reaches 25,000 bits and then moves over to follow the (16, 2) curve. Thus, the buffer control has effectively limited the maximum buffer-state to approximately 25,000 bits for a large range of channel rates. As the channel rate is reduced, the amount of time spent in the lower data-rate mode increases. Percentage figures beside points on the curve indicate the percentage of time the coder was in the high data-rate mode for that particular channel rate.

The percentage of time spent in the low-resolution mode is quite low until the curve approaches the (16, 2) curve. Thus, assuming a buffer of say 40,000 bits, subsampling enables the channel rate to be

reduced from about 375 bits per line to about 225 bits per line. At this level the low-resolution mode is still only used about 10 percent of the time.

The subsampling curve of Fig. 4, however, only gives the story for one level of activity. In Fig. 5 the curves show the effect of subsampling for three amounts of activity. Before one can decide on an operating point for a coding system, that is, a channel rate and a buffer size, one must decide on the maximum level of activity which will be tolerated before additional degradation of the signal takes place either in the form of buffer overload, or, for instance, further reduction in resolution. If a curve is available for this level of activity then an operating point can be selected, for instance, just below the sharp upward turn of the curve.

A corollary of the above is that given a buffer of a particular size the position of the barrier beyond which subsampling is used should be placed as close to the top of the buffer as is possible without overflow occurring (over the allowed range of data activity), or before another stage of resolution-reduction is invoked. In this way the amount of time spent in the high-resolution mode will be maximized. If two stages of subsampling are used then the barriers associated with each

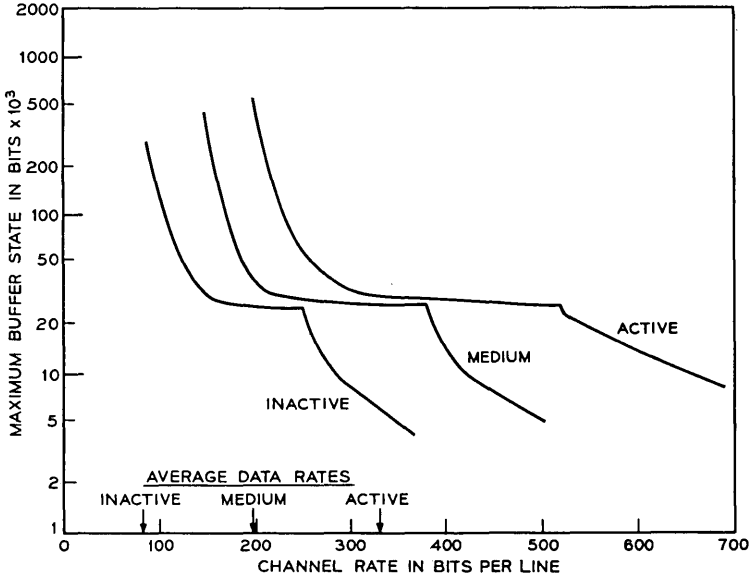

Fig. 5—The channel-rate vs buffer-state curves for buffer-controlled subsampling.

transition should be placed close together and near the top of the buffer. However, if the barriers are too close together then activity rates which would normally be handled by the first stage of subsampling will be handled by the second stage of subsampling. If on the other hand the barriers are too far apart then the first stage of subsampling will be entered prematurely.

For practical reasons one may want to change control only at the beginning of each field. Thus the whole field would be either subsampled or not depending on the state of the buffer prior to the start of the field. This condition was simulated and the results, which are shown in the dashed curve of Figure 6, indicate the importance of being able to change from one mode to another within a field. Without this provision an increase in buffer size of up to 70 percent is required, depending on the operating point.

3.4 *Activity-Controlled Subsampling*

Reduction of spatial resolution by subsampling in the moving area affects picture quality very little because the image is already blurred

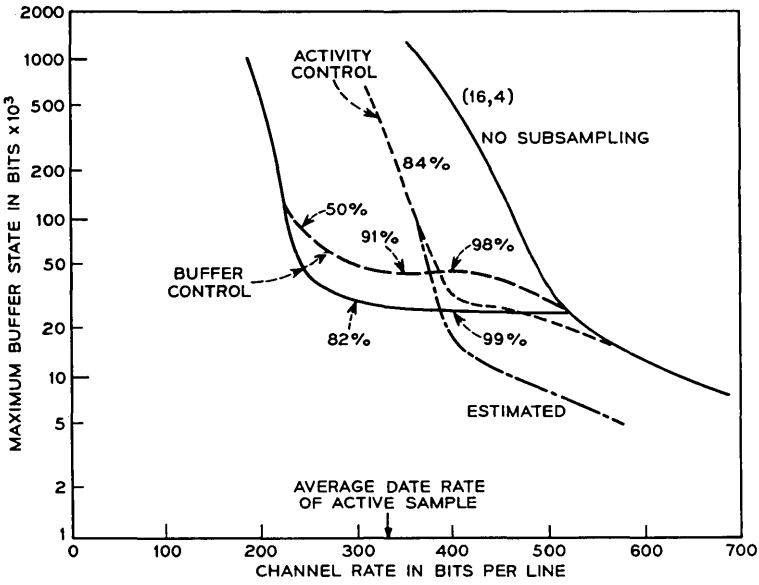

Fig. 6—The effect of activity control on subsampling (dotted curve) is compared with buffer control (dashed curve). With activity control, subsampling is invoked when more than 50,000 bits are required to code the previous field. The active data sample was used.

by the camera.* Also, the human observer is quite tolerant of blurring in a moving image.

The state of the buffer provides some measure of the amount of movement in a picture, but this measure is delayed in time because the buffer acts like an integrator and responds after the fact. A better estimate of the amount of activity is the amount of data generated in a field.

In order to simulate activity-controlled subsampling, the amount of data generated during a field was compared with a threshold. If it exceeded the threshold, subsampling was introduced in the next field. In Fig. 6 the buffer-state versus channel-rate curve for this condition with a threshold of 50,000 bits per field is shown as a dotted curve. Of course, for activity-controlled subsampling the amount of time spent in the high-resolution modes does not vary with channel rate or buffer state and in the example considered it was 84 percent.

One cannot speak of within-field activity control because a single activity figure is derived for the whole field. Subsampling active fields, in effect, alters the structure of the data being smoothed by the buffer, converting it into lower activity data but with a higher mean-to-peak ratio. Thus, the resulting channel-rate versus buffer-state curve should be similar in shape to the curve obtained without control but shifted to the left and down, as shown in Fig. 3 for decreasing amounts of activity.

The result, shown in Fig. 6, is inconsistent with the above in that the activity-controlled curve converges with the curve obtained without control as the channel rate increases. The reason for this is artifactual and stems from the way the control is derived. If one field is active enough to introduce subsampling in the next field, the subsampling will reduce the amount of activity so that the following field will not be subsampled. Thus, with active data, fields will alternate between subsampling and no subsampling. For operating points to the right of the elbow of the uncontrolled curve there will not be enough smoothing to carry the surplus generated in the field that is not subsampled into the next field, and one would expect the curves in the two cases to coincide.

One could overcome this problem by deriving an activity control that was based on the data rate prior to subsampling or (as was used by Candy, et al., in the buffer control case[4]) build hysteresis into the threshold so that the decision to stop subsampling would not be made

* The camera target integrates light falling on it over one frame period and in that time a fast moving object can move a distance of 4 or 5 pels.

until the data rate fell to about half the threshold used in the decision to switch to subsampling in the first place. The dot-dash curve is an estimate of what the channel-rate versus buffer-state curve would look like if this modified type of activity control was employed.

In comparison, we see that buffer-controlled subsampling introduces a horizontal platform between the fully sampled curve and another curve with half the number of amplitude bits assigned to the segmented pels. On the other hand, activity-controlled subsampling produces a horizontal shift of the fully sampled curve to the left.

The curves of Figs. 4 and 6 suggest the interesting possibility that perhaps buffer-controlled subsampling could be added to activity-controlled subsampling. This would give the advantage of having the subsampling phased with the data peaks when the amount of activity is moderate, but having the powerful limiting effect of buffer-controlled subsampling for active-data sources. From knowing the effect of both of the methods of subsampling one could estimate quite accurately the curve resulting from the combined strategy. The results of a simulation of the combined strategy is shown in Fig. 7 where all the conditions

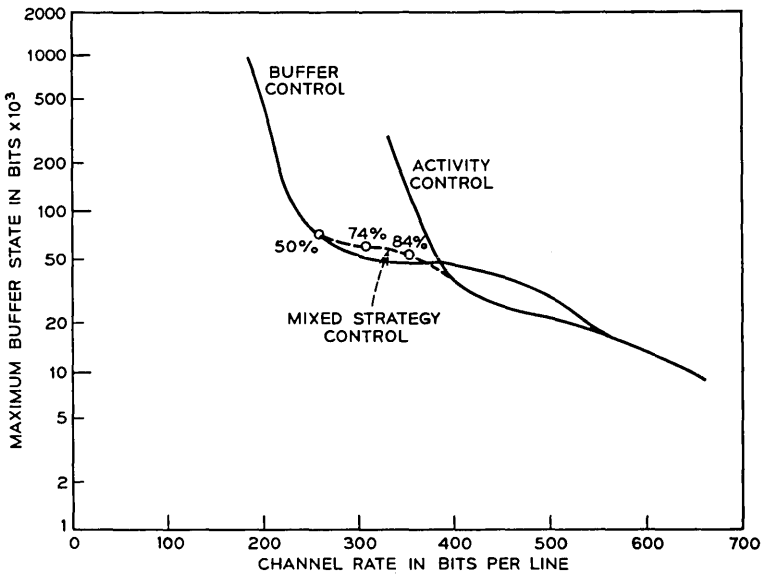

Fig. 7—A mixed strategy is employed. Activity control and buffer control are combined producing the dashed curve which makes a transition from the activity control curve to the buffer control curve as the channel rate decreases. The active data sample was used.

are the same as for the results of Figs. 4 and 6, and control is only exercised at the end of a field.

3.5. *Data Interleaving*

As mentioned previously, an efficient operating point for a coder-buffer combination is likely to be just below the elbow of the channel-rate versus buffer-state curve. At this point the buffer is smoothing within a field but providing very little smoothing from field-to field. As one would expect the average data generation rate for *Picturephone* schemes is not uniform within a frame but peaks toward the bottom.

The data generation rate as a function of vertical position within the field is shown in Fig. 8 for a single field of data. The data rate of this particular field is a local maximum, taken from the active data sample. The peak data rate is 850 bits/line occurring toward the bottom of the picture (probably associated with the model's shoulders) while the average rate is 517 bits/line giving a mean-to-peak ratio of 0.61. For less-active data samples the ratio is even more favorable, 0.47 and 0.35 for a local maximum taken from the medium-activity data sample and the inactive data sample respectively. Plots of the vertical distribution

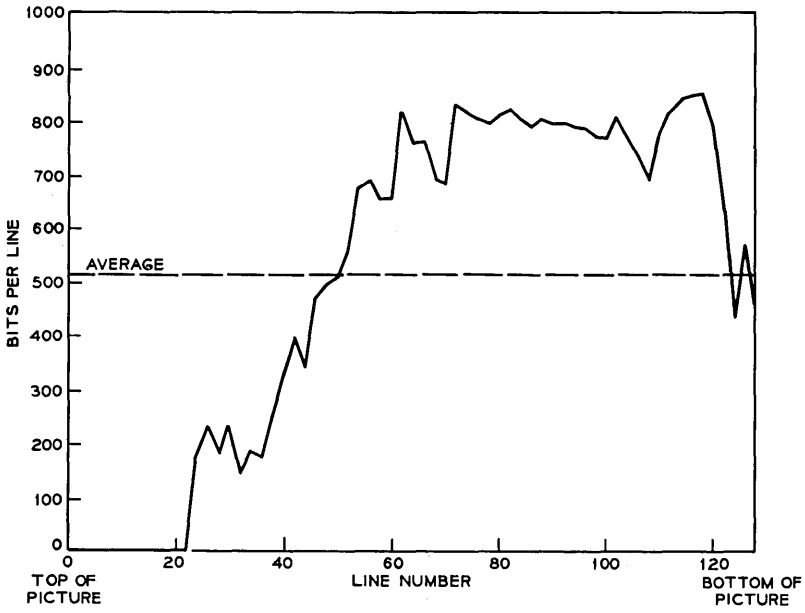

Figure 8—Vertical distribution of data-generation rate throughout field.

of data for adjacent fields, as one would expect, are very similar. Presmoothing of the data can be achieved if instead of reading out the data in the order in which they are generated the data are read so that a line coming from an area having a high average-data-generation rate will be succeeded by a line from an area having a low average-data-generation rate. This arrangement could only be achieved, in general, by having a memory capable of storing an appreciable portion of a frame of coded data at the transmitter to interleave the data and a similar arrangement at the receiver to put the data back in the correct order. In such a situation the advantage to be gained over spending the same amount of money on additional buffer capacity may be quite negligible.

In certain types of coders such as conditional PCM replenishment[7] and conditional in-frame encoding[8] the signal is stored in the transmitter frame memory in much the same form as the transmitted signal. In other coders such as the conditional element-line encoder[8] the signal stored in the frame memory can be converted to the same form as the transmitted data without a great deal of storage (a line memory in the case of the element-line encoder). Thus the frame memory can also be used to interleave the data by providing readout taps at points within a field. In such situations additional memory is required to label the information which is to be transmitted but this only amounts to an increase of about 5 percent in the size of the frame memory.

It is a simple matter to simulate data interleaving since the complete data is recorded on a digital disk in the form of two 8-bit numbers for each line and the data can be read from the disk in any order. The lines were taken in the order 1, 33, 65, 97; 2, 34, 66, 98; 3 $\cdots$ 127; 32, 64, 96, 128; 129, 161, 193, 225; 130 $\cdots$ 160, 192, 224, 256. Some small improvement may be obtained by using the order 1, 65, 33, 97; $\cdots$ over the one above.

The effect of 4:1 data interleaving is shown in Fig. 9, for the medium-active data sample. As would be expected, data interleaving has little effect with large buffers where smoothing takes place over many frames. However, at the elbow the curve for interleaving continues to fall until at a channel rate of 450 bits per line the maximum buffer states with and without data interleaving differ by more than a factor of 10. The difference in the 99-percent points (1080 bits as against 55 with data interleaving) is even larger.

IV. DISCUSSION AND CONCLUSIONS

With little or no buffering a frame-to-frame coder requires a large channel rate. As the size of the buffer is increased, the required channel

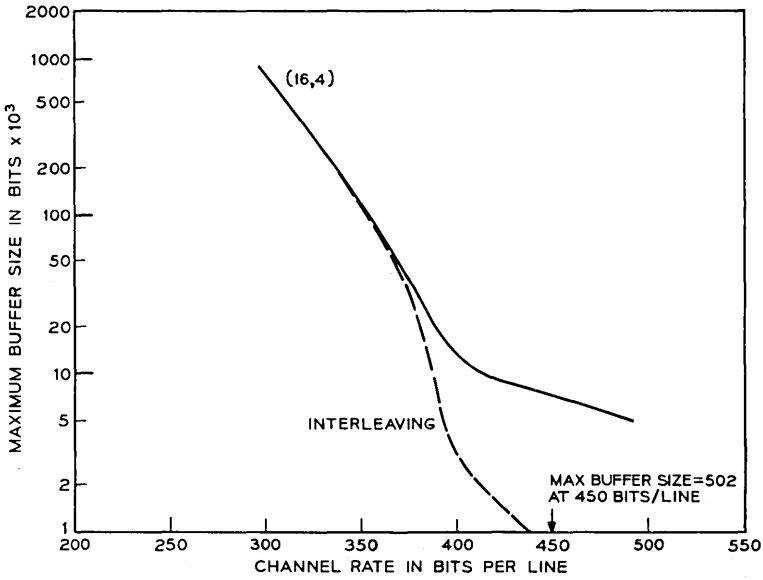

Fig. 9—Compared with normal buffering (solid-line curve) 4:1 data interleaving reduces the required buffer size by a factor of ten at higher channel rates.

rate decreases quite rapidly until the buffer is large enough to smooth the data over an entire field. Beyond this point there is very little improvement until the buffer is large enough to smooth the data from one period of active movement to the adjacent inactive period. Buffers large enough to do this (greater than 10^6 bits), however, introduce transmission delays which are intolerable in normal conversations.

The curve of maximum buffer-state versus channel-rate summarizes the buffer requirement of a coder for a particular level of activity and enables one to explore possible tradeoffs in the selection of a suitable operating point for a coder. For active movement and a 50,000-bit buffer, the use of simple frame-to-frame coding results in nearly a two-to-one saving over the channel rate required by an in-frame coder giving roughly equal picture quality. Further reduction is obtained if the rate of data generation during periods of peak activity is controlled by using either the amount of activity in the picture or the state of the buffer as the controlling variable.

It is assumed that the coder can switch between one of two modes—a normal mode and a reduced resolution mode, which has about half the data generation rate. A simple buffer threshold control effectively

clamps the buffer state to the value of the threshold until the coder is operating predominantly in the reduced resolution mode. If the control signal is only permitted to change the coder mode at the end of a field then the clamping action is less effective, since the buffer, in the worst case, may have to accommodate a large amount of data generated in a busy field prior to switching. This results in an increase in required buffer size of up to 70 percent depending on the channel rate.

Activity control, on the other hand, does not change the basic shape of the buffer-state curve but instead makes the coder appear as though it has a lower overall data rate. Activity control is also an effective method of reducing the average data rate which is the most important parameter in TASI-like channel-sharing schemes.

Ideally one would like to use the speed of the moving object as the control signal rather than the data generation rate because the reduced data-rate mode would then be used only when the subjective effect on picture quality is very small.

Buffer control and activity control can be combined so that when either the buffer threshold or the activity threshold is exceeded the coder switches to the reduced data-rate mode. The activity control operates more rapidly than the buffer control, enabling the reduced data-rate mode to be restricted more to the periods of peak activity. For small buffer sizes, however, the addition of activity control would probably help picture quality very little. The combined operating mode may find application where a channel sharing and buffer sharing arrangement is applied to a small number of users. In such an arrangement both the average data rate and the peak data rate are important.

Most of the advantage in buffering is obtained by smoothing data over a field. This gain is possible only because the data are not generated at a uniform rate throughout the field but tend to be concentrated near the middle and bottom of the picture. If data from different places in the field are interleaved the resulting bit stream can be smoothed with a much smaller buffer. A four-fold interleave was simulated and the size of the buffer at the elbow point was reduced by a factor of four. For slightly larger channel rates the reduction in buffer size was greater than a factor of 10. The frame memory can only be used to obtain the temporary storage required for data interleaving when the data in the frame memory is in the same form as the transmitted data or when the data can be converted economically to be of the same form. A small, but interesting class of coders falls in this category.

V. ACKNOWLEDGMENT

I especially thank B. G. Haskell and R. F. W. Pease for their suggestions and advice. In addition B. G. Haskell was largely responsible for transferring the data to the computer, and W. G. Scholes was ever ready to help with the data acquisition.

REFERENCES

1. Jesty, L. C., "Television as a Communication Problem," Proc. IEEE *99*, pt. III A (May 1952), p. 761. See also Kell, R. D.: British Patent No. 341811, 1929.
2. Seyler, A. J., "The Coding of Visual Signals to Reduce Channel-Capacity Requirements," Proc. IEEE *109* (September 1962), pp. 676–684.
3. Brainard, R. C., Rowlinson, D. E., and Cutler, C. C., "*Picturephone*® Communication with Delay," private communication.
4. Candy, J. C., Franke, Mrs. M. A., Haskell, B. G., and Mounts, F. W., "Transmitting Television as Clusters of Frame-to-Frame Differences," B.S.T.J., *50*, No. 6 (July–August 1971), pp. 1889–1917.
5. Pease, R. F. W., and Limb, J. O., "Exchange of Spatial and Temporal Resolution in Television Coding," B.S.T.J., *50*, No. 1 (January 1971), pp. 191–200.
6. Limb, J. O., and Pease, R. F. W., "A Simple Interframe Coder for Video Telephony," B.S.T.J., *50*, No. 6 (July–August 1971), pp. 1877–1888.
7. Mounts, F. W., "A Video Encoding System Employing Conditional Picture Element Replenishment," B.S.T.J., *48*, No. 7 (September 1969), pp. 2545–2554.
8. Limb, J. O., and Pease, R. F. W.,"Frame-to-Frame Coding by Transmission of Conditional In-Frame Coded Signal", to be published.

Copyright © 1972 American Telephone and Telegraph Company
THE BELL SYSTEM TECHNICAL JOURNAL
Vol. 51, No. 1, January, 1972
Printed in U.S.A.

Buffer and Channel Sharing by Several Interframe *Picturephone*® Coders

By B. G. HASKELL

(Manuscript received August 5, 1971)

Simulations are described which test the feasibility of several conditional replenishment type Picturephone *coders sharing the same transmission channel. Channel sharing takes advantage of the fact that many different users are rarely in rapid motion at the same time. Thus, when the data from several sources is averaged together prior to transmission, it is much more uniform than that from a single source. Since the peaks in the averaged data are smaller than with a single source, less buffering is required, and the channel rate required for transmission is much closer to the average data rate generated. Results indicate that by combining twelve sources prior to transmission, a 2:1 reduction in the bit rate of the system described by Candy, et al.,*[1] *can be obtained. This means that twelve* Picturephone *sources could share a 12 megabits per second (one way) transmission facility.*

I. INTRODUCTION AND SUMMARY

In Ref. 1 a frame-to-frame coding system for *Picturephone* signals is described which operates at 2 Mb/s and uses a number of techniques to reduce the bit rate required for transmission. For the most part, only picture elements that change significantly are transmitted in each frame period.[2] These elements are addressed in clusters and transmitted as frame differences; and since information is generated at an irregular rate, the data is buffered prior to transmission. When the buffer starts to fill, indicating active motion, only every other changed picture element is transmitted,[3,4] the unsampled elements being replaced by the average of their neighbors. When the buffer fills completely, replenishment is stopped for one frame period allowing the buffer to empty before resuming transmission.

Two-to-one subsampling in the changing parts of the picture has been shown to be subjectively invisible during rapid motion.[1,4] Frame repeating on the other hand, is quite visible, but since it is rarely used

(only during periods of camera panning or violent motion) it is not too objectionable.

The rate at which data is generated by the system is very irregular due to random spacing of changed elements within the field and due to variations in movement on the part of the subject. It is practical to provide enough buffering to smooth the data over a field time. However, it is not practical to smooth the data between peaks in human movement because of the expense involved and because of the transmission delay which such a large buffer would introduce.[1,5] Thus, the channel capacity which must be provided to accommodate active movement is much larger than the long-term average data rate generated by the system, and unless some sort of stuffing information is generated,[1] such as forced replenishment, the transmission channel is idle much of the time.

An obvious method to utilize the channel more efficiently is to transmit the data from several interframe coders over a shared channel, allocating more capacity and buffer space to those sources which happen to require it at a given moment and less to those which are producing relatively little data. Since separate *Picturephone* conversations can be assumed to be independent, the combined data on a per source basis should be much less peaked than that from a single source, or in statistical terms, if the data from N_S independent, identically distributed sources is averaged, then the variance is reduced by a factor of N_S (the mean is unchanged). This will not only reduce the required channel capacity, but it will also reduce the required buffering.

A number of schemes have been proposed.[6-8] Most of them are variations of the system shown in Fig. 1. Unbuffered data from the various sources is first stored in individual prebuffers, then transferred to the principal buffer via the multiplexing switch, and finally transmitted over a single high-capacity data channel to the receiver where the inverse operation takes place. The switch may rotate either sequentially or nonsequentially and either at a constant rate or at a variable rate. In any event, some source labeling information must be sent so that at the receiver a given block of data is identified with the correct source.

If the individual sources are far removed from the high-capacity channel and its associated multiplexing switch, then it may be desirable to buffer the data as in Ref. 1 prior to transmission to the prebuffers of Fig. 1. In this case each prebuffer should be preceded by a device which removes the stuffing information from the incoming constant-rate data stream before it is fed to the prebuffer.

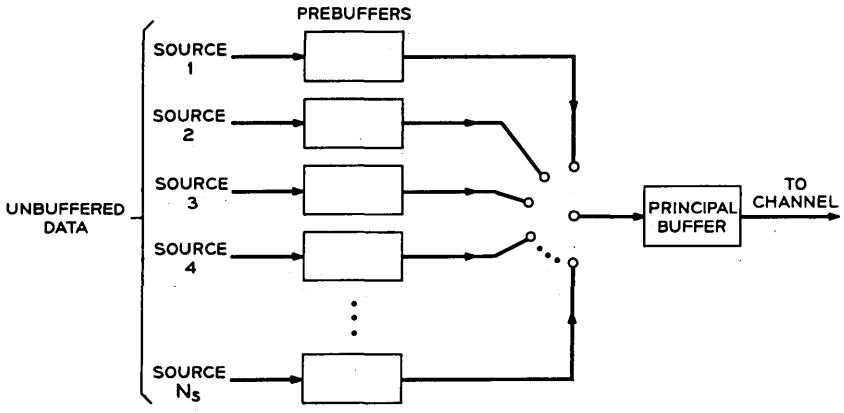

Fig. 1—Channel and buffer sharing system for sources which generate data at an irregular rate.

In order to simulate the system of Fig. 1, one hour of unbuffered data from a single source was stored on a digital disk. The data included all types of activity in the proportion in which they could be expected to occur in actual *Picturephone* conversations. The simultaneous occurrence of N_S independent conversations was then simulated by starting each conversation at a different point on the digital disk. This method of simulation avoids the necessity of constructing a reliable statistical model for the data; however, it does require a large amount of random access storage.

Controlling the coding mode of a single source according to the number of bits in a buffer as is done in Ref. 1 reduces the peak data rate considerably, but it does not result in the minimum long-term average data rate, a more important parameter where channel sharing is concerned. Furthermore, if the prebuffers were the only ones available, they would probably not be large enough to perform this task effectively. Thus, in the simulations the number of significant changes per field was used to control the transitions between full sampling in the changed area, sampling every other changed picture element (2:1 subsampling), and sampling every fourth changed picture element (4:1 subsampling).

Sections II and III describe the method of acquisition of the data and various statistical results obtained from it. Section IV describes simulations of single interframe coders using different techniques to control the coding mode according to the amount of activity in the scene. Required buffer size versus channel rate curves are obtained under the assumption that the buffer is at least large enough to smooth

the data over a field period. Simulation results for shared-buffer/shared-channel systems are described in Section V.

The simulations indicate that there is indeed considerable advantage in several interframe coders sharing a buffer and a channel. Using the techniques of Ref. 1, a channel rate of 2.0 Mb/s (one way) is required to transmit the data from a single *Picturephone* source. However, with a moderate amount of buffering (about the same as that of a single frame-to-frame coder[1]), combining five sources prior to transmission reduces the required one-way channel rate to 1.2 Mb/s on a per source basis, i.e., five sources over a 6-Mb/s transmission facility. With 12 sources per shared channel a transmission rate of 1.0 Mb/s per source can be achieved with relatively little buffering. Significantly more savings in channel rate is obtained only by sharing a very much larger number of sources. As the number of sources per shared channel increases, the bit rate per source approaches 0.6 Mb/s asymptotically.

II. ACQUISITION OF DATA

Frame-to-frame television picture coders are, at present, only in the experimental stage. Thus, it is not possible to test in real time the feasibility of sharing transmission channels. Computer simulations can be carried out, however, by storing a long sample of unbuffered data from a single source on a digital disk and simulating the simultaneous occurrence of N_S *Picturephone* conversations by starting each conversation at a different point on the digital disk. As long as the starting points are not close together the conversations simulated in this manner will be independent.

The apparatus used to generate the data was essentially the same as in Ref. 1. The picture was scanned with 271 lines at 30 frames per second (two interlaced fields per frame) producing a nominally 1-MHz signal. This was sampled at about 2 MHz and coded as 8-bit PCM ($0 \cdots 255$) so that all processing could be done digitally. A picture element was deemed to have changed significantly if the magnitude of its frame-to-frame difference was greater than four out of a possible 255. However, two exceptions to this criterion were made: (*i*) if a significant change was preceded and followed by two insignificant changes, then the change was deemed insignificant, and (*ii*) if two clusters of significant changes were separated by three or less insignificant changes, then the clusters were joined by relabeling the intervening elements as significant changes.

For each field, two numbers were recorded: the number of significant

changes and the number of clusters requiring addressing. These were then stored on a digital disk via a Honeywell DDP-224 digital computer. Other data such as line sync words are generated, at least in these simulations, at a constant rate and, therefore, do not require storage. The bit rate for each field can then be computed by assigning four bits to each significant change, 12 bits to each cluster requiring addressing, and then adding the bits which occur at a constant rate.

Storing only two numbers per field makes it impossible to simulate phenomena that occur because of the irregular distribution of data within fields. It also requires that in all simulations buffers must be large enough to smooth these irregularities over a field time. More will be said about this point in later sections.

It was intended that these data should represent as much as possible those that would result in practice. To accomplish this goal, product-trial video tapes of actual *Picturephone* conversations were obtained and used as a guide as to the amount of motion which could be expected. A subject was placed in front of a TV camera whose output was being coded by the interframe coder, and, at the same time, the product-trial video tape was played through a monitor which was visible to the subject. The subject was then instructed to mimic as much as possible the motion displayed on the monitor.

Violent activity such as camera panning or flipping the mirror to display printed material was simulated by waving a large card in front of the camera. Such behavior occasionally caused changes in nearly 90 percent of the picture area. Simultaneous movement by more than one person in the scene (this rarely occurred) was simulated by the subject moving closer to the camera to more nearly approximate the area in motion.

Data were recorded for one hour, using two subjects; the scene for both the simulation and the product trial was a standard office with average lighting. The dress of the subjects was somewhat more colorful than that of the individuals in the video tape, however. But since this will tend to make the results conservative, if anything, it was not considered to be a drawback.

III. STATISTICAL CHARACTERISTICS OF THE DATA

The long-term average characteristics of movement by the typical single *Picturephone* user are shown in Fig. 2 where the probability of the number of changes per field exceeding n versus n is plotted, i.e., 1 − probability distribution function of number changes per field.

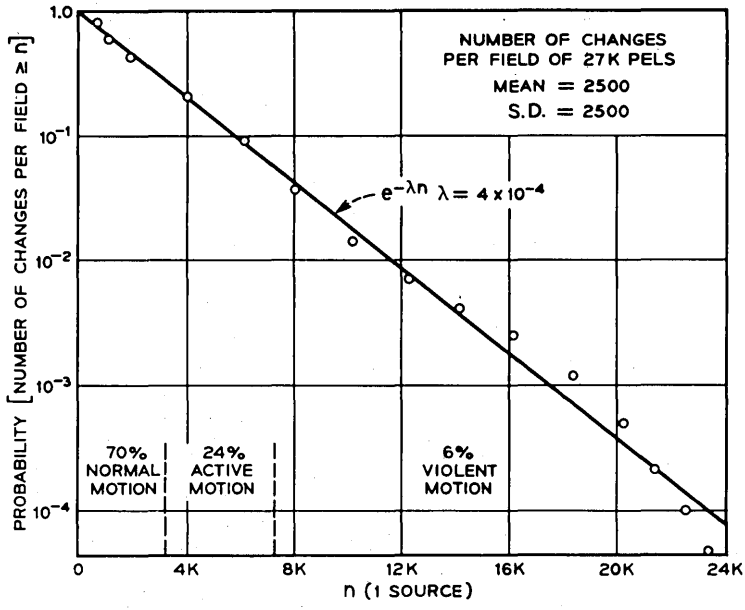

Fig. 2—Probability that the number of changes per field exceeds the threshold value n. Points lie very close to the exponential $e^{-\lambda n}$ with $\lambda = 4 \times 10^{-4}$.

The curve is very close to the exponential $e^{-\lambda n}$ (for $\lambda = 4 \times 10^{-4}$) over much of its range. The exponential shape agrees with results obtained by Seyler[9] for certain types of commercial television material, but, as reported by Pease,[10] the curve tends to be much lower (i.e., a smaller proportion of the picture changing on the average).

Inactive conversation (less than 11 percent of the picture changing) comprises about 70 percent of the data. Active motion (between 11 percent and 25 percent of the picture changing) comprises about 24 percent of the data, and violent motion (more than 25 percent of the picture changing) comprises the remaining six percent of the data. Thus, an interframe coder which was designed to accommodate active motion would fully use the required channel capacity only about 6 percent of the time. For the remainder of the time, stuffing information would have to be transmitted to maintain synchronization within the system.

Figures 3 to 6 show the curves corresponding to Fig. 2 when data streams from more than one source are averaged together prior to transmission. Simultaneous occurrence of several *Picturephone* con-

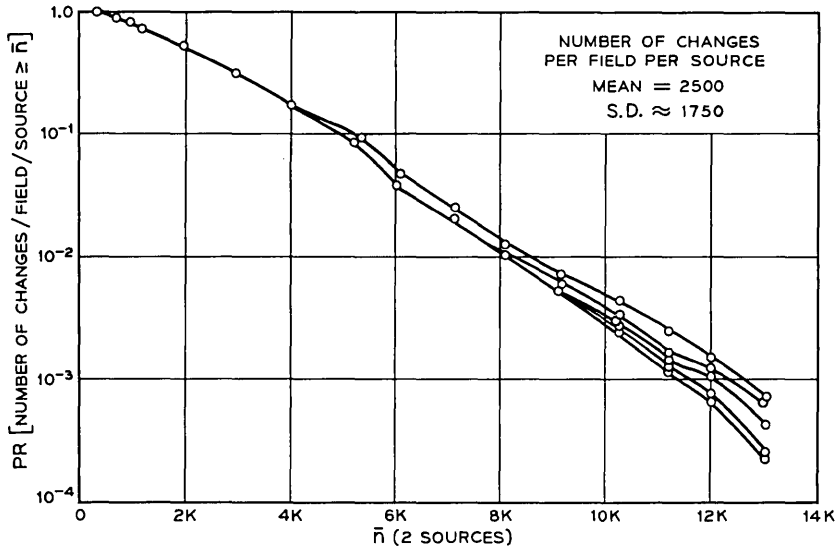

Fig. 3—Probability that the number of changes per field per source exceeds $\bar{n}$ when data from *two sources* is combined. Multiplicity of curves results from different starting positions in the data.

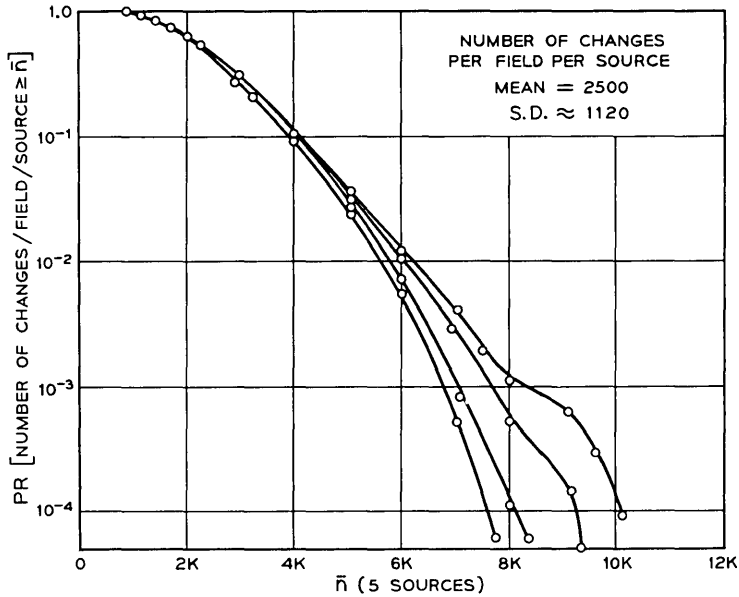

Fig. 4—Probability that the number of changes per field per source exceeds $\bar{n}$ when data from *five sources* is combined.

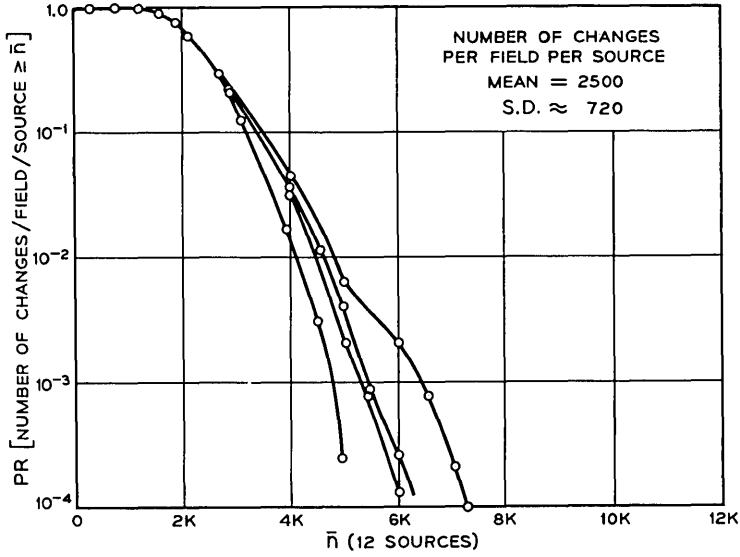

Fig. 5—Probability that the number of changes per field per source exceeds $\bar{n}$ when data from *twelve sources* is combined.

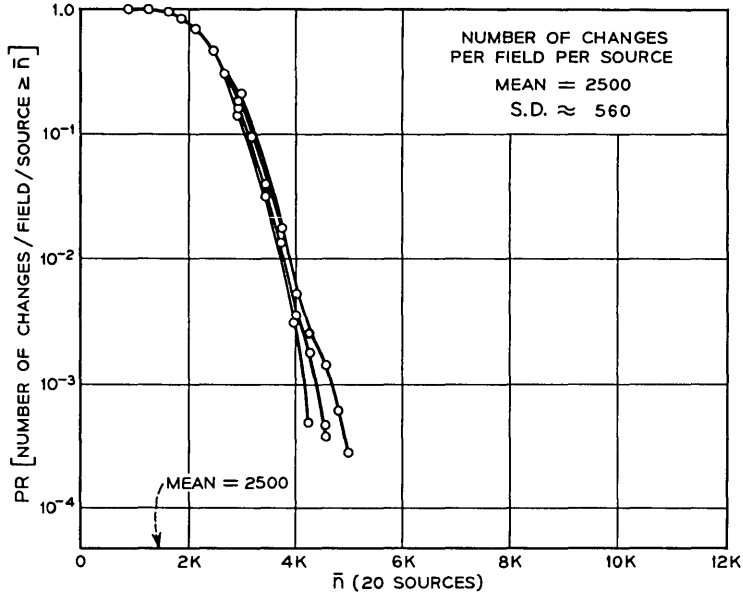

Fig. 6—Probability that the number of changes per field per source exceeds $\bar{n}$ when data from *twenty sources* is combined.

versations was simulated by starting each conversation at a different point on the digital disk. The multiplicity of curves in each figure results from various choices for these starting positions. The number of changes per field per message source is obtained by adding the number of changes per field contributed by each message source and dividing by N_S , the number of sources. The probability of this quantity exceeding $\bar{n}$ versus $\bar{n}$ is plotted in Figs. 3 to 6 for $N_S = 2, 5, 12$ and 20 respectively. As the number of sources increases, the variation of the data from the mean decreases indicating that the data are becoming more and more uniform.

When the starting positions of the separate conversations on the digital disk are changed, the results vary, especially in the tails of the distribution. This occurs because the tails are determined completely by the alignment of movement peaks in the data from each of the several sources, and when the relative positions of these peaks are changed the alignment will also change.

Figures 3 to 6, which were obtained experimentally, are very close to those obtained analytically using the exponential $\lambda e^{-\lambda n}$ as the probability density function of n for the single-source case. For more than 15 sources ($N_S \geqq 15$) the central limit theorem begins to come into effect and $\bar{n}$ is very nearly Gaussian with mean λ^{-1}, i.e., 2500 changes, and variance $(N_S\lambda^2)^{-1}$.

The large spread and consequent large possible deviation from the mean of the data from a single source is only one reason why buffering is difficult. The other reason is the high field-to-field correlation in the data due to the fact that motion in successive fields is very much the same.[1] Figure 7 shows the normalized autocorrelation function of the number of changes per field (this function is independent of N_S). According to the curve there is still a 50 percent correlation between fields which are as much as one second apart.

For a single source, transmission channels become saturated and buffers become filled only during periods of rapid motion. Thus, one is less interested in the long-time average correlation in the data as shown in Figure 7 and is more interested in how long the large peaks in the data rate are going to last. Figure 8 indicates the average durations of data peaks for a single source. If n, the number of changes per field, rises above some threshold value T during field i and does not go below T again until field j, then the duration of the peak is $(j - i)$ fields. From Fig. 8 it is seen that although periods of high data rates are quite rare, when one does occur chances are that it will last for at least several fields. In fact, for human conversations large peaks in the data can last for a

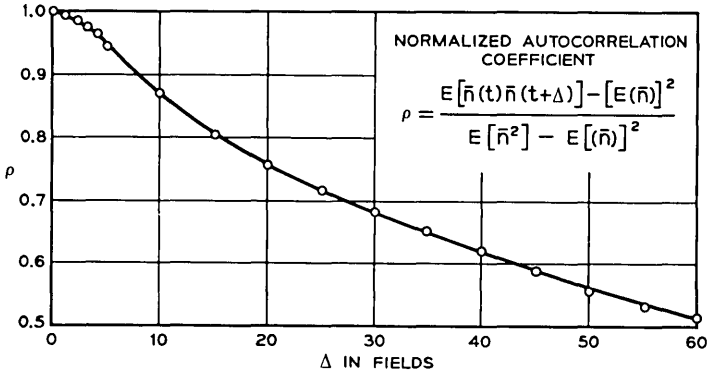

Fig. 7—Normalized autocorrelation coefficient of the number of changes per field. There is still a 50-percent correlation between fields which are 1 second apart.

few seconds, a period much too long to allow complete smoothing by a buffer because of the transmission delay that would be introduced.[1,5]

Combining data from several sources prior to transmission reduces the impact of these peaks considerably. Figures 9 to 12 show the average durations of peaks in $\bar{n}$, the number of changes per field per source,

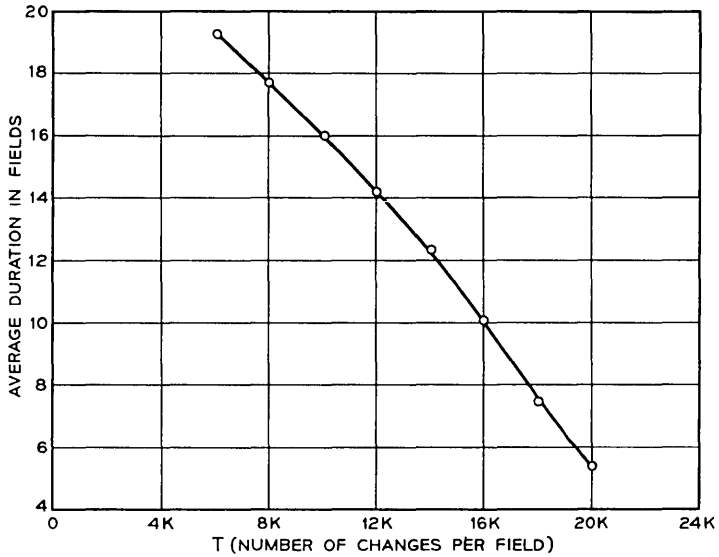

Fig. 8—Average duration of peaks in the number of changes per field. A peak starts when n rises above T and ends when n falls back below T.

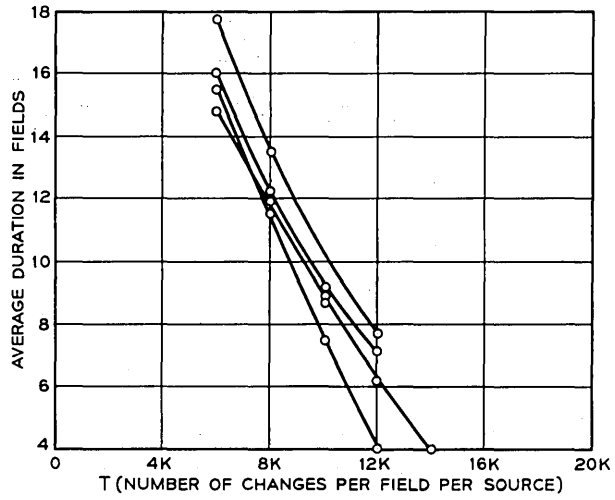

Fig. 9—Average duration of peaks in the number of changes per field per source when data from *two sources* is combined.

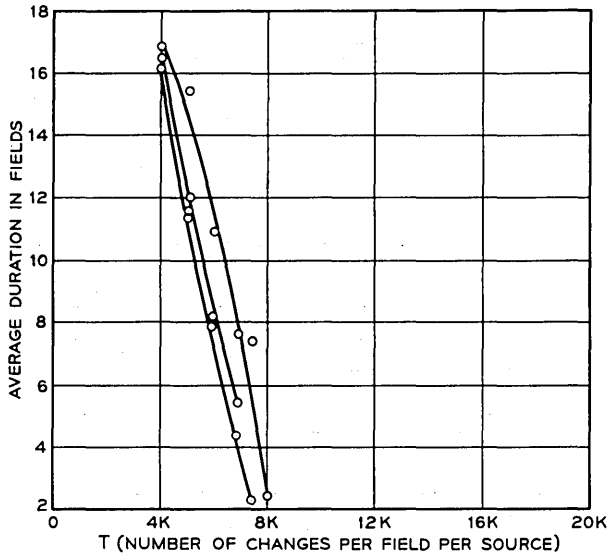

Fig. 10—Average duration of peaks in the number of changes per field per source when data from *five sources* is combined.

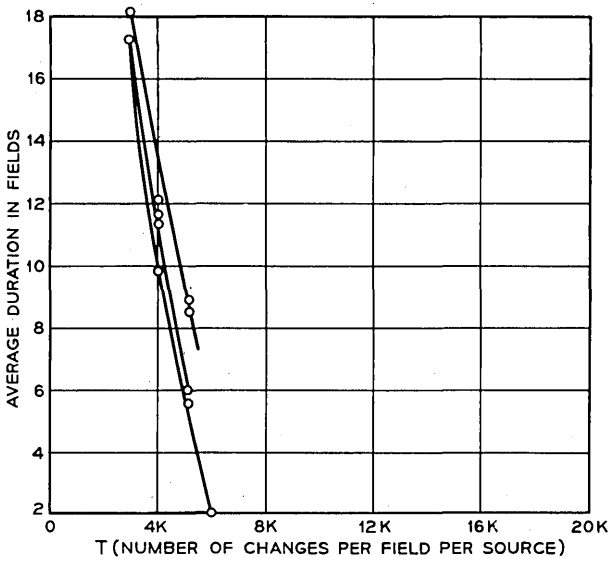

Fig. 11—Average duration of peaks in the number of changes per field per source when data from *twelve sources* is combined.

when N_S = 2, 5, 12, and 20 sources. As before, the multiplicity of curves represents changes in the digital disk starting positions. As N_S, the number of sources per shared channel increases, the magnitudes of large data peaks decrease due to the probable misalignment of peaks from the several data sources.

IV. SIMULATION OF SINGLE INTERFRAME CODERS

A number of simulations were carried out of frame-to-frame coders operating by themselves without channel or buffer sharing. These simulations differ from those of Ref. 5 in that the data used represent all types of motion in the relative proportions that could be expected in *Picturephone* transmission, whereas in Ref. 5 each segment of data represented a particular level of activity. Also, two stages of data-rate reduction were employed in these simulations, whereas in Ref. 5 only 2:1 subsampling was used.

Several features of real-time interframe coders could not be simulated using the data described in Sections II and III. *First*, since the number of changes and the number of clusters were recorded on a per-field basis, behavior within a field could not be simulated. Thus, it is always

assumed that buffers are large enough to smooth the data over a field period. For a bad case suppose that all of the data for a busy field occurred in the bottom half of the picture. Then for a 2 Mb/s transmission rate (≈33,000 bits per field), a buffer capable of storing 16,500 bits would be required to smooth over a field period. Even assuming a large buffer, however, small queue lengths cannot be represented accurately in systems where extra stuffing information is generated during periods when the buffer is empty.

Second, raising the threshold, which determines a significant frame difference during periods of violent motion, as was done in Ref. 1 requires feedback to the interframe coder; this was not employed during the collection of these data. However, the absence of this feature should not affect the results very much since during periods of high activity it is not a particularly effective technique for data reduction (see Fig. 16 in Ref. 1). Furthermore, use of a constant threshold in the simulations would tend to make the results conservative, if anything.

A third effect which could not be simulated adequately was switching between the various stages of data-rate reduction. Switching from 2:1 subsampling to full sampling, for example, requires that extra information be transmitted to update those picture elements which

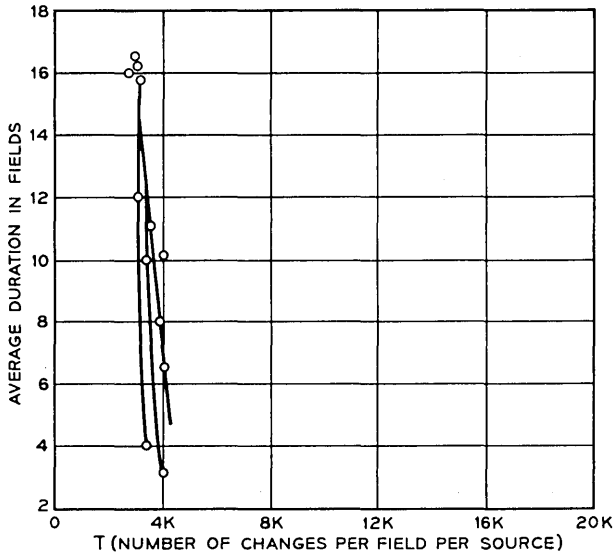

Fig. 12—Average duration of peaks in the number of changes per field per source when data from *twenty sources* is combined.

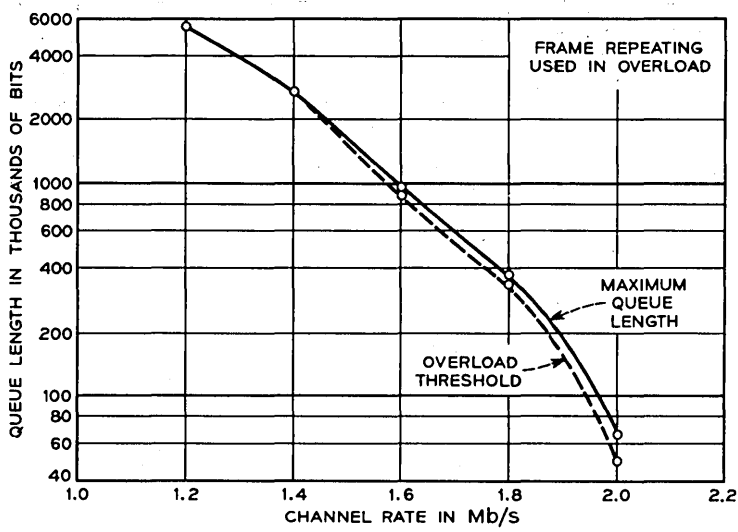

Fig. 13—Buffer requirements versus channel rate for a single source and 0.11-percent probability of overload. Overload detected via queue length at end of previous field. Frame repeating used in overload.

were previously being derived through interpolation. This switch need not take place in one frame-time, however. In a bad case where 60 to 70 percent of the picture changes during subsampling and the interpolation is completely unsuccessful, only about 600 extra picture elements per field need be transmitted to produce a full resolution picture in 0.5 seconds. When switching from 4:1 subsampling to 2:1 subsampling, only 300 extra picture elements per field need be transmitted. In view of these facts, it is felt that the switching itself can be carried out in practice in such a way as to have little effect on simulation results.

Initially, schemes similar to Ref. 1 were simulated where the number of bits in the buffer, i.e., queue length, was used to determine the usage of 2:1 subsampling or frame repeating. Twelve bits were assigned to each cluster that required addressing and four bits to each frame difference that was transmitted. When the buffer was more than 20 percent full, 2:1 subsampling in the changing area was switched in. When the queue length exceeded some higher threshold value, a whole frame was repeated thus requiring no transmission for the duration of that frame.

In the first simulation, the queue length at the end of the previous

field was used to control subsampling and repeating in the present field. Using the channel rate and buffer size of Ref. 1, namely 2 Mb/s and 67,000 bits, overflow occurred during 0.11 percent of the frames, i.e., about 1 second in a 15-minute conversation. For other channel rates, Fig. 13 shows the buffer sizes and threshold values required to maintain a 0.11 percent probability of visible degradation due to buffer filling.

If instead, one controls the subsampling and repeating by the queue length requirements in the present field, the results are changed very little, as can be seen by comparing Figs. 13 and 14. This is due to the high correlation in the amount of movement in successive fields.

The effect on the picture of frame repeating during periods of violent movement is quite noticeable,[1] and it is speculated that this degradation might be made less objectionable if 4:1 subsampling were used instead of frame repeating.[1,4] A simulation was carried out to see what the effect on buffer requirements would be of switching to a 4:1 subsampling mode when the queue length at the end of the previous field was above some threshold. Figure 15 shows the buffer size and threshold versus channel rate required to maintain a 0.11 percent probability of buffer overload. The buffer sizes are significantly larger than those of Figure 13.

With 4:1 subsampling, however, a higher usage of this mode may be

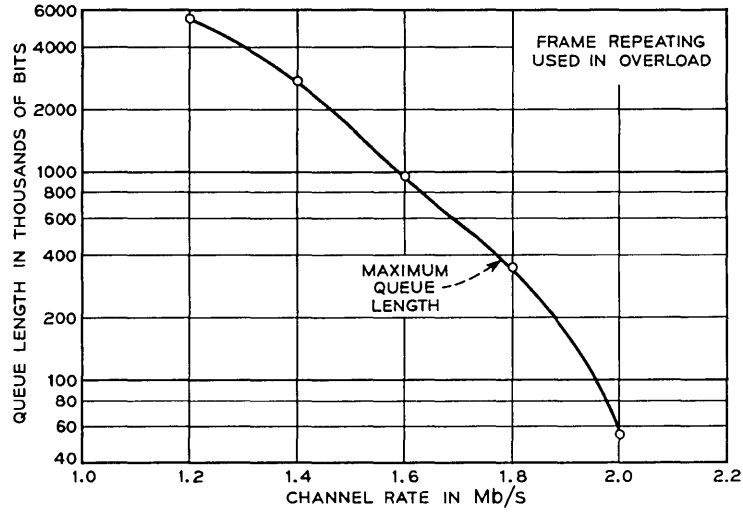

Fig. 14—Buffer requirements versus channel rate for a single source and 0.11-percent probability of overload. Overload detected via queue length in present field. (Curve is very close to that of Fig. 13.)

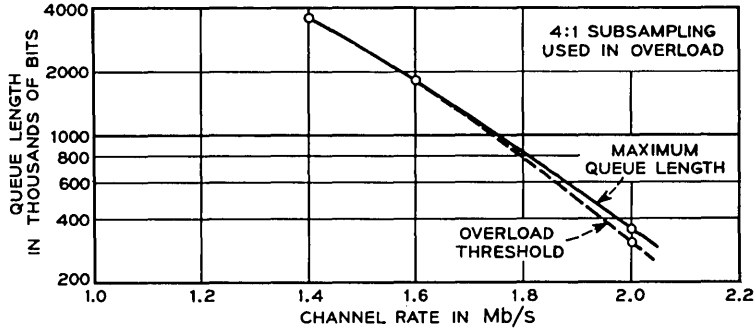

Fig. 15—Buffer requirements versus channel rate for a single source and 0.11-percent probability of overload. 4:1 subsampling used in overload. (Curve is higher than that of Fig. 13.)

tolerated since the degradation is expected to be less than with frame repeating. Exactly how much can be tolerated is not known, but if the frequency of usage is allowed to rise to 0.23 percent, then the curve of Fig. 16 is obtained (which matches very closely the buffer requirements of Figure 13 where frame repeating is used).

In the above schemes a drastic data-rate reduction is made if buffer overflow threatens. This has the effect of emptying the buffer so that

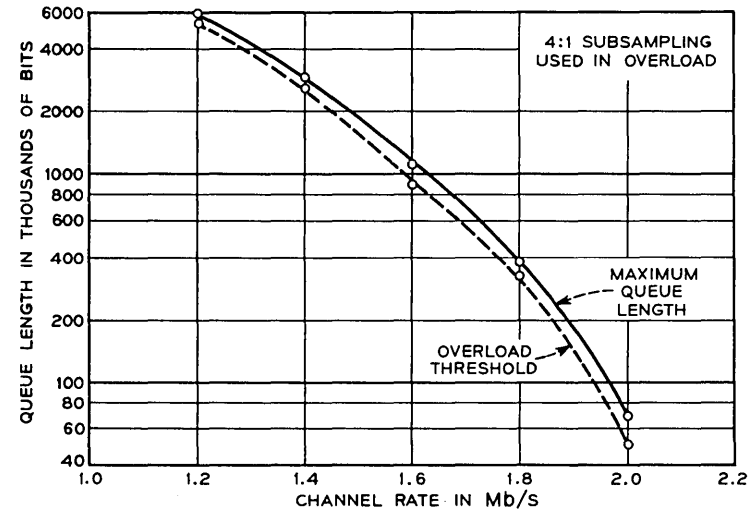

Fig. 16—Buffer requirements versus channel rate for a single source and 0.23-percent probability of overload. 4:1 subsampling used in overload. (Curve is close to that of Fig. 13.)

the next few fields can be sent with good resolution even though rapid motion is occurring. Thus, during violent movement only 1 in 4 or 1 in 8 frames is degraded. The visible degradation is annoying, however, during the whole period of violent motion. Thus, although only 0.11 percent of the frames are degraded, the visible impairment may be objectionable during all violent motion (0.88 percent of the time) since the intervening unimpaired frames do not reduce the visibility of the phenomenon.

When channel sharing is contemplated, system performance depends on the long-term average data rate. Thus, 2:1 subsampling should be employed not only when the buffer starts to fill but during all periods of active movement; similarly, 4:1 subsampling should be used during all periods of very violent movement. To simulate techniques of this type the number of significant changes in the previous field was used to control the coding in the present field. If the number of changes

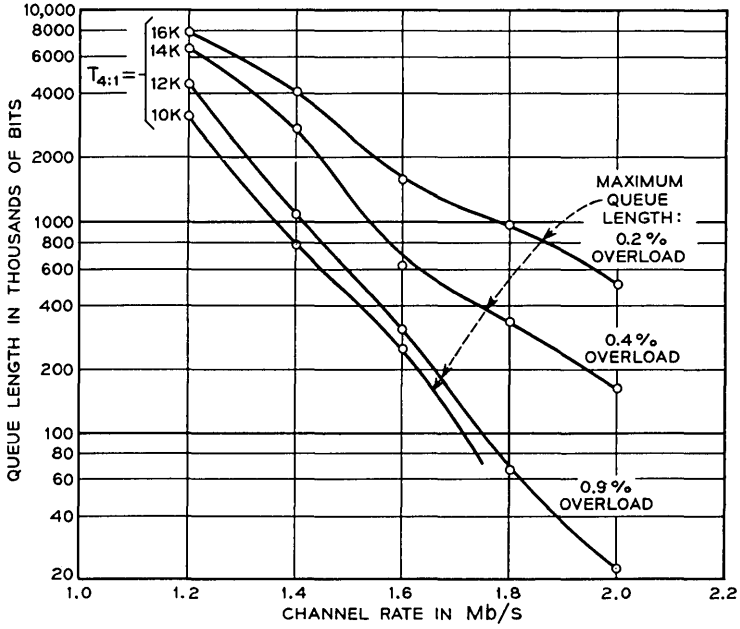

Fig. 17—Buffer requirements versus channel rate for a single source where subsampling is controlled according to the number of changes in the previous field. If the number of changes exceeds $T_{2:1}$ then 2:1 subsampling is used; if the number of changes exceeds $T_{4:1}$ then 4:1 subsampling is used. Variations in $T_{2:1}$ do not affect the results if $T_{2:1} \ll T_{4:1}$. Also shown for each value of $T_{4:1}$ is the percentage of the time in overload, i.e., when 4:1 subsampling is used.

exceeds the value $T_{2:1}$ then 2:1 subsampling is used; if the number of changes exceeds $T_{4:1}$, i.e., during violent motion, then 4:1 subsampling is used. In practice, only frame differences corresponding to sampled picture elements should be examined since the interpolation itself introduces frame differences independent of movement. Buffer size versus channel rate curves for various values of $T_{4:1}$ are given in Fig. 17 along with the percentage of time that overload, i.e., 4:1 subsampling, is used. Variations in $T_{2:1}$ do not seem to affect these results as long as $T_{2:1}$ is much smaller than $T_{4:1}$.

The value of $T_{4:1}$ for which the buffer requirements most closely approximated those of Figures 13 and 16 where queue length control is used is between 13,000 and 14,000 changes per field. This corresponds to very violent motion (about half the picture changing) and occurs only about 0.5 percent of the time (see Fig. 2). Statistics of the bit stream with $T_{4:1}$ = 13,400 changes per field and $T_{2:1}$ = 3000 changes per field are given in Figures 18 and 19. From these figures it is again apparent that large peaks in the bit rate occur very rarely, but when they do occur they can last for an appreciable period of time.

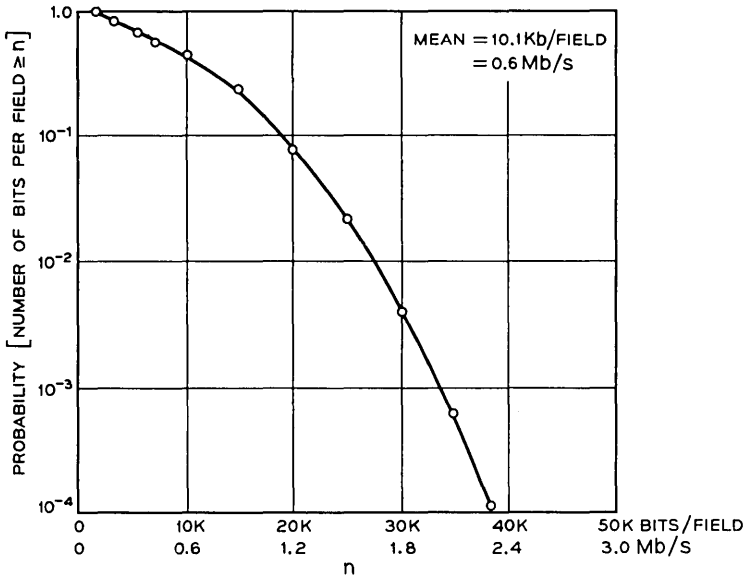

Fig. 18—Statistical characteristics of the single-source bit stream with subsampling controlled by the number of changes in the previous field. $T_{2:1}$ = 3000; $T_{4:1}$ = 13,400. Probability that the number of bits per field exceeds n is plotted versus n. Also shown is n in Mb/s.

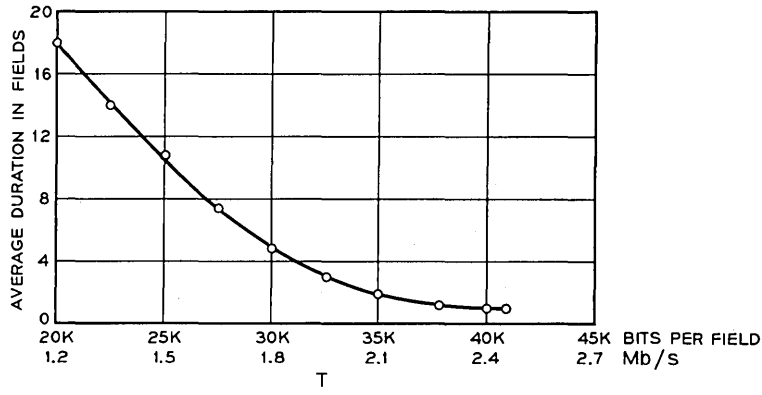

Fig. 19—Average duration of peaks in the bit rate above T for a single source with subsampling controlled by the number of changes in the previous field. $T_{2:1} = 3000$; $T_{4:1} = 13{,}400$.

Smaller values of $T_{4:1}$ require smaller buffers; however, the picture degradation will be more objectionable. Just how small $T_{4:1}$ can be made depends on the actual 4:1 subsampling scheme used and on the subjective requirements of the viewer. However, as we shall see in the next section, when combining sources prior to transmission, variations in $T_{4:1}$ do not seem to affect the results significantly. $T_{2:1}$ then becomes much more important in the performance of the system.

V. SIMULATION OF SHARED BUFFER-SHARED CHANNEL SYSTEMS

The system that will be considered in this section is shown in Fig. 1. Unbuffered data from each interframe coder or buffered data from which the stuffing information has been removed enter the prebuffers at the left to await transfer to the principal buffer via the time division multiplexer. The prebuffers should be capable of storing one or two lines of coded information if excessive transmission of source identification bits is to be avoided. The multiplexing switch can either rotate at a constant rate or stop at the output of each prebuffer only long enough to transfer data. A variable rotation rate will, in general, require less buffering and alleviate certain synchronizing problems. Similarly, the switch can access each prebuffer either sequentially or nonsequentially according to some control strategy which gives higher priority to more active sources. Nonsequential access will, in general, require smaller buffers; however, some means must then be provided for preventing one source from hogging the channel. Other configura-

tions are also possible; e.g., with a nonuniform switch rotation rate the principal buffer might be removed by making the prebuffers larger.

On rare occasions the combined data from all sources will be too much for the system to transmit, and some data will have to be deleted. If the coder itself can be told that data are being deleted, then it can be done without introducing too much picture degradation in the same way as in the single-source coder.[1] However, if rapid feedback to the coder is not feasible, then the responsibility for minimizing picture degradation in the event of buffer overflow falls entirely on the various receiver systems. This could happen in the situation depicted in Fig. 20, where the signal has successfully passed through N shared channel transmission systems and upon reaching the Nth switching station it finds that there is a momentary shortage of transmission capacity requiring the deletion of data according to some predetermined strategy. For example, half the transmitted samples along a line might be deleted, thus requiring interpolation at the receiver, or an entire line of data

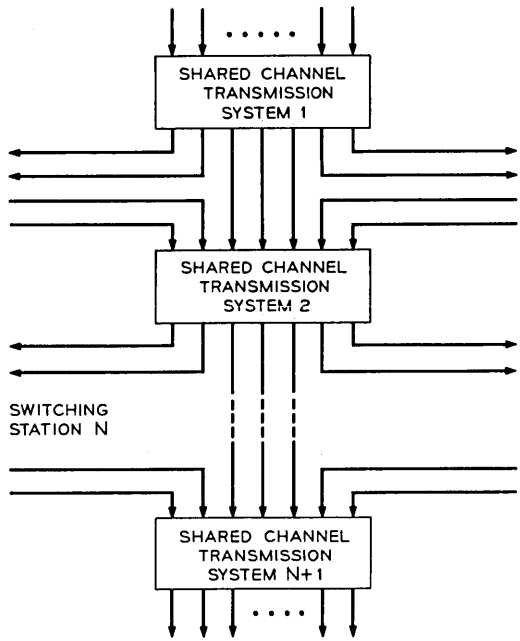

Fig. 20—Cascaded shared channel transmission systems where feedback to the original coder is impractical.

might be dropped at the Nth switching station and replaced by the average of the line above and the line below at the receiver.[11]

In the simulations which were carried out to study the channel sharing system of Fig. 1, 2:1 or 4:1 subsampling was assumed to have already taken place for each incoming field in which the number of significant changes exceeded $T_{2:1} = 3000$ or $T_{4:1} = 13{,}400$, respectively. A value of three thousand changes per field represents moderate to active motion on the part of the subject and is probably near the minimum value which could be used to control 2:1 subsampling in practice, since subsampling during slow movement results in noticeable aliasing defects in the picture. A value of 13,400 changes per field corresponds to violent motion, where nearly 50 percent of the picture area is changing. The choice of $T_{4:1}$ should not be crucial to the picture quality as long as it is in the range of violent motion; thus, for comparison purposes it was chosen so that the resulting single-source buffer requirements approximated those of Fig. 16, where subsampling was controlled by the queue length in the buffer. The effects of varying $T_{2:1}$ and $T_{4:1}$ will be discussed later.

Since the data were recorded only at the field rate, the queue length within the transmitter buffer could be examined in the simulations only at certain times. Thus, as in the single-source case, small queue lengths are not represented accurately. Unlike the single-source case, however, a certain amount of in-field data smoothing takes place because of the data interleaving[5] mechanism at the multiplexer switch. If more than just a few sources are combined, it is highly unlikely that television lines from the various sources will come from the same area of the picture. Thus, while one line from one source may come from an active area near the bottom of the picture, other lines from other sources will come from quiet areas near the top of the picture. Furthermore, as the transmission rate per source is reduced, the amount of buffering per source required for in-field smoothing decreases. Thus, if the data from each source occurred in the bottom half of the field, and all the sources were more or less in vertical synchronism, then 16K of buffering per source would be required for in-field data smoothing at 2 Mb/s per source. However, only 8K of buffering would be required at 1 Mb/s per source, and much less is required if, as seems likely, the sources are not in vertical synchronism.

The maximum queue length per source is plotted versus the channel rate per source in Figures 21 to 25 for systems in which 1, 2, 5, 12 and 20 sources respectively share the same transmission channel. As before,

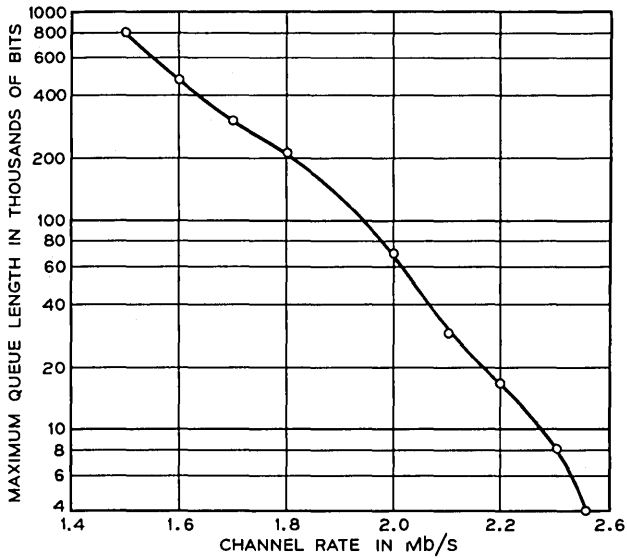

Fig. 21—Buffer requirements versus channel rate for a single source. (Same as Fig. 17 with $T_{4:1} = 13{,}400$, $T_{2:1} = 3000$.) 4:1 subsampling used when the number of changes in previous field exceeds $T_{4:1}$. Variations in $T_{2:1}$ have little effect.

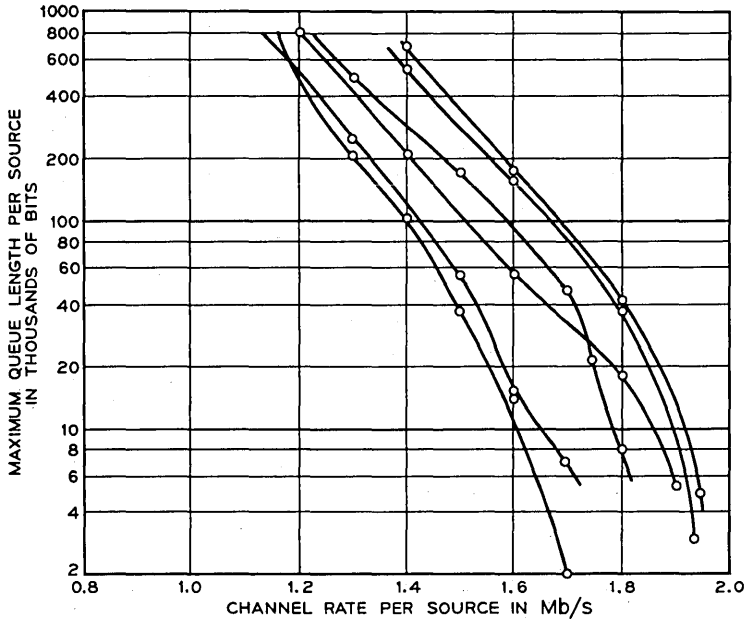

Fig. 22—Buffer requirements versus channel rate when data from *two sources* is combined prior to transmission. Multiplicity of curves results from different starting positions in the data. $T_{4:1} = 13{,}400$; $T_{2:1} = 3000$.

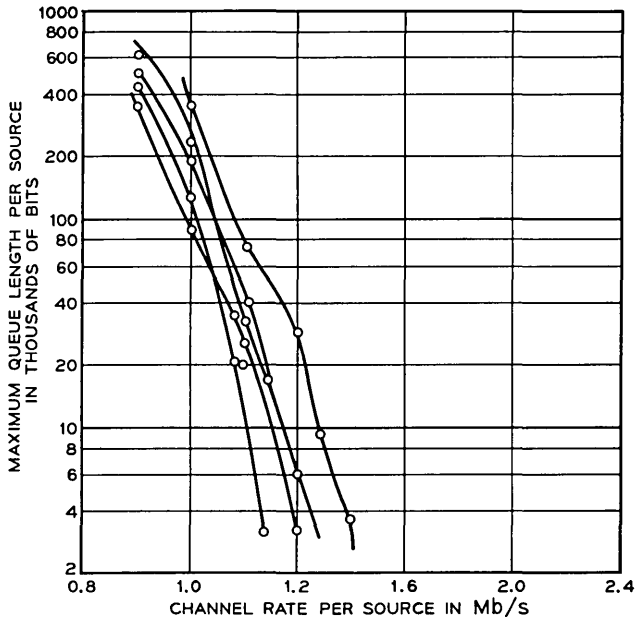

Fig. 23—Buffer requirements versus channel rate when data from *five sources* is combined prior to transmission.

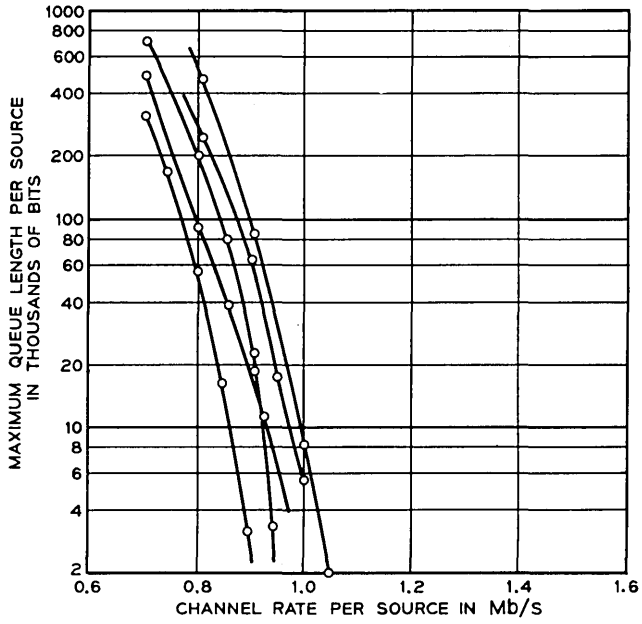

Fig. 24—Buffer requirements versus channel rate when data from *twelve sources* is combined prior to transmission.

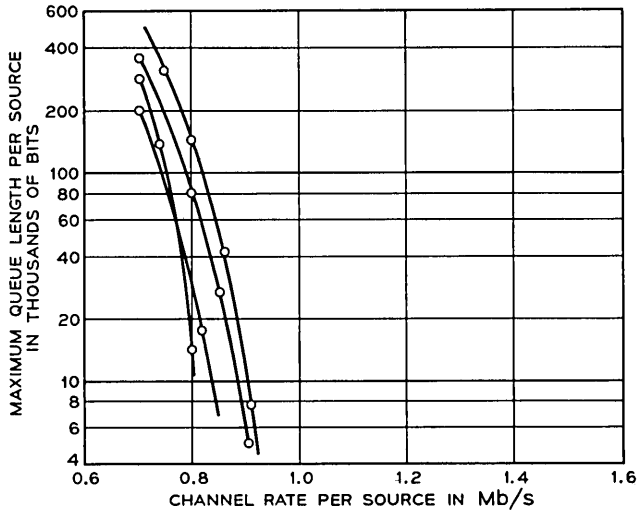

Fig. 25—Buffer requirements versus channel rate when data from *twenty sources* is combined prior to transmission.

the simultaneous occurrence of several conversations is simulated by starting each one at a different place in the data. Different sets of starting positions yield different curves. 2:1 subsampling was assumed when the number of changes per field exceeded $T_{2:1} = 3000$, and 4:1 subsampling was assumed when the number of changes per field exceeded $T_{4:1} = 13{,}400$. If buffer sizes of the order of 70,000 bits per source are not considered unreasonable, then the approximate channel rate per source required to transmit N_S sources, without buffer overflow, is given in Table I.

In every case where more than one source was simulated, changing the starting positions in the recorded data caused significant variation in the maximum queue length measurement. Results differing by a factor of ten were obtained in some cases. This occurs because the maximum queue length depends crucially on the lining up of data peaks from separate sources, and this is likely to be quite erratic as the starting position for each source is varied.

When more than four sources shared a channel, variations in $T_{4:1}$, the number of changes per field beyond which 4:1 subsampling was assumed, had little effect compared with the effect shown in Fig. 17 on a single source. Variations in $T_{2:1}$, however, had more and more of an effect as the number of sources per shared channel increased, whereas

TABLE I—CHANNEL RATE VERSUS NUMBER OF SOURCES
(BUFFER SIZE = 70,000 BITS/SOURCE; NO OVERFLOW)

Number of Sources, N_S	Channel Rate per Source (Mb/s)
1	2.0
2	1.7
5	1.2
12	0.90
20	0.85

with a single source no effect was observed at all. This occurs because of the higher sensitivity to the average data rate as opposed to the peak data rate when the number of sources per shared channel is large.

The curves also tend to become much steeper as the number of sources is increased. This is to be expected since as the rate of the combined data becomes more and more uniform, buffering will become less and less effective in reducing the required channel rate. If the principal transmitter buffer is reduced in size to the point where it is barely large enough to smooth data peaks within a field (the simulations are invalid for buffer sizes smaller than this), then the approximate channel rate per source required to transmit N_S sources, without buffer overflow, is given in Table II. Comparison with Table I shows that for more than five sources, large buffers result in relatively little improvement in bit rate.

Exactly how large the principal buffer must be to smooth the data within a field is difficult to specify because of the many factors that were discussed earlier in this section. In the simulations, however, the data are already smoothed over a field period regardless of the buffer size. Thus, the results in Table II can be obtained by simply setting the size of the principal buffer equal to zero in the simulations.

TABLE II—CHANNEL RATE VERSUS NUMBER OF SOURCES
(BUFFER LARGE ENOUGH ONLY FOR IN-FIELD SMOOTHING;
NO OVERFLOW)

Number of Sources, N_S	Channel Rate per Source (Mb/s)
1	2.4
2	2.0
5	1.3
12	1.05
20	0.92

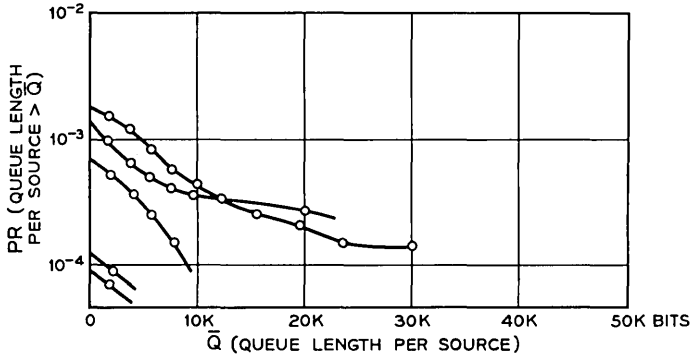

Fig. 26—Probability that the buffer queue length exceeds $\bar{Q}$ when data from *five sources* is combined. Channel rate = 1.25 Mb/s.

Up to now only the maximum queue length attained during the simulation has been considered. This maximum occurs only once, however. For nearly all the remaining time the queue length is much less than this. Thus, if a small probability of buffer overflow is allowed, the buffer size which would be required in practice could be somewhat less than is indicated in Figs. 21 to 25. Or, equivalently, for a given buffer size the required channel rate could be somewhat less.

Queue length probability distributions for 5, 12, and 20 sources and various channel rates are given in Figs. 26 to 28 for various starting

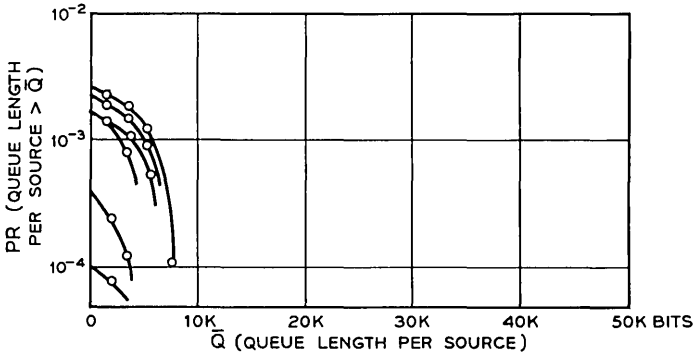

Fig. 27—Probability that the buffer queue length exceeds $\bar{Q}$ when data from *twelve sources* is combined. Channel rate = 1.0 Mb/s.

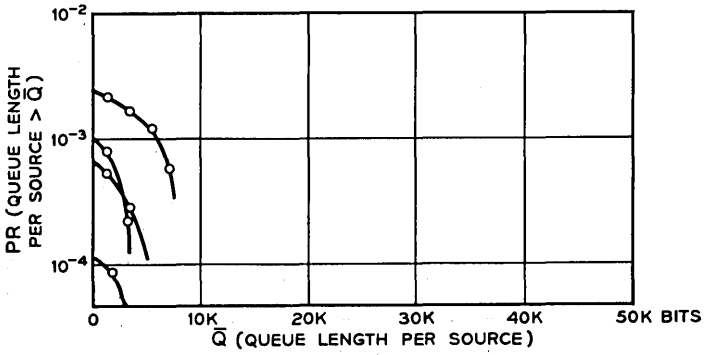

Fig. 28—Probability that the buffer queue length exceeds $\bar{Q}$ when data from *twenty sources* is combined. Channel rate = 0.9 Mb/s.

positions on the digital disk. These channel rates, which are also shown in Table III, were chosen so that with buffering of only a few thousand bits/source, i.e., enough for smoothing the data over a field period, overflow occurred less than about 0.1 percent of the time. Compared with the 0.5 percent probability of 4:1 subsampling, buffer overflow occurred one fifth as often.

Comparison of Tables II and III shows that as the number of sources per shared channel increases, the bit rate saving obtained by allowing a small probability of buffer overflow becomes less and less. This result further substantiates the fact that as the number of sources increases, the combined data become uniform enough so that buffering is of very little importance.

TABLE III—CHANNEL RATE VERSUS NUMBER OF SOURCES.
(BUFFER LARGE ENOUGH ONLY FOR IN-FIELD SMOOTHING. BUFFER OVERFLOW OCCURRED LESS THAN 0.1 PERCENT OF THE TIME.)

Number of Sources, N_S	Channel Rate per Source (Mb/s)
1	2.0
2	1.7
5	1.25
12	1.0
20	0.90

VI. CONCLUSION

The basic concept of sharing a buffer and a transmission channel between several interframe coders has been discussed with particular reference to the system in Ref. 1, which requires 2.0 Mb/s to transmit a single *Picturephone* signal. Several simulations were described, and it was concluded that five sources could be combined and transmitted on a 6-Mb/s facility with about the same amount of buffering as in Ref. 1; i.e., 1.2 megabits/second and 70,000 bits of buffering per source. With a minimal amount of buffering (a few thousand bits per source) a 2:1 reduction of the bit rate in Ref. 1 can be obtained if twelve sources are combined prior to transmission; i.e., 1.0 megabits/second per source. Combining more than twelve sources results in relatively little reduction in the required channel rate.

As in Ref. 5 the results of this paper can be used with appropriate scaling for other coding schemes as long as the ratio of addressing bits per cluster to amplitude bits per significant change (12 bits/4 bits, here) is maintained and the 2:1 and 4:1 subsampling is brought in at about the same time. Thus, if 9 bits were to be used for addressing a cluster and 3 bits per significant change, then the channel rate and queue length scales should be all multiplied by 2/3.

The simulations could have been carried out more easily had there been available a reliable statistical model of human movement in *Picturephone* scenes. Section III goes a long way toward providing such a model. For a single source the number of significant changes per field has an exponential probability density function in the region of interest; however, there is a strong field-to-field correlation resulting in large data peaks which can last for many fields. It is this characteristic that makes channel sharing so effective in reducing the required bit rate.

VII. ACKNOWLEDGMENTS

Mrs. M. A. Franke and F. W. Mounts constructed much of the hardware used to collect the data. K. A. Walsh acted as a subject. Helpful discussions were also held with J. C. Candy, R. F. W. Pease, J. O. Limb and W. G. Scholes.

REFERENCES

1. Candy, J. C., Franke, Mrs. M. A., Haskell, B. G., and Mounts, F. W., "Transmitting Television as Clusters of Frame-to-Frame Differences," B.S.T.J., *50*, No. 6 (July–August 1971), pp. 1889–1917.

2. Mounts, F. W., "A Video Encoding System with Conditional Picture-Element Replenishment," B.S.T.J., *48,* No. 7 (September 1969), pp. 2545–2554.
3. Seyler, A. J., "The Coding of Visual Signals to Reduce Channel-Capacity Requirements," Proc. IEE, *109,* (September 1962), pp. 676–684.
4. Limb, J. O., and Pease, R. F. W., "Exchange of Spatial and Temporal Resolution in Television Coding," B.S.T.J., *50,* No. 1 (January, 1971), pp. 191–200.
5. Limb, J. O., "Buffering of Data Generated by the Coding of Moving Images," B.S.T.J., this issue, pp. 239–259.
6. Seitzer, D., "Instantaneous Priority Multiplexing of Gray Pictures," IEEE Trans. on Commun. Technology, (October 1970), p. 690.
7. Urquhard-Pullen, D. I., "Improvements Relating to Multiplexed Transmission Systems," British Patent No. 1057024.
8. Cutler, C. C., and Mounts, F. W., private communication.
9. Seyler, A. J., "Probability Distribution of TV Frame Differences," Proc. IREE Australia, (1965), p. 355.
10. Pease, R. F. W., "Frame Difference Signals for a Personal Communication Television System of 271 Lines," internal memorandum.
11. Pease, R. F. W., and Limb, J. O., "A Simple Interframe Coder for Video Telephony," B.S.T.J., *50,* No. 6 (July–August 1971), pp. 1877–1888.

Copyright © 1972 American Telephone and Telegraph Company
THE BELL SYSTEM TECHNICAL JOURNAL
Vol. 51, No. 1, January, 1972
Printed in U.S.A.

Optimal Test Point Selection for Sequential Manufacturing Processes

By M. R. GAREY

(Manuscript received June 23, 1971)

Consider a manufacturing process, such as the production of complex semiconductor devices, which consists of the sequential application of n possibly unreliable operations, t_1 , t_2 , $\cdots$, t_n . Let c_i be the cost incurred in performing operation t_i , and let p_i be the probability that t_i will be performed successfully. Clearly one would prefer to reject immediately any item as soon as a faulty operation has been performed upon it in order to avoid the unnecessary cost of further processing that item. For this purpose, we shall assume that, immediately following each operation t_i , it is possible to apply a perfectly reliable test T_i , for determining whether or not the item should be rejected at that point, where the cost incurred by applying T_i depends only upon the point i of test application and the last previous point at which such a test was applied. Since the application of tests entails additional costs, careful analysis is required to determine which tests are sufficiently useful to justify that additional cost. Using a dynamic programming approach, we derive a useful and efficient algorithm which utilizes the test and operation costs, along with the operation failure probabilities, to determine a set of testing points which will result in the minimal expected manufacturing cost. We then show how it is possible to further improve upon our algorithm for the particular case in which all test costs depend only upon the point of test application.

Certain types of products, such as many semiconductor devices, are manufactured by performing a linear sequence of individual operations, where many of the individual operations have a nonnegligible probability of yielding an undesired result. In such cases it would be preferable to immediately reject a faulty item to avoid the unnecessary, and useless, cost of further processing that item. However, the introduction of tests into the manufacturing process, for determining

whether or not an item should be rejected, will itself introduce additional costs in such a way that the total expected cost of the manufacturing process may increase. In addition, certain choices of test points, though reducing the total expected cost, may be considerably more costly than certain other choices of test points. We shall present an efficient and useful algorithm that uses the various test and operation costs, along with the operation failure probabilities, to determine an optimal set of testing points, which minimizes the expected cost of the entire manufacturing process.

Consider a manufacturing process consisting of n individual operations, or tasks, t_1 , t_2 , $\cdots$, t_n , which are to be performed sequentially in the fixed order of their indices. Associated with each task t_i are the cost $c_i > 0$ incurred by performing t_i and the success probability p_i , $0 < p_i \leqq 1$, that operation t_i will have the proper result, assuming all previous operations were successful. Immediately after any operation t_i it is possible to perform a perfectly reliable test T_i which determines whether or not all previous operations, including t_i , have been successful, that is, whether or not the item should be rejected at that point. The cost for performing test T_i is given by $C_i > 0$. We justify this simple testing cost by noting that in many manufacturing procedures of this type the major determinant of testing cost is merely the cost of removing the item from the assembly line and preparing it for test application. However, we shall later generalize the testing cost to allow a dependence upon the previously untested operations. We now develop an algorithm which uses the knowledge of these costs and probabilities to determine a choice of test points (a subset of the T_i) which results in the lowest possible expected manufacturing cost per item processed. This is equivalent to minimizing the expected cost per fault-free item produced, because the introduction of tests into the process does not change the probability, given by $\prod_{i=1}^{n} p_i$, that an item is successfully processed by all n tasks. The tests merely serve to reject already faulty items to avoid the cost of useless additional processing.

We solve this problem by the method of dynamic programming.[1] Following each operation t_i it is necessary to decide whether or not test T_i should be applied. To make this decision we need only compute the minimal expected costs for completing the process assuming that T_i is or is not utilized and choose the smaller. The computations of these two expected costs use the cost of T_i , the probability p that the item is not faulty at this point, and the cost of t_{i+1} . For the case that T_i is used, we also need the minimal expected cost for completing the

process under the assumption that the item is fault-free before t_{i+1} is performed. For the case that T_i is not used, we need the minimal expected cost for completing the process under the assumption that the item is not faulty with probability p before t_{i+1} is performed.

Formally, let a state of the process be described by $[j, p]$, with $1 \leqq j \leqq n$ and $0 < p \leqq 1$, where the process is in state $[j, p]$ if and only if operation t_i has just been applied and the resulting item is fault-free with probability p. There is also a "reject" state R entered when a test rejects a faulty item. The initial state of the process is $[1, p_1]$, and the final states are all those states of the form $[n, p]$, $0 < p \leqq 1$, plus the reject state R. The transitions between states are determined by the decisions on whether or not to apply a test before the next operation. If the process is in state $[j, p]$ and test T_j is not applied, the next state will be $[j + 1, p \cdot p_{j+1}]$. If the process is in state $[j, p]$ and test T_j is applied, the next state will be either $[j + 1, p_{j+1}]$, with probability p, or R, with probability $1 - p$. The problem is to find a sequence of states to transform the process from the initial state to any final state, with minimal expected total process cost.

Let $K[j, p]$ be the minimum expected cost to get from state $[j, p]$ to a final state and let $S[j, p]$ be the corresponding optimal set of test points T_k. We then have

$$K[j, p] = \min \begin{cases} C_j + p \cdot (c_{j+1} + K[j + 1, p_{j+1}]) \\ c_{j+1} + K[j + 1, p \cdot p_{j+1}] \end{cases}$$

and $S[j, p]$ equals either $S[j + 1, p_{j+1}] \cup \{T_j\}$ or $S[j + 1, p \cdot p_{j+1}]$, depending upon whether the first or second expression is smaller. For a final state $[n, p]$, $0 < p \leqq 1$, we have $K[n, p] = 0$ and $S[n, p]$ empty. (In our basic model, the final test will never be applied, since it can only increase the total expected cost. However, the results can also be applied if test T_n is always required as a final product quality check, in which case $K[n, p] = C_n$ and $S[n, p] = \{T_n\}$.)

The difficulty with using these equations to obtain an optimal solution is that, since p can take any value from 0 to 1, there are an infinite number of equations to solve. Fortunately, for states of the form $[j, p]$, p can take only a finite number of possible values, $\prod_{k=1}^{j} p_k$, $\prod_{k=2}^{j} p_k$, $\cdots$, $\prod_{k=j}^{j} p_k$, depending upon the last test which had been applied. Thus, if none of the tests T_i, T_{i+1}, $\cdots$, T_{j-1} were applied, and either $i = 1$ or T_{i-1} was applied, then $p = \prod_{k=i}^{j} p_k$. Accordingly we shall now describe a state of the process by (j, i), $i \leqq j$, where the process is in state (j, i) if and only if

(*i*) operation t_j has just been applied,
(*ii*) none of the tests T_i , T_{i+1} , $\cdots$, T_{j-1} were applied, and
(*iii*) either $i = 1$ or T_{i-1} was applied.

The initial state is then state (1, 1) and the final states are of the form (n, i), $1 \leqq i \leqq n$, plus the reject state R. If the process is in state (j, i), the next state will be either $(j + 1, j + 1)$, with probability p, or R, with probability $1 - p$, if T_j is applied or $(j + 1, i)$ if T_j is not applied. With $K(j, i)$ and $S(j, i)$ defined in the same way as previously, the dynamic programming equations become

$$K(j, i) = \min \begin{cases} C_j + \left(\prod_{k=i}^{j} p_k\right) \cdot (c_{j+1} + K(j + 1, j + 1)) \\ c_{j+1} + K(j + 1, i) \end{cases}$$

and $S(j, i)$ equals either $S(j + 1, j + 1) \cup \{T_j\}$ or $S(j + 1, i)$, depending upon whether the first or second expression is smaller. We also have $K(n, i) = 0$ and $S(n, i)$ empty for $1 \leqq i \leqq n$. This set of equations can be solved iteratively to determine the optimal solution.

Observe now that no additional complications arise if we generalize the test costs to allow a dependence upon the state (j, i). Accordingly we redefine the cost of test T_j , when the previously untested operations are t_i , t_{i+1} , $\cdots$, t_j , to be given by $C_{j,i} > 0$, allowing the additional dependence upon i. We can then rewrite our dynamic programming equations as

$$K(j, i) = \min \begin{cases} C_{j,i} + \left(\prod_{k=i}^{j} p_k\right) \cdot (c_{j+1} + K(j + 1, j + 1)) \\ c_{j+1} + K(j + 1, i) \end{cases}$$

with $K(n, i) = 0$ for $1 \leqq i \leqq n$, with $S(j, i)$ corresponding as before. The following algorithm uses these equations to iteratively solve for the optimal set of test points.

Algorithm 1. *Computation of Optimal Testing Points*

(a) For each i, $1 \leqq i \leqq n$, set
$K(n, i) \leftarrow 0$ and $S(n, i) \leftarrow \varnothing$ (empty set).
(b) Set $j \leftarrow n - 1$.
(c) Set $i \leftarrow j$ and $P \leftarrow 1$.
(d) Set $P \leftarrow P \cdot p_i$.
(e) Compute

$$K(j, i) = \min \begin{cases} C_{j,i} + P \cdot (c_{j+1} + K(j + 1, j + 1)) \\ c_{j+1} + K(j + 1, i) \end{cases}$$

and set $S(j, i)$ to $S(j + 1, j + 1) \cup \{T_i\}$ or $S(j + 1, i)$, depending, respectively, on whether the first or second expression is smaller.

(f) If $i > 1$, set $i \leftarrow i - 1$ and go to (d).

(g) If $j > 1$, set $j \leftarrow j - 1$ and go to (c).

(h) The optimal set of test points is given by $S(1, 1)$ and yields a manufacturing process with total expected cost per item processed of $c_1 + K(1, 1)$.

Notice that it is not necessary to actually construct and save all the optimal partial sets $S(j, i)$ but merely to note whether or not test T_i is included in $S(j, i)$. The optimal test set can be constructed directly from this information upon completion of the algorithm. The number of operations performed by the algorithm is at most proportional to the square of the number of tasks in the manufacturing procedure under analysis. Thus the algorithm can be economically used for extremely large problems when programmed for a digital computer, and many problems can be reasonably solved by hand calculation. The details of the algorithm are illustrated with a small example in Appendix A.

Notice that if physical constraints prevent the application of a test following certain tasks, this can be handled in the algorithm merely by automatically setting $K(j, i)$ to $c_{i+1} + K(j + 1, i)$ whenever T_i is not allowed. This is equivalent to combining tasks t_i and t_{i+1} into a single task having cost $c_i + c_{i+1}$ and success probability $p_i \cdot p_{i+1}$.

We now return briefly to the original case where the cost of test T_i depends only upon j and show how Algorithm 1 can be improved for this case. We let

$$D(j, i) = C_i + \left(\prod_{k=i}^{j} p_k\right)(c_{i+1} + K(j + 1, j + 1)) - c_{i+1} - K(j + 1, i).$$

Thus $D(j, i)$ is merely the difference of the two expressions which must be compared in order to determine whether or not to apply test T_i when in state (j, i). An optimal solution is formed by choosing to apply test T_i from state (j, i) if and only if $D(j, i) < 0$. We can then prove the following theorem.

Theorem 1: For all j, $1 < j < n$, and all i, $1 < i < j$, $D(j, i) \geqq D(j, i - 1)$.

The proof of Theorem 1 is given in Appendix B. Simply stated, Theorem 1 tells us that, for fixed j, the difference function $D(j, i)$ changes sign only once. In particular, it implies that if test T_i is to be applied in state (j, i), then test T_i should also be applied in each of the

states $(j, i-1), (j, i-2), \cdots, (j, 1)$. This enables us to modify step (e) of Algorithm 1, when all test costs depend only on j, to omit the computation of $c_{i+1} + K(j+1, i)$ in determining $K(j, i)$ whenever $T_i \in S(j, i+1)$. In fact, for very large problems, one might consider using a binary search, for each j, to discover the value $i = i_o$ at which $D(j, i)$ changes sign. Once that point has been found, each $K(j, i)$ can be computed by evaluating only one of the two expressions in the minimization, the proper one being determined by whether i is less than i_o or greater than i_o. Though the number of operations required will still increase proportionally to n^2, this method will substantially reduce the actual number of operations performed.

A related problem with tests which merely test for the success or failure of a single operation, all of which must be applied, but which are not restricted as to point of application in the process sequence is solved as a special case in Ref. 2. The algorithm given there requires time bounded by the square of the number of tasks in the production sequence. A more general problem has tests which each determine the success or failure of some particular subset of the tasks. Any one of the tests may be applied at any point in the manufacturing process and will determine the success or failure of all operations which belong to its test set and which have already been performed. The problem solved in this paper had those test sets restricted to being of the form $\{t_1, t_2, \cdots, t_k\}$, which enabled us to give an efficient optimization algorithm. The best known algorithms for the general problem, however, require an amount of time which may be exponential in the number of tasks, restricting their usefulness to only very small problems.

Another related problem has been considered by T. S. Ellington.[3] In his problem, one has a number of alternative methods for accomplishing each task, the alternatives having different cost and success probabilities, and one would like to select the best method for each task in order to obtain the minimum expected cost. Though Ellington was able to give an efficient algorithm for making this selection, it was based on the assumption that each task is automatically tested immediately after it is applied. If, however, we also allow choice as to test points, the problem becomes more complicated. One cannot merely combine our algorithm with Ellington's, though both are dynamic programming algorithms, because they work from opposite ends of the process sequence. The development of an efficient algorithm to simultaneously select optimal test points and optimal task alternatives remains an open problem which could have substantial practical importance in the design of actual manufacturing processes.

ACKNOWLEDGEMENTS

The author is indebted to D. Slepian, W. B. Joyce, W. M. Boyce, and H. O. Pollak for their invaluable suggestions and encouragement.

APPENDIX A

Optimization Algorithm Example

We illustrate the application of the optimization algorithm with the following small example:

	c_i	p_i	C_i
t_1	10	.9	7
t_2	10	.8	8
t_3	25	.9	4
t_4	20	.8	12
t_5	30	.8	10
t_6	15	.9	12

If no tests are applied, the expected cost of the process is simply the sum of the c_i or 110. If all tests, except the last (which can only increase the total expected cost), are applied, the expected cost of the process is

$$c_1 + C_1 + p_1(c_2 + C_2 + p_2 \cdot (c_3 + C_3 + p_3 \cdot (c_4 + C_4 + p_4 \cdot (c_5 + C_5 + p_5 \cdot (c_6))))) \cong 101.77.$$

We now show the successive computations performed in applying the optimization algorithm.

$K(6, i) = 0$ for all i	no test
$K(5, 5) = \min (10 + .8(15), 15) = 15$	no test
$K(5, 4) = \min (10 + .64(15), 15) = 15$	no test
$K(5, 3) = \min (10 + .576(15), 15) = 15$	no test
$K(5, 2) = \min (10 + .4608(15), 15) = 15$	no test
$K(5, 1) = \min (10 + .41472(15), 15) = 15$	no test
$K(4, 4) = \min (12 + .8(45), 45) = 45$	no test
$K(4, 3) = \min (12 + .72(45), 45) = 44.4$	test
$K(4, 2) = \min (12 + .576(45), 45) = 37.92$	test
$K(4, 1) = \min (12 + .5184(45), 45) = 35.328$	test
$K(3, 3) = \min (4 + .9(65), 64.4) = 62.5$	test
$K(3, 2) = \min (4 + .72(65), 57.92) = 50.8$	test
$K(3, 1) = \min (4 + .648(65), 55.328) = 46.12$	test

$$K(2, 2) = \min (8 + .8(87.5), 75.8) = 75.8 \qquad \text{no test}$$
$$K(2, 1) = \min (8 + .72(87.5), 71.12) = 71 \qquad \text{test}$$
$$K(1, 1) = \min (7 + .9(85.8), 81) = 81 \qquad \text{no test}$$

These all are computed by simply following the optimization algorithm as given, noting by "test" or "no test" whether the first or second value was smaller. The optimal solution has expected cost $c_1 + 81 = 91$, which is appreciably smaller than the two "obvious" solutions. We remind the reader that the cost per fault-free item produced is obtained simply by dividing the cost per item processed by $\prod_{i=1}^{n} p_i$, the probability that the processed item is fault free. Thus, in this case, the optimal solution has cost per fault-free item approximately equal to 233, compared to 282 if no tests are used and 261 if all tests are used. Considerably greater benefits may be derived when the algorithm is applied to processes with a larger number of tasks.

To determine which tests are applied in the optimal solution, one notes first that T_1 is not applied since "no test" was indicated for $K(1, 1)$. Since T_1 is not applied, we go to $K(2, 1)$ which indicates that T_2 should be used. Since T_2 is applied, we go to $K(3, 3)$ which indicates that T_3 should be used. Since T_3 is applied, we go to $K(4, 4)$ which indicates that T_4 should not be applied. Next, since T_4 is not used, we go to $K(5, 4)$ which indicates T_5 is not used. Finally, $K(6, 4)$ indicates that T_6 is not used. Thus, the optimal solution uses only two tests, T_2 and T_3.

If one is required to apply T_6, the optimal solution can be computed similarly to have expected cost 98.6. It uses only tests T_2, T_4, and T_6. In this case, the solution which uses no tests other than T_6 has expected cost 122, and the solution which uses all the tests has expected cost 106.75. We emphasize again that, even though the gain from applying the optimization algorithm to this small example is not insubstantial, considerably greater savings can be obtained with larger, more realistic problems.

APPENDIX B

Proof of Theorem 1

Let

$$D(j, i) = C_i + \left(\prod_{k=i}^{j} p_k\right)(c_{j+1} + K(j + 1, j + 1)) - c_{j+1} - K(j + 1, i).$$

Theorem 1: For all j, $1 < j < n$, and all i, $1 < i \leqq j$, $D(j, i) \geqq D(j, i - 1)$.

Proof. Suppose $D(j, i) < D(j, i-1)$. Then

$$D(j, i-1) - D(j, i) = \left(\prod_{k=i}^{j} p_k\right)(p_{i-1} - 1)(c_{i+1} + K(j+1, j+1)) + K(j+1, i) - K(j+1, i-1) > 0.$$

Then

$$K(j+1, i) - K(j+1, i-1) > \left(\prod_{k=i}^{j} p_k\right)(1 - p_{i-1})(c_{i+1} + K(j+1, j+1)).$$

We shall show that this inequality is never satisfied; that is, for all j, $2 < j \leqq n$, and for all i, $1 < i \leqq j$,

$$(*) \qquad K(j, i) - K(j, i-1) \leqq \left(\prod_{k=i}^{j-1} p_k\right)(1 - p_{i-1})(c_i + K(j, j)).$$

We prove (*) by induction on j, running from n down to 3. If $j = n$, we have that $K(n, i) = K(n, i-1)$, so that the left side of (*) is zero. Since the right side is nonnegative, the inequality is clearly satisfied.

Now suppose that (*) holds for all j, $m < j \leqq n$, and all i, $1 < i \leqq j$. We shall show that it must then hold for $j = m$.

To do this, we first prove a useful intermediate inequality,

$$p_m(c_{m+1} + K(m+1, m+1)) \leqq c_m + K(m, m).$$

We consider two cases. If $D(m, m) < 0$,

$$c_m + K(m, m) = c_m + p_m(c_{m+1} + K(m+1, m+1)) \geqq p_m(c_{m+1} + K(m+1, m+1)).$$

If $D(m, m) \geqq 0$, $c_m + K(m, m) = c_m + c_{m+1} + K(m+1, m)$. By the induction hypothesis, we have

$$K(m+1, m+1) - K(m+1, m) \leqq (1 - p_m)(c_{m+1} + K(m+1, m+1)).$$

Rewriting, we obtain

$$c_{m+1}K(m+1, m) \geqq p_m(c_{m+1} + K(m+1, m+1)),$$

which completes the proof of the intermediate inequality.

We now prove (*) for $j = m$, using two cases.

Case 1. $D(m, i-1) < 0$. Since $D(m, i-1) < 0$,

$$K(m, i-1) = C_m + \left(\prod_{k=i-1}^{m} p_k\right)(c_{m+1} + K(m+1, m+1)).$$

It is always the case that

$$K(m, i) \leqq C_m + \left(\prod_{k=i}^{m} p_k\right)(c_{m+1} + K(m + 1, m + 1)).$$

Thus,

$$\begin{aligned} K(m, i) - K(m, i - 1) &\leqq \left(\prod_{k=i}^{m} p_k\right)(1 - p_{m-1})(c_{m+1} + K(m + 1, m + 1)) \\ &= \left(\prod_{k=i}^{m-1} p_k\right)(1 - p_{m-1})[p_m(c_{m+1} + K(m + 1, m + 1))] \\ &\leqq \left(\prod_{k=i}^{m-1} p_k\right)(1 - p_{m-1})[c_m + K(m, m)], \end{aligned}$$

using the intermediate inequality proved earlier. This completes the proof of (*) for Case 1.

Case 2. $D(m, i - 1) \geqq 0$. Since $D(m, i - 1) \geqq 0$,

$$K(m, i - 1) = c_{m+1} + K(m + 1, i - 1).$$

It is always the case that $K(m, i) \leqq c_{m+1} + K(m + 1, i)$. Thus, $K(m, i) - K(m, i - 1) \leqq K(m + 1, i) - K(m + 1, i - 1)$. By the induction hypothesis,

$$\begin{aligned} K(m + 1, i) - K(m + 1, i - 1) &\leqq \left(\prod_{k=i}^{m} p_k\right)(1 - p_{i-1})(c_{m+1} + K(m + 1, m + 1)) \\ &= \left(\prod_{k=i}^{m-1} p_k\right)(1 - p_{i-1})[p_m(c_{m+1} + K(m + 1, m + 1))] \\ &\leqq \left(\prod_{k=i}^{m-1} p_k\right)(1 - p_{i-1})[c_m + K(m, m)], \end{aligned}$$

again using the previously proved intermediate inequality. This completes the proof of (*) for Case 2.

Theorem 1 follows by induction.

REFERENCES

1. Bellman, R., *Dynamic Programming*, Princeton University Press, Princeton, New Jersey, 1957.
2. Garey, M. R., "Optimal Task Sequencing with Precedence Constraints," to be published.
3. Ellington, T. S., "Cost Optimization Utilizing Reference Techniques (COURT)," Western Electric Engineer, *15*, No. 1 (1971), pp. 25–32.

Copyright © 1972 American Telephone and Telegraph Company
THE BELL SYSTEM TECHNICAL JOURNAL
Vol. 51, No. 1, January, 1972
Printed in U.S.A.

The General Second-Order Twin-T and Its Application to Frequency-Emphasizing Networks

By E. LUEDER

(Manuscript received June 8, 1971)

The general conditions for reducing the third-order transfer function of a twin-T by one are derived using Euclid's algorithm. The conditions presently used impose narrower constraints than necessary on the twin-T, thus leaving fewer free parameters to optimize the circuit. With the new method the zeros of the twin-T transfer function can be placed in both the left- and the right-half s-plane.

The advantages of the twin-T with additional free parameters in second-order RC-active filters are appreciable. For example, in the medium-selectivity frequency-emphasizing network (MSFEN), the gain needed to realize a given pole Q may be up to 70 times smaller than that required with previous methods, while the stability of the pole is improved typically by a factor of 2. Thus, an MSFEN with the general second-order twin-T is capable of realizing a wider range of pole Q's than was possible previously, while the sensitivity of the pole Q is reduced.

I. INTRODUCTION

The twin-T as represented in Fig. 1 consists of the three resistors R_1 , R_2 , R_3 and the three capacitors C_1 , C_2 , C_3 . A straightforward analysis provides its Y-matrix as

$$Y = \begin{bmatrix} \dfrac{as^3 + s^2(b+f) + s(c+g) + 1}{R_s(R_pC_3s + 1)(R_3C_ss + 1)} & -\dfrac{as^3 + bs^2 + cs + 1}{R_s(R_pC_3s + 1)(R_3C_ss + 1)} \\ -\dfrac{as^3 + bs^2 + cs + 1}{R_s(R_pC_3s + 1)(R_3C_ss + 1)} & \dfrac{as^3 + s^2(b+d) + s(c+e) + 1}{R_s(R_pC_3s + 1)(R_3C_ss + 1)} \end{bmatrix}, \tag{1a}$$

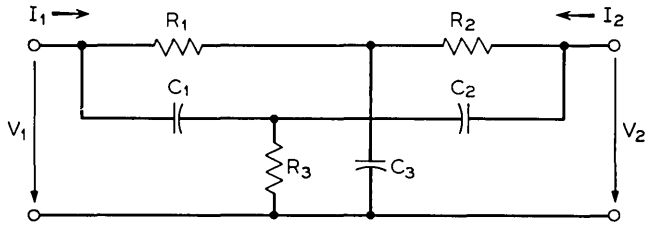

Fig. 1—The twin-T.

where

$$\left.\begin{aligned} a &= R_1R_2R_3C_1C_2C_3 & e &= R_1C_3 + R_sC_2 \\ b &= R_sR_3C_1C_2 & f &= R_2C_3(R_1C_1 + R_3C_s) \\ c &= R_3C_s & g &= R_sC_1 + R_2C_3 \\ d &= R_1C_3(R_2C_2 + R_3C_s) & R_s &= R_1 + R_2\ ;\quad C_s = C_1 + C_2 \\ & & R_p &= \frac{R_1R_2}{R_s} \end{aligned}\right\}. \tag{1b}$$

The transfer function of the unloaded twin-T is

$$T(s) = \frac{V_2}{V_1}\bigg|_{I_2=0} = -\frac{Y_{21}}{Y_{22}} = \frac{as^3 + bs^2 + cs + 1}{as^3 + (b + d)s^2 + (c + e)s + 1}. \tag{2}$$

The elements of Y and the transfer function $T(s)$ are of the third degree in s. The properties of the twin-T are very useful in second-order RC-active filter sections.[1,2] One of these properties is to allow right-half-plane zeros of $T(s)$ in the unshaded region of Fig. 2 which is bounded by the line with an angle of 60 degrees.[3] An important application in RC-active filters is based on the fact that one needs less gain of the amplifier to realize a high-pole Q if $T(s)$ has right-half-plane zeros.[4] However, as is well known, for the RC-active filter applications, the degree in s of either $T(s)$ or of the elements of Y has to be reduced to second order by creating a common divider in the numerator and the denominator of $T(s)$ or the elements of Y. To achieve this several special solutions are known,[5] some of which will be listed later. All of them, however, either impose more constraints than necessary on the values of the components of the twin-T, or they destroy the possibility of right-half-plane zeros. Some solutions are approximations which hold only in the neighborhood of the imaginary axis. This paper will derive the general condition for the reduction by one of the degree

in s. This will lead to only one constraint, leaving additional free components of the twin-T. This fact has a variety of applications in network theory. As an example it will be used in Section V to optimize and to extend the capabilities of the second-order FEN. Another application is the precision tuning of second-order RC-active filter sections.[6] The reduction of the degree of $T(s)$ by one will be dealt with in the following section.

II. THE TRANSFER FUNCTION T(s) OF SECOND DEGREE

The degree of $T(s)$ in equation (2) is reduced by one by creating a common divider in the numerator and the denominator of $T(s)$ or, in other words, by creating a coinciding zero and pole of $T(s)$ which can be cancelled. The condition under which a pole and a zero coincide may be found by using Euclid's algorithm.[7] This algorithm and its application to $T(s)$ are presented in the Appendix. The result is the following: $T(s)$ is of second degree in s if

$$d(d^2 + e^2b) - e(e^2a + cd^2) = 0. \tag{3}$$

The common divider of $T(s)$ is

$$D(s) = s + \frac{e}{d}. \tag{4}$$

Dividing the numerator and the denominator of $T(s)$ by $D(s)$ and considering equation (3) provides the transfer function of second degree in s

$$T(s) = \frac{s^2 + \left(\frac{b}{a} - \frac{e}{d}\right)s + \frac{d}{ea}}{s^2 + \left(\frac{b}{a} - \frac{e}{d} + \frac{d}{a}\right)s + \frac{d}{ea}}. \tag{5}$$

Now we have to check the condition (3) in further detail. Inserting

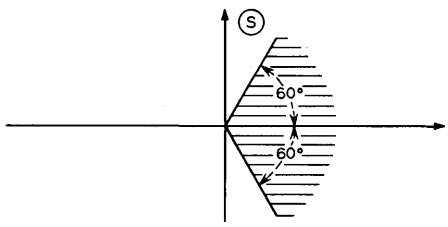

Fig. 2—The possible location of zeros of $T(s)$.

a, b, c, d, and e from (1b) in (3) and then rearranging equation (3) yields

$$(R_1R_2C_3 - R_3R_sC_s)\left(\left(\frac{d}{e}\right)^2 - R_1R_3C_1C_3\right) = 0. \tag{6}$$

Obviously equation (6) provides two separate conditions for the pole-zero cancellation; namely,

$$\left(\frac{d}{e}\right)^2 = R_1R_3C_1C_3 \tag{7}$$

or

$$R_1R_2C_3 = R_3R_sC_s\,. \tag{8}$$

The coefficients of $T(s)$ in equation (5) depend upon the choice of condition (7) or (8). The two solutions are:

Case 1. $T(s)$ as in equation (5), with $\left(\frac{d}{e}\right)^2 = R_1R_3C_1C_3\,.$ (9a)

Case 2. $T(s)$ as in equation (5), with

$$R_1R_2C_3 = R_3C_sR_s\,. \tag{9b}$$

Case 2 should be worked out in further detail. Inserting (8) in (5) yields the result

$$T(s) = \frac{s^2 + \frac{d}{ae}}{s^2 + \frac{d}{a}s + \frac{d}{ae}} \tag{9c}$$

[where again constraint (8) holds].

In Case 1 the zeros of $T(s)$ may be in the left- or in the right-half plane since in the numerator the coefficient of s can be positive or negative. The zeros of $T(s)$ in Case 2 however always lie on the imaginary axis.

As can be seen, the cancellation of poles and zeros is guaranteed in all cases by only one condition; namely, either equation (7) or equation (8). Thus from the six parameters of the twin-T, five are left at our disposal.

III. THE Y-MATRIX OF SECOND DEGREE

The condition for the reduction of the degree in all four elements of Y in equation (1a) is obvious. One of the two first-order factors of the denominator has to be contained in all numerators. We divide

the numerators by one of those first-order factors and set the rest of the division equal to zero. This provides the one condition

$$R_pC_3 = R_3C_s \; ; \tag{10a}$$

that is, the two first-order factors of the denominator are equal. Inserting R_p from equation (1b) in (10a) yields

$$R_1R_2C_3 = R_3R_sC_s \; , \tag{10b}$$

which is the same condition as equation (8). Dividing all numerators in Y by $(sR_pC_3 + 1)$ and inserting $R_3 = (R_1R_2C_3/R_sC_s)$ from (10b) yields the second-order Y-matrix

$$Y = \begin{bmatrix} \dfrac{s^2R_1R_2C_1C_2\dfrac{C_3}{C_s} + s(R_sC_1 + R_2C_3) + 1}{R_s(sR_pC_3 + 1)} & -\dfrac{s^2R_1R_2C_1C_2\dfrac{C_3}{C_s} + 1}{R_s(sR_pC_3 + 1)} \\ -\dfrac{s^2R_1R_2C_1C_2\dfrac{C_3}{C_s} + 1}{R_s(sR_pC_3 + 1)} & \dfrac{s^2R_1R_2C_1C_2\dfrac{C_3}{C_s} + s(R_sC_2 + R_1C_3) + 1}{R_s(sR_pC_3 + 1)} \end{bmatrix} . \tag{11}$$

Again the pole-zero cancellation is guaranteed by only one constraint leaving five parameters of the twin-T at our disposal. Before we consider an application, let us look at some special cases for the constraints (7) or (10b).

IV. SPECIAL CASES

We fulfill the condition (7) or (10b) by selecting one or more of the remaining five free parameters of the twin-T in a special way. This will simplify sometimes the equations for $T(s)$ and Y. We shall list the following six special cases.

(*i*) $$R_1 = R_2 = 2R_3 = R; \qquad C_1 = C_2 = \frac{C_3}{2} = C.$$

With this choice of values the conditions (7) and (10b) are satisfied simultaneously. So we shall obtain a second order $T(s)$ with zeros on the imaginary axis and a Y-matrix of second order.
From (9c) we get

$$T(s) = \frac{s^2 + \dfrac{1}{R^2C^2}}{s^2 + \dfrac{4}{RC}s + \dfrac{1}{R^2C^2}} \; ,$$

and from (11) we get

$$Y = \begin{bmatrix} \dfrac{s^2R^2C^2 + 4RCs + 1}{2R(sRC + 1)} & -\dfrac{s^2R^2C^2 + 1}{2R(sRC + 1)} \\ -\dfrac{s^2R^2C^2 + 1}{2R(sRC + 1)} & \dfrac{s^2R^2C^2 + 4RCs + 1}{2R(sRC + 1)} \end{bmatrix}.$$

This symmetrical twin-T with the two free parameters R and C has been used in the filters described in Refs. 1 and 2.

(*ii*) $R_2 = \rho R_1$; $R_3 = \dfrac{\rho}{1 + \rho} R_1$; $C_2 = \dfrac{C}{\rho}$; $C_3 = C_1 \dfrac{\rho + 1}{\rho}$; $\rho \geqq 0$.

The conditions (7) and (10b) are again satisfied simultaneously. Thus we get a $T(s)$ of second degree with zeros on the imaginary axis. From (9c) we obtain

$$T(s) = \frac{s^2 + \left(\dfrac{1}{R_1C_1}\right)}{s^2 + 2\dfrac{\rho + 1}{\rho}\dfrac{1}{R_1C_1}s + \left(\dfrac{1}{R_1C_1}\right)^2}.$$

This so-called potentially symmetrical twin-T has been used in Ref. 5.

(*iii*) $$R_1 = R_3 = R; \qquad C_1 = C_3 = C.$$

With this choice of values only condition (7) is satisfied. We, therefore, expect a $T(s)$ of second degree. Since condition (10a) is not fulfilled, the Y-matrix will remain of third-degree. In this case we get from (5) with (7)

$$T(s) = \frac{s^2 + \dfrac{1}{RC}\dfrac{R}{R_2}s + \dfrac{1}{RCR_2C_2}}{s^2 + \dfrac{1}{RC}\left(2\dfrac{R}{R_2} + 1 + \dfrac{RC}{R_2C_2}\right)s + \dfrac{1}{RCR_2C_2}}.$$

Obviously, only zeros in the open left-half plane are possible.

(*iv*) $$R_2C_2 = R_3(C_1 + C_2) = R_1(C_2 + C_3).$$

This choice satisfies only (7) and yields the transfer function

$$T(s) = \frac{s^2 + \dfrac{1}{R_2C_3}s + \dfrac{1}{R_2^2C_2^2}\left(1 + \dfrac{C_2}{C_1}\right)}{s^2 + \left[\dfrac{1}{R_2C_3} + \dfrac{2}{R_2C_2}\left(1 + \dfrac{C_2}{C_1}\right)\right]s + \dfrac{1}{R_2^2C_2^2}\left(1 + \dfrac{C_2}{C_1}\right)},$$

where again no right-half-plane zeros are possible.

(*v*) $$R_1C_1 = R_2C_2 = R_3C_3 .$$

Again this special choice satisfies only constraint (7). Equations (5) and (7) yield

$$T(s) = \frac{s^2 + \frac{1}{R_1C_1}\left(\frac{R_3}{R_1} + \frac{R_3}{R_2} - 1\right)s + \frac{1}{R_1^2C_1^2}}{s^2 + \frac{1}{R_1C_1}\left(\frac{R_3}{R_1} + \frac{R_3}{R_2} + \frac{R_1}{R_3} + \frac{R_1}{R_2}\right)s + \frac{1}{R_1^2C_1^2}}.$$

Obviously this transfer function is capable of realizing right-half-plane zeros.

(*vi*) $$R_1 = R_3 = R; \qquad C_2 = \frac{R}{R + R_2}\sqrt{C_1C_3}.$$

This choice satisfies (7) and yields the transfer function

$$T(s) = \frac{s^2 + \frac{R(C_1 + \sqrt{C_1C_3}) + R_2(C_1 - C_3)}{RR_2C_3(C_1 + \sqrt{C_1C_3})}s + \frac{(R + R_2)(C_1 + \sqrt{C_1C_3})}{R^2R_2C_1(C_3 + \sqrt{C_1C_3})\sqrt{C_1C_3}}}{s^2 + \left[\frac{R(C_1 + \sqrt{C_1C_3}) + R_2(C_1 - C_3)}{RR_2C_3(C_1 + \sqrt{C_1C_3})} + \frac{(R + R_2)(C_1 + \sqrt{C_1C_3})}{RR_2C_1\sqrt{C_1C_3}}\right]s + \frac{(R + R_2)(C_1 + \sqrt{C_1C_3})}{R^2R_2C_1(C_3 + \sqrt{C_1C_3})\sqrt{C_1C_3}}},$$

which is capable of realizing right-half-plane zeros. An application for the general second-order twin-T will be demonstrated in the following section.

V. FREQUENCY-EMPHASIZING NETWORKS (FENS) WITH GENERAL TWIN-TS

The so-called medium-selectivity FEN (MSFEN)[2] is shown in Fig. 3. Its transfer function is

$$\frac{V_{out}}{V_{in}} = T_0(s) = -\frac{R_F}{R_G}\frac{1}{1 + \mu\beta T(s)}, \tag{12}$$

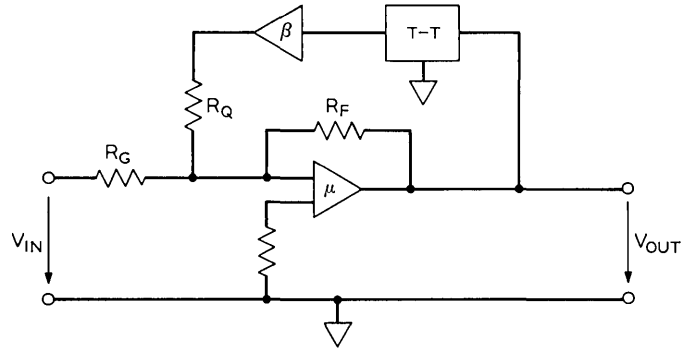

Fig. 3—A frequency-emphasizing network.

where $\beta \geqq 1$ is the gain of the noninverting amplifier in the feedback loop,

$$\mu = \frac{R_F}{R_G} \tag{13}$$

is the gain of the inverting amplifier in the forward path, and $T(s)$ designates the transfer function of the unloaded twin-T. Inserting $T(s)$ from (9a), which enables realization of right-half-plane zeros, we get from (12)

$$T_0(s) = -\frac{R_F}{R_G} \frac{s^2 + \left(\frac{b}{a} - \frac{e}{d} + \frac{d}{a}\right)s + \frac{d}{ae}}{(1 + \mu\beta)\left[s^2 + \left(\frac{b}{a} - \frac{e}{d} + \frac{d}{a}\frac{1}{1 + \mu\beta}\right)s + \frac{d}{ae}\right]} \tag{14}$$

with constraint equation (7). We want to realize the following transfer function of a FEN

$$T_{\text{FEN}}(s) = -K \frac{s^2 + \frac{\omega_0}{q_z}s + \omega_0^2}{s^2 + \frac{\omega_0}{q_p}s + \omega_0^2}. \tag{15a}$$

$| T_{\text{FEN}}(j\omega) |$ has a maximum at $\omega = \omega_0$ where $| T_{\text{FEN}}(j\omega_0) | = | q_p/q_z |$. In order to get a frequency-emphasizing network

$$q_p > | q_z |. \tag{15b}$$

We immediately get from equation (15a) the following requirements for (14a):

$$\omega_0^2 = \frac{d}{ae}, \tag{16a}$$

$$\frac{\omega_0}{q_z} = \frac{b}{a} - \frac{e}{d} + \frac{d}{a}, \tag{16b}$$

$$\frac{\omega_0}{q_p} = \frac{b}{a} - \frac{e}{d} + \frac{d}{a}\frac{1}{1 + \mu\beta}, \tag{16c}$$

and from (14b):

$$\left(\frac{d}{e}\right)^2 = R_1R_3C_1C_3. \tag{16d}$$

The last requirement $K = R_F/R_G[1/(1 + \mu\beta)]$ can always be satisfied by R_G which does not occur in (16a) through (16d).

We simplify the equations (16a) through (16d). Inserting (16b) into (16c) we get

$$\frac{d}{a} = \left(1 + \frac{1}{\mu\beta}\right)\omega_0\left(\frac{1}{q_z} - \frac{1}{q_p}\right) \triangleq x. \tag{17a}$$

Inserting (17a) in (16a), (16a) in (16d), and (17a) and (16a) in (16b) we get

$$e\omega_0^2 = x, \tag{17b}$$

$$R_1R_3C_1C_3 = a^2\omega_0^4, \tag{17c}$$

$$-\frac{b}{a} + \frac{1}{a\omega_0^2} + \frac{\omega_0}{q_z} = x. \tag{17d}$$

With a, b, d, e from (16) we obtain, finally,

$$\frac{(R_2C_2 + R_3C_1 + R_3C_2)}{R_2R_3C_1C_2} = x, \tag{18a}$$

$$(R_1C_3 + R_1C_2 + R_2C_2)\omega_0^2 = x, \tag{18b}$$

$$-\frac{(R_1 + R_2)}{R_1R_2C_3} + R_2C_2\omega_0^2 + \frac{\omega_0}{q_z} = x, \tag{18c}$$

$$1 = R_1R_2^2R_3C_1C_2^2C_3\omega_0^4, \tag{18d}$$

where (18d) has been used to simplify (18c). This nonlinear system of four equations with the seven unknowns: R_i, $i = 1, 2, 3$, C_i, $i = 1, 2, 3$, and $\mu\beta$ contained in x may be solved by choosing three unknowns in such a way that all solutions are realizable, that is they are positive real numbers. Picking R_1, R_2, C_3 and solving for R_3, C_1, C_2, and x does not give a feasible solution. We pick now R_2, C_2 and x and solve for R_1, R_3, C_1 and C_3. From (18b, c) we get

$$R_1C_3 = \frac{x}{\omega_0^2} - R_2C_2 - R_1C_2 = \frac{R_1 + R_2}{R_2}\left[\frac{1}{\frac{\omega_0}{q_z} + R_2C_2\omega_0^2 - x}\right]. \tag{19}$$

The equation on the right side of (19) yields

$$R_1 = \frac{\left(\frac{x}{\omega_0^2} - R_2C_2\right)\left(\frac{\omega_0}{q_z} + R_2C_2\omega_0^2 - x\right) - 1}{\frac{1}{R_2} + C_2\left(\frac{\omega_0}{q_z} + R_2C_2\omega_0^2 - x\right)}. \tag{20a}$$

From (19) we obtain, further,

$$C_3 = \frac{R_1 + R_2}{R_1 R_2} \frac{1}{\frac{\omega_0}{q_z} + R_2 C_2 \omega_0^2 - x}, \tag{20b}$$

with R_1 in equation (20a).

Eliminating C_1 in (18a) and (18d) and solving for R_3 yields

$$R_3 = \frac{x - \frac{1}{R_2 C_2} - (R_2 C_2)^2 \omega_0^4 R_1 C_3}{R_1 R_2 C_2^2 C_3 \omega_0^4}, \tag{20c}$$

while (18d) provides

$$C_1 = \frac{1}{R_1 R_2^2 C_2^2 R_3 C_3 \omega_0^4}. \tag{20d}$$

From (17a) we obtain

$$\mu\beta = \frac{1}{\frac{x}{\omega_0\left(\frac{1}{q_z} - \frac{1}{q_p}\right)} - 1}. \tag{20e}$$

The solution for R_1, R_3, C_1, C_3 and $\mu\beta$ has to be positive. C_3 is positive if

$$\frac{\omega_0}{q_z} + R_2 C_2 \omega_0^2 - x > 0. \tag{21a}$$

With equation (21a) the denominator of (20a) is positive; thus the numerator also has to be positive, which yields

$$x^2 - x\left(\frac{\omega_0}{q_z} + 2\omega_0^2 R_2 C_2\right) + \omega_0^2 + \frac{\omega_0^3 R_2 C_2}{q_z} + \omega_0^4 R_2^2 C_2^2 < 0.$$

This is satisfied for

$$x \in \left[\frac{\omega_0}{2q_z} + \omega_0^2 R_2 C_2 - \omega_0\sqrt{\frac{1}{4q_z^2} - 1}, \frac{\omega_0}{2q_z} + \omega_0^2 R_2 C_2 + \omega_0\sqrt{\frac{1}{4q_z^2} - 1}\right]. \tag{21b}$$

The square root in (21b) is always real since the numerator of equation (14a) or (15a) belongs to a passive RC-two port where $q_z < \frac{1}{2}$ always holds. For the requirement $\mu\beta \geqq 0$ we get from (20e)

$$x > \omega_0\left(\frac{1}{q_z} - \frac{1}{q_p}\right) \tag{21c}$$

which, with (15b), is always satisfied as long as $|q_z| < q_p$. Finally $R_3 > 0$ yields

$$x > \frac{1}{R_2C_2} + (R_2C_2)^2R_1C_3\omega_0^4 .$$

With R_1 in equation (20a) and C_3 in equation (20b) we then obtain

$$x^2 - x\left(\frac{2}{R_2C_2} + \frac{\omega_0}{q_z}\right) + \frac{1}{R_2^2C_2^2} + \omega_0^2 + \frac{\omega_0}{q_zR_2C_2} < 0.$$

This is fulfilled for

$$x \,\varepsilon\, \left(\frac{\omega_0}{2q_z} + \frac{1}{R_2C_2} - \omega_0\sqrt{\frac{1}{4q_z^2} - 1},\ \frac{\omega_0}{2q_z} + \frac{1}{R_2C_2} + \omega_0\sqrt{\frac{1}{4q_z^2} - 1}\right). \qquad (21d)$$

We now have to check the compatibility of the inequalities (21a) through (21d). It can be shown easily that the upper bound in (21b) guarantees (21a), which must no longer be considered. The inequalities (21b) and (21d) have a range in common if the upper bound of (21b) is higher than the lower bound of (21d) and if the lower bound of (21b) is lower than the upper bound of (21d). This is satisfied if

$$R_2C_2 \,\varepsilon\, \left[\frac{1}{\omega_0}\left(\frac{1}{2q_z} - \sqrt{\frac{1}{4q_z^2} - 1}\right),\ \frac{1}{\omega_0}\left(\frac{1}{2q_z} + \sqrt{\frac{1}{4q_z^2} - 1}\right)\right]. \qquad (22a)$$

Then the common range of (21b) and (21d) is $x \,\varepsilon\, \{\max$ [lower bounds of (21b) and (21c)], min [upper bounds of (21b) and (21d)]$\}$. This yields

$$x \,\varepsilon\, \left[\frac{\omega_0}{2q_z} + \omega_0^2R_2C_2 - \omega_0\sqrt{\frac{1}{4q_z^2} - 1},\ \frac{\omega_0}{2q_z} + \frac{1}{R_2C_2} + \omega_0\sqrt{\frac{1}{4q_z^2} - 1}\right]$$

$$\text{if} \quad R_2C_2 > \frac{1}{\omega_0}, \qquad (22b)$$

and

$$x \,\varepsilon\, \left[\frac{\omega_0}{2q_z} + \frac{1}{R_2C_2} - \omega_0\sqrt{\frac{1}{4q_z^2} - 1},\ \frac{\omega_0}{2q_z} + \omega_0^2R_2C_2 + \omega_0\sqrt{\frac{1}{4q_z^2} - 1}\right]$$

$$\text{if} \quad R_2C_2 < \frac{1}{\omega_0}. \qquad (22c)$$

The inequality (21c) may be satisfied if the upper limit of (22b) and (22c) respectively is larger than the limit in (21c). This yields for (22b)

$$\frac{1}{R_2C_2} > \frac{\omega_0}{2q_z} - \frac{\omega_0}{q_p} - \omega_0\sqrt{\frac{1}{4q_z^2} - 1}, \qquad (22d)$$

and for (22c)

$$R_2C_2 > \frac{1}{\omega_0}\left(\frac{1}{2q_z} - \sqrt{\frac{1}{4q_z^2} - 1} - \frac{1}{q_p}\right). \tag{22e}$$

Obviously (22a) also guarantees (22e); (22a) and (22d) are compatible if the lower bound of (22a) is lower than the bound for R_2C_2 in (22d). Again, this is always satisfied as can be easily shown. Thus we get the two following sets of constraints:

Case 1.

$$R_2C_2 > \frac{1}{\omega_0}. \tag{23a}$$

$$R_2C_2 \in \left[\frac{1}{\omega_0}\left(\frac{1}{2q_z} - \sqrt{\frac{1}{4q_z^2} - 1}\right), \frac{1}{\omega_0}\left(\frac{1}{2q_z} + \sqrt{\frac{1}{4q_z^2} - 1}\right)\right]. \tag{23b}$$

$$x \in \left[\frac{\omega_0}{2q_z} + \omega_0^2 R_2C_2 - \omega_0\sqrt{\frac{1}{4q_z^2} - 1}, \frac{\omega_0}{2q_z} + \frac{1}{R_2C_2} + \omega_0\sqrt{\frac{1}{4q_z^2} - 1}\right]. \tag{23c}$$

$$x > \omega_0\left(\frac{1}{q_z} - \frac{1}{q_p}\right). \tag{23d}$$

Case 2.

$$R_2C_2 < \frac{1}{\omega_0}. \tag{24a}$$

$$R_2C_2 \in \left[\frac{1}{\omega_0}\left(\frac{1}{2q_z} - \sqrt{\frac{1}{4q_z^2} - 1}\right), \frac{1}{\omega_0}\left(\frac{1}{2q_z} + \sqrt{\frac{1}{4q_z^2} - 1}\right)\right]. \tag{24b}$$

$$x \in \left[\frac{\omega_0}{2q_z} + \frac{1}{R_2C_2} - \omega_0\sqrt{\frac{1}{4q_z^2} - 1}, \frac{\omega_0}{2q_z} + \omega_0^2 R_2C_2 + \omega_0\sqrt{\frac{1}{4q_z^2} - 1}\right]. \tag{24c}$$

$$x > \omega_0\left(\frac{1}{q_z} - \frac{1}{q_p}\right). \tag{24d}$$

Equations (20a) through (20e) and the constraints (23) and (24) represent the solution to the design of an FEN. For a given q_p the gain $\mu\beta$ should become as small as possible. This enlarges the bandwidth of the amplifier and provides a more stable gain. As equation (20e) shows, $\mu\beta$ becomes small if x is chosen as large as possible.

G. Malek[8] has written a computer program which provides solutions to equations (20a) through (20e) satisfying the constraints (23) and

(24). The user may specify the spread in the values of the resistors and the capacitors that can be tolerated. The program will give him a solution with the given spread and with a minimum value of the gain $\mu\beta$.

With G. Malek's program the following FENs have been designed. (*i*) Given: $\omega_0 = 5 \times 10^4$ 1/second; $q_p = 60$; tolerable spread in the values of the Rs and Cs is 1:9.5; $\mu\beta$ should be as small as possible. The result is

$$R_1 = 16.821K \quad R_2 = 50.00K \quad R_3 = 22.556K \quad \mu\beta = 11.4$$

$$C_1 = 546pF \quad C_2 = 320pF \quad C_3 = 3010pF \quad q_z = 0.3.$$

(*ii*) Given: $\omega_0 = 5 \times 10^4$ 1/second; $q_p = 60$; tolerable spread 1:4.5; and again $\mu\beta$ as small as possible. The result is

$$R_1 = 25.6K \quad R_2 = 50.0K \quad R_3 = 16.5K \quad \mu\beta = 13.4$$

$$C_1 = 647pF \quad C_2 = 375pF \quad C_3 = 1674pF \quad q_z = 0.3.$$

(*iii*) Given: $\omega_0 = 5 \times 10^4$ 1/second; $q_p = 500$; tolerable spread 1:3; and $\mu\beta$ as small as possible. The result is

$$R_1 = 41.4K \quad R_2 = 50.0K \quad R_3 = 22.5K \quad \mu\beta = 20.16$$

$$C_1 = 413pF \quad C_2 = 370pF \quad C_3 = 1208pF \quad q_z = 0.25.$$

A great variery of further solutions may be found by G. Malek's program. If we would realize the three FENs with potentially symmetrical twin-Ts with the same spread in values, we would require a gain $\mu\beta = 133$ in the first case, $\mu\beta = 153$ in the second, and $\mu\beta = 1499$ in the third case. Thus the gain in the new circuits is a factor of 10 to 75 times smaller, resulting in increased bandwidth and stability.

The deviation of q_p with respect to temperature has been measured by G. Malek[8]. In the temperature range of 10°C to 70°C, q_p of the new circuit changed by 9 percent in comparison to 19.5 percent in the case of a potentially symmetrical twin-T.

VI. CONCLUSIONS

Conditions have been derived which guarantee that the transfer function or the Y-matrix of a general twin-T is of second degree in s. As a result, five parameters of the twin-T are at our disposal. Since this number is larger than in the commonly used approaches, more effective use can be made of a twin-T. It has been demonstrated in the case of an MSFEN that the gain required to realize a given pole Q

may be reduced by a factor up to 70, while the stability of the pole may typically be improved by a factor of 2. The topological structure of the MSFEN, however, is the same as in the building blocks presently used.

APPENDIX

Given the two polynomials $N_0(s)$ and $N_1(s)$ where the degree of N_1 does not exceed that of N_0 . We wish to find the largest common divider of N_0 and N_1 using Euclid's algorithm.[7] This algorithm is described below by the (a) equations, while the (b) equations are only used for the proof.

We form

$$\frac{N_0(s)}{N_1(s)} = A_1(s) + \frac{N_2(s)}{N_1(s)} \tag{25a}$$

or

$$N_0(s) = A_1(s)N_1(s) + N_2(s). \tag{25b}$$

where the degree of N_2 is smaller than the degree of N_0 .

A common divider of N_0 and N_1 is a zero which both have in common. At those zeros, N_0 and N_1 vanish; thus N_2 in equation (25b) also must vanish. So the common zero is also contained in N_1 and N_2 . Thus we continue by

$$\frac{N_1(s)}{N_2(s)} = A_2(s) + \frac{N_3(s)}{N_2(s)} \tag{26a}$$

or

$$N_1(s) = A_2(s)N_2(s) + N_3(s). \tag{26b}$$

With the same reasoning as before, the common zero is contained in N_2 and N_3 where the degree of N_3 is smaller than the degree of N_1 . Continuing in the same manner we get

$$\frac{N_{\nu-1}(s)}{N_\nu(s)} = A_\nu(s) + \frac{N_{\nu+1}(s)}{N_\nu(s)} \tag{27a}$$

or

$$N_{\nu-1}(s) = A_\nu(s)N_\nu(s) + N_{\nu+1}(s). \tag{27b}$$

If $N_{\nu+1}(s) \equiv 0$ then N_ν is the largest common divider. This can be seen, considering that $N_{\nu-1}$ and N_ν have the same common divider

as N_0 and N_1 . For $N_{\nu+1} \equiv 0$ we get from (27b)

$$N_{\nu-1}(s) = A_\nu(s)N_\nu(s), \tag{28}$$

which shows that the largest divider N_ν is also contained in $N_{\nu-1}$.

If we want the common divider to be of the first degree in s then we continue dividing as above until an $N_\nu(s)$ of the first degree and a rest of zero degree remains. Now we put the rest $N_{\nu+1}(s) \equiv 0$ from which we derive the one condition for a common factor of the first degree in N_0 and N_1 .

We apply this technique to $T(s)$ in equation (2), where

$$N_0(s) = as^3 + (b + d)s^2 + (c + e)s + 1,$$
$$N_1(s) = as^3 + bs^2 + cs + 1.$$

We ask for the one condition for which a common divider of the first degree occurs. Applying the algorithm, we get

Step 1: $$N_2 = +(ds^2 + es) = +ds\left(s + \frac{e}{d}\right).$$

Step 2: $$N_3 = \left(b - \frac{ea}{d}\right)s^2 + cs + 1.$$

At this point we may use a shortcut, which is always possible and which saves a considerable amount of time. We are to find the common divider of N_2 and N_3 . Since N_2 is of the second degree we may factor it as shown above. One of the roots of the first order must be the common divider; ds cannot be a root of $N_3(s)$, thus

$$D(s) = s + \frac{e}{d} \tag{29}$$

must be the divider we are after. Dividing N_3 by $s + e/d$ we get the following rest which we set equal to zero

$$d(d^2 + e^2b) - e(d^2c + e^2a) = 0. \tag{30}$$

Equation (6) is the constraint guaranteeing that $D(s)$ is the common divider of $N_0(s)$ and $N_1(s)$. Dividing $N_0(s)$ and $N_1(s)$ by $D(s)$ and considering (30) we get

$$N_0(s) = \left(s + \frac{e}{d}\right)\left(as^2 + \left(b + d - \frac{ea}{d}\right)s + \frac{d}{e}\right), \tag{31a}$$

$$N_1(s) = \left(s + \frac{e}{d}\right)\left(as^2 + \left(b - \frac{e}{d}a\right)s + \frac{d}{e}\right), \tag{31b}$$

and

$$T(s) = \frac{N_1(s)}{N_0(s)} = \frac{as^2 + \left(b - \frac{e}{d}a\right)s + \frac{d}{e}}{as^2 + \left(b + d - \frac{ea}{d}\right)s + \frac{d}{e}}. \tag{31c}$$

REFERENCES

1. Sallen, R. P., and Key, E. L., "A Practical Method of Designing RC-Active Filters," IRE Trans., *CT-2*, No. 1 (March 1955), pp. 74–85.
2. Moschytz, G. S., "FEN Filter Design Using Tantalum and Silicon Integrated Circuits," Proc. IEEE, *58*, No. 4 (April 1970), pp. 550–556.
3. Seshu, S., and Reed, M. B., *Linear Graphs and Electrical Networks*, Reading, Massachusetts: Addison-Wesley, 1961.
4. Moschytz, G. S., Class notes on linear active networks. Lecture 10, BTL out-of-hours course (Spring 1970).
5. Moschytz, G. S., "A General Approach to Twin-T Design and Its Application to Hybrid Integrated Linear Active Networks," B.S.T.J., *49*, No. 6 (July–August 1970), pp. 1105–1149.
6. Lueder,E., "Precision Tuning of Hybrid RC-Active Filters with Nonideal Amplifiers," unpublished work.
7. Weber, H., *Lehrbuch der Algebra, 1*, New York: Chelsea Publishing Comp., 1898.
8. Malek, G., unpublished work.

Contributors to This Issue

GEORGE H. BEBBINGTON, B.A., 1960, Rutgers University; currently working towards an M.A. at Newark State College; Bell Laboratories, 1952—. Mr. Bebbington is presently a member of the Rubber and Crosslinked Plastics Group. He has worked on the development of wire and cable insulation and jacketing compounds and also on public health, ozonization, and deterioration problems. Member, New York Rubber Group of the Rubber Division of the American Chemical Society.

RICHARD A. CONNOLLY, B.S. (Forestry), 1952, University of Maine; Master of Forestry, 1954, Yale School of Forestry; Bell Laboratories, 1956—. Mr. Connolly's work is concerned with the performance of materials used in buried, marine, and atmospheric environments of interest to the Bell System. Member, Society of Industrial Microbiology, Society of American Foresters, ASTM D20 Committee concerned with the resistance of plastics to microorganisms.

DONALD W. DAHRINGER, B.S.Ch.E., 1955, Newark College of Engineering; M.S.Ch.E., 1959, Polytechnic Institute of Brooklyn; Bell Laboratories, 1961—. Mr. Dahringer has worked in the area of organic materials development. He is currently a Bell System consultant on adhesives and bonding technology. Member, ACS, A.I.Ch.E., NJSPE, Omicron Delta Kappa, Phi Lambda Upsilon, Iota Tau.

JOHN B. DECOSTE, B.S.Ch.E., Cooper Union; Bell Laboratories, 1928—. Mr. DeCoste's career has been in chemical research directed toward the adoption of organic polymeric material for use in the telephone plant. He holds two patents and has published a number of papers on the properties of polyethylene and poly(vinyl chloride) as well as on standardization in plastics. Member, ACS, Society of Plastics Engineers, ASTM.

DONALD L. DUTTWEILER, B.E.E., 1966, Rensselaer Polytechnic Institute; M.S., 1967, and Ph.D., 1970, Stanford University; Bell Laboratories, 1970—. Since joining Bell Laboratories, Mr. Duttweiler has been concerned with various analytical problems in the area of digital communications. Member, IEEE, Eta Kappa Nu, Tau Beta Pi, Sigma Xi.

MICHAEL R. GAREY, B.S., 1967, M.S., 1969, and Ph.D., 1970, University of Wisconsin; Bell Laboratories, 1970—. Mr. Garey's recent interests have been in the fields of graph theory, combinatorial analysis, and discrete optimization, with particular emphasis on the design of efficient computational algorithms. Member, Association for Computing Machinery, Mathematical Association of America.

BARRY G. HASKELL, B.S., 1964, M.S., 1965, and Ph.D. (Electrical Engineering), 1968, University of California; Research Assistant, University of California, 1965–68; Bell Laboratories, 1968—. Mr. Haskell is engaged in TV picture processing studies. Member, IEEE, Phi Beta Kappa, Sigma Xi.

THEODORE H. KLEIN, B.S. (Chemistry), 1953, Upsala College; Bell Laboratories, 1967—. Mr. Klein's major interests at Bell Laboratories have been reinforced plastics and substrates for flexible circuitry. Member, American Society For Testing and Materials; Bell Laboratories Representative to Society of Plastic Industries.

T. K. KWEI, B.S. (Chemistry), 1949, National Chiao-Tung University, China; M.S. (Chemical Engineering), 1954, University of Toronto; Ph.D. (Chemistry), 1958, Polytechnic Institute of Brooklyn; Standard Oil Company of Indiana; Interchemical Corporation; Bell Laboratories, 1965—. Mr. Kwei is interested in the mechanical properties of polymers and diffusion in polymers. He has published some forty-five papers on chemical subjects.

JOHN O. LIMB, B.E.E., 1963, and Ph.D., 1967, University of Western Australia; Research Laboratories, Australian Post Office, 1966–1967; Bell Laboratories, 1967—. Mr. Limb has worked on the coding of picture signals to reduce channel capacity requirements. More recently this has included the coding of color pictures. He is now working on methods of reducing redundancy in moving pictures for *Picturephone*® visual telephone applications.

ERNST LUEDER, Dipl. Ing., 1958, Dr.-Ing., 1962, Habilitation, 1967, University of Stuttgart (Germany); Bell Laboratories, 1968–1971. At Stuttgart Mr. Lueder was engaged in network synthesis, theory of nonlinear and electromechanical circuits, and system theory. While at Bell Laboratories he specialized in design of *RC*-active filters. Mr.

Lueder is presently professor of network theory and system theory at the University of Stuttgart. Member, German Associations of Engineers VDE and NTG.

DIETRICH MARCUSE, Diplom Vorpruefung, 1952, Dipl. Phys., 1954, Berlin Free University; D.E.E., 1962, Technische Hochschule, Karlsruhe, Germany; Siemens and Halske (Germany), 1954–57; Bell Laboratories, 1957—. At Siemens and Halske, Mr. Marcuse was engaged in transmission research, studying coaxial cable and circular waveguide transmission. At Bell Laboratories, he has been engaged in studies of circular electric waveguides and work on gaseous masers. He spent one year (1966–1967) on leave of absence from Bell Laboratories at the University of Utah where he wrote a book on quantum electronics. He is presently working on the transmission aspect of a light communications system. Member, IEEE, Optical Society of America.

JAMES MCKENNA, B.Sc. (Mathematics), 1951, Massachusetts Institute of Technology; Ph.D. (Mathematics), 1961, Princeton University; Bell Laboratories, 1960—. Mr. McKenna has done research in quantum mechanics, electromagnetic theory, and statistical mechanics. He has recently been engaged in the study of nonlinear partial differential equations that arise in solid state device work, and in the theory of stochastic differential equations.

RUSSELL J. MINER, Bell Laboratories, 1961—. Since joining the Plastics Research and Development Department, Mr. Miner has been involved in the study of the effects of soil burial, electron irradiation, and outdoors aging on plastic materials used in the Bell System as well as the flame and fire retardance properties of these materials.

J. A. MORRISON, B.Sc., 1952, King's College, University of London; Sc.M., 1954, and Ph.D., 1956, Brown University; Bell Laboratories, 1956—. Mr. Morrison has been doing research in a variety of problems in mathematical physics and applied mathematics. His recent interests have included perturbation techniques for nonlinear oscillations and propagation in random media. He was a Visiting Professor of Mechanics at Lehigh University during the Fall semester 1968. Member, American Mathematical Society, SIAM, Sigma Xi.

FRANK X. VENTRICE, B.S. (Chemistry) and graduate work, 1960, Brooklyn College; Bell Laboratories, 1961—. Prior to joining Bell Laboratories, Mr. Ventrice did research on soil suspending agents at Colgate-Palmolive. At Bell Laboratories, as a member of the Casting Resins and Organic Finishes Group, he is doing research and development on epoxies, polyurethanes, silicone, styrene-polyesters, and waxes. Mr. Ventrice is currently a Bell System consultant on casting and encapsulating materials. Member, ACS.

CONTENTS

(Continued from front cover)

GENERAL ARTICLES


Bell System